Univerzita Karlova

Přírodovědecká fakulta

Studijní program: Geologie

Mgr. Šárka Kubínová

Minerální a chemické změny během krystalizace magmatu a tvorby pozdně variských intruzí a žil v moldanubické zóně Českého masívu

Mineral and chemical changes of magma crystallization during formation of post-Variscan intrusions and veins in the Moldanubian Zone of the Bohemian Massif

Disertační práce

Školitel: prof. Ing. Shah Wali Faryad, CSc.

Konzultant: doc. RNDr. Kryštof Verner, Ph.D.

Praha, 2019

„The true genius shudders at incompleteness and usually prefers silence to saying

the something which is not everything that should be said."

- Edgar Allan Poe -

Prohlášení

Prohlašuji, že jsem závěrečnou práci zpracovala samostatně a za spolupráce ostatních členů výzkumného týmu. Všechny použité informační zdroje a literatura jsou řádně uvedeny. Tato práce ani její podstatná část nebyla předložena k získání jiného nebo stejného akademického titulu.

Declaration

I certify that this thesis is my own work and it was created by collaboration with the other members of research team. I cite all used sources of information and literature. This work, neither its important part, wasn't submit to obtain the other or the same academic title.

V Praze, 6.6.2019

In Prague, 6.6.2019

.....

Šárka Kubínová

Poděkování

Předkládaná práce byla sestavena na základě poznatků z několika let trvajícího výzkumu, do nějž různou měrou přispěla spousta lidí, kteří si zaslouží můj upřímný vděk. Největší zásluhy na dokončení této práce má můj školitel, profesor Shah Wali Faryad. Z celého srdce mu děkuji za vřelý přístup, cenné rady a ochotu pomoci. Rovněž mu děkuji za odborné vedení při zpracování této disertační práce a materiální zajištění. Srdečné poděkování si zaslouží i zesnulý docent František Holub, který byl mým školitelem v průběhu bakalářského a magisterského stupně studia a z jehož výzkumné práce jsem čerpala inspiraci pro sestavení této disertační práce. Společně s mým současným školitelem mi poskytl spoustu nově nabytých znalostí a zkušeností, a oba mi budou velkým vzorem nejen v profesním, ale i osobním životě.

Déle děkuji všem spoluautorům a spolupracovníkům za jejich příspěvky do jednotlivých částí této práce, poskytnuté konzultace a pomoc při terénním výzkumu, odběru vzorků a získávání dat.

Touto cestou bych rovněž ráda poděkovala svým rodičům za velkou podporu, trpělivost a poskytnutí zázemí po celou dobu mého studia. Velké díky si zaslouží i kamarádi a kolegové z Ústavu petrologie a strukturní geologie Univerzity Karlovy.

Závěrem děkuji všem institucím, které podpořily jednotlivé části této práce finančně. Jedná se o Grantovou Agenturu České republiky (výzkumný projekt č. 13-06958S, 18-03160S) a Přírodovědeckou Fakultu Univerzity Karlovy (výzkumný projekt Progress Q45 a GAUK 1194019).

Acknowledgements

The presented thesis includes the results of several years of research. Many people participated in various parts of this research and everyone deserves my sincere gratitude. The greatest merit for completion of this thesis goes to my supervisor, Professor Shah Wali Faryad. I thank him with all my heart for his honest attitude, valuable advice and willingness to help me. As well, I thank him for professional guidance in processing of this thesis and material assurance. Heartfelt thanks also belong to deceased Docent František Holub. He was my supervisor during my bachelor and master degree study and his research works were the source of inspirations for compilation of my thesis. He together with my recent supervisor provided me a lot of new experiences and both two will be my models not only in my future professional but also in personal life.

I also thank all my co-authors and collaborators for their contributions to the individual parts of this work, for provided consultations and for help with fieled works, sampling and data acquisition.

As well, I would like to thank my parents for big support, patience and providing me a great background throughout my study. Great thanks also belong to all my friends and colleagues from the Institute of Petrology and Structural Geology at the Charles University.

Finally, I thank all the institutions that provide the financial support to individual parts of this work. These are Grant Agency of the Czech Republic (researcher project number 13-06958S, 18-03160S) and the Faculty of Science at the Charles University (researcher project Progress Q45 and GAUK 1194019).

Český abstrakt

Pozdně variské hořčíkem bohaté draselné až ultradraselné magmatické horniny vytvářejí početné žíly, žilné roje a několik plutonických těles při hranici mezi Moldanubickou Zónou a Telesko-Barrandienskou jednotkou v Českém Masivu. Přesto, že představují objemově menší skupinu magmatických hornin, jsou klíčové k pochopení generování tavenin a proseců plášťové metasomatózy, a diferenciace taveniny v mělčích hloubkách. Kromě toho jsou považovány za indikátory tektonického vývoje této části Českého Masivu během finálních stádií Variské Orogeneze. V současnosti jsou předmětem diskuze několika autorů zejména z pohledu jejich geneze, vmístění a geodynamického významu.

Předkládaná disertační práce je kompilace čtyř vědeckých publikací zaměřených na petrologické stadium vybraných (ultra)-draselných žilných hornin z několika lokalit nacházejících se při západním okraji Moldanubické Zóny. Studium minerálních struktur, chemického složení minerálů a celohorninových vzorků společně se studiem magnetických staveb a struktruních terénních vztahů, a stanovení stáří nám umožnilo popsat krystalizační historii těchto hornin, diskutovat jejich vývoj od vzniku taveniny k výstupu a vmístění magmatu, a vytvořit model sekvence Variských orogenních procesů v Moldanubické části Českého Masivu.

Předmětem zájmu jsou vápenato-alkalické lamprofyry (*minety*, *spessartity*, *kersantity)* a příbuzné horninové typy (*vaugnerit*, *syenitové porfyry*). Všechny tyto horninové druhy mají podobnou minerální asociaci mírně se odlišující modálním množstvím jednotlivých minerálů vzhledem k danému horninovému typu. Obsahují olivín anebo mastkové pseudomorfózy po olivínu, biotit, klinopyroxen, ortopyroxen, amfibol anebo jeho pseudomorfózy, a kalcit. Felsické faze jsou reprezentovány K-živcem, plagioklasem a křemenem. Běžnými akcesorickými minerály jsou apatit, Cr-spinel, titanit, zirkon and opakní fáze (Fe-Ti oxidy a sulfidy Fe, Cu, Ni). Sekundární minerály vytvořené během pozdního stadia krystalizace jsou mastek, serpentin, karbonát, biotit, klinopyroxen, amfibol, chlorit a křemen. Ve studovaných vzorcích byly rovněž pozorovány různé typy ocelli. Jedná se o (*i*) křemen s reakčními lemy klinopyroxenu a menším množstvím K-živce, (*ii*) kalcitové ocelli, a (*iii*) multifázové ocelli tvořené plagioklasem a biotitem, méně amfibolem a K-živcem, a příležitostně karbonátem a křemenem.

Studované žilné horniny nesou známky minerální krystalizace, která probíhala v několika stádiích. Pozorované struktury minerálů společně s obsahem hlavních prvků v analyzovaných minerálech a jejich kompoziční zonálnost svědčí o variacích ve složení taveniny a fluid a teplotně-tlakových změnách během formování žil. Hlavní prvky a komponenty, které ovlivnily vznik a stabilitu minerální fází jsou CO_2, H_2O, F, Si a Na. Stádia minerální krystalizace, rozlišené v této práci, dokládají začátek krystalizace z mateřské taveniny ve svchním plášti. Poté byla reziduální tavenina ovlivněna frakcionací a kontaminací korovým materiálem během svého výstupu. Na závěr,

minerální reakce v subsolidových podmínkách a únik volatilních komponent ovlivnily růst minerálů během posledního krystalizačního stádia.

Chemické složení všech analyzovaných celohorninových vzorků ukazuje běžné geochemické znaky, které byly pozorované v podobných horninových typech ve Variském Orogenu. Těmito znaky jsou především vysoké obsahy K, volatílií (hlavně H_2O a CO_2) a inkompatibilních prvků (značně vysoké poměry LILE/HFSE a obsahy REE s obohacením LREE vzhledem k HREE). Vzorky zároveň ukazují znaky odvozené z pláště, kterými jsou vysoké obsahy Mg, Cr a Ni. Navzdory těmto základním geochemickým podobnostem, je mezi analyzovanými vzorky možné pozorovat variace v prvkových koncentracích, zejména oscilace v poměrech některých inkompatibilních prvků jako Ce, Sr, Nb a Zr. Geochemické složení studovaných žil indikuje, že zdrojové magma bylo vytvořeno nízkým stupněm parciálního tavení metasomatizovaného volatiliemi bohatého peridotitu ve svrchním plášti (pravděpodobně v poli stability spinelu nebo dokonce při hranici polí stability spinelu a granátu), a následně ovlivněno frakcionací a krustální kontaminací, což je v souladu s pozorovanými minerálními strukturami a chemickým složením minerálů.

Nové U-Pb datování vaugneritu a syenitového porfyru dává podobné stáří (338.59 ± 0.68 Ma a 337.87 ± 0.21 Ma). Stanovené stáří obou žil je blízké stáří draslíkem bohatých syenitových plutonů v Moldanubické Zóně.

Magnetické stavby vybraných žil dokládají jejich formování tokem magmatu uvnitř žíly. V jednom případě však lamprofyrová žíla ukázala kombinaci volného toku magmu a tlakově řízeného pohyb magmatu. Jednotlivé žíly mají paralelní orientace ve směru Z-V až SZ-JV. Jsou téměř kolmé ke směru Středočeského Plutonického Komplexu (SPK) a rovněž k magmatickým stavbám v jednotlivých plutonech SPK a k regionálním metamorfním stavbám pozorovaným v metamorfovaných horninách Moldanubické Zóny. Výstup a vmístění magmatu v žilách byl přisouzen k regionálnímu napěťovému poli ZSZ-VJV konvergence během formování Variského Orogenu.

English abstract

The late-Variscan magnesium-rich potassic to ultrapotassic igneous rocks create numerous dykes, dyke swarms and several plutonic bodies at the boundary between the Moldanubian Zone and the Teplá-Barrandian Block of the Bohemian Massif. They represent a volumetrically smaller group of igneous rock but they are the key to understand generation of melt and processes of mantle metasomatism and shallow-level magma differentiation. In addition, they are considered as an indicator of the tectonic evolution of this part of the Bohemian Massif during the final stages of the Variscan orogenesis. Currently, they are the subject of discussion by several authors in terms of their genesis, emplacement time and geodynamic significance.

The presented thesis is a compilation of four scientific publications that are aimed at the petrological study of selected (ultra)-potassic dyke rocks from several localities at the western border of the Moldanubian Zone. The study of mineral textures, mineral chemistry and whole-rock geochemistry together with magnetic fabrics, structural field relations and age determinations allowed us to describe the crystallization history of these rocks, discuss their evolution from melt generation to magma ascent and emplacement, and form the model of sequence of Variscan orogenic processes in the Moldanubian part of the Bohemian Massif.

The objects of interest are calc-alkaline lamprophyres (*minettes*, *spessartites*, *kersantites*) and related rock-types (*vaugnerite*, *syenite porphyries*). These rock-types all have similar mineral assemblages with slightly different modal amounts of individual minerals in relation to the rock-type. They contain olivine and/or talc pseudomorphs after olivine, biotite, clinopyroxene, orthopyroxene, amphibole and/or its pseudomorphs, and calcite. The felsic phases are represented by K-feldspar, plagioclase and quartz. Apatite, Cr-spinel, titanite, zircon and opaque phases (Fe-Ti oxides and sulphides of Fe, Cu, Ni) are common accessory minerals. Late-stage secondary minerals are talc, serpentine, carbonate, biotite, clinopyroxene, amphibole, chlorite and quartz. Moreover, various types of ocelli were observed in the studied samples. These are (*i*) quartz with reaction rims of clinopyroxene and minor K-feldspar, (*ii*) calcite ocelli, and (*iii*) multiphase ocelli formed by plagioclase and biotite, minor amphibole and K-feldspar, and occasionally by carbonate and quartz.

The studied dyke rocks preserve the evidence of multistage crystallization. The observed mineral textures together with the major element concentrations in analyzed minerals and their compositional zoning are the expression of variations in composition of melt and fluid and temperature-pressure changes during formation of dykes. The main elements and components that affect the formation and stability of mineral phases are CO_2, H_2O, F, Si and Na. The stages of mineral crystallization, distinguished in this work, demonstrate they started their crystallization from parental melt in the upper mantle. Then the residual melt was affected by both fractionation and contamination by crustal material during the magma ascent. Finally, the mineral reactions in

subsolidus conditions and escape of volatiles affected the growth of minerals during the last crystallization stage.

The bulk rock chemistry of all analyzed samples show common geochemical features that were observed in similar rock-types around the Variscan orogeny. These features are especially high contents of K, volatiles (mainly H_2O and CO_2) and incompatible elements (notably high LILE/HFSE ratios and REE contents with enrichment of LREE relative to HREE). The samples show mantle-derived signatures such as high contents of Mg, Cr and Ni. Despite of these basic geochemical similarities, it is possible to see variations in element concentrations in the analyzed samples, mainly the oscillations in ratios of some incompatible elements such as Ce, Sr, Nb and Zr. The whole-rock geochemistry of studied dykes indicates that the source magma was formed by a low-degree of partial melting of metasomatic volatile-rich peridotite in the upper mantle (probably in the spinel stability field or even at the boundary between the spinel and garnet stability field), and subsequently affected by the fractionation and crustal contamination which is consistent with observed mineral textures and mineral chemistry.

The new U-Pb dating of vaugnerite and syenite porphyry yielded similar ages (338.59 ± 0.68 Ma and 337.87 ± 0.21 Ma). The determined ages of both dykes are close to the age of potassium-rich syenite plutons in the Moldanubian Zone.

The magnetic fabrics of the selected dykes assume their formation by magma flow within the dyke. But in one case a lamprophyre dyke showed the combination of both magma free flow and forcefully driven magma movement. The individual dykes have parallel orientation in W-E to NW-SE direction. They are almost perpendicular to the Central Bohemian Plutonic Complex (CBPC) trending as well as to the magmatic fabrics in the individual plutons of CBPC and to the regional metamorphic fabrics observed in the metamorphic rocks of the Moldanubian Zone. The magma ascent and emplacement in the dykes were attributed to the regional stress field of WNW-ESE convergence during the formation of Variscan Orogeny.

List of published articles presented in the thesis

Kubínová, Š., Faryad, S. W., Verner, K., Schmitz, M., Holub, F. (2017). Ultrapotassic dykes in the Moldanubian Zone and their significance for understanding of the post-collisional mantle dynamics during Variscan orogeny in the Bohemian Massif. Lithos 272–273, 205–221.

Authors contribution: 70 %

Kubínová, Š., Faryad, S. W. (2019). Mineral textures of olivine minette and their significance for crystallization history of parental magma; an example from the Moldanubian Zone (the Bohemian Massif). Mineralogy and Petrology, DOI: 10.1007/s00710-019-00658-y.

Authors contribution: 80 %

Hrouda, F., Verner, K., Kubínová, Š., Buriánek, D., Faryad, S. W., Chlupáčová, M., Holub, F. V. (2016). Magnetic fabric and emplacement of dykes of lamprophyres and related rocks of the Central Bohemian Dyke Swarm (Central European Variscides). Journal of Geosciences 61, 335–354.

Authors contribution: 30 %

Hrouda, F., Faryad, S. W., Kubínová, Š., Verner, K., Chlupáčová, M. (2019) Simultaneous free flow and forcefully driven movement of magma in lamprophyre dykes as indicated by magnetic anisotropy: Case study from the Central Bohemian Dyke Swarm, Czech Republic. Geosciences 9(3), 104.

Authors contribution: 30 %

It is to confirm the above given partial involvement (in percentage) of Šárka Kubínová in the fieldwork and sampling, making of the petrographic descriptions, responsibility for the collecting, processing and presentation of chemical data, as well as the calculation and determination of temperature and pressure during minerals crystallization. Discussion produced by the student following detailed consultations with the supervisor.

.....

Prof. Shah Wali Faryad (supervisor)

Table of contents

CHAPTER 1

HIGH-POTASSIC MAGNESIUM-RICH IGNEOUS ROCKS

1.1 Introduction

Recent results of research on magnesium-rich potassic to ultrapotassic mantle-derived rocks, exposed along the orogenic belts on the Earth, show their importance for mantle dynamics during plate convergence and help to characterize the crust and mantle interaction during these large-scale geological processes. These rocks form a volumetrically smaller group of igneous rocks but they are genetically important as they record the thermal and geochemical fingerprints of the lithosphere beneath the region. Their mineralogical and geochemical features can be used to obtain information about the composition of lithospheric mantle and its local chemical variations, to the extent of metasomatic processes in the upper mantle, to the origin of melt and its shallow-level magma mixing, fractionation and contamination by crustal material, and to characterization of the ascent and emplacement of magma. The investigation, understanding and clarification of origin, evolution and emplacement of these igneous rocks is still in progress and a lot of questions are debated.

Generally, potassic to ultrapotassic magmatism is associated with late-collisional (convergent) to post-collisional (divergent) tectonic settings, or with stable (within plate) continental tectonic settings. This type of magmatic activity includes the formation of five main rock-groups: *calc-alkaline lamprophyres* (or *lamprophyres sensu stricto* according to Streckeisen (1979) or *shoshonitic lamprophyres* according to Rock 1977), *alkaline lamprophyres*, *ultramafic lamprophyres (*or *melilitic lamprophyres)*, *lamproites* (or *lamproitic lamprophyres*) and *kimberlites*. Also, some transitional rock-types between the individual rock-varieties of above mentioned (ultra)-potassic rock-groups and/or gradations of lamprophyres and lamproites into the „normal“ igneous rocks of similar bulk composition were observed (Rock, 1991 and references therein). The calc-alkaline lamprophyres are commonly associated with a subduction related environment (Garza et al., 2013; Guo et al., 2004; Karsli et al., 2014; Krmíček et al.,2014; Ma et al., 2014; O'Leary et al., 2009; Owen, 2008; Pandey et al., 2017a, 2018; Rock, 1984, 1991), whereas the alkaline lamprophyres and lamproites occur in post-collisional settings and also in continental intra-plate settings (Chalapathi Rao et al., 2012; Chen and Zhai, 2003; Conticelli et al., 2009; Fritschle et al., 2013; Lu et al., 2015; Meshram et al., 2015; Orejana et al., 2008; Rock, 1977, 1991; Stoppa et al., 2014; Ubide et al., 2014), and ultramafic lamprophyres and kimberlites are typically found in within plate settings (Beard et al., 1996; Rock, 1991; Tappe et al., 2004, 2006, 2008).

Lamprophyres are a unique type of mesocratic to melanocratic (rarely ultramafic) rocks which mainly form dykes and usually also small intrusions. They have a specific mineral texture („lampropohyric texture“) that is characterized by euhedral mafic phenocrysts (typically hydrous phases such as dark mica (biotite to phlogopite in composition) and/or calcic amphibole, and also clinopyroxene, orthopyroxene and olivine) occurring in a fine-grained matrix composed from the same mafic phases and from felsic minerals (the most abundant feldspars, and minor or free foids and quartz). They often contain abundant apatite which can form not only grains in the matrix but also phenocrysts. The presence of carbonates (both primary and/or secondary) is characteristic. Lamprophyres often undergo subsolidus autometasomatic alteration or deuteric processes in response to the high volatile contents in the residual melt. The replacement of olivine, pyroxene, biotite and plagioclase and the occurrence of ocelli (vesicles filled by most often carbonates and quartz) are very common. Also, some lamprophyres contain xenocrysts of quartz or feldspars, or mafic enclaves and even xenoliths (e.g. Rock 1991 and references therein).

Based on recent studies (e.g. Bédard, 1994; Guo et al., 2004, 2006; Karsli et al., 2014; Moayyed et al., 2008; Pandey et al., 2017a; Plá Cid et al., 2006; Wenzel et al., 1997; Woodard et al., 2014), the parental lamprophyric magmas represent the primary melts derived by low-degree partial melting of heterogenous metasomatised mantle. Moreover, some authors propose the origin of lamprophyres by mixing of mantle-derived basaltic or lamproite melts with crustally-derived silicic melts (Rock, 1991; Prelevic et al., 2004), or even by mixing of upwelling basaltic melt with ultrapotassic upper-mantle-derived melts (Thompson et al., 1990), or by crustal-level mixing of basic and alkaline mantle-derived melts (Xu et al., 2007).

The principal geochemical features of lamprophyres are high concentrations of mantle-compatible elements such as high MgO, Cr and Ni and high Mg# values, and elevated contents of mantle-incompatible elements such as alkalis, volatiles (mainly H_2O and CO_2), F, Cl, S, P_2O_5, LILE (Rb, Ba, Cs), Th, U and REE (especially LREE), and also the mantle isotopic composition of Nd and crustal isotopic composition of Sr and Pb (e.g. Rock, 1991; Scarrow et al., 2008). These geochemical features were linked to low-degree partial melting of lithospheric mantle peridotites, affected by metasomatism and by mixing mantle and crustal melts, and modified by fractional crystallization and assimilation of crustal material during magma ascent. Lamprophyres show a wide spectrum of geochemical composition that reflect (i) their tectonic setting, (ii) local geochemical variations in mantle source, (iii) melting conditions, (iv) composition of material entering into the subduction zone, (v) composition of the assimilated surrounding rocks and (vi) type and extent of modifying processes (differentiation, magma mixing etc.). They can be ultrabasic to intermediate and peraluminic to perpotassic in composition and may have various sodium-potassium ratios. Their Na_2O-K_2O contents vary from high sodium (sodic-potassic varieties) to considerable predominance of potassium over sodium (mildly even strongly potassic varieties). In case of (ultra)-potassic

varieties, the elevated K_2O contents (up to several weight percent) cannot be derived from normal mantle peridotite. It requires geochemical and/or mineralogical enrichments of the mantle source. This enrichment can occur by melting of phlogopite in the mantle peritodite (Conceição and Green, 2004; Foley, 1992a, b; Förster et al., 2017) and/or by the remelting of crustally derived sediments (Pan et al., 2017; Su et al., 2017). Moreover, Vaughan and Scarrow (2003) deduced that the variations in the degree of potassium-rich metasomatism of the upper mantle are controlled by the initiation and location of lithospheric strike-slip shear zones.

1.2 Classification and nomenclature of lamprophyres and related rocks

For clarity, a brief review on classification and nomenclature of lamprophyres and related rocks is given below. It should be noted that definition and classification of lamprophyre rocks were subject to extensive changes during the last decades and a lot of works with diverse concepts were published. Various aspects of this classification and nomenclature were implemented by Le Bas and Streckeisen (1991), Le Maitre (1989), Le Maitre et al. (2002), Mitchell (1994), Rock (1991), Streckeisen (1979), Tappe et al. (2005) and Woolley et al. (1996), and a brief review is listed in Krmíček and Krmíčková (2010). In this thesis, the classification of Le Maitre et al. (2002) is used. As the most common subduction-related potassium-rich rocks are *calc-alkaline lamprophyres* accompanied by *lamproites* and *alkaline lamprophyres*, the nomenclature linked below is aimed to these rock-types. Moreover, these rock-types are presented across the European Variscan belt and they are genetically linked with the individual stages of orogen formation. From this view, they could be collectively called as *orogenic lamprophyres* and *orogenic lamproites*.

1.2.1 Lamprophyres

The name „*lamprophyre*“ derives from the Greek words „lampros“ and „porphyros“ and means „glistening porphyry“ (Rock, 1991). The name was first used by Gümbel (1874) for dark-colored dyke rocks with numerous lustrous biotite phenocrysts in a feldspar matrix. He initially distinguished two varieties of lamprophyres - *minette* and *kersantite*. Later, Rosebhusch (1887) added to these rocks mafic dykes with amphibole phenocrysts (*vogesite*, *spessartite*, *camptonite*). These five varieties of lamprophyres represent the „true lamprophyres“ which were originally distinguished and classified as lamprophyres. During the 20th century, the lampropohyre group was added to by many newly described rocks which were similar to the lamprophyres in some features and their classification into common igneous rocks was difficult. The lamprophyre rock-group grew beyond the few sub-groups to include numerous rock varieties which missed the initial concept.

By recent definition of Le Maitre et al. (2002), *lamprophyres* represent a diverse rock-group that is difficult to distinguish chemically from other normal igneous rocks. They are distinguished on the following traditional characteristics: (*i*) they usually form dykes, (*ii*) they are not simply textural varieties of common plutonic or volcanic rocks, (*iii*) they are mesocratic to melanocratic (M' = 35-90), rarely holomelanocratic (M' > 90) rocks with porphyritic texture, (*iv*) they usually contain essential biotite (or Fe-phlogopite) and/or amphibole, and sometimes clinopyroxene and olivine, (*v*) if feldspars and/or feldspathoids are present, they are restricted to the matrix, (*vi*) hydrothermal alteration of olivine, pyroxene, biotite, and plagioclase, when present, is common, (*vii*) calcite, zeolites, and other hydrothermal minerals may appear as primary phases, (*viii*) their contents of K_2O and/or Na_2O, H_2O, CO_2, S, P_2O_5 and Ba are relatively high compared with other rocks with similar composition. The recommended classification is based on mineralogical criteria and seven types are distinguished according to the predominant mafic and felsic minerals (Tab.1).

Tab. 1 Classification and nomenclature of lamprophyres based on their mineralogy (according Le Maitre et al., 2002).

Light-coloured constituents		Predominant mafic minerals		
feldspar	foid	biotite > hornblende, □± diopsidic augite, (± olivine)	hornblende, diopsidic augite, ± olivine	brown amphibole, Ti-augite, olivine, biotite
or > pl	-	*minette*	*vogesite*	-
pl > or	-	*kersantite*	*spessartite*	-
or > pl	feld > foid	-	-	*sannaite*
pl > or	feld > foid	-	-	*camptonite*
-	glass or foid	-	-	*monchiquite*

or = alkali feldspar; pl = plagioclase; feld = feldspar; foid = feldspathoid.

In addition to these lamprophyre varieties, Rock (1984) divided *soda-minette,* where dominant mafic mineral is sodic amphibole and/or pyroxene, and K-feldspar dominates over plagioclase.

The *minette*, *kersantite*, *spessartite* and *vogesite* form the group of calc-alkaline lamprophyres, while *sannaite*, *camptonite* and *monchiquite* constitute alkaline lamprophyres. The *soda-minette* represents a transition variety between the calc-alkaline and alkaline lamprophyre groups (Streckeisen, 1979; Rock, 1977, 1984, 1991).

1.2.2 Plutonic lamprophyric rocks

A few ultrapotassic igneous rocks have been described that form mainly plutonic bodies and also dykes. These are geochemically similar to lamprophyres (it was assumed that they were generated from the lamprophyric magmas), but they do not have typical lamprohyric texture. They are medium- to coarse-grained and typically contain phenocrysts of Mg-rich biotite (to phlogopite) and/or ampbibole and also often feldspars. There are several varieties with local names as below:

Durbachite represents porphyric melanocratic variety of syenite that contains large grains of biotite, amphibole and K-feldspar in a matrix composed by biotite, amphibole, K-feldspar and a little quartz. It is chemical equivalent of minettes. The rock was first described by Sauer (1892) and its name come from Durbach in the Central Black Forest, Germany.

Vaugnerite is aphiric diorite to melasyenite composed of biotite, amphibole and plagioclase with K-feldspar, quartz and abundant accessory apatite. It forms dykes or small bodies and it is a chemical equivalent of kersantites and partly of minettes. Its name is after Vaugneray (near Lyon) in French Massif Central, France where it was described by Fournet (1861).

Redwitzite is lamprophyric rock of variable composition. It represents amphibole-biotite-(pyroxene) dioritoids and gabbroids which are characterized by the presence of large biotite phenocrysts. Originally was described by Willmann (1919) and named after Marktredwitz, Fichtelgebirge in NE Bavaria, Germany.

Appinite is variable group of volatile-rich amphibole- or clinopyroxene-rich hornblendites to melagranites. They contain amphibole in a matrix formed by plagioclase and/or K-feldspar with or without quartz. It is a chemical equivalent of vogesite and spessartite. Name is after Appin in Caledonides, Scotland (Bailey and Maufe, 1916).

1.2.3 Lamproites

The name „*lamproite*“ was introduced by Niggli (1923) for extrusive rocks of lamprophyric aspect. Today, the term *lamproite* have completely different meaning and it is used for intrusive and extrusive rocks with specific geochemical and mineralogical composition.

Lamproites classification scheme of Le Maitre et al. (2002) is based on the combination of mineralogical and chemical criteria. The mineralogical criteria are characterized by the presence of (not necessarily of all) primary minerals including: (*i*) Ti-rich, Al-poor phlogopite phenocrysts and (*ii*) poikilitic phlogopite in the matrix, (*iii*) Ti-K- rich richterite, (*iv*) forsteritic olivine, (*v*) Al-Na-poor diopside, (*vi*) Fe-rich leucite, (*vii*) Fe-rich sanidine. Based on the presence of one dominant mineral together with two or three other major minerals, the specific lamproite names are distinguished (for example „diopside-sanidine-phlogopite lamproite“ that corresponds with historial

name „orendite“). The presence of minerals that preclude the classification of a rock as a lamproite include: primary plagioclase, melillite, monticellite, kalsilite, nepheline, Na-rich alkali feldspar, sodalite, nosean, hauyne, melanite, schorlomite or kimzeyite. The chemical criteria include: (*i*) ultrapotassic character (molar K_2O / Na_2O > 3), (*ii*) molar K_2O / Al_2O_3 > 0.8, (*iii*) peralkaline character (molar (K_2O + Na_2O) / Al_2O_3 > 1), and (*iv*) both FeO and CaO < 10%, TiO_2 1–7%, Ba > 2000 ppm (commonly > 5000 ppm), Sr > 1000 ppm, Zr > 500 ppm and La > 200 ppm.

1.3 Potassic to ultrapotassic igneous rocks in the European Variscides

The late- to post-Variscan potassic to ultrapotassic igneous rocks including calc-alkaline lamprophyres and their plutonic equivalents (mainly durbachites and vaugnerites), and minor alkaline lamprophyres, lamproites, redwitzites and related rock-types are observed throughout the European Variscan basement rocks. They form plutonic bodies and dykes and they were observed (Fig. 1) in *the Bohemian Massif* (Awdankiewicz, 2007, 2010; Abdelfadil et al., 2013; Holub, 1997; Holub et al., 1997; Gerdes et al., 2000; Janoušek and Holub, 2007; Kotková et al., 2010; Kovaříková et al., 2007; Krmíček, 2010; Krmíček et al., 2016; Leichmann and Gaweda, 2001; Mazur et al., 2007; Pivec et al., 2002; Siebel et al., 2003; Štemprok et al., 2008, 2014; Verner et al., 2008; Wenzel et al., 1997, 2000; Zeitlhofer et al., 2016), in *the Schwarzwald* (*Black Forest*, e.g. Hegner et al., 1998; Schaltegger, 2000), in *the Vosges* (Schaltegger et al., 1996), in *the French Massif Central* (Couzinié et al., 2014; Martin et al., 2017; Montel, 1988; Sabatier 1980, 1991), in *the Armorican Massif* (Caroff et al., 2015) and in *the Iberian Massif* (Bea et al., 1999; Errandonea-Martin et al., 2018; Scarrow et al., 2011). These massifs represent tectonostratigraphic units of the Variscan Belt (according to Franke, 2000) which are formed by allochthonous and autochthonous parts separated by several suture zones (Fig. 1). The recent position of individual units is the result of the complex Carboniferous-Devonian convergence and subsequent collisions of microcontinents initially separated from the north periphery of Gondwana by spreading in the newly born Rheic Ocean. These microcontinents (the Armorican Terrane Assemblage) drifted to the north and finally accreted to Laurussia and completed the Variscan Belt. (For more details about the formation and evolution of Variscan orogenic belt and its terranes see Ballouard et al., 2017; Dias et al., 2016; Edel, 2001; Edel et al., 2003, 2013; Faure et al., 2017; Fernández et al., 2016; Finger et al., 2007; Franke, 2000; Franke et al., 1995, 2017; Jastezębski et al., 2015; Kroner and Romer, 2013; Murphy et al., 2016; Nance et al., 2010, 2012; Pouclet et al. 2017; Schulmann et al., 2009, 2014; Tait et al., 1997, von Raumer et al., 2003; Winchester et al., 2002.). Thus, the Variscan Orogen has a complex structure resulting from the stacking of terranes.

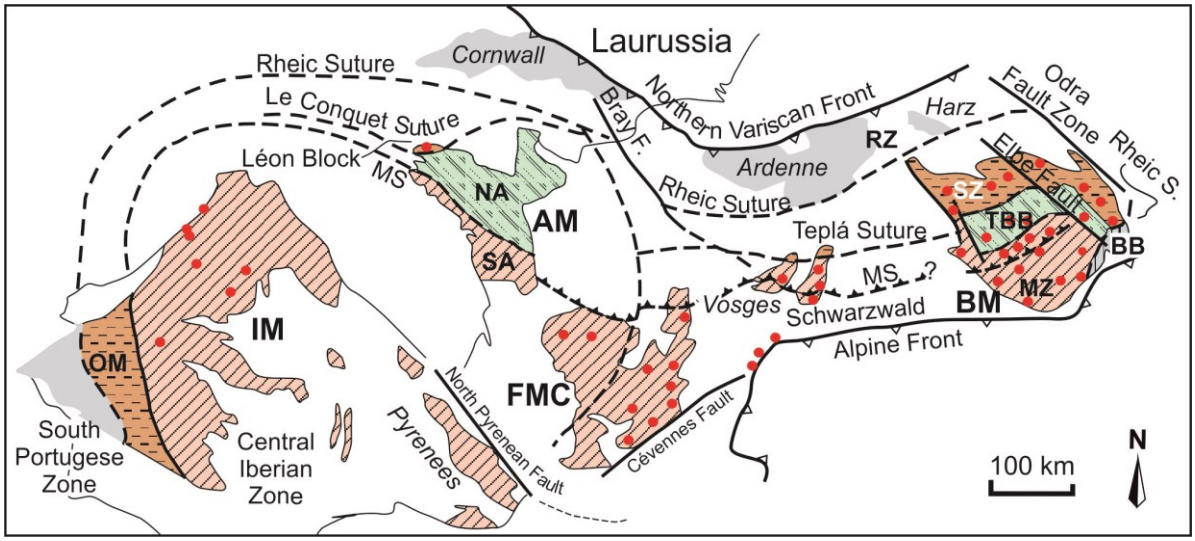

Fig. 1 The occurrence of (ultra)-potassic igneous rocks (red circles) in the lithotectonic units along the European Variscan Belt. For clarity, the red circles do not show individual localities but correspond to the broader area of occurrence of dykes or plutonic bodies or both together (taken from: Awdankiewicz, 2007; Bea et al., 1999; Caroff et al., 2015; Couzinié et al., 2014; Errandonea-Martin et al., 2018; Hegner et al., 1998; Holub, 1997; Kovaříková et al., 2007; Krmíček, 2010; Martin et al., 2017; Sabatier, 1991; Scarrow et al., 2011; Štemprok et al., 2014; von Raumer et al., 2014; Wenzel et al., 1997; Zeitlhofer et al., 2016). Basement units are: AM = Armorican Massif, BB = Brunovistulian Block, BM = Bohemian Massif, FMC = French Massif Central, IM = Iberian Massif, MZ = Moldanubian Zone, NA = North Armorica, OM = Ossa-Morena Zone, RZ = Rhenohercynian Zone, SA = South Armorica, SZ = Saxothuringian Zone, MS = Moldanubian suture.

The above mentioned massifs are characterized by the presence of subduction-related igneous rock-series. All massifs record episodic magmatic activity which style was changed in response to the evolving Variscan orogen. Based on the main igneous rock-types, the several subsequent magmatic pulses were divided by Finger et al. (1997) and Schaltegger (1997). As the magmatic activity evolved from calc-alkaline to alkaline and/or peralkaline and medium-potassic to high-potassic, magmatic activity include the initial more voluminous granitoid magmatism followed by lesser volume potassic to ultrapotassic magmatism. The main subsequent magmatic pulses can be divided:

(i) *calc-alkanine magmatism* forming composite plutons of granites, granodiorites, monzogranites and monzodiorites which are syn-orogenic to late-orogenic.

(ii) *calc-alkaline high-potassic magmatism* including plutonic bodies and dykes of (mela)granitoids-(mela)syenitoids and calc-alkaline lamprophyric rock-types (vaugnerite, durbachite, minette, kersantite, spessartite, vogesite). They are late- to post-orogenic.

(iii) (per)-alkaline (ultra)-potassic magmatism formed rocks with alkaline lamprophyric and lamproitic affinitites (sannaite, campronite, monchiquite, alkaline minette,

lamproite). They are post-orogenic and were formed during syn-collisional extension.

Von Raumer et al. (2014) stated that the K-Mg-rich igneous rocks in the European Variscides were derived by partial melting of enriched subcontinental mantle source during a late-collisional stage of Variscan orogenesis. The mantle melting was probably caused by the existence of thermal anomalies which were created by slab windows and the sinking of the subducted slab into the mantle. As melt formation during plate convergence reflect the plate movement, Schaltegger (1997) concluded that the distribution of Variscan high-K igneous rocks trace the paleosutures. The significance of these rocks as the tracer of suture zones was discussed also by Edel (2001). Both these authors stated that the formation of K-Mg-rich rocks is in relation to wrenching and orogeny parallel extension. Consistently, von Raumer et al. (2014) concluded that these rocks are distributed above the suture zone but their recent geographical occurrences do not detect any obvious plate-tectonic context.

1.4 The Bohemian Massif and Variscan magmatic activity

The Bohemian Massif forms the eastern segment of the European Variscan orogenic belt (Fig. 2a) and is formed by several lithotecnonic units that consist of basement rocks affected by various degrees of metamorphism and deformation and intruded by the variable types of igneous rocks. These units are represented by two crustal blocks (the Brunovistulian and the Teplá-Barrandian) and two zones (the Moldanubian and the Saxothuringian). The zones, in contrast with blocks, are characterized by the presence of high- to ultrahigh-pressure rocks (eclogites, garnet peridotites) creating lenses and boudins within the amphibolite-granulite facies metamorphic rocks (gneisses, migmatites and granulites) formed during Variscan orogenesis. (For more details about basement units, their metamorphism and age relations see Faryad et al. 2015; Košler et al. 2014; Kröner et al. 1988; Medaris et al. 2006; Schulmann et al. 2005; Wendt et al. 1993). The Moldanubian Zone is placed in the southern part of the Bohemian Massif and it lies between the Brunovistulian Block in the south-east and the Teplá-Barrandian Block in the north-west. The Saxothuringian Zone forms the northern part of the Bohemian Massif and is separated from the Moldanubian Zone by the the Teplá-Barrandian Block.

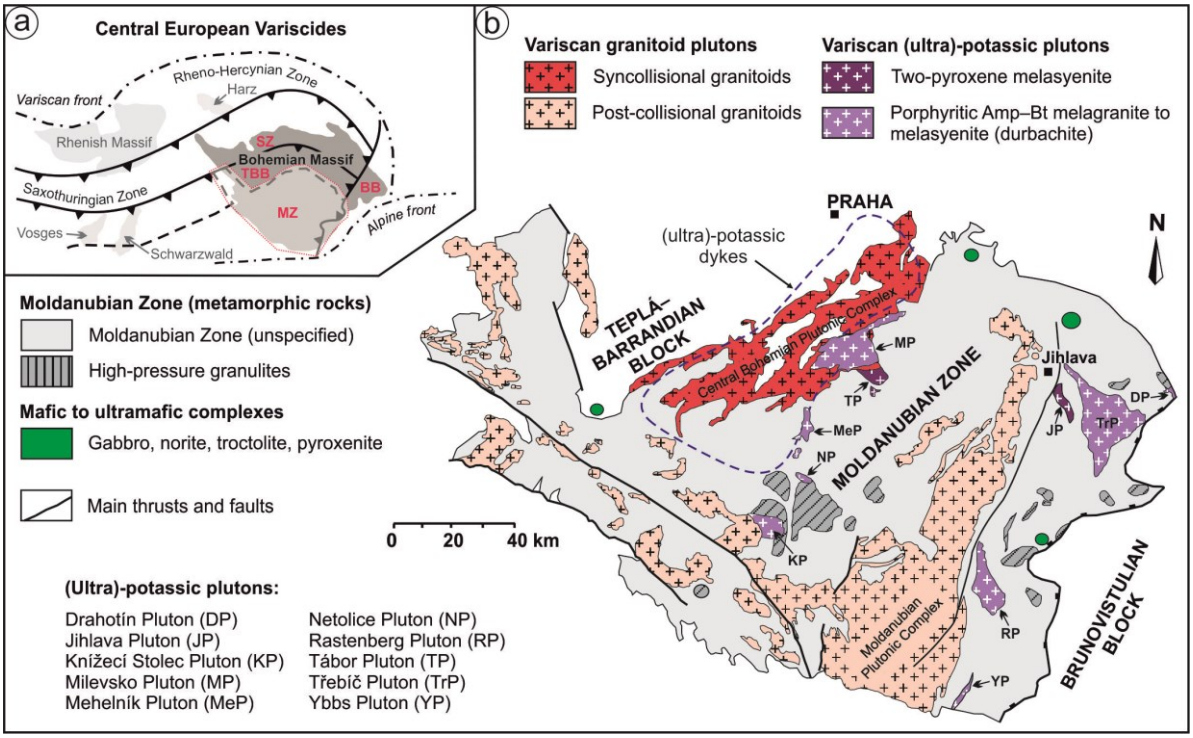

Fig. 2 (a) The simplified map of the Central European Variscides showing the position of the Bohemian Massif and its lithotectonic units (BB - Brunovistulian Block, MZ - Moldanubian Zone, SZ - Saxothuringian Zone, TBB - Teplá-Barrandien Block) (modified from Franke, 2000). **(b)** The geological map of the Moldanubian Zone of the Bohemian Massif (modified from Holub, 1997; Faryad et al., 2015, 2016, Janoušek and Holub, 2007) showing Variscan granitoids and (ultra)-potassic plutonic bodies. The dashed line define occurence of (ultra)-potassic dyke in theWestern Moldanubian Zone.

The Moldanubian Zone represents an exhumed lower- to mid-crustal orogenic root (Schulmann et al., 2005). It is formed by medium-grade (the Monotonous and Varied units) and high-grade (the Gföhl Unit) metamorphic rocks that are intruded by Variscan plutonic rocks and dykes. In general, the overall structure of the Moldanubian Zone was created in consequence of stacking several lithotectonic units at ~ 360 to 345 Ma and their subsequent high-temperature low-pressure (HT-LP) metamorphism, anatexis and late-Variscan wrench tectonics (for more details see e.g. Faryad and Žák 2016; Faryad et al. 2010; Franke 2006; Lardeaux et al. 2014; Schulmann et al., 2009; Žák et al., 2014). The metamorphic rock-types are represented by biotite paragneisses to migmatites and small bodies of amphibolites, schists, marbles and metaquartzites. The protoliths have determined the Paleoproterozoic to Devonian ages (Friedl et al., 2004; Janoušek et al., 2006; Košler et al., 2014; Kröner et al., 1988; Schulmann et al., 2005; Wendt et al., 1993).

The Teplá-Barrandian Block originally formed a part of the Cadomian accretionary wedge that was deformed (compressed) during the early stages of Variscan orogeny. It is formed of low- to medium-grade metamorphic rocks (slates, metagraywackes, metasiltstones, metaconglomerates) with protoliths of Neoproterozoic ages. These metamorphic rocks are intruded by Cambro-Ordovician

granitoids and they are covered by a folded, but unmetamorphosed, volcanosedimentary sequences of Paleozoic age (for more details see e.g. Hajná et al. 2017; Chlupáč et al. 1998; Schulmann et al. 2009; Žák et al. 2014).

The contact area between the relatively cold rocks of the Teplá-Barrandian Block and the hot, rapidly exhumed rocks of the Moldanubian Zone represents a significant tectonic boundary that permits the formation of various plutonic bodies, smaller intrusions and dykes of Variscan age (Fig. 2b). These igneous rocks have wide compositional range from mafic to felsic types and they are represented by mainly calc-alkaline, minor peraluminous and lesser peralkaline rock-series. It was assumed that they was created by several magmatic pulses generated from heterogenous mantle sources in relatively narrow time-intervals (see e.g. Holub et al. 1997b) Based on the compositions and ages of these Variscan igneous rocks, the four main groups can be subdivided. The first two groups represent granitoid complexes that form two belts, *the Central Bohemian Plutonic Complex* (*CBPC*) and *the Moldanubian Plutonic Complex* (*MPC*), with different ages and relations to the Variscan geotectonic processes (e.g. Finger et al. 1997; Holub et al. 1997b; Schalterger 1997; Žák et al. 2014). The older (c. 355–345 Ma) *CBPC* is located at the western border of the Moldanubian Zone and it is composed by subduction-related calc-alkaline granitoids (Holub et al. 1997a,b; Janoušek et al. 2004; Žák et al. 2014). The younger (c. 330–300 Ma) *MPC* lie in the eastern part of the Moldanubian Zone and it is formed by peraluminous (S-type) anatectic granitoids that were created by extensive migmatitization and isothermal decompression of the surrounding pelitic rocks (Žák et al. 2011). The third group is represented by several isolated plutons and dyke swarms of potassic to ultrapotassic rocks which are separated into two belts oriented almost in the NE-SW direction, the "*Western HP and Durbachite belt*" (including *the Milevsko Pluton*, *the Tábor Pluton*, *the Mehelník Pluton*, *the Netolice Pluton*, *the Knížecí Stolec Pluton*, several smaller bodies and numerous dykes) and "*Eastern HP and Durbachite belt*" (formed by *the Třebíč Pluton*, *the Jihlava Pluton*, *the Drahotín Pluton*, *the Rastenberg Pluton*, smaller bodies and dykes) with determined ages 346–335 Ma (Finger et al., 2007; Holub 1997; Janoušek and Gerdes 2003; Janoušek et al. 2010; Kotková et al., 2010; Krmíček 2010; Kubínová et al. 2017). The last group represents ~ 340 Ma mafic to ultramafic rocks (gabbro, norite, trocolite, pyroxenite) (Ackerman et al. 2013; Faryad et al. 2015, 2016). As some of these rocks are unmetamorphosed and the others record the signs of amphibolite-granulite metamorphism, they were assumed to be pre-Variscan in age.

The *CBPC* was created by several magmatic pulses which gave rise the various granitoids and subordinate mafic rocks (e.g. Holub et al. 1997b; Žák et al., 2014). The main rock groups consists: (*i*) the medium-K calc-alkaline rocks (quartz diorites to granodiorites) of *the Sázava Pluton* (~ 354 Ma; Janoušek et al. 2004), (*ii*) the high-K to shoshonitic calc-alkaline rocks (monzogabbros, quartz monzonites to granodiorites) of *the Blatná Composite Pluton* (~ 346 Ma; Janoušek et al.

2010), and (*iii*) the ultrapotassic rocks (melasyenites to melagranites of durbachite serie) of the *Milevsko* (~ 343 Ma, Holub et al. 1997a) and *Tábor* (336 Ma, Janoušek et al. 2013) *plutons*.

The magmatic rocks of the CBPC and adjacent metamorphic rocks of the Moldanubian Zone and the Teplá-Barrandian Block are intruded by abundant dykes and dyke swarms (~ 340 to 335 Ma; Holub et al. 1997b, 2009, 2012) which are distributed in an almost rectangular area (~ 30 × 100 km) that is elongated approximately in the NNE-SSW direction and mostly covers the whole area of CBPC and adjacent units (Fig. 2b). The dykes are petrographically variable and geochemically diverse. They are mafic to felsic in composition and they are represented by mainly calc-alkaline and minor peralkaline rock-series including rock-types with high-potassic to ultra-potassic and even shoshonitic affinity. The rock-types consist of lamprophyric rocks (spessartite, kersantite, minette, vaugnerite), variable types of porphyries (gabbrodiorite to granodiorite, (mela)-syenite to melagranite in compositions), and lamproitic rocks (lamproite, peralkaline minette and related rocks) (Holub et al. 1997b, 2007, 2009, 2012; Krmíček, 2010). Their diverse geochemical character declare the multiple magmatic pulses which come from heterogenous mantle sources and/or crustal sources in relatively narrow time-intervals (for a brief overview see Holub 1999, 2007).

(*i*) *The medium- to higher-potassic calc-alkaline dykes* (spessartites, kersantites, gabbrodiorite to granodiorite porphyries) were emplaced mainly into the oldest granitoids of the CBPC (Sázava Pluton) and also into the adjacent low-grade metasedimentary rocks of the Teplá-Barrandian Block. The average thickness of these dykes is ~ 1–6 m (rarely up to 10 m). (*ii*) *The high- to ultra-potassic calc-alkaline dykes* (minettes, vaugnerites and (mela)-syenite to melagranite porphyries) were emplaced into partly exhumed paragneisses to migmatites of the Moldanubian Zone and into the older intrusive bodies of the CBPC (Sázava and Blatná Pluton), but not into ultrapotassic plutons and younger intrusions of the CBPC. The thickness of dykes varies from 0.5–1.5 m (rarely up to 3 m) for minettes and vaugnerites, and 5–25 m for melasyenite to melagranite porphyries. The lengths of all these potassic dykes mentioned above are often limited to less than 1–2 km, perhaps due to segmentation of dykes by younger faults. Their intrusive contacts are sharp and discordant to the metamorphic and magmatic fabrics in the host rocks. The remarkable feature of these dykes is their orientations, which are parallel in a W-E to NW-SE direction (i.e. almost perpendicular to the CPBC trend and to the main foliation and nappe stacked basement rocks of the Moldanubian Zone). The horizontal distances between parallel dykes are 0.5–1.0 km which indicates the high density of dyking.

1.5 Study area

The different varieties of potassic to ultrapotassic dyke rocks were selected for study. These include calc-alkaline lamprophyres (*minettes*, *spessartites*, *kersantites*) and related rocks (*vaugnerite*,

syenite porphyries) which intrude the various host rocks (plutonic and metamorphic) from the broader area between the Moldanubian Zone and Teplá-Barrandian Block.

Three dykes of minette, vaugnerite and syenite porphyry intrude the migmatized paragneisses in the western part of the Moldanubian Zone. Ten studied dykes occur within the granitoids of the CBPC. These comprise four minettes, spessartite and syenite porphyry in Sázava Pluton, and two minettes and two syenite porphyries in Blatná Pluton. Three dykes (kersantite and two spessartites) penetrate the metasiltstones and metagraywackes in the eastern part of the Teplá-Barrandian Block. The closer localization and description of individual localities is listed in the next chapters (Chapter 2–5).

1.6 Subjects of research and main aims of the thesis

This thesis includes papers focused on petrological, mineralogical and geochemical study as well as on investigations of magnetic fabrics and structural field relations of the late- to post-Variscan potassic to ultrapotassic dykes (calc-alkaline lamprophyres and related rock-types) that represent a part of dyke swarms occurring together with the smaller bodies and several larger plutons of Mg-rich potassic rock in the western part of the Moldanubian Zone, and also intruding into granitiods of the Central Bohemian Plutonic Complex and metasediments of the eastern border of Teplá-Barrandian Block. Dykes are believed to be a good indicator of magmatic processes including generation of primary melt at mantle depths and its modification by fractionation and crustal contamination. In addition to petrology, the study of their magnetic fabrics and structural field relations allow to understand the mechanism of magma ascent within the dykes and its final emplacement.

Despite extensive and long-time study of the Bohemian Massif and the reconstruction of its Variscan evolution, many questions are still debated. For example, the recent main controversial topic is the kinematic character of Variscan subduction and position of individual lithotectonic units. As the Bohemian Massif is characterized by the biggest occurrence of lamprophyre dykes in the European Variscides, a detailed investigation of these dyke rocks can be helpful to the characterization of lithospheric mantle beneath the Variscan Orogen. Our research brings new knowledge at the field of investigation focused on evolution of the Bohemian Massif at the time of Variscan orogenesis. As the Bohemian Massif represents the biggest uncovered well-preserved part of the European Variscides it has a key role for understanding the tectonic evolution of the whole Variscan orogenic belt.

To trace the magmatic history of selected dyke rocks, a complex approach involving petrological, mineralogical and geochemical methods is applied in this thesis. Special attention is given to (*i*) the mineral textures witch can be used for the reconstruction of crystallization succession

of rock-forming minerals and allow us to distinguish the stages of mineral crystallization, and (*ii*) mineral chemistry and its zoning which permit to understand why and under what conditions these crystallization stages occur. In combination with (*iii*) whole-rock geochemistry it is possible to characterize the origin of melt and its subsequent evolving including fractional crystallization and crustal contamination. To understand the magma ascent and emplacement, (*iv*) the study of magnetic fabrics is very useful and together with (*v*) the structural field relations can be used to interpret the formation of dykes in relation to the regional stress field during the Variscan orogenesis. The last part of research include (*vi*) the ID-TIMS analyses of minerals in different rock-types that were used to the determine their ages and allow us to compare these ages with ages of the other Variscan dykes and discuss the timing of this type of magmatic activity in the Bohemian Massif and also discuss the existence of different magmatic pulses in relation to the time-period. The combination of above mentioned approaches was used to discuss the geodynamic significance of dyke rocks and allow us to reconstruct the succession of Variscan orogenic processes in the Moldanubian Zone and define a petrogenetic model including potassic magmatism. Also, a comparison of studied dykes with the potassium-rich syenite plutons in the Moldanubian Zone is included and their relationships are debated.

Three dyke rocks of *vaugnerite*, *syenite porphyry* and *olivine minette* were selected for detailed study of mineral textures and mineral chemistry. Moreover, the major and trace element bulk rock chemistry was analyzed in samples of *vaugnerite* and *syenite porphyry*. And also, these two dykes were used to determe the absolute age by U-Pb dating. In total 14 dykes of *minettes*, *spessartites*, *kersantites* and *syenite porphyries* were investigated by magnetic fabris. In addition, a *kersantite-spessartite composite dyke* was studied in more detail. Its magnetic fabrics were combined with mineral textures and completed by mineral chemistry and major element bulk rock chemistry.

References

Abdelfadil, Kh.M., Romer, R.L., Seifert, Th., Lobst, R., 2013. Calc-alkaline lamprophyres from Lusatia (Germany) - Evidence for a repeatedly enriched mantle source. Chemical Geology 353, 230–245.

Ackerman, L., Pašava, J., Erban, V., 2013. Re-Os geochemistry and geochronology of the Ransko gabbro-peridotite massif, Bohemian Massif. Mineralium Deposita 48, 799–804.

Awdankiewicz, M., 2007. Late Paleozoic lamprophyres and associated mafic subvolcanic rocks of the Sudetes (SW Poland): petrology, geochemistry and petrogenesis. Geologia Sudetica, 39, 11–97.

Awdankiewicz, M., 2010. Petrogenesis of the Late Paleozoic lamprophyres and related mafic rocks of the Sudetes, SW Poland. Mineralogia, Special Papers 37, 20–25.

Bailey E.B., Maufe, H.B., 1916. The geology of Ben Nevis and Glen Coe, and the surrounding country. Memoirs. Geological Survey of Scotland, Edinburgh, Sheet 53, 1–247.

Ballouard, C., Poujol, M., Boulvais, P., Zeh., A., 2017. Crustal recycling and juvenile addition during lithospheric wrenching: The Pontivy-Rostrenen magmatic complex, Armorican Massif (France), Variscan belt. Gondwana Research 49, 222–247.

Bea, F., P. Montero, and J. F. Molina (1999), Mafic precursors, peraluminous granitoids, and late lamprophyres in the Avila batholith: A model for the generation of Variscan batholiths in Iberia. Journal of Geology 107, 399–419.

Beard, A. D., Downes, H., Vetrin, V., Kempton, P. D., Maluski, H., 1996. Petrogenesis of Devonian lamprophyre and carbonatite minor intrusions, Kandalaksha Gulf (Kola Peninsula, Russia). Lithos 39, 93–119.

Bédard, J.H., 1994. Mesozoic east North American alkaline magmatism: Part 1. Evolution of Monteregian lamprophyres, Québec, Canada. Geochimica et Cosmochimica Acta 58, 95–112.

Caroff, M., Labry, C., Le Gall, B., Authemayou, Ch., Grosjean, D.B., Guillong, M., 2015. Petrogenesis of late-Variscan high-K alkali-calcic granitoids and calc-alkalic lamprophyres: The Aber-Ildut/North-Ouessant complex, Armorican Massif, France. Lithos 238, 140–155.

Chalapathi Rao, N.V., Dharma Rao, C.V., Das, S., 2012. Petrogenesis of lamprophyres from Chhota Udepur area, Narmada rift zone, and its relation to Deccan magmatism. Journal of Asian Earth Sciences 45, 24–39.

Chen, B., Zhai, M., 2003. Geochemistry of late Mesozoic lamprophyre dykes from the Taihang Mountains, north China, and implications for the sub-continental lithospheric mantle. Geological Magazine 140, 87–93.

Chlupáč, I., Havlíček, V., Kříž, J., Kukal, Z., Štorch, P., 1998. Paleozoic of the Barrandian (Cambrian to Devonian). Czech Geological Survey, Prague, 183 pp.

Conceição, R.V., Green, D.H., 2004. Derivation of potassic (shoshonitic) magmas by decompression melting of phlogopite + pargasite lherzolite. Lithos 72, 209–229.

Conticelli, S., Guarnieri, L., Farinelli, A., Mattei, M., Avanzinelli, R., Bianchini, G., Boari, E., Tommasini, S., Tiepolo, M., Prelević, D., Venturelli, G., 2009. Trace elements and Sr–Nd–Pb isotopes of K-rich, shoshonitic, and calc-alkaline magmatism of the Western Mediterranean Region: genesis of ultrapotassic to calc-alkaline magmatic associations in a post-collisional geodynamic setting. Lithos 107, 68–92.

Couzinié, S., Moyen, J.-F., Villaros, A., Paquette, J.-L., Scarrow, J.H., Marignac, C., 2014. Temporal relationships between Mg-K mafic magmatism and catastrophic melting of the Variscan crust in the southern part of Velay Complex (Massif Central, France). Journal of Geosciences 59 (1), 69–86.

Dias, R, Ribeiro, A, Romão, J., Coke, C., Moreira, N., 2016. A review of the arcuate structures in the Iberian Variscides; constraints and genetic models. Tectonophysics 681, 170–194.

Edel, J.B., 2001. The rotations of the Variscides during the Carboniferous collision: paleomagnetic constraints from the Vosges and the Massif Central (France). Tectonophysics 332, 69–92.

Edel, J.B., Schulmann, K., Holub, F.V., 2003. Anticlockwise and clockwise rotations of the Eastern Variscides accommodated by dextral lithospheric wrenching: palaeomagnetic and structural evidence. Journal of the Geological Society 160, 209–218.

Edel, J.B., Schulmann, K., Skrzypek, E., Cocherie, A., 2013. Tectonic evolution of the European Variscan belt constrained by palaeomagnetic, structural and anisotropy of magnetic susceptibility data from the Northern Vosges magmatic arc (eastern France). Journal of the Geological Society, London 170, 785–804.

Errandonea-Martin, J., Sarrionandia, F., Carracedo-Sánchez, M., Gil Ibarguchi, J.I., Eguíluz, L., 2018. Petrography and geochemistry of late- to post-Variscan vaugnerite series rocks and calc-alkaline lamprophyres within a cordierite-bearing monzogranite (the Sierra Bermeja Pluton, southern Iberian Massif). Geologica Acta 16, 237–255.

Faryad, S.W., Žák, J., 2016. High-pressure granulites of the Podolsko complex, Bohemian Massif: an example of crustal rocks that were subducted to mantle depths and survived a pervasivemid-crustal high-temperature overprint. Lithos 246–247, 246–260.

Faryad, S.W., Nahodilová, R., Dolejš, D., 2010. Incipient eclogite facies metamorphism in the Moldanubian granulites revealed by mineral inclusions in garnet. Lithos 114, 54–69.

Faryad, S.W., Kachlík, V., Sláma, J., Hoinkes, G., 2015. Implication of corona formation in a metatroctolite to the granulite facies overprint of HP-UHP rocks in the Moldanubian Zone (Bohemian Massif). Journal of Metamorphic Geology 33, 295–310.

Faryad, S.W., Kachlík, V., Sláma, J., Jedlicka, R., 2016. Coincidence of gabbro and granulite formation and their implication for Variscan HT metamorphism in the Moldanubian Zone (Bohemian Massif), example from the Kutná Hora Complex. Lithos 264, 56–69.

Faure, M., Li, X.-H., Lin, W., 2017. The northwest-directed ‘‘Bretonian phase’’ in the French Variscan Belt (Massif Central and Massif Armoricain): A consequence of the Early Carboniferous Gondwana–Laurussia collision. Comptes Rendus Geoscience 349, 126–136.

Fernández, R.D., Arenas, R., Pereira, M.F., Sánchez-Martínez, S., Albert, R., Parra, L.-M.M., Pascual, F.-J.R., Matas, J., 2016. Tectonic evolution of Variscan Iberia: Gondwana-Laurussia collision revisited. Earth-Science Reviews 162, 269–292.

Finger, F., Roberts, M.B., Haunschmid, B., Schermaier, A., Steyrer, H.B., 1997. Variscan granitoids of Central Europe: their typology, potential sources and tectonothermal relations. Mineralogy and Petrology 61, 67–96.

Finger, F., Gerdes, A., Janoušek, V., René, M., Riegler, G., 2007. Resolving the Variscan evolution of the Moldanubian sector of the Bohemian Massif: the significance of the Bavarian and the Moravo-Moldanubian tectonometamorphic phases. Journal of Geosciences 52 (1–2), 9–28.

Foley, S.F., 1992a. Petrological characterization of the source components of potassic magmas: geochemical and experimental constraints. Lithos 28, 187–204.

Foley, S.F., 1992b. Vein-plus-wall-rock melting mechanisms in the lithosphere and the origin of potassic alkaline magmas. Lithos 28, 435–453

Förster, M.W., Prelević, D., Schmück, H.R., Buhre, S., Veter, M., Mertz-Kraus, R., Foley, S.F., Jacob, D.E., 2017. Melting and dynamic metasomatism of mixed harzburgite + glimmerite mantle source: Implications for the genesis of orogenic potassic magmas. Chemical Geology 455, 182–191.

Fournet, J., 1861. Geologie lyonnaise. Lyon, 1, 744 pp.

Franke,W., 2006. The Variscan orogen in Central Europe: construction and collapse. Geological Society, London, Memoirs 32, 333–343.

Franke,W., 2000. The mid-European segment of the variscides: tectonostratigraphic units, terrane boundaries and plate tectonic evolution. In: Franke,W., Haak, V., Oncken, O., Tanner, D. (Eds.), Orogenic Processes: Quantification and Modelling in the Variscan Belt. Geological Society, London, Special Publication 179, pp. 35–61.

Franke, W., Dallmeyer, R.D., Weber, K., 1995. XI. Geodynamic evolution. In: Dallmeyer, R.D., Franke, W., Weber, K. (eds) Pre-Permian Geology of Central and Eastern Europe. Springer, Berlin, pp. 579–593.

Franke, W., Cocks, L.R.M., Torsvik, T. H., 2017. The Palaeozoic Variscan oceans revisited. Gondwana Research 48, 257–284.

Friedl, G., Finger, F., Paquette, J.L., von Quadt, A.,McNaughton, N.J., Fletcher, I.R., 2004. Pre-Variscan geological events in the Austrian part of the Bohemian Massif deduced from U-Pb zircon ages. International Journal of Earth Sciences 93, 802–823.

Fritschle, T., Prelević, D., Foley, S.F., Jacob, D.E., 2013. Petrological characterization of the mantle source of Mediterranean lamproites: Indications from major and trace elements of phlogopite. Chemical Geology 353, 267–279.

Garza, A.O., Dostal, J., Keppie, J.D., Paz-Moreno, F.A., 2013. Mid-Tertiary (25–21 Ma) lamprophyres in NW Mexico derived from subduction-modified subcontinental lithospheric mantle in an extensional backarc environment following steepening of the Benioff zone. Tectonophysics 590, 59–71.

Gerdes, A., Wörner, G., Finger, F., 2000. Hybrids, magma mixing and enriched mantle melts in post-collisional Variscan granitoids: the Rastenberg pluton, Austria. In: Franke W., Haak V., Oncken O., Tanner D. (eds) Orogenic Processes: Quantification and Modelling in the Variscan belt. Geological Society, London, Special Publication 179, 415–431.

Guo, F., Fan, W., Wang, Y., Zhang, M., 2004. Origin of early cretaceous calc-alkaline lamprophyres from the Sulu orogen in eastern China: implications for enrichment processes beneath continental collisional belt. Lithos 78, 291–305.

Guo, Z., Wilson, M., Liu, J., Mao, Q., 2006. Post-collisional, potassic and ultrapotassic magmatism of the northern Tibetan plateau: constraints on characteristics of the mantle source, geodynamic setting and uplift mechanisms. Journal of Petrology 47 (6), 1177–1220.

Gümbel, C.W., 1874. Die palaolithischen Eruptivgesteine des Fichtelgebirges. Weiss, Munich, 50 pp.

Hegner, E., Kölbl-Ebert, M., Loeschke, J., 1998. Post-collisional Variscan lamprophyres (Black Forest, Germany): $^{40}Ar/^{39}Ar$ phlogopite dating, Nd, Pb, Sr isotope, and trace element characteristics. Lithos 45, 395–411.

Hajná, J., Žák, J., Dörr, W., 2017. Time scales and mechanisms of growth of active margins of Gondwana: a model based on detrital zircon ages from the Neoproterozoic to Cambrian Blovice accretionary complex, Bohemian Massif. Gondwana Research 42, 63–83.

Holub, F.V., 1997. Ultrapotassic plutonic rocks of the durbachite series in the Bohemian Massif: petrology, geochemistry and petrogenetic interpretation. Journal of Geological Sciences - Economic Geology, Mineralogy 31, 5–26.

Holub, F.V., Cocherie, A., Rossi, P., 1997a. Radiometric dating of granitic rocks from the Central Bohemian Plutonic Complex (Czech Republic): constraints on the chronology of thermal and tectonic events along the Moldanubian-Barrandian boundary. Comptes Rendus de l'Académie des Sciences Paris 325, 19–26.

Holub, F.V., Machart, J., Manová, M., 1997b. The Central Bohemian Plutonic Complex: Geology, chemical composition and genetic interpretation. Sborník geologických věd, Ložisková geologie, mineralogie LG 31, 27–50.

Holub, F.V., Studená, M., Vosk, M., 2007. Dolerites and gabbro to diorite porphyries in the Central Bohemian Plutonic Complex (in Czech). Zprávy o geologických výzkumech v roce 2006, 127–129.

Holub, F.V., Verner, K., Schmitz, M.D., 2012. Temporal relations of melagranite porphyry dykes and durbachitic plutons in South Bohemia (in Czech). Zprávy o geologických výzkumech v roce 2011, Česká geologická služba, 23–25.

Holub, F.V., Verner, K., Studená, M., Orságová, L., 2009. Dyke swarms of ultrapotassic melasyenite to melagranite porphyries from the Central Bohemian Plutonic Complex and the Šumava part of the Moldanubicum (in Czech). Zprávy o geologických výzkumech v roce 2008, Česká geologická služba, 17–20.

Holub, F.V., 1999. Geochemistry and significance of dyke swarms in the Central Bohemian Plutonic Complex. Geolines 8, 28.

Holub, F.V., 2007. Dyke swarms in the area of the Central Bohemian Plutonic Complex: their matter variations and relationships to the plutonic rocks (in Czech). 3. sjezd České geologické společnosti, Volary.

Janoušek, V., Gerdes, A., 2003. Timing the magmatic activity within the Central Bohemian Pluton, Czech Republic: conventional U-Pb ages for the Sázava and Tábor intrusions and their geotectonic significance. Journal of the Czech Geological Society 48, 70–71.

Janoušek, V., Holub, F.V., 2007. The causal link between HP-HT metamorphism and ultrapotassic magmatism in collisional orogens: case study from the Moldanubian Zone of the Bohemian Massif. Proceedings of the Geologists Association 118, 75–86.

Janoušek, V., Brainthwaite, C.J.R., Bowes, D.R., Gerdes, A., 2004. Magma mixing in the genesis of Hercynian calc-alkaline granitoids: an integrated petrographic and geochemical study of the Sázava intrusion, Central Bohemian Pluton, Czech Republic. Lithos 78, 67–99.

Janoušek, V., Gerdes, A., Vrána, S., Finger, F., Erban, V., Friedl, G., Braithwaite, C.J.R., 2006. Low-pressure granulites of the Lišov massif, southern Bohemia: Viséan metamorphism of Late Devonian plutonic arc rocks. Journal of Petrology 47, 705–744.

Janoušek, V., Wiegand, B., Žák, J., 2010. Dating the onset of Variscan crustal exhumation in the core of the Bohemian Massif: new U-Pb single zircon ages from the high-K calc-alkaline granodiorites of the Blatná suite, Central Bohemian Plutonic Complex. Journal of the Geological Society, London 167, 347–360.

Janoušek, V., Holub, F.V., Gerdes, A., Verner, K., 2013. Two-pyroxene syenitoids from the Moldanubian Zone of the Bohemian Massif: peculiar magmas derived from a strongly enriched lithospheric mantle source. Geophysical Research Abstracts 15, EGU2013–11746.

Jastezębski, M., Żelaźniewicz, A., Murtezi, M., Larionov, A.N., Sergeev, S., 2015. The Moldanubian Thrust Zone - A terrane boundary in the Central European Variscides refined based on lithostratigraphy and U-Pb zircon geochronology. Lithos 220–223, 116–132.

Karsli, O., Dokuz, A., Kaliwoda, M., Uysal, I., Aydin, F., Kandemir, R., Fehr, K.T., 2014. Geochemical fingerprints of Late Triassic calc-alkaline lamprophyres fromthe Eastern Pontides, NE Turkey: a key to understanding lamprophyre formation in a subduction-related environment. Lithos 196, 181–197.

Kotková, J., Schaltegger, U., Leichmann, J., 2010. Two types of ultrapotassic plutonic rocks in the Bohemian Massif - Coeval intrusions at different crustal levels. Lithos 115, 163–176.

Košler, J., Konopásek, J., Sláma, J., Vrána, S., 2014. U-Pb zircon provenance of Moldanubian metasediments in the Bohemian Massif. Journal of Geological Society 171, 83–95.

Kovaříková, P., Siebel, W., Jelínek, E., Štemprok, M., Kachlík, V., Holub, F.V., Blecha, V., 2007. Petrology, geochemistry and zircon ages for redwitzite at Abertamy, NW Bohemian Massif (Czech Republic): tracing the mantle component in Late Variscan intrusions. Chemie der Erde 67, 151–174.

Krmíček, L., 2010. Pre-Mesozoic lamprophyres and lamproites of the Bohemian Massif (Czech Republic, Poland, Germany, Austria). Mineralogia, Special Papers 37, 37–46.

Krmíček, L., Romer, R.L., Ulrych, J., Glodny, J., Prelević, D., 2016. Petrogenesis of orogenic lamproites of the Bohemian Massif: Sr-Nd-Pb-Li isotope constraints for Variscan enrichment of ultra-depleted mantle domains. Gondwana Research 35, 198–2016.

Krmíček, L., Krmíčková, M., 2010. Recent view on a definition and classification of lamprophyres. Mineralogia, Special Papers 37, 47–48.

Krmíček, L., Halavínová, M., Romer, R.L., Vašinová Galiová, M., Vaculovič, T., 2014. Phlogopite/matrix, clinopyroxene/matrix and clinopyroxene/phlogopite trace element partitioning in a calc-alkaline lamprophyre: new constraints from the Křižanovice minette dyke (Bohemian Massif). Journal of Geosciences 59, 87–96.

Kroner, U., Romer, R.L., 2013. Two plates – many subduction zones: the Variscan orogeny reconsidered. Gondwana Research 24, 298–329.

Kröner, A., Wendt, I., Liew, T.C., Compston, W., Todt, W., Fiala, J., Vaňková, V., Vaněk, J., 1988. U-Pb zircon and Sm-Nd model ages of high-grade Moldanubian metasediments, Bohemian Massif, Czechoslovakia. Contributions to Mineralogy and Petrology 99, 257–266.

Kubínová, Š., Faryad, S.W., Verner, K., Schmitz, M., Holub, F., 2017. Ultrapotassic dykes in the Moldanubian Zone and their significance for understanding of the post-collisional mantle dynamics during Variscan orogeny in the Bohemian Massif. Lithos 272–273, 205–221.

Lardeaux, J.M., Schulmann, K., Faure, M., Janoušek, V., Lexa, O., Skrzypek, E., Edel, J.B., Štípská, P., 2014. The Moldanubian Zone in French Massif Central, Vosges/Schwarzwald and Bohemian Massif revisited: differences and similarities. In: Schulmann K., Martínez Catalán J.R., Lardeaux J.M., Janoušek V., Oggiano G. (eds) The Variscan Orogeny: Extent, Timescale and the Formation of the European Crust. Geological Society, London, Special Publications 405, 7 –44.

Le Bas, M. J., Streckeisen, A. L., 1991. The IUGS systematic of igneous rocks. Journal of the Geological Society 148, 825–833.

Leichmann, J., Gaweda, A., 2001. Klodsko-Zloty Stok and Niemcza Zone Granitoids - a shallow level intrusion of Durbachites in the Rhenohercynian Zone. Mitteilungen der Österr. Mineral. Gesellschaft, Wien 146, 169–170.

Le Maitre, R. W., Bateman, P., Dudek, A., Keller, J., Lameyre, M., Le Bas, M. J., Sabine, P. A., Schmid, R., Sϕrensen, H., Streckeisen, A., Woolley, A. R., Zanettin, B., 1989. A Classification of Igneous Rocks and a Glossary of Terms. Recommendations of the International Union of Geological Sciences Subcommission on the Systematics of Igneous Rocks. Blackwell Scientific Publications, Oxford, 193 pp.

Le Maitre, R.W., Streckeisen, A., Zanettin, B., Le Bas, M.J., Bonin, B., Bateman, P., Bellieni, G., Dudek, A., Efremova, S., Keller, J., Lameyre, J., Sabine, P.A., Schmid, R., Sørensen, H., Woolley, A.R., 2002. Igneous Rocks. A Classification and Glossary of Terms. Recommendations of the International Union of Geological Sciences Subcommission on the Systematics of Igneous Rocks, 2nd edn. Cambridge University Press, Cambridge, 236 pp.

Lu, Y.J., McCuaig, T.C., Xiang Li, Z., Journdan, F., Hart, C.J.R., Hou, Z.Q., Tang, S.H., 2015. Paleogene post-collisional lamprophyres in western Yunnan, western Yangtze Craton: mantle source and tectonic implications. Lithos 233, 139–161.

Ma, L., Jiang, S.Y., Hou, M.L., Dai, B.Z., Jiang, Y.H., Yang, T., Zhao, K.D., Pu, W., Zhu, Z.Y., Xu, B., 2014. Geochemistry of Early Cretaceous calc-alkaline lamprophyres in the Jiaodong Peninsula: implication for lithospheric evolution of the eastern North China Craton. Gondwana Research 25, 859–872.

Martin, A.M., Médard, E., Righter, K., Lanzirotti, A., 2017. Intraplate mantle oxidation by volatile-rich silicic magmas. Lithos 292–293, 320–333.

Mazur, S., Aleksandrowski, P., Turniak, K., Awdankiewicz, M., 2007. Geology, tectonic evolution and Late Palaeozoic magmatism of the Sudetes - an overview. In: Kozłowski A., Wiszniewska J. (eds) Granitoids in Poland. AM Monograph, KNM PAN-WG UW, Warszawa pp 59–87.

Medaris, L.G., Beard, B.L., Jelínek, E., 2006. Mantle-derived, UHP garnet pyroxenite and eclogite in the Moldanubian Gföhl Nappe, Bohemian Massif: a geochemical review, new P-T determinations, and tectonic interpretation. International Geology Review 48, 765–777.

Meshram, T.M., Shukla, D., Behera, K.K., 2015. Alkaline lamprophyre (camptonite) from Bayyaram area, NE margin of the Eastern Dharwar Craton, southern India. Current Science 109 (11), 1931–1934.

Mitchell, R. H., 1994. The lamprophyre facies. Mineralogy and Petrology 51, 137–146.

Moayyed, M., Moazzen, M., Calagari, A. A., Jahangri, A., Modjarrad, M., 2008. Geochemistry and petrogenesis of lamprophyric dykes and the associated rocks from Eslamy peninsula, NW Iran: Implications for deep-mantle metasomatism. Chemie der Erde 68, 141–154.

Montel J.M., 1988. First discovery of an orthopyroxene bearing vaugnerite: petrography, geochemistry, and implications on the genesis fo vaugnerites. Comptes Rendus de l'Académie des Sciences de Paris 306, 985–990.

Murphy, J.B., Quesada, C., Gutiérrez-Alonso, G., Johnston, S.T., Weil, A., 2016. Reconciling competing models for the tectono-stratigraphic zonation of the Variscan orogen in Western Europe. Tectonophysics 681, 209–219.

Nance, R.D., Gutiérrez-Alonso, G., Keppie, J.D., Linnemann, U., Murphy, J.B., Quesada, C., Strachan, R.A., Woodcock, N.H., 2010. Evolution of the Rheic Ocean. Gondwana Research 17, 194–222.

Nance, R.D., Gutiérrez-Alonso, G., Keppie, J.D., Linnemann, U., Murphy, J.B., Quesada, C., ., Strachan, R.A., Woodcock, N.H., 2012. A brief history of the Rheic Ocean. Geoscience Frontiers 3(2), 125–135.

Niggli, P., 1923. Gesteins- und Mineralprovinzen. Borntraeger, Berlin, 602 pp.

O'Leary,M.S., Lira, R., Dorais,M.J., Tassinari, C.C., 2009. Post-collisional lamprophyric event in Sierra Norte, Cordoba, Argentina: mineralogical, geochemical and isotopic characteristics. Journal of South American Earth Sciences 28, 277–287.

Orejana, D., Villaseca, C., Billström, K., Paterson, B.A., 2008. Petrogenesis of Permian alkaline lamprophyres and diabases from the Spanish Central System and their geodynamic context within western Europe. Contributions to Mineralogy and Petrology 156, 477–500.

Owen, J.P., 2008. Geochemistry of lamprophyres from the Western Alps, Italy: implications for the origin of an enriched isotopic component in the Italian mantle. Contributions to Mineralogy and Petrology 155, 341–362.

Pan, F.B., Jin, C., Jia, B.J., Liu, R., He, X., Gao, Z., Tao, L., Zhou, X.C., Zhang, L.Q., 2018. A late Mesozoic short-lived shift from fluid-dominated to sediment-dominated mantle metasomatism in the northeast South China Block and its tectonic implications. Lithos 310-311, 288–301.

Pandey, A., Chalapathi Rao, N.V., Pandit, D., Pankaj, P., Pandey, R., Sahoo, S., Kumar, A., 2017a. Subduction-tectonics in the evolution of the eastern Dharwar craton, southern India: Insights from the post-collisional calc-alkaline lamprophyres at the western margin of the Cuddapah basin. Precambrian Research 298, 235–251.

Pandey, A., Chalapathi Rao, N.V., Chakrabarti, R., Pandit, D., Pankaj, P., Kumar, A., Sahoo, S., 2017b. Petrogenesis of a Mesoproterozoic shoshonitic lamprophyre dyke from theWajrakarur kimberlite field, eastern Dharwar craton, southern India: Geochemical and Sr-Nd isotopic evidence for amodified sub-continental lithospheric mantle source. Lithos 292–293, 218–233.

Pandey, A., Chalapathi Rao, N.V., Chakrabarti, R., Pankaj, P., Pandit, D., Pandey, R., Sahoo, S., 2018. Post-collisional calc-alkaline lamprophyres from the Kadiri greenstone belt: Evidence for the Neoarchean convergence-related evolution of the Eastern Dharwar Craton and its schist belts. Lithos 320–321, 105–117.

Pivec, E., Holub, F.V., Lang, M., Novák, J.K., Štemprok, M., 2002. Rock-forming minerals of lamprophyres and associated mafic dykes from the Krušné hory/Erzgebirge (Czech Republic). Journal of the Czech Geological Society 47, 23–32.

Plá Cid, J., Rios, D. C., Conceição, H., 2006. Petrogenesis of mica-amphibole-bearing lamprophyres associated with the Paleoproterozoic Morro do Afonso syenite intrusion, eastern Brazil. Journal of South American Earth Sciences 22, 98–115.

Pouclet, A., Álvaro, J.J., Bardintzeff, J.-M., Imaz, A.G., Monceret, E., Vizcaïno, D., 2017. Cambrianeearly Ordovician volcanism across the South Armorican and Occitan domains of the Variscan Belt in France: Continental break-up and rifting of the northern Gondwana margin. Geoscience Frontiers 8, 25–64.

Prelevic, D., Foley, S.F., Cvetkovi, V., Romer, R.L., 2004. Origin of minette by mixing of lamproite and dacite magmas in Veliki Majdan, Serbia. Journal of Petrology 45, 759–792.

Rock, N. M. S., 1977. The nature and origin of lamprophyres: some definitions, distinctions, and derivations. Earth-Science Reviews, 13, 123–169.

Rock, N. M. S., 1984. Nature and origin of calc-alkaline lamprophyres: minettes, vogesites, kersantites and spessartites. Earth Sciences, 74, 193–227.

Rock, N.M.S., 1991. Lamprophyres. Blackie, London 225 pp.

Rosenbusch, H., 1887. Mikroskopische Physiographie der Mineralien und Gesteine. Band II, Massige Gesteine. Schweizerbartsche, Stuttgart, 877 pp.

Sabatier, H., 1980. Vaugnérites and granites, a peculiar association of basic and acid rocks. Bulletin de Minéralogie 103, 507–522.

Sabatier, H., 1991. Vaugnerites: special lamprophyre-derived mafic enclaves in some Hercynian granites from Western and Central Europe. In: Didier J., Barbarin B. (eds) Enclaves and Granite Petrology. Developments in Petrology, Amsterdam, Elsevier, 63–81.

Sauer, A., 1892. Der Granitit von Durbach im nordlichen Schwarzwalde und seine Grenzfacies von Glimmersyenit (Durbachite). Mittheilungen der Grossherzoglich Badischen Geologischen Landesanstalt Heidelberg 2, 231–276.

Scarrow, J.H., Bea, F., Montero, P., Molina, J.F., 2008. Shoshonites, vaugnerites and potassic lamprophyres: similaritites and differences between „ultra“-high-K rocks. Earth and Environmental Science Transactions of the Royal Society of Edinburg 99, 159–175.

Scarrow, J.H., Molina, J.F., Bea, F., Montero, P., Vaughan, A.P.M., 2011. Lamprophyre dikes as tectonic markers of late orogenic transtension timing and kinematics: a case study from the Central Iberian Zone. Tectonics 30 (TC4007), 1–22.

Schalterger, U., 1997. Magma pulses in the Central Variscan Belt: episodic melt generation and emplacement during lithospheric thinning. Terra Nova 9 (5/6), 242–245.

Schaltegger, U., 2000. U-Pb geochronology of the Southern Black Forest batholith (Central Variscan belt): timing of exhumation and granite emplacement. International Journal of Earth Sciences 88, 814–828.

Schaltegger, U., Schneider, J.L., Maurin, J.C., Corfu, F., 1996. Precise U-Pb Chronometry of 345-340 Ma old magmatism related to syn-convergence extension in the southern Vosges (Central Variscan Belt). Earth and Planetary Science Letters 144, 403–419.

Schulmann, K., Kröner, A., Hegner, E., Wendt, I., Konopásek, J., Lexa, O., Štípská, P., 2005. Chronological constraints on the pre-orogenic history, burial and exhumation of deep-seated rocks along the eastern margin of the Variscan orogen, Bohemian Massif, Czech Republic. American Journal of Science 305, 407–448.

Schulmann, K., Konopásek, J., Janoušek, V., Lexa, O., Lardeaux, J.-M., Edel, J.-B., Štípská, P., Ulrich, S., 2009. An Andean type Palaeozoic convergence in the Bohemian Massif. Comptes Rendu Geoscience 341, 266–286.

Schulmann, K., Martínez Catalán, J.R., Lardeaux, J.M., Janoušek, V., Oggiano, G., 2014. The Variscan Orogeny: Extent, Timescale and the Formation of the European Crust. Geological Society, London, Special Publications 405, 1–6.

Siebel, W., Chen, F., Satir, M., 2003. Late-Variscan magmatism revised: new implications from Pb-evaporation zircon ages on the emplacement of redwitzites and granites in NE Bavaria. International Journal of Earth Sciences 92, 36–53.

Stoppa, F., Rukhlov, A.S., Bell, K., Schiazza,M., Vichi, G., 2014. Lamprophyres of Italy: early Cretaceous alkaline lamprophyres of Southern Tuscany, Italy. Lithos 188, 97–112.

Streckeisen, A., 1979. Clasification and nomenclature of volcanic rocks, lamprophyres, carbonatites, and melilitic rocks: Recommendations and suggestions of the IUGS Subcommission on the systematice of igneous rocks. Geology, 7, 331–335.

Štemprok, M., Dolejš, D., Holub, F.V., 2014. Late Variscan calc-alkaline lamprophyres in the Krupka ore district, Eastern Krušné hory/Erzgebirge: their relationship to Sn-W mineralization. Journal of Geosciences 59, 41–68.

Štemprok, M., Seifert, T., Holub, F.V., Chlupáčová, M., Dolejš, D., Novák, J.K., Pivec, E., Lang, M., 2008. Petrology and geochemistry of Variscan dykes from the Jáchymov (Joachimsthal) ore district, Czech Republic. Journal of Geosciences 53, 65–104.

Su, H.M., Jiang, S.Y., Zhang, D.Y., Wu, X.K., 2017. Partial melting of subducted sediments produced early Mesozoic calc-alkaline lamprophyres from northern Guanxi Province, South China. Scientific Reports 7.

Tappe, S., Foley, S. F., Jenner, G. A., Kjarsgaard, B. A., 2005. Integrating ultramafic lamprophyres into the IUGS classification of Igneous rocks: Rationale and implications. Journal of Petrology, 46 (9), 1893–1900.

Tappe, S., Foley, S.F., Jenner, G.A., Heaman, L.M., Kjarsgaard, B.A., Romer, R.L., Stracke, A., Joyce, N., Hoefs, J., 2006. Genesis of ultramafic lamprophyres and carbonatites at Aillik Bay, Labrador: a consequence of incipient lithospheric thinning beneath the North Atlantic craton. Journal of Petrology 47, 1261–1315.

Tappe, S., Foley, S.F., Kjarsgaard, B.A., Romer, R.L., Heaman, L.M., Stracke, A., Jenner, G.A., 2008. Between carbonatite and lamproite - diamondiferous Torngat ultramafic lamprophyres formed by carbonate-fluxed melting of cratonic MARID-type metasomes. Geochimica et Cosmochimica Acta 72, 3258–3286.

Tappe, S., Jenner, G. A., Foley, S. F., Heaman, L., Besserer, D., Kjarsgaard, B. A., Ryan, B., 2004. Torngat ultramafic lamprophyres and their relation to the North Atlantic Alkaline Province. Lithos 76, 491–518.

Tait, J.A., Bachtadse, V., Franke, W., Soffel, H.C., 1997. Geodynamic evolution of the European Variscan fold belt: palaeomagnetic and geological constraints. Geologische Rundschau 86, 585–598.

Thompson, R.N., Leat, P.T., Dickin, A.P., Morrison, M.A., Hendry, G.L., Gibson, S.A., 1990. Strongly potassic mafic magmas from lithospheric mantle source during continental extension and heating: evidence from Miocene minettes of northwest Colorado, U.S.A. Earth and Planetary Science Letters 98, 139–154.

Ubide, T., Galé, C., Arranz, E., Lago, M., Larrea, P., 2014. Clinopyroxene and amphibole crystal populations in a lamprophyre sill from the Catalonian Coastal Ranges (NE Spain): a record of magma history and a window to mineral-melt partitioning. Lithos 184-187, 225–242.

Vaughan, A.P.M., Scarrow, J.H., 2003. K-rich mantle metasomatism control of localization and initiation of lithospheric strike-slip faulting. Terra Nova 15, 163–169.

Verner, K., Žák, J., Nahodilová, R., Holub, F., 2008. Magmatic fabrics and emplacement of the cone-sheet-bearing Knížecí Stolec durbachitic pluton (Moldanubian Unit, Bohemian Massif): implications for mid-crustal reworking of granulitic lower crust in the Central European Variscides. International Journal of Earth Sciences 97, 19–33.

von Raumer, J.F., Stampfli, G.M., Bussy, F., 2003. Gondwana-derived microcontinents - the constituents of the Variscan and Alpine collisional orogens. Tectonophysics 365, 7–22.

von Raumer, J.F., Finger, F., Veselá, P., Stampfli, G.M., 2014. Durbachites-vaugnerites - a geodynamic marker in the central European Variscan orogen. Terra Nova 26, 85–95.

Wendt, J.I., Kröner, A., Fiala, J., Todt,W., 1993. Evidence from zircon dating for existence of approximately 2.1 Ga old crystalline basement in southern Bohemia, Czech Republic. Geologische Rundschau 82, 42–50.

Wenzel, Th., Mertz, D.F., Oberhänsli, R., Becker, T., Renne, P.R., 1997. Age, geodynamic setting, and mantle enrichment processes of a K-rich intrusion from the Meissen massif (northern Bohemian massif) and implications for related occurrences from the mid-European Hercynian. Geologische Rundschau 86, 556–570.

Wenzel, T., Oberhänsli, R., Mezger, K., 2000. K-rich plutonic rocks and lamprophyres from the Meissen Massif (northern Bohemian Massif): geochemical evidence for variability enriched lithospheric mantle sources. Neues Jahrbuch für Mineralogie - Abhandlungen 175(3), 249–293.

Willmann, K., 1919. Die Redwitzite, eine neue Gruppe von granitischen Lamprophyren. Zeitschrift der Deutschen Geologischen Gesellschaft, Berlin 71, 1–33.

Winchester, J.A., Pharaoh, T.C., Verniers, J., 2002. Paleozoic amalgamation of the Central Europe: an introduction and synthesis of new results from recent geological and geophysical investigations. Geological Society, London, Special Publications 201, 1–18.

Woodard, J., Kietäväinen, R., Eklund, O., 2014. Svecofennian post-collisional shoshonitic lamprophyres at the margin of the Karelia Craton: Implications for mantle metasomatism. Lithos 205, 379–393.

Woolley, A. R., Bergman, S. C., Edgar, A. D., Le Bas, M. J., Mitchell, R. H., Rock, N. M. S., Scott Smith, B. H., 1996. Clasification of lamprophyres, lamproites, kimberlites, and the kalsilic, melilitic and leucitic rocks. The Canadian Mineralogist 34, 175–186.

Xu, X., Zhang, B., Qin, K., Mao, Q., Cai, X., 2007. Origin of lamprophyres by the mixing of basic and alkaline melts in magma chamber in Beiya area, western Yunnan, China. Lithos 99, 339–362.

Žák, J., Verner, K., Finger, F., Faryad, S.W., Chlupáčová,M., Veselovský, F., 2011. The generation of voluminous S-type granites in the Moldanubian unit, Bohemian Massif, by rapid isothermal exhumation of the metapelitic middle crust. Lithos 121, 25–40.

Žák, J., Verner, K., Janoušek, V., Holub, F.V., Kachlík, V., Finger, F., Hajná, J., Tomek, F., Vondrovic, L., Trubač, J., 2014. A plate-kinematic model for the assembly of the Bohemian Massif constrained by structural relations around granitoid plutons. Geological Society, Special Publications 405, 169–196.

Zeitlhofer, H., Grasemann, B., Petrakakis, K., 2016. Variscan potassic dyke magmatism of durbachitic affinity at the southern end of the Bohemian Massif (Lower Austria). International Journal of Earth Sciences 105, 1175–1197.

CHAPTER 2

ULTRAPOTASSIC DYKES IN THE MOLDANUBIAN ZONE AND THEIR SIGNIFICANCE FOR UNDERSTANDING OF THE POST-COLLISIONAL MANTLE DYNAMICS DURING VARISCAN OROGENY IN THE BOHEMIAN MASSIF

Šárka Kubínová [a], Shah Wali Faryad [a], Kryštof Verner [a], Mark Schmitz [b], František Holub [a]

[a] *Institute of Petrology and Structural Geology, Charles University, Albertov 6, Prague 12843, Czech Republic*

[b] *Boise State University, 1910 University Drive, Boise, USA*

Status: Published in Lithos (2017)

ABSTRACT

We report mineral textures, geochemistry and age relations of two ultrapotassic dykes from a dyke swarm in the Western part of the Moldanubian Zone at contact to the Teplá-Barrandian Block. The dykes have orientation almost perpendicular to the NNE-SSW trending of the Central Bohemian Plutonic Complex and cross cut metamorphic foliation in basement gneisses and migmatites. Based on mineral compositions and geochemistry, the dykes show close relations to Mg-K syenite plutons in theMoldanubian Zone. The two dykes are vaugnerite and syenite in compositions and contain talc pseudomorphs after olivine within a fine-grained matrix that consists of K-feldspar, phlogopite, small amount of clinopyroxene and accessory quartz, apatite, titanite and sulphides of Fe, Cu, Ni. The syenite porphyry dyke cross cuts the vaugnerite. It contains quartz phenocrysts and comparing to vaugnerite has lower modal content of talc pseudomorphs.

The vaugnerite and syenite porphyry have high K_2O (6 to 7 wt.%) and mg-number (0.66–0.74), but low CaO and Na_2O contents. The vaugnerite is markedly rich in P_2O_5 (> 2 wt.%) and comparing to syenite porphyry has higher amount of mantle-incompatible elements (e.g. Rb, Cs, Ba, Pb, Th, U), V and Cr. ID-TIMS analyses on titanite in vaugnerite and on zircon in syenite porphyry yielded 338.59±0.68 and 337.87±0.21 Ma, respectively. Mineral and bulk rock chemistry of the dykes indicates that the source magma was formed by a low degree of partial melting of a highly anomalous domain in the upper mantle which subsequently fractionated and was contaminated with crustal material during its ascent. Formation of ultrapotassic magma is explained by transcurrent

shear zones in the mantle lithosphere that occurred due to block rotation and post-collisional mantle dynamics initiated by slab break-off and asthenosphere upwelling into the Moldanubian accretionary complex during the Variscan Orogeny.

***Keywords**: dyke swarm, ultrapotassic magmatism, Variscan orogeny, Bohemian Massif*

2.1 Introduction

The Moldanubian Zone of the Bohemian Massif (Fig. 1) is known for the presence of (ultra)-potassic igneous rocks that form plutons of Mg-K syenite (durbachite) and dykes of vaugnerite, minette, syenite porphyry, kersantite, lamproites (Holub, 1997; Krmíček et al., 2011). This K-rich magmatism is considered as an indicator of evolving mantle dynamics that occurred along the European Variscan orogenic belt (Fig. 1a, Abdelfadil et al., 2014; Couzinié et al., 2014; Finger et al., 2007; Gerdes et al., 2003; Janoušek and Holub, 2007; Krmíček et al., 2016; Štemprok et al., 2014; von Raumer et al., 2013; Zeitlhofer et al., 2016). In the Moldanubian Zone of the Bohemian Massif, the (ultra)-potassic rocks occur mostly along two NNE-SSW-orientated belts (Fig. 1b) and the origin of their formation is the subject of controversy. According to Janoušek and Holub (2007), the ultrapotassic magma derived from anomalous mantle sources contaminated by crustal material and their formation was related to subduction of the Saxothuringian plate beneath the Teplá-Barrandian Block (the Teplá suture in Fig. 1a) and it was coeval with the granulite facies metamorphism in the Moldanubian Zone (Schulmann et al., 2014). Relations of lamproites dykes and ultrapotassic plutons in theMoldanubian Zone to the subduction of Rhenohercynian oceanic basin (Rhenohercynian suture in Fig. 1a) are assumed by Kroner and Romer (2013) and Krmíček et al. (2016). According to von Raumer et al. (2014), the ultrapotassic rocks along the whole Variscan Orogeny (Eastern Alps, Alpine External Massifs with those of Corsica, the French Massif Central, Black Forest, Vosges and the Bohemian Massif, Fig. 1a) were created by slab windows and/or the sinking of the subducted Rhenohecynian slab into the mantle. Available geochronological dating shows wide range of ages of this magmatism that includes ages of 293–343 Ma from the Bohemian Massif (Holub et al., 1997; Kusiak et al., 2010; Verner et al., 2008; von Seckendorf et al., 2004), 305 Ma from vaugnerite in the French Central Massif (Couzinié et al., 2014) and 265 Ma from lamprophyre in the Central Iberian Zone (Scarrow et al., 2011). Based on recent results of petrological study (Faryad et al., 2013, 2015), the main processes of metamorphism and formation of igneous rocks in the Moldanubian Zone were operated by subduction and subsequent collision of the Moldanubian plate beneath the Teplá-Barrandian Block (the Moldanubian suture in Fig. 1a).

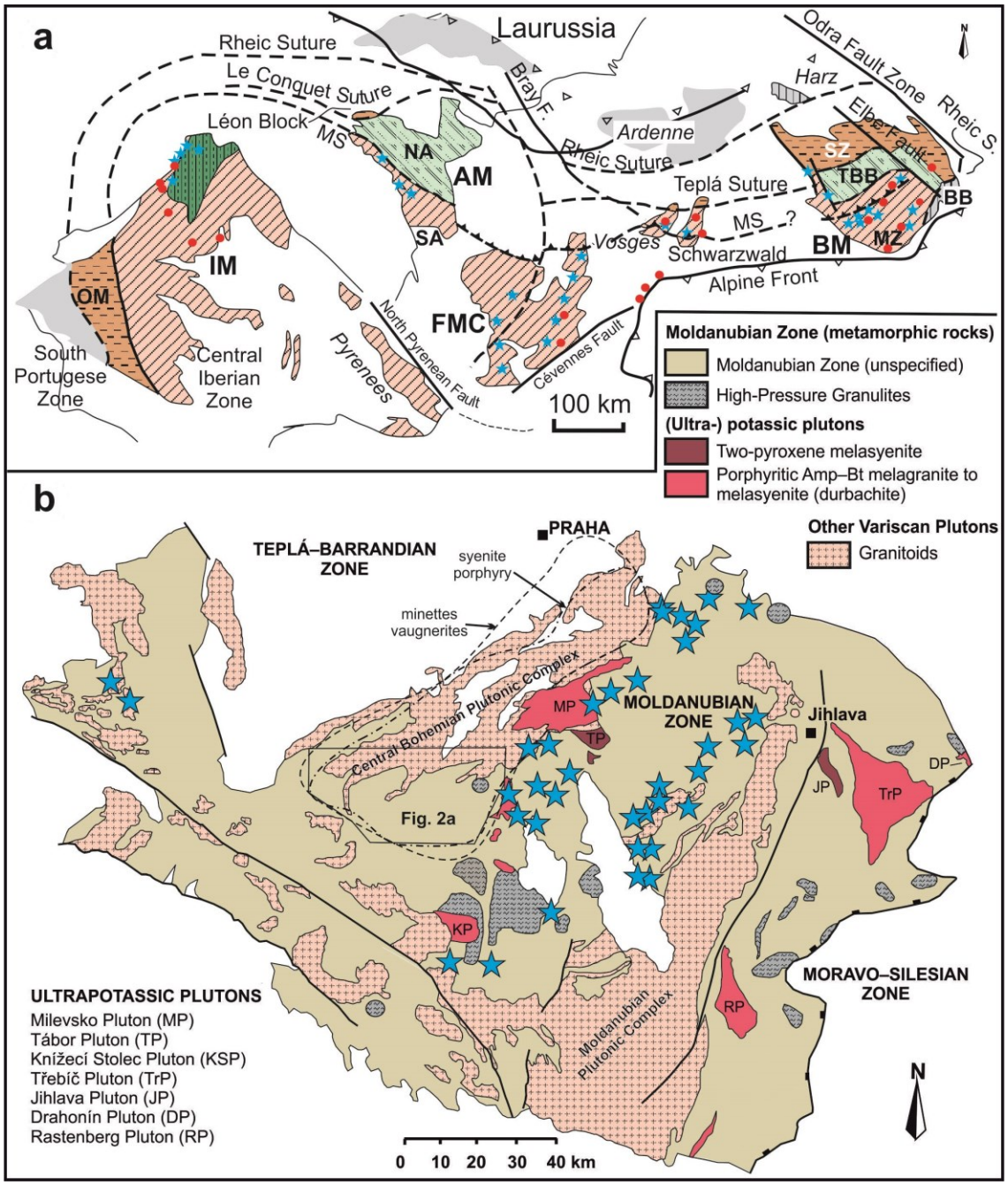

Fig. 1 a) Position of the pre-Carboniferous Moldanubian type allochthonous units along the European Variscan Belt with presumed Moldanubian suture (Faryad et al., 2013; Franke, 2000). The red circles are occurrences of ultrapotassic magmatic rocks (after von Raumer et al., 2014) and the blue stars indicate distribution of HP-UHP rocks (Faryad and Kachlík, 2013). Basement units: AM = Armorican Massif, BB = Brunovistulian Block, BM = Bohemian Massif, FMC = French Massif Central, IM = Iberian Massif, MZ = Moldanubian Zone, NA = North Armorica, OM = Ossa-Morena Zone, SA = South Armorica, SZ = Saxothuringian Zone, MS = Moldanubian suture, b) Moldanubian Zone in the Bohemian Massif with Variscan granitoid plutons and ultrapotassic plutons. The dashed and dot-dashed lines delineate the occurrences of dykes of minettes-vaugnerite and syenite porphyry, respectively (for detail see Fig. 2a). Stars indicate distribution of retrogressed eclogite from the amphibolite facies Monotonous and Varied units.

In this work, we present detailed petrology, geochemistry and age data of two dykes of vaugnerite and syenite porphyry that occur within migmatized gneisses of the Monotonous unit in the Moldanubian Zone. Field relations show that the vaugnerite dyke is relatively older than the syenite porphyry but both cross cut the older granite apophyses which follow metamorphic fabrics in the gneisses and are parallel to the SSW-NNE directed Central Bohemian Plutonic Complex (Fig. 1b). By combination of mineral textures and compositional variations in minerals and bulk rock chemistry we attempt to clarify the origin and source of the ultrapotassic magma and analyse subsequent processes of its fractionation and assimilation with crustal material during magma ascendance. The results of this work are used to discuss the relations of ultrapotassic magmatism to mantle dynamics during post-subduction history and granulite facies metamorphism in the Moldanubian Zone.

2.2 Geological setting

The Bohemian Massif, representing the easternmost segment of the European Variscides, is formed by two crustal blocks (the Brunovistulian and the Teplá-Barrandian, Fig. 1) and two zones (the Moldanubian and the Saxothuringian) with various rocks affected by degrees of metamorphism and deformation. The Saxothuringian Zone occupies the northern part of the Bohemian Massif, while the Moldanubian Zone is located in the southern part of the Bohemian Massif between the Teplá-Barrandian Block in the north-west and the Brunovistulian Block in the east (Fig. 1). The Moldanubian Zone is formed by medium-grade (the Monotonous and Varied units) and high-grade (the Gföhl Unit) metamorphic rocks with Paleoproterozoic to Devonian protolith ages (Friedl et al., 2004; Janoušek et al., 2006; Košler et al., 2014; Kröner et al., 1988; Schulmann et al., 2005; Wendt et al., 1993) that are intruded by numerous bodies of Variscan granitoids. In general, the overall structure of the Moldanubian Zone is the result of stacking of several lithotectonic units at ~360 to 345 Ma followed by HT-LP metamorphism, anatexis and late-Variscan wrench tectonics (for review see Schulmann et al., 2009; Žák et al., 2014; Faryad and Žák, 2016).

In the Moldanubian Zone, magmatic rocks of Variscan age can be classified into four groups. The first two groups are represented by granitoid complexes that are exposed along two belts, the Central Bohemian Plutonic Complex (CBPC) and the Moldanubian Plutonic Complex (MPC) (Fig. 1b). These two complexes differ from each other by age and their relations to Variscan geotectonic processes (e.g. Finger et al., 1997; Holub et al., 1995; Schalterger, 1997; Žák et al., 2014). The older (c. 355–345 Ma) CBPC straddles the border of the Teplá-Barrandian Block and is formed by subduction related calc-alkaline granitoid plutons (Janoušek et al., 2006; Žák et al., 2014). The younger MPC is composed of peraluminous (S-type) anatectic granitoids (c. 330–300 Ma) and it was formed by extensive migmatitization and isothermal decompression of the surrounding pelitic rocks

(Žák et al., 2011). The third group is represented by potassic-ultrapotassic rocks (346–337 Ma) that form several isolated plutons (Fig. 1b) and dyke swarms (Holub et al., 1997; Janoušek and Gerdes, 2003; Janoušek et al., 2010). The last group of Variscan igneous rocks has mafic and ultramafic composition (gabbro, norite, trocolite, pyroxenite) and around 340 Ma age (Ackerman et al., 2013; Faryad et al., 2015, 2016). Some of the mafic-ultramafic rocks are unmetamorphosed, but others record amphibolite-granulite facies conditions and therefore were assumed to be pre-Variscan in age.

The (ultra)-potassic rocks form larger plutons (the two Mg-K syenite plutons the Třebíč and the Milevsko pluton occupy c. 500 and 220 km^2, respectively), smaller bodies and dyke swarms. The dykes have composition of spessartite, gabbrodiorite, minette, vaugnerite (the name used for high-potassic rocks in the French Massif Central by Sabatier, 1980), kersantite, melasyenite and melagranite. In the western part of the Moldanubian Zone, they are distributed over about 30 × 100 km area that mostly covers the CBPC (Fig. 1b). The dykes have orientation almost E-W and intrude not only the basement rocks, but also granitic rocks of the CBPC. They have thickness of ~ 25 m for melagranite to melasyenite porphyries and about 3 m for minettes and vaugnerites. The vaugnerite and syenite porphyry dykes selected for this study occur within migmatized paragneisses at Nihošovice (Fig. 2). The paragneisses consist of quartz, feldspar and biotite, and rarely sillimanite, garnet and cordierite for which temperatures of 630–720 °C at 0.4 GPa are estimated (Vrána et al., 1995). Two superimposed metamorphic foliations can be defined in the paragneisses. The earlier, steeply to moderately dipping foliation (compositional banding) has a regional NNE-SSW strike. This foliation was heterogeneously reworked into flat-lying or gently to NW dipping schistosity with well-developed N-S mineral or stretching lineations. Several sheets of leucogranite are present in the migmatites and paragneisses. They are mostly parallel to the regional metamorphic foliation and originated by melt segregated from the host migmatites. Both these foliations are discordantly truncated by sharp intrusive contacts with the WNW-ESE directed syenite porphyry dyke and also by the vaugnerite dyke (Fig. 2b). The intrusive contacts of vaugnerite with the country rocks are sharp, dipping steeply to the south. The syenite porphyry has discordant intrusive contacts to the vaugnerite and therefore, the syenite porphyry intrusion must be relatively younger. The light grey syenite porphyry usually contains melanocratic enclaves (up to 10 × 10 cm in size). Both dykes reveal chilled margins represented by very fine-grained matrix.

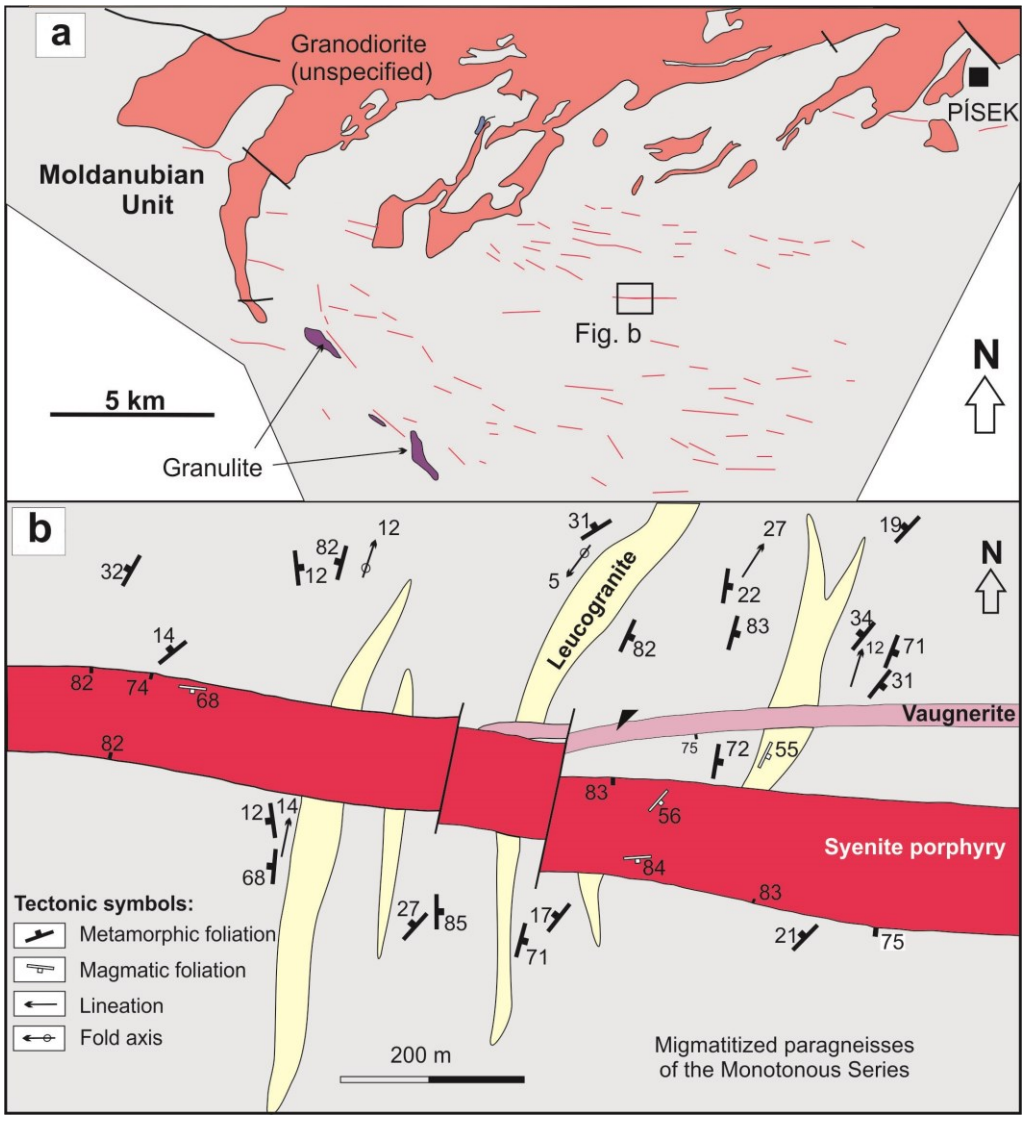

Fig. 2. (a) Distribution of the vaugnerite-minette and syenite porphyry dykes in the western sector of the Moldanubian Zone of the Bohemian Massif. (b) detail of the vaugnerite and syenite porphyry dykes, cross cutting the migmatised paragneisses with leucogranite apophyses.

2.3 Analytical methods

Chemical analyses were obtained with the JEOL JXA-8530F microprobe equipped with wavelength- and energy-dispersive spectrometers (WDS and EDS) at the Department of Petrology and Structural Geology, Charles University in Prague. The operating conditions were 15 kV and 30 nA beam current for spot analyses and 20 kV and 120 nA for element mappings. Standards were quartz (Si), corundum (Al), periclase (Mg), magnetite (Fe), rhodonite (Mn), calcite (Ca), rutile (Ti), chromium oxide (Cr), vanadinite (V), albite (Na), sanidine (K), apatite (P, F). Representative analyses of selected minerals are given in Table 1. Mineral abbreviations are: ab = albite, am =

amphibole, bt = biotite, cpx = clinopyroxene, fo = forsterite, ksp = K-feldspar, s = serpentine, tc= talc.

Major- and trace-element for the whole rock analyses were carried out at the Activation Laboratories Ltd. (Ontario, Canada) according to Code 4Litho package following lithium metaborate/tetraborate fusion and inductively coupled plasma-mass spectrometry (ICP-MS); loss on ignition (LOI) was measured according to standard gravitative method (www.actlabs.com).

U-Pb isotope dilution analyses of zircon and titanite were performed at Boise State University. All titanite crystal fragments were cleaned in ethanol under high-energy ultrasonic agitation, then fluxed in dilute HNO_3 for 30 min prior to rinsing and dissolution. Zircon was subjected to a modified version of the chemical abrasion method of Mattinson (2005), reflecting a preference to prepare and analyse carefully selected single crystals. Zircon crystals selected on the basis of clarity and morphology were annealed in quartz crucibles in a muffle furnace at 900 °C for 60 h, chemically abraded (Mattinson, 2005) using a single abrasion step in concentrated HF at 180 °C for 12 h. All samples were spiked with an enriched ^{205}Pb-^{233}U-^{235}U tracer (BSU-1B calibrated against EARTHTIME gravimetric standards), and dissolved in concentrated HF at 220 °C for 48 h in PFA fluoropolymer capsules nested within PTFE fluoropolymer-lined high-pressure steel dissolution vessels. After dissolution, drying to salts, and reequilibration in 6 M HCl at 180 °C for 12 h, the Pb and U were separated from the solutions using dilute HBr and HCl-based anion exchange chromatography. Isotope ratio analyses were performed on purified Pb and U aliquots dried with a silica gel emitter on single Re filaments, using an IsotopX Phoenix X62 thermal ionization mass spectrometer (TIMS), through a combination of single collector ion-counting (Pb^+) and static multicollector Faraday cup (UO_2^+) measurement modes. Further details of ID-TIMS analysis are described by Davydov et al. (2010) and Schmitz and Davydov (2012).

U-Pb dates and uncertainties for each analysis were calculated from the measured ratios using the algorithms of Schmitz and Schoene (2007) and the U decay constants of Jaffey et al. (1971). Analytical uncertainties were propagated from non-systematic errors, including counting statistics, instrumental fractionation, tracer subtraction, and blank subtraction. These error estimates should be considered when comparing our $^{206}Pb/^{238}U$ dates with isotope dilution analyses from other laboratories that used tracer solutions calibrated against the EARTHTIME gravimetric standards. When comparing our dates with those derived from other decay schemes (e.g., $^{40}Ar/^{39}Ar$, ^{187}Re-^{187}Os), the uncertainties in tracer calibration (0.03 %; Condon et al., 2015; McLean et al., 2015) and U decay constants (0.108 %; Jaffey et al., 1971) should be added to the analytical error in quadrature. Quoted errors for calculated weighted mean U-Pb dates are thus of the form ± X(Y)[Z], where X is solely analytical uncertainty, Y is the combined analytical and tracer uncertainty, and Z is the combined analytical, tracer and ^{238}U decay constant uncertainty.

2.4 Petrology and mineral chemistry

The vaugnerite and syenite porphyry were sampled across the dyke from center to contact with the host rock. In total, 4 samples of vaugnerite, 5 samples of syenite porphyry and two enclaves in the syenite porphyry were taken for detailed study.

2.4.1 Vaugnerite

The vaugnerite is mostly fine-grained with pseudomorphs of talc (phenocrysts of former olivine up to 1.2 mm in size, Fig. 3) and phenocrysts of clinopyroxene (with length of 1.5 mm) and biotite. Clinopyroxene is mostly replaced by amphibole. The matrix is formed by biotite, feldspar, amphibole, calcite, quartz and apatite. Some apatite grains may reach length of 0.5 mm. Accessory amounts of titanite and opaque mineral are also present.

2.4.1.1. Pseudomorphs after olivine

More than 30 % modal amounts of pseudomorphs are present in the rocks. They are represented by two or more zones. The central part of the pseudomorphs is mostly represented by talc which in some pseudomorphs have optical orientation in one direction, suggesting topotactic replacement after a former single crystal. In the mantle part of some pseudomorphs, talc with calcite can be observed. The outermost zone is formed by biotite, but small amounts of tremolite can also be present. As no relic of precursor phase was found in the pseudomorphs, their formation from olivine instead of magnesite or orthopyroxene is favoured by their pyramidal shapes (Fig. 3a, b) and by high Ni content in talc (Table 1). In addition, minor amounts of Ni sulphide are also present in or around the pseudomorphs.

Table 1 Selected microprobe analyses of minerals from vaugnerite and syenite porphyry

Sample	SK8		SK4				LR782-1	SK4	LR783
Rock	Vaugnerite		Syenite porphyry				Vaugn.	Syen. p	Syen. p.
Mineral	Biotite						Pyroxene		Amphib.
Position	t	t	t-r	In cpx	In cpx	In ps	t-c	t-c	m
SiO_2	40.28	39.61	41.25	38.55	37.54	38.22	54.10	54.46	51.68
TiO_2	3.05	3.59	1.44	2.91	5.38	5.29	0.16	0.14	0.55
Al_2O_3	12.22	11.98	11.97	13.72	13.78	13.57	0.40	0.58	3.44
Cr_2O_3	0.52	0.16	0.39	0.23	0.79	0.68	0.03	0.59	0.00
FeO	6.07	9.10	5.75	12.29	9.81	7.25	6.30	4.30	10.61
MnO	0.00	0.00	0.00	0.00	0.07	0.00	0.22	0.14	0.35
MgO	21.78	19.23	22.92	16.50	16.33	19.27	17.08	17.94	16.35
CaO	0.00	0.00	0.07	0.25	0.08	0.08	21.49	21.84	11.22
Na_2O	0.08	0.08	0.05	0.11	0.00	0.08	0.14	0.21	0.68
K_2O	10.05	9.99	9.77	9.41	9.83	9.92	0.00	0.00	0.30
BaO	0.29	0.33	0.30	0.29	0.88	1.02	0.00	0.00	0.00
F	0.50	0.39	0.86	0.61	0.34	0.60	0.00	0.00	0.00
Total	94.84	94.47	94.77	94.90	94.85	95.97	99.91	100.20	95.18
Si	2.983	2.993	3.042	2.949	2.887	2.863	1.988	1.981	7.491
Ti	0.170	0.204	0.080	0.168	0.311	0.298	0.004	0.004	0.060
Al	1.067	1.067	1.040	1.238	1.249	1.198	0.017	0.025	0.587
Cr	0.030	0.009	0.023	0.014	0.048	0.040	0.001	0.017	0.578
Fe^{3+}	0.000	0.000	0.000	0.000	0.000	0.000	0.009	0.004	0.578
Fe^{2+}	0.376	0.575	0.354	0.786	0.631	0.454	0.184	0.127	0.708
Mn	0.000	0.000	0.000	0.000	0.005	0.000	0.007	0.004	0.043
Mg	2.405	2.167	2.520	1.882	1.872	2.151	0.936	0.973	3.533
Ca	0.000	0.000	0.006	0.020	0.006	0.006	0.846	0.851	1.742
Na	0.011	0.012	0.007	0.017	0.000	0.011	0.010	0.015	0.192
K	0.950	0.963	0.919	0.918	0.964	0.948	0.000	0.000	0.055
Ba	0.009	0.010	0.009	0.009	0.027	0.030	0.000	0.000	0.000
F	0.117	0.093	0.201	0.148	0.083	0.142	0.000	0.000	0.000
X_{Mg}	0.86	0.79	0.88	0.71	0.75	0.83	0.84	0.88	0.83

t - tabular grain in the matrix, cpx - clinopyroxene, ps - pseudomorph, c - core, r - rim, m - matrix

Table 1 continued

Sample	SK8	SK4		SK8	SK8	LR782-1	Sample	SK8	LR783
Rock	Vaugn.	Syenite porph.		Vaugnerite				Vaugn.	Syen. p
Mineral	K-feldspar			Talc	Spinel			Apatite	
Position	m	c	r	ps	m	ps			m
SiO_2	64.73	64.37	64.25	61.33	0.23	0.88	CaO	52.83	53.31
TiO_2	0.00	0.00	0.00	0.00	0.96	1.35	SrO	1.16	1.06
Al_2O_3	18.17	19.35	18.93	0.25	3.64	3.95	FeO	0.37	0.25
Cr_2O_3	0.00	0.00	0.00	0.00	61.27	56.95	MgO	0.51	0.00
FeO	0.00	0.00	0.00	2.10	29.16	31.15	Ce_2O_3	0.00	0.32
MnO	0.00	0.00	0.00	0.00	2.01	1.48	P_2O_5	42.32	42.51
NiO	0.00	0.00	0.00	0.38	0.00	0.00	SiO_2	0.63	0.62
MgO	0.00	0.00	0.00	28.67	0.81	1.04	Cl	0.08	0.00
CaO	0.00	0.31	0.42	0.05	0.00	0.00	F	3.78	3.86
Na_2O	0.20	2.38	2.46	0.00	0.00	0.00	Total	101.6	101.92
K_2O	16.63	12.47	12.69	0.04	0.00	0.00	O=F,Cl	1.610	1.624
BaO	0.48	2.08	0.73	0.00	0.00	0.00	Total	100.0	100.301
V_2O_5	0.00	0.00	0.00	0.00	0.33	0.61			
ZnO	0.00	0.00	0.00	0.00	1.51	2.60	Ca	9.117	9.187
Total	100.2	100.96	99.48	92.81	99.91	100.01	Sr	0.108	0.099
							Fe	0.050	0.033
Si	3.004	2.980	2.975	3.992	0.008	0.032	Mg	0.122	0.000
Ti	0.000	0.000	0.000	0.019	0.026	0.037	Ce	0.000	0.019
Al	0.994	1.056	1.033	0.000	0.156	0.168	P	5.771	5.789
Cr	0.000	0.000	0.000	0.000	1.760	1.623	Si	0.101	0.100
Fe^{3+}	0.000	0.000	0.000	0.000	0.000	0.028	Cl	0.021	0.000
Fe^{2+}	0.000	0.000	0.000	0.114	0.886	0.911	F	1.926	1.962
Mn	0.000	0.000	0.000	0.000	0.062	0.045			
Ni	0.000	0.000	0.000	0.020	0.000	0.000			
Mg	0.000	0.000	0.000	2.783	0.044	0.056			
Ca	0.000	0.015	0.021	0.003	0.000	0.000			
Na	0.018	0.213	0.221	0.000	0.000	0.000			
K	0.984	0.736	0.749	0.003	0.000	0.000			
Ba	0.009	0.038	0.013	0.000	0.000	0.000			
V	0.000	0.000	0.000	0.000	0.008	0.015			
Zn	0.000	0.000	0.000	0.000	0.050	0.090			
Anorthite	0.000	0.015	0.021	Spinel	4.16	5.03			
Albite	0.017	0.215	0.221	Galaxite	5.89	4.06			
Orthoclase	0.976	0.740	0.748	Hercynit	0.57	8.94			
Celsian	0.007	0.030	0.011	Gahnite	4.80	7.75			
				Chromit	83.76	73.12			

ps - pseudomorph, c - core, r - rim, m - matrix

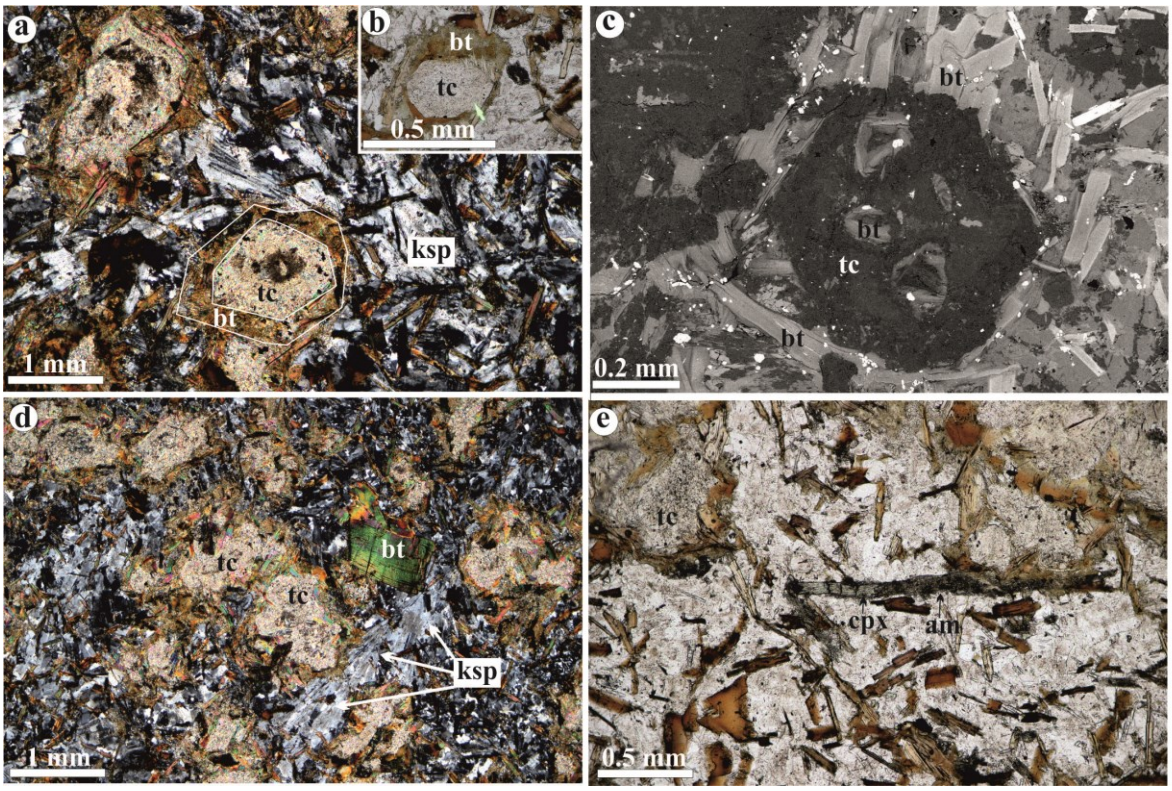

Fig. 3. Microtextural relationships of minerals and their pseudomorphs in vaugnerite (a, b, d and (e) are polarized microscope and (c) is backscattered electron image). (a, b) shows pseudomorphs of talc with carbonate after automorphic grains of olivine. Note that the talc has corona of biotite delineated by lines in (a). The matrix is formed mostly by K-feldspar and biotite. (c) is detail of pseudomorph after olivine filled by talc. (d) shows phenocryst of biotite with pseudomorphs after olivine. (e) exhibits columnar shaped pyroxene replaced by amphibole with biotite and pseudomorphs after olivine.

2.4.1.2. Biotite

At least three to four textural types of biotite were observed. In addition to rare phenocrysts (about 1 mm in size; *type I*), thin tabular crystals of biotite are present in the matrix (*type II*). The biotite crystals have orientation in different directions, but in some cases, they together with feldspar show flow structure around the talc pseudomorphs. The large porphyric grains of biotite are partly deformed (Fig. 3d). The next type of biotite forms inclusions in clinopyroxene and K-feldspar. All three varieties have dark red-brown colour and are phlogopite in composition with high X_{Mg} ranging from 0.73–0.83 (Fig. 4, Table 1). Their Ti contents vary between 0.33–0.39 apfu (Fig. 4a). The last type is biotite to phlogopite in composition (with X_{Mg} = 0.65–0.89) that has (red)-brown to green-brown colour and is inside and around the pseudomorphs after olivine (distinguished as *Type III* of biotite in Fig. 4). It contains 0.30–0.43 apfu Ti. Fluorine content in biotite types range between 0.08 and 0.25 apfu and correlates well with XMg (Fig. 4b). The higher fluorine contents occur usually in biotite of pseudomorphs. Regardless, the different textural varieties of biotite have relatively high Si (5.83–5.92 apfu) with Al = 1.99–2.19 apfu (Fig. 4c).

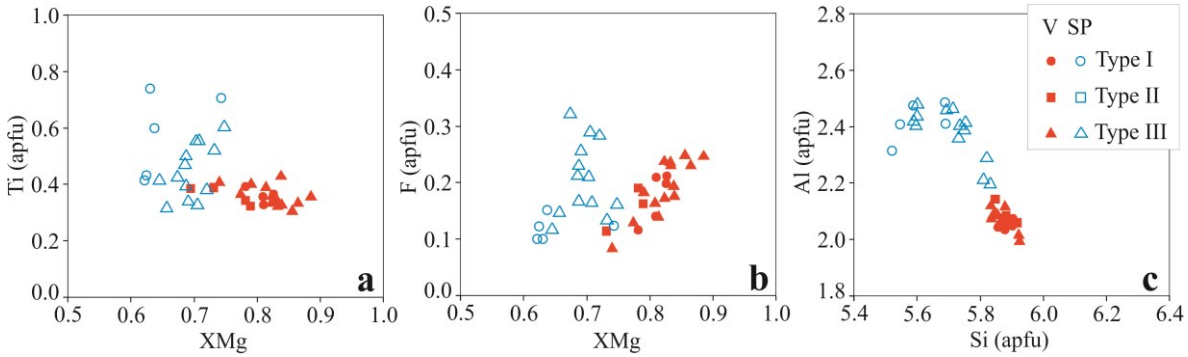

Fig. 4. Covariations diagrams of X_{Mg}:Ti (a), X_{Mg}:F (b) and Si:Al (c) of biotite from vaugnerite (V) and syenite porphyry (SP). Type I = phenocrysts, type II = tabular grains in the matrix, type III = small grains inside and around the talc pseudomorphs after olivine.

2.4.1.3. Clinopyroxene

Clinopyroxene forms columnar crystals (Fig. 3e) and it is mostly replaced by amphibole. Similar to biotite, it has orientation in different directions. Relatively fresh grains contain inclusions of apatite. In composition it is diopsidic augite with X_{Mg} = 0.82–0.84 (Table 1). It has low Al_2O_3 = 0.40–0.55 wt.%, Cr_2O_3 = 0.02–0.07 wt.% and Na_2O = 0.15–0.24 wt.%. The TiO_2 content is below 0.26 wt.%.

2.4.1.4. Amphibole

Two varieties of amphibole are present in vaugnerite. The first variety forms pseudomorphs after clinopyroxene (Fig. 3e). In most cases, it has dusty appearance due to myriads of minute globular opaque grains. It is actinolite in composition with XMg = 0.73–0.77 and Si = 7.8–7.9 apfu. The second variety is tremolite and forms small needles in the corona of olivine pseudomorphs with biotite or occurs within the pseudomorphs with talc and calcite.

2.4.1.5. Feldspars

K-feldspar is the main constituent of the matrix. It forms up to 1 mm long grains that seem to flow around the pseudomoprhs (Fig. 3a, c) and has inclusions of biotite and pyroxene or amphibole. It is mostly orthoclase in composition with 2 mol% albite component and shows perthitic texture with albite exsolutions. All feldspar analyses contain Ba with 0.77–1.34 mol% celsian component. Some analyses show up to 9 mol% albite content. Small amounts of albite, forming separate grains in the matrix, are also present.

2.4.1.6. Apatite

Apatite is present in the matrix and forms up to 0.2 mm long crystals. It occurs also as inclusions in biotite and has relatively high fluorine content (2.93–3.76 wt.% F). It contains Sr (1.08–1.28 wt.% SrO) and minor content of Ce, Fe and Mg (Table 1).

2.4.1.7. Other minerals

Titanite (< 0.2 mm in size) is present in the matrix. It has relatively high ZrO_2 = 2.3 wt.%, Nb_2O_5 = 1.53 wt.%, SnO = 1.4 wt.%, La_2O_3 = 0.27 wt.%, Ce_2O_3 = 0.53 and Al_2O_3 = 1.53 wt.%. In one sample, *spinel* was found to occur in the matrix and within talc pseudomorph. It is chromite (73–83 mol%) with small amount of spinel, gahnite and galaxsite components (Table 1). *Carbonate* analysed from the pseudomorphs is calcite with less than 1 % magnesite, siderite and rodochrosite components. Calcite with magnesite content of about 4 mol% is also present in the pseudomorphs. *Opaque phases* analysed by energy dispersive spectrometer are nickel sulphide and pyrrhotite. *Quartz* is present as interstitial phase in the matrix.

2.4.2 Syenite porphyry

The syenite porphyry is characterized by authomorphic phenocrysts of alkali feldspars (up to 2 × 5 mm), clinopyroxene (up to 0.5 × 2 mm), amphibole (0.2 × 3 mm), biotite (up to 1 mm) and rarely quartz (up to 2 mm) in a very fine-grained matrix (Fig. 5). It rarely contains pseudomorphs of talc, similar to that in the vaugnerite. The matrix is fine-grained to aphanitic in the central part of the syenite porphyry dyke and changes to glassy at the contact with surrounding rocks. It consists of alkali feldspar, quartz, biotite, amphibole and accessory amounts of apatite, opaque phases and zircon.

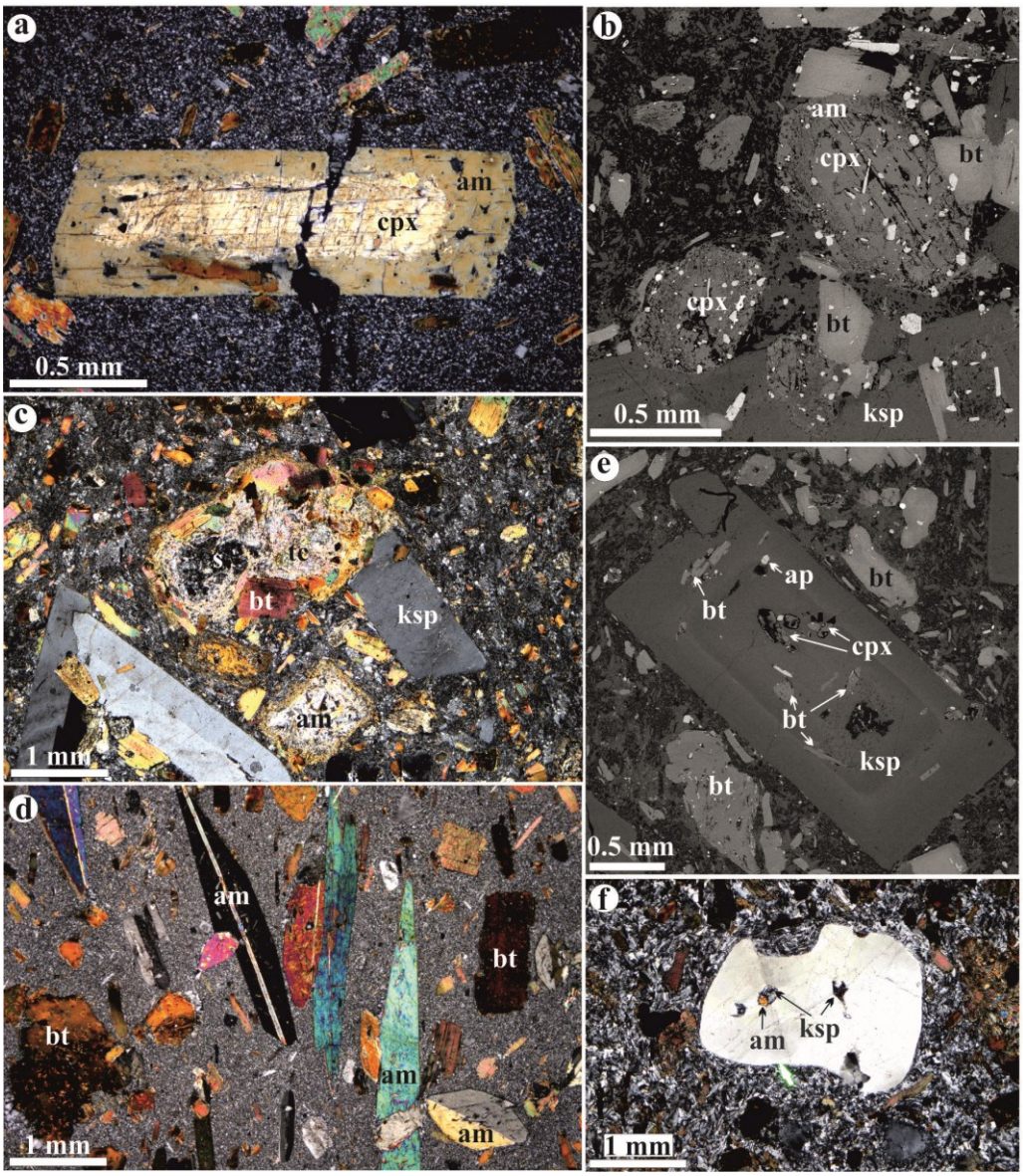

Fig. 5. Photomicrographs (a, c, d, f) and BSE (b, e) fromsyenite porphyry. (a) clinopyroxene crystal in a fine grainedmatrix is topotactically replaced along the rims by amphibole. (b) two clinopyroxene phenocrysts with apatite inclusions show magmatic corrosion along the rims, where new amphibole forms. In the lower part of image phenocryst of K-feldspar encloses clinopyroxene and biotite. (c) indicates pseudomorphs of talc (tc) and serpentine (s) after olivine and amphibole (am) after clinopyroxene. (d) phenocrysts of amphibole, having almost parallel orientation in the fine-grained matrix. (e) Compositional zoning in K-feldspar with inclusions of clinopyroxene, biotite and apatite. (f) phenocryst of quartz with inclusions of amphibole and K-feldspar shows magmatic corrosion along the rims.

2.4.2.1. Pseudomorphs

Two varieties of pseudomorphs are present in the syenite porphyry. The first (up to 3.5 mm in size) is formed by talc and minor serpentine (Fig. 5c) and seems to be similar to that in vaugnerite formed by replacement of olivine. It is less common and reach only about 5–8 vol.% of the rock. The

second, rarer, pseudomorphs (0.5 mm in size) are formed by amphibole of tremolite composition (X_{Mg} 0.90–1.00).

2.4.2.2. Biotite

Similar to vaugnerite, three textural types of biotite are present in syenite porphyry. The red-brown phenocrysts of biotite (*Type I*) have tabular shapes and contain inclusions of apatite and rarely of zircon. Cores of some large grains are scattered by small rutile and ilmenite crystals. Large biotite crystals are partly deformed and along cleavage and rims replaced by chlorite. Matrix grains (*Type II*) are small about 0.04 mm in size. Based on the classification by Foster (1960), both types are biotite and Mg-biotite. It has $X_{Mg} > 0.62$ and the highest $X_{Mg} = 0.75$ is present in some phenocrysts. The last type forms brown to green-brown biotite grains (*Type III*; X_{Mg} = 0.64–0.75) inside and around the pseudomorphs after olivine. Comparing to biotite from vaugnerite, it has higher Ti (0.30–0.78 apfu) and Al (2.21–2.48 apfu), but lower X_{Mg} (0.62–0.75) and Si (5.54–5.85 apfu, Fig. 4). Fluorine content is similar to that in biotite from vaugnerite (Fig. 4).

2.4.2.3. Clinopyroxene

Tabular grains of clinopyroxene are partly replaced by amphibole. Some grains have a thin replacement zone of amphibole (Fig. 5b). It contains inclusions of apatite and biotite. In composition it is diopsidic augite with X_{Mg} = 0.84–0.90 with low Al_2O_3 = 0.53–0.65 wt.%, Cr_2O_3 = 0.02–0.67 wt.% and Na_2O = 0.15–0.22 wt.%. The TiO_2 content is below 0.24 wt.%.

2.4.2.4. Amphibole

Light green amphibole forms either separate tabular grains (with length up to 1.5 mm, Fig. 5d) or clusters of small grains after clinopyroxene (Fig. 5c). It is mostly actinolite with X_{Mg} = 0.65–0.78, but some authomorphic grains have composition at transition between actinolite and magnesio-hornblende with X_{Mg} = 0.78–0.85. The large tabular grains with typical amphibole shape (Fig. 5d) could have formed by topotactic replacement of igneous amphibole. This variety has higher TiO_2 = 0.60–0.65wt.%, Al_2O_3 = 3.5wt.% and X_{Na} = Na/(Na+Ca) = 0.1 (Table 1) comparing to actinolite with TiO_2 = 0.1–0.2 wt.%, Al_2O_3 = 1.5–2.0 wt.% and X_{Na} = Na/(Na + Ca) = 0.04.

2.4.2.5. Alkali feldspar

Alkali feldspar is the dominant phase in the rock, where it forms long tabular phenocrysts with typical carlsbad twining. The phenocrysts may contain inclusions of biotite, clinopyroxene, amphibole, opaque minerals and apatite. They are weakly deformed and fractured. It is orthoclase in

composition with 75–96 mol% Or and small amounts of Ba (up to 1.76 mol% Celsian component). Albite content is high in the phenocrysts (12–22 mol% Ab) comparing to that in the matrix (3–6 mol% Ab). Some porphyric grains show systematic compositional zoning (Fig. 5e) with core having higher celsian content (7.0 mol%) that decreases to 2.6 mol% at the rim. The decrease of celsian in the rim is compensated by all three component orthoclase, albite and anorthite (Table 2). Pure albite is also present in the fine-grained matrix.

2.4.2.6. Apatite

In addition to small inclusions in biotite, amphibole, alkali feldspar and clinopyroxene, relatively large (0.05 mm long) columnar apatite crystals are present in the matrix. Similar to apatite in the vaugnerite it has high (up to 3.7 wt.%) fluorine content with SrO = 1.05–1.17 wt.%.

2.4.2.7. Quartz

Quartz occurs in the fine-grained matrix, but rarely large phenocrysts are also present. They show magmatic corrosion along the rims and undulose extinction with subgrain formation.

2.4.2.8. Other minerals

Zircon is present as an inclusion in biotite. *Nickel sulphide* is also present, but calcite was not observed. Very fine-grained *ilmenite* and *rutile* with knee-shaped twins are scattered in core of some biotite crystals.

2.4.3 Mafic enclaves in the syenite porphyry

The selected enclaves are similar in mineral composition and they consist of K-feldspar, biotite, amphibole and small amounts of apatite and accessory amounts of titanite and opaque phases. From the syenite porphyry they differ by higher content of amphibole pseudomorphs after clinopyroxene. In addition to tabular biotite (up to 0.5 mm in size) and amphibole pseudomorphs (up to 1 mm), they contain phenocrysts of K-feldspar (up to 3mmin size). Amphibole forms either separate tabular grains (up to 0.3 mm) or clusters of small grains with small amounts of biotite. Less frequent are pseudomorphs of talc with opaque phases. Both biotite and amphibole contain inclusions of apatite.

2.5 Major and trace element geochemistry

The whole-rock geochemical data (Table 2) indicates that all analysed samples are ultrapotassic (according to definition of Foley et al. (1987), K_2O > 5.8 wt.%, K_2O/Na_2O > 2.2 and MgO > 3.52 wt.%). Based on the $K_2O + Na_2O$: SiO_2 ratios (Le Bas et al., 1986) the vaugnerite plots in the field of basaltic trachyandesite, while enclaves and syenite porphyry in the fields of trachyandesite and trachyte, respectively (Fig. 6a). All rock samples are metaluminious (by alumina saturation of Shand (1927)) and have a considerable dominance K_2O content over Na_2O content (vaugnerite shows higher K_2O/Na_2O = 5.76–8.49 then syenite porphyry with K_2O/Na_2O = 2.24–3.02, enclaves have K_2O/Na_2O = 3.16–3.44). Using the classification diagram of Scarrow et al. (2009), the vaugnerite and enclaves plot in the field of K-lamprophyre and syenite porphyry is similar to some silica-rich durbachite out of these field (Fig. 6b). Vaugnerite has the highest MgO content (> 9.88 wt.%) and mg-number (= molar MgO/(MgO + FeO)) in the range of 0.72–0.74. Syenite porphyry show the lowest MgO content (> 3.5 wt.%) and its mg-number is 0.66–0.67. Enclaves have > 6.6 wt.% MgO and mg = 0.67–0.70.

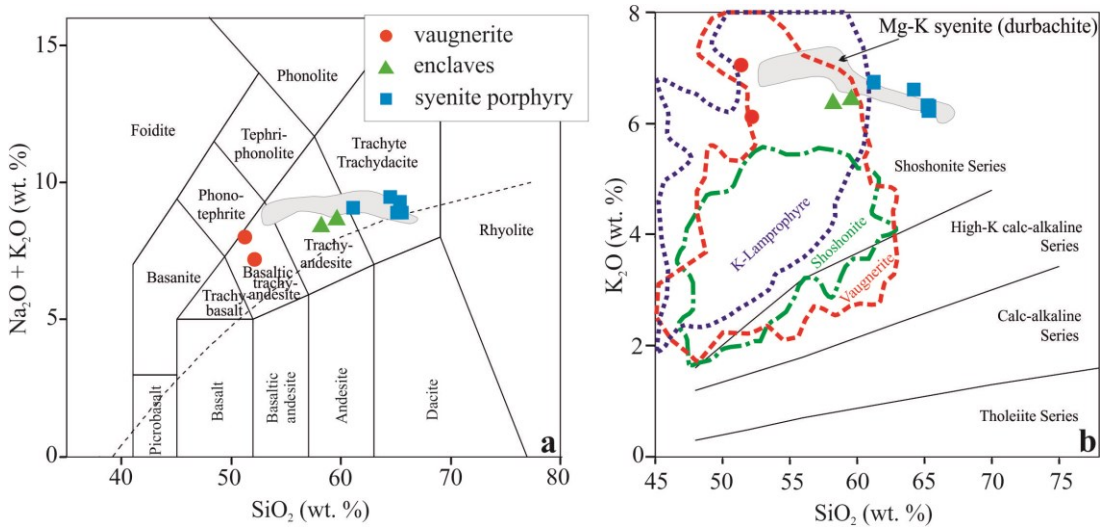

Fig. 6. (a) Total alkali-silica classification diagram (Le Bas et al., 1986) for vaugnerite and syenite porphyry. (b) K_2O (wt.%) vs SiO_2 (wt.%) diagram (according to Scarrow et al., 2009) for the same samples as plotted in (a). The dividing lines show the classification boundaries from Rickwood (1989). Data have been normalized to 100 wt.% volatile-free. The grey fields are Mg-K syenite (data from Holub, 1997; Janoušek et al., 2000).

Systematic variation of some major elements from the vaugnerite, through the enclaves to the syenite porphyry can be seen by strong positive correlations of CaO, FeO, TiO_2 and P_2O_5 and Cr_2O_3 (not shown) with MgO (Fig. 7). The Na_2O and Al_2O_3 contents show a decrease with increase of MgO (Fig. 7d, e). Systematic variation from vaugnerite to syenite porphyry can be observed also in the contents of some transit elements. Higher contents of V (233–255 ppm), Cr (363–410 ppm) occur in vaugnerite than that in syenite porphyry with V = 52–84 ppm, Cr = 220–310 ppm.

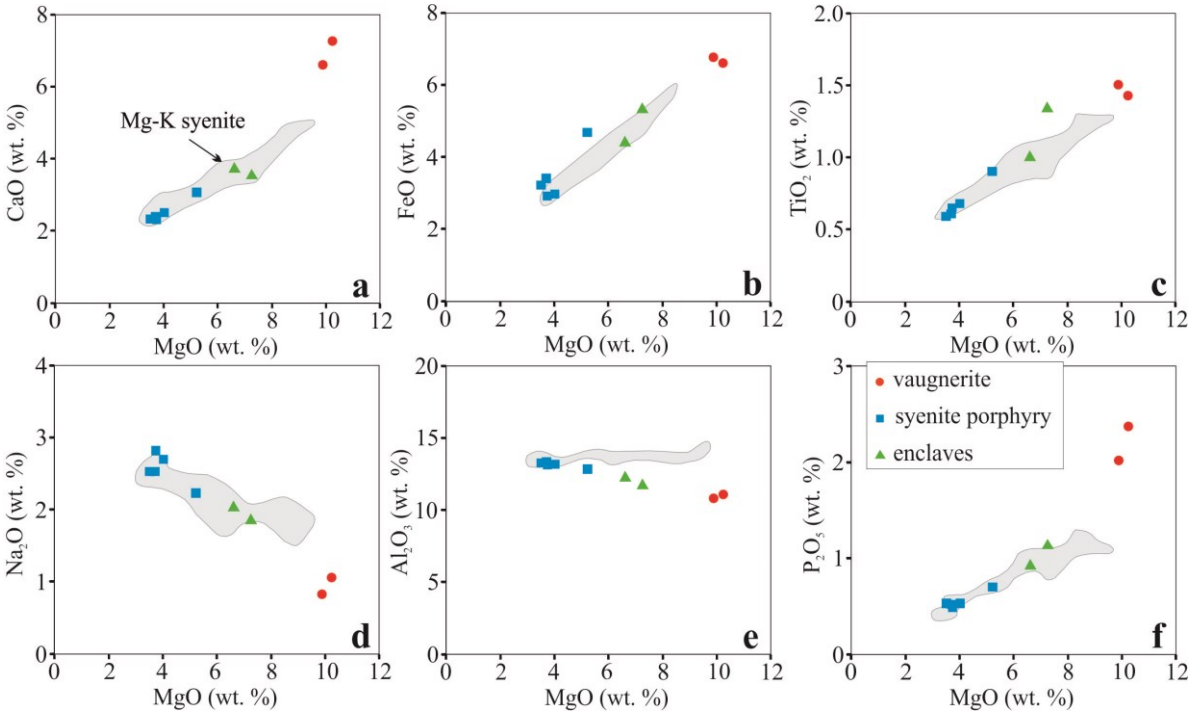

Fig. 7. Selected major element oxide (wt.%) concentrations vs. MgO content (wt.%) illustrating the broad compositional range of vaugnerite and syenite porphyry. All the major element data have been recalculated to 100 wt.% on a volatile-free basis (Table 2). Mg-K syenite (the grey fields, data from Holub, 1997; Janoušek et al., 2000) are also shown for comparison.

The spider plot of primitive mantle-normalized contents of selected trace and minor elements for the studied samples (Fig. 8a) shows variable enrichment of strong incompatible elements. Primitive mantle-normalized concentrations indicate enrichment in the range from several times primitive mantle for less incompatible elements (such as Ti and Y) to several hundred and even > 1000 times for more incompatible elements (such as K, Rb, Th, U or Pb). Analysed samples have typical high ratios of the most large ion lithophile elements (LILE), such as Rb or K, and high ratios of Th and U in relation to the high field strength elements (HFSE) for instance, the very high Th/Nb ratios (1.7–2.1). The primitive mantle-normalized incompatible trace element patterns are distinguished by significantly negative Nb-Sr-Ti and positive Pb anomalies, despite the generally high contents of Nb, Sr and Ti in the rocks. Concentration of some mantle incompatible elements is not systematic. The Y is higher in vaugnerite, but higher Hf, Ta, U values are recorded in the syenite porphyry. Similarly unsystematic variations in both rocks are present in Zr, Th, Nb, Rb and Sr contents.

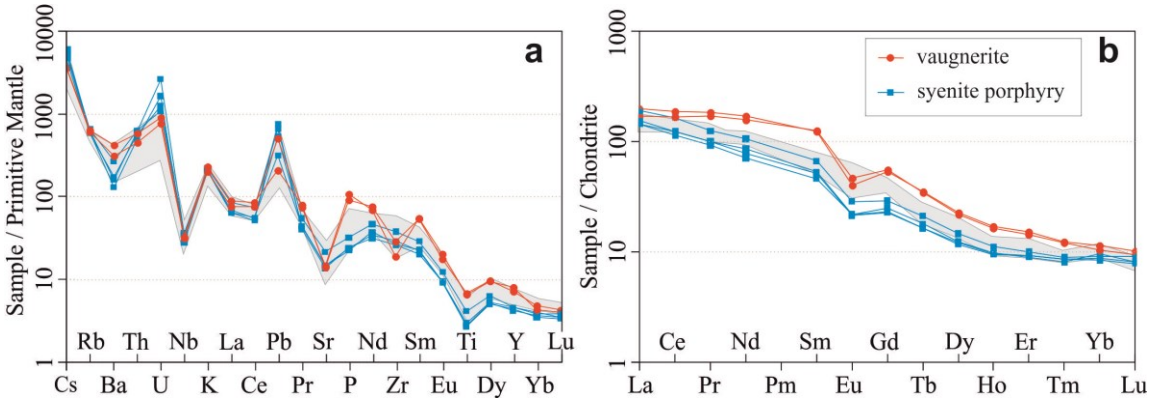

Fig. 8. (a) Primitive mantle-normalized trace element variation diagrams and (b) chondrite-normalized REE patterns for the studied rocks. Coefficients for normalization are after Sun and McDonough (1989) and Boynton (1984). The grey fields in (a) and (b) indicates Mg-K syenite (data are from Holub, 1997and Janoušek et al., 2000).

The chondrite-normalized REE (rare earth elements) diagram (Fig. 8b) show smooth curves with enrichment of light REE (LREE) compared to the heavy REE (HREE). The average concentrations of REE are higher in the vaugnerite than in the syenite porphyry. Both rocks show negative europium anomaly with Eu/Eu* 0.46–0.52 in vaugnerite and 0.56–0.63 in syenite porphyry (Fig. 8b). The La_n/Yb_n ratios are in the range of 15.14–20.86 and there is no systematic variation among different rocks types.

Table 2 Whole-rock major (wt.%) and trace element (ppm) analyses from ultrapotassic dykes.

Rock	Vaugnerite		Syenite porphyry				Xenolith		
Sample	LR 781	LR 782	LR 783	LR 786	LR 788	LR 2447	LR 784	LR 785	LR 787
SiO_2	52.16	51.38	65.26	65.35	65.37	61.24	64.23	59.59	58.23
TiO_2	1.43	1.51	0.65	0.59	0.61	0.90	0.68	1.00	1.34
Al_2O_3	11.09	10.83	13.13	13.27	13.35	12.85	13.18	12.22	11.70
Fe_2O_3	1.47	1.51	0.77	0.72	0.76	1.04	0.70	0.82	1.07
FeO	6.61	6.78	2.92	3.22	3.41	4.69	2.97	4.39	5.32
MnO	0.11	0.12	0.06	0.06	0.07	0.10	0.06	0.09	0.10
MgO	10.24	9.88	3.74	3.52	3.71	5.22	4.02	6.62	7.26
CaO	7.27	6.62	2.32	2.33	2.39	3.07	2.51	3.72	3.53
Na_2O	1.06	0.83	2.82	2.53	2.53	2.23	2.70	2.03	1.85
K_2O	6.11	7.05	6.32	6.22	6.30	6.74	6.61	6.42	6.36
P_2O_5	2.37	2.02	0.49	0.53	0.52	0.70	0.53	0.92	1.13
Σ	99.92	98.52	98.48	98.34	99.02	98.79	98.19	97.82	97.89
mg	73.43	72.22	65.87	66.08	65.98	66.50	66.57	69.71	67.30
K_2O/Na_2O	5.76	8.49	2.24	2.46	2.49	3.02	2.45	3.16	3.44

Table 2 continued.

Rock	Vaugnerite		Syenite porphyry			
Sample	LR 781	LR 782	LR 783	LR 786	LR 788	LR 2447
Sc	22	24	-	10	10	13
V	246	252	58	52	55	84
Cr	440	410	-	220	220	310
Co	35	34	14	13	14	20
Ni	60	66	62	70	81	130
Cu	30	26	18	20	11	20
Zn	120	73	45	50	47	80
Ga	18	18	20	20	18	21
Rb	393	407	407	387	375	420
Sr	316	295	316	291	309	459
Y	37	33	21	20	19	21
Zr	212	324	302	296	329	429
Nb	22.6	23.6	25.2	20.1	24.8	26.0
Sn	13	8	12	9	7	15
Sb	13.3	< 0.2	-	< 0.2	< 0.2	1.7
Cs	28.8	29.3	48.1	42.9	37.4	42.7
Ba	2214	2969	1132	920	1224	1894
Hf	6.1	8.6	10.1	8.7	9.4	11.5
Ta	1.86	1.78	2.40	2.71	2.64	2.41
Pb	35.9	15.1	22.6	53.8	38.2	47.3
Th	38.4	49.3	52.8	43.2	49.1	54.2
U	16.3	19.1	55.6	34.8	26.3	22.7
La	52.7	61.1	44.7	44.8	47.7	58.8
Ce	135	152	100	91.9	99.3	133
Pr	20.8	22.3	12.2	11.3	12.3	15.3
Nd	94.1	103	51.5	42.6	47.1	63.6
Sm	24.4	24.1	10.3	9.0	10.2	13.1
Eu	3.43	2.97	1.60	1.61	1.56	2.12
Gd	14.4	13.8	6.5	5.6	5.9	7.5
Tb	1.62	1.65	0.85	0.77	0.78	1.03
Dy	7.07	7.24	3.98	3.75	3.89	4.70
Ho	1.17	1.22	0.72	0.68	0.69	0.81
Er	3.01	3.18	1.88	1.95	1.93	2.11
Tm	0.39	0.40	0.26	0.28	0.28	0.29
Yb	2.16	2.39	1.99	1.74	1.83	1.90
Lu	0.30	0.33	0.26	0.25	0.26	0.29
Eu/Eu*	0.52	0.46	0.56	0.63	0.57	0.60
La_n/Yb_n	16.45	17.24	15.14	17.36	17.57	20.86

2.6 Radiometric dating

2.6.1 U/Pb dating of vaugnerite

Nine single-grain analyses of titanite from the vaugnerite sample (LR782) yielded relatively radiogenic Pb isotopic data, with modest amounts of common Pb (Tables 3 and 4, Fig. 9a, b). Titanite grains were dissolved in two exploratory batches. Of the four grains initially dissolved, two were translucent, honey coloured (s1-s2), while two were more turbid and brown (s3-s4). Isotopic results from s3 and s4 showed greater dispersion relative to s1 and s2 (Fig. 9a), thus the five crystals dissolved in the second batch were of the translucent, honey-coloured character similar to s1 and s2. Analyses s3 and s4 were discarded from further consideration. In the remaining crystals, radiogenic ^{206}Pb comprised 80–89% of the budget, thus making the calculation of model U-Pb dates somewhat sensitive to the choice of initial common Pb. To establish the initial common Pb composition incorporated into the titanites, a three-dimensional "total-Pb" $^{238}U/^{206}Pb$-$^{207}Pb/^{206}Pb$-$^{206}Pb/^{204}Pb$ isochron (Ludwig, 1998) was fit to the seven remaining titanite grains, resulting in common Pb plane intercepts at $(^{206}Pb/^{204}Pb)_i$ = 17.56 ± 0.51 and $(^{207}Pb/^{204}Pb)_i$ = 15.57 ± 0.12 (Fig. 9b). These compositions were used to calculate model radiogenic U/Pb ages for the seven titanite analyses. Calculated $^{206}Pb/^{238}U$ dates were statistically equivalent, ranging from 337.4 to 340.0 Ma, with a weighted mean of 338.59 ± 0.68 Ma (95% confidence interval, including geologic scatter). The age of igneous crystallization is interpreted from this weighted mean $^{206}Pb/^{238}U$ date.

2.6.2 U/Pb dating of syenite porphyry

Seven single-grain analyses of zircon from sample LR788 yielded concordant U-Pb dates (Table 3, Fig. 9c). The five oldest $^{206}Pb/^{238}U$ dates are equivalent with a weighted mean of 337.87 ± 0.21 Ma (95% confidence interval, including geologic scatter; Fig. 9d). The age of igneous crystallization is interpreted from this weighted mean $^{206}Pb/^{238}U$ date. Two other analyses with concordant dates yielded slightly younger $^{206}Pb/^{238}U$ dates, suggesting these grains suffered minor Pb loss. Two other grains yielded discordant dates, due to the presence of inherited components that are considerably older.

Table 3 Radiogenic U-Pb isotope ratio and age data

Grain (a)	Th/U (b)	$^{206}Pb^*$ x10^{-13}mol (c)	mol % $^{206}Pb^*$ (c)	Pb*/Pbc (c)	Pbc (pg) (c)	$^{206}Pb/^{204}Pb$ (d)	$^{208}Pb/^{206}Pb$ (e)	Radiogenic Isotopic Ratios: $^{207}Pb/^{206}Pb$ (e)	% err (f)	$^{207}Pb/^{235}U$ (e)	% err (f)	$^{206}Pb/^{238}U$ (e)	% err (f)	corr. coef.	Radiogenic Isotopic Dates: $^{207}Pb/^{206}Pb$ (g)	± (f)	$^{207}Pb/^{235}U$ (g)	± (f)	$^{206}Pb/^{238}U$ (g)	± (f)
LR782 titanite (vaugnerite)																				
s4	1.76	4.417	85.42%	2.31	63.5	120.5	0.554	0.053983	0.82	0.41836	0.85	0.056207	0.226	0.281	370	18	354.9	2.6	352.52	0.78
s5	**2.15**	**2.474**	**82.91%**	**2.06**	**42.9**	**102.9**	**0.678**	**0.053380**	**0.99**	**0.39868**	**1.03**	**0.054169**	**0.266**	**0.249**	**345**	**22**	**340.7**	**3.0**	**340.06**	**0.88**
t8	**1.73**	**2.191**	**79.80%**	**1.55**	**46.7**	**87.0**	**0.547**	**0.053321**	**1.20**	**0.39703**	**1.23**	**0.054005**	**0.319**	**0.213**	**342**	**27**	**339.5**	**3.6**	**339.06**	**1.05**
t9	**1.64**	**4.550**	**87.46%**	**2.69**	**55.0**	**140.1**	**0.518**	**0.053424**	**0.73**	**0.39760**	**0.77**	**0.053977**	**0.193**	**0.323**	**347**	**16**	**339.9**	**2.2**	**338.89**	**0.64**
s1	**1.36**	**7.743**	**83.39%**	**1.82**	**129.9**	**105.8**	**0.429**	**0.053196**	**0.95**	**0.39573**	**0.98**	**0.053953**	**0.258**	**0.246**	**337**	**22**	**338.5**	**2.8**	**338.75**	**0.85**
t6	**1.56**	**2.694**	**85.72%**	**2.28**	**37.8**	**123.1**	**0.494**	**0.053101**	**0.81**	**0.39455**	**0.85**	**0.053889**	**0.218**	**0.287**	**333**	**18**	**337.7**	**2.4**	**338.35**	**0.72**
s2	**1.73**	**8.024**	**89.00%**	**3.18**	**83.5**	**159.8**	**0.545**	**0.053196**	**0.61**	**0.39486**	**0.65**	**0.053834**	**0.170**	**0.349**	**337**	**14**	**337.9**	**1.9**	**338.02**	**0.56**
t7	**1.74**	**3.507**	**79.48%**	**1.52**	**76.2**	**85.7**	**0.550**	**0.053210**	**1.23**	**0.39423**	**1.26**	**0.053735**	**0.326**	**0.209**	**338**	**28**	**337.5**	**3.6**	**337.41**	**1.07**
s3	1.59	2.455	85.81%	2.31	34.2	123.8	0.501	0.053314	0.81	0.39233	0.84	0.053371	0.216	0.289	342	18	336.1	2.4	335.18	0.71
LR788 zircon (syenite porphyry)																				
z4	0.250	16.0134	99.96%	661	0.58	41148	0.078	0.087030	0.091	1.02902	0.180	0.085754	0.132	0.873	1361.2	1.8	718.44	0.93	530.38	0.67
z1	0.521	3.5525	99.91%	323	0.28	19248	0.164	0.054043	0.079	0.41842	0.140	0.056153	0.069	0.932	372.9	1.8	354.92	0.42	352.19	0.24
z6	**0.482**	**2.1646**	**99.83%**	**176**	**0.31**	**10630**	**0.152**	**0.053227**	**0.090**	**0.39509**	**0.150**	**0.053836**	**0.069**	**0.928**	**338.5**	**2.0**	**338.08**	**0.43**	**338.03**	**0.23**
z5	**0.064**	**7.2675**	**99.96%**	**724**	**0.22**	**49004**	**0.020**	**0.053259**	**0.063**	**0.39533**	**0.128**	**0.053835**	**0.070**	**0.966**	**339.8**	**1.4**	**338.25**	**0.37**	**338.02**	**0.23**
z3	**0.099**	**8.7642**	**99.96%**	**708**	**0.28**	**47471**	**0.031**	**0.053227**	**0.057**	**0.39489**	**0.125**	**0.053808**	**0.068**	**1.001**	**338.5**	**1.3**	**337.93**	**0.36**	**337.86**	**0.22**
z2	**0.516**	**6.8461**	**99.95%**	**636**	**0.27**	**37966**	**0.163**	**0.053245**	**0.065**	**0.39497**	**0.129**	**0.053800**	**0.070**	**0.964**	**339.3**	**1.5**	**337.99**	**0.37**	**337.81**	**0.23**
z8	**0.481**	**6.1935**	**99.91%**	**350**	**0.44**	**21087**	**0.152**	**0.053237**	**0.067**	**0.39469**	**0.131**	**0.053770**	**0.070**	**0.958**	**338.9**	**1.5**	**337.79**	**0.38**	**337.63**	**0.23**
z9	0.085	13.3510	99.95%	545	0.54	36662	0.027	0.053185	0.074	0.39384	0.134	0.053707	0.071	0.919	336.7	1.7	337.17	0.38	337.24	0.23
z7	0.250	5.4083	99.86%	195	0.65	12491	0.079	0.053223	0.085	0.39345	0.142	0.053616	0.072	0.889	338.3	1.9	336.89	0.41	336.69	0.24

Notes: (a) each analysis is a single grain or grain fragment; analyses in bold used in the weighted mean calculations.

(b) Model Th/U ratio calculated from radiogenic $^{208}Pb/^{206}Pb$ ratio and $^{207}Pb/^{235}U$ date.

(c) Pb* and Pbc are radiogenic and common Pb, respectively. mol % $^{206}Pb^*$ is with respect to radiogenic and blank Pb.

(d) Measured ratio corrected for spike and fractionation only. Samples were spiked with the BSU1B tracer, with an external Pb fractionation correction of 0.18 ± 0.02 (1-sigma) %/amu (atomic mass unit), based on analysis of NBS-981 and NBS-982.

(e) Corrected for fractionation, spike, common Pb, and initial disequilibrium in $^{230}Th/^{238}U$. Up to 0.5 pg of common Pb is assigned to procedural blank with composition of $^{206}Pb/^{204}Pb = 18.042 \pm 0.61\%$; $^{207}Pb/^{204}Pb = 15.537 \pm 0.52\%$; $^{208}Pb/^{204}Pb = 37.686 \pm 0.63\%$ (1-sigma). Excess over blank was assigned to initial common Pb, using the Stacey and Kramers (1975) two-stage Pb isotope evolution model at 338 Ma (LR788 zircon), or a 3-D total-Pb regression estimate (LR782 titanite).

(f) Errors are 2-sigma, propagated using algorithms of Schmitz and Schoene (2007).

(g) Calculations based on the decay constants of Jaffey et al. (1971). $^{206}Pb/^{238}U$ and $^{207}Pb/^{206}Pb$ ratios and dates corrected for initial disequilibrium in $^{230}Th/^{238}U$ using Th/U [magma] = 3.

Table 4 Total sample U-Pb isotope ratio data

Grain (a)	$\frac{^{238}U}{^{206}Pb}$ (b)	% err (c)	$\frac{^{207}Pb}{^{206}Pb^*}$ (b)	% err (c)	$\frac{^{204}Pb}{^{206}Pb}$ (b)	% err (c)	ρ 8/6-7/6 (d)	ρ 8/6-4/6 (d)	ρ 7/6-4/6 (d)	$\frac{^{206}Pb}{^{204}Pb}$ (b)	% err (c)	$\frac{^{207}Pb}{^{204}Pb}$ (b)	% err (c)	ρ 6/4-7/4 (d)
LR782 titanite (vaugnerite)														
s1	**15.4683**	**0.076**	**0.19113**	**0.129**	**0.009424**	**0.202**	**-0.743**	**0.136**	**0.411**	**106.11**	**0.202**	**20.281**	**0.190**	**0.784**
s2	**16.5463**	**0.076**	**0.14430**	**0.178**	**0.006225**	**0.294**	**-0.681**	**-0.070**	**0.700**	**160.65**	**0.294**	**23.183**	**0.212**	**0.801**
s3	16.1137	0.126	0.17003	0.434	0.007975	0.642	-0.898	-0.728	0.939	125.39	0.642	21.319	0.279	0.844
s4	15.2163	0.096	0.17452	0.238	0.008244	0.359	-0.748	-0.353	0.810	121.31	0.359	21.171	0.217	0.766
s5	**15.3391**	**0.127**	**0.19427**	**0.353**	**0.009629**	**0.499**	**-0.866**	**-0.651**	**0.905**	**103.86**	**0.499**	**20.176**	**0.234**	**0.767**
t6	**15.9403**	**0.118**	**0.17068**	**0.394**	**0.008032**	**0.583**	**-0.880**	**-0.682**	**0.926**	**124.50**	**0.583**	**21.249**	**0.264**	**0.826**
t7	**14.8139**	**0.097**	**0.22320**	**0.205**	**0.011615**	**0.289**	**-0.857**	**-0.369**	**0.723**	**86.10**	**0.289**	**19.217**	**0.200**	**0.705**
t8	**14.8106**	**0.130**	**0.22011**	**0.326**	**0.011398**	**0.443**	**-0.920**	**-0.683**	**0.887**	**87.73**	**0.443**	**19.312**	**0.216**	**0.714**
t9	**16.2236**	**0.092**	**0.15704**	**0.268**	**0.007082**	**0.427**	**-0.764**	**-0.399**	**0.834**	**141.21**	**0.427**	**22.176**	**0.252**	**0.810**

Notes: (a) each analysis is a single grain or grain fragment; analyses in bold used in regression calculations.
(b) Total sample ratios are corrected for fractionation, spike, and blank Pb only.
(c) Errors are 2-sigma, propagated using algorithms of Schmitz and Schoene (2007).
(d) ρ (8/6-7/6) = correlation coefficient between $^{238}U/^{206}Pb$ and $^{207}Pb/^{206}Pb$; ρ (8/6-4/6) = correlation coefficient between $^{238}U/^{206}Pb$ and $^{204}Pb/^{206}Pb$; ρ (7/6-4/6) = correlation coefficient between $^{207}Pb/^{206}Pb$ and $^{204}Pb/^{206}Pb$; ρ (6/4-7/4) = correlation coefficient between $^{206}Pb/^{204}Pb$ and $^{207}Pb/^{204}Pb$.

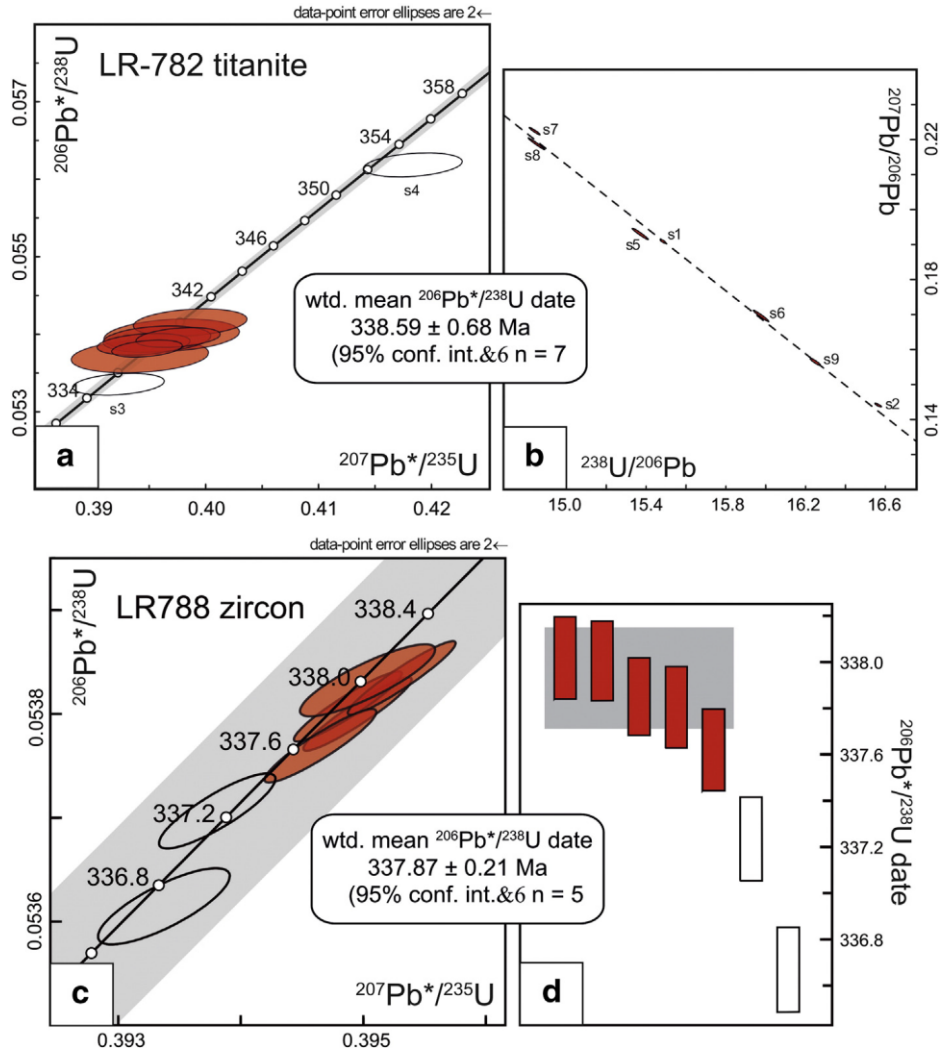

Fig. 9. (a) Conventional (radiogenic U-Pb isotope ratio) concordia diagram for titanite from vaugnerite sample LR782; b) total sample U-Pb isotope ratio Tera-Wasserburg diagram illustrating correlated titanite analyses from LR782; c) conventional (radiogenic U-Pb isotope ratio) concordia diagram for zircon from syenite porphyry sample LR788; d) ranked age plot for LR788 zircons.

2.7 Discussion

2.7.1 Mineral textures and crystallization history of the vaugnerite and syenite porphyry dykes

Mineral textures in the vaugnerite indicate at least two stages of crystallization that occurred under different P-T-X conditions (Fig. 10). The oval-shaped pseudomorphs with orthorhombic contours, which are formed of talc with relatively high nickel content, support their formation after olivine. Equilibrium phases of this early stage of crystallization were olivine, apatite, biotite (type I) and clinopyroxene. This is consistent with the result of melting experiments of Parat et al. (2010) on durbachite, where olivine as a liquidus phase co-crystallized with biotite and clinopyroxene. Apatite,

forming as an inclusion in biotite, suggests that it crystallized prior to or coeval with biotite. It is not clear, if all of the amphiboles are pseudomorphous after clinopyroxene or if some could have formed by transformation of igneous amphibole, but the original amphibole is not present in the studied samples.

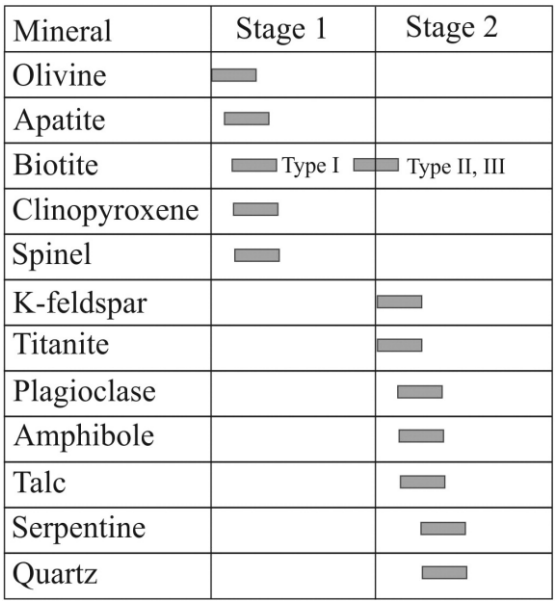

Fig. 10. Generalized succession of mineral crystallization in the investigated vaugnerite and syenite porphyry dykes. Biotite: type I = phenocrysts, type II = tabular grains in the matrix, type III = small grains inside and around the talc pseudomorphs after olivine.

The biotite around olivine pseudomorphs formed by interaction of the olivine phenocrysts with surrounding melt in the matrix. Since the formation of this biotite type could occur transitionally between the first and second stages, biotite occurring inside of the pseudomorphs, clearly relates to the second stage. The high X_{Mg} in this biotite probably reflects a local compositional gradient resulting from the transformation of former olivine. The high fluorine and titanium contents in biotite around and inside of pseudomorphs could be due to the transformation of original Ca-Na (?) amphibole into actinolite or tremolite which contains negligible amounts of fluorine and titanium in the analyses. As titanite occurs only in the matrix, it is possible that it was formed during this stage of crystallization. The biotite in the matrix (type II) was probably formed at the transition between the first and second crystallization stage. The second crystallization stage in the vaugnerite occurred in a SiO_2-rich environment. In addition to the stabilization of K-feldspar instead of biotite and formation of free quartz in the matrix, the replacement of olivine into talc instead of serpentine also supports silica saturated conditions during crystallization of matrix minerals. Carbonatization by CO_2-charged aqueous fluids is the logical cause of the talc + dolomite alteration, however depending on the fluid pressure and water activity tremolite-actinolite amphibole can be stabilized (Platt and Mitchell, 1982; Slaughter et al., 1975).

Similar to that in the vaugnerite, the presence of pseudomorphs after olivine, apatite and some biotite and clinopyroxene in the syenite porphyry could have crystallized during the first stage. However, this crystallization occurred after significant fractionation which is supported by the only small or minor amounts of olivine pseudomorphs, but higher content of free quartz. (The modal amounts of biotite and pseudomorphs after olivine decrease from vaugnerite (~20 and 20 wt.%) to syenite porphyry (~10 and 10 wt.%), respectively; while the clinopyroxene content is similar in both at about 10 wt.%.) Pseudomorphs of actinolite after clinopyroxene and biotite in coronas and within the pseudomorphs after olivine relate to the second stage. The phenocrysts of alkali feldspar with inclusions of apatite, and clinopyroxene clearly formed during the second stage of crystallization that occurred in a silica-rich environment. The corroded quartz xenocrysts suggest that the assimilation of country rocks was likely played a major role in the evolution of the magma composition and phase relations (e.g. Clarke, 2007; Thorkelson, 1992).

As minerals formed during the first stage in both the vaugnerite and syenite porphyry were transformed to other phases or reequilibrated during cooling, only biotite and clinopyroxene could be treated to trace compositional change between the first and second stage of magma crystallization. Based on the high concentration of fluorine, titanium and high X_{Mg}, the biotite in vaugnerite and syenite porphyry is comparable with that (up to 1.0 wt.% F, 1.3–7.3 wt.% TiO_2 and X_{Mg}= 0.73–0.90) from ultrapotassic alkaline rocks of mantle origin (Edgar and Arima, 1983; Edgar et al., 1996). The X_{Mg} and TiO_2 values in biotite and X_{Mg} in clinopyroxene from our samples are close to that from melting experiment on durbachite by Parat et al. (2010). The experiment carried out by these authors was in the temperature range of 900–1100 °C at 0.1, 0.2 and 1.0 GPa and they produced olivine at 1100 and 1000 °C, biotite and clinopyroxene at 1000 and 900 °C. The biotite from their experiment had however very low F (< 0.05wt.%),which was probably related to low fluorine content in the starting material. The clinopyroxene has relatively higher Al_2O_3 = 1.56–5.93 wt.% (average 3.26 wt.% from 26 analyses) in comparison to that in the clinopyroxene from durbachite (0.48 wt.%) and from our samples (vaugnerite, Al_2O_3 = 0.45–0.55 wt.% and syenite porphyry, Al_2O_3 = 0.53–0.65 wt.%). No systematic relationship occurs in the variation of Al_2O_3 contents in clinopyroxene with pressure and temperature changes in the experiments.

The compositional and modal relations of minerals, including the high fluid contents (F, CO_2, H_2O) in minerals from the study dykes indicate close similarity with the ultrapotassic rocks of lamprophyre composition (Edgar et al., 1996; Mitchell and Bergman, 1991). Mass balance calculations between mineral modes and bulk rock composition indicate a decrease of modal contents of early crystallized phases (olivine + phlogopite + apatite + clinopyroxene) from about 50% in vaugnerite to 20 mol% in the syenite porphyry. In addition to higher calcite and apatite contents in the vaugnerite, fluorine and H_2O are incorporated in biotite, which has 3–4 magnitudes higher content in the vaugnerite.

2.7.2 Origin of the vaugnerite-syenite porphyry magma and its relation to Mg-K syenite magmatism in the Moldanubian Zone

There is general agreement that the ultrapotassic rocks in the Bohemian Massif crystallized from magma originated by melting of an anomalous lithospheric mantle contaminated by mature crustal material (Holub, 1997; Janoušek and Holub, 2007; Krmíček et al., 2016; von Raumer et al., 2013). A mantle origin for the vaugnerite and syenite porphyry magma is supported by the presence and chemistry of early crystallized minerals in the rock. The occurrence of phlogopite as well as of F-rich apatite and carbonate reflect partial melting of a previously metasomatized spinel-lherzolite mantle source or pre-enriched phlogopite-bearing mantle (Foley et al., 1987; Mahéo et al., 2009).

The mantle metasomatism was operated by the influx of high K (and also Ba) fluids, rich in H_2O or CO_2. (Kempton, 1987; Roden et al., 1984). High concentration of volatiles (CO_2, F) may have resulted in lowering of melting temperature of normal peridotite to produce potassic magma. Negative Ti and Nb anomalies (Fig. 8a) as well as positive correlation between these two elements can be explained by the presence of Ti-rich residual minerals, e.g. rutile in the mantle source region or they could be inherited from crustal components present in the source (Guo et al., 2006; Williams et al., 2004). The negative Eu anomaly along with enrichment with light REE suggest partial melting in the presence of residual phlogopite, which buffered K and Nb concentrations in the lithospheric mantle which had been enriched by sediment component (Turner et al., 1999). The high F and P_2O_5 contents accommodated in phlogopite and apatite are comparable with those in some lamproite rocks (e.g. Edgar and Mitchell, 1997; Hughes, 1982). The low SiO_2 and high Al_2O_3 contents of biotite from the syenite porphyry in comparison to that in vaugnerite suggests relatively low-pressure (and possibly low-temperature) conditions for their formation (Arai,1984).

The formation of ultrapotassic magma is generally assumed to occur at relatively great depth by low degrees of partial melting (e.g. Conceição and Green, 2004; Condamine and Médard, 2014; Green and Pearson, 1986; Gupta, 2015; Mallik et al., 2015). The lack of plagioclase as a phenocryst in both vaugnerite and syenite porphyry suggests that the early equilibrium phases crystallized below the depths of plagioclase stability field. The minor albite in the matrix could have crystallized coeval with or even later than K-feldspar at lower pressures in crustal positions. Lanthanum is highly incompatible in minerals such as spinel and garnet, while Yb is incompatible in spinel but compatible in garnet (K_D for Yb in garnet is > 3; Thirlwall et al., 1994). The relatively low La/Yb ratio of around 2.2 in the vaugnerite suggests that the melting must have occurred at depth in the spinel stability field (Moyen, 2009; Williams et al., 2004). This is in agreement with the presence of Cr-rich spinel in the vaugnerite. It should however be noted that the Cr content enlarges the stability field of spinel to higher pressure (e.g. Klemme, 2004).

When using MgO as a fractionation index, the progressive decrease of CaO, FeO, TiO_2, P_2O_5 (Fig. 7) can be explained by fractional crystallization from vaugnerite to syenite porphyry, which is consistent with petrographical observations indicating that pseudomorphs after olivine, biotite, apatite and clinopyroxene phenocrysts predominate in the vaugnerite. On the other hand, the slight increase of Al_2O_3 from vaugnerite to syenite porphyry may relate to crustal assimilation (Conticelli, 1998; Taylor and McLennan, 1985). The increase of SiO_2 could relate both to fractionation and contamination of felsic crustal material during magma ascent to the surface. However, the input of crustal material into the original magma is supported by the presence of quartz phenocrysts in the syenite porphyry. Mass balance calculations, using the OPTIMASBA software (Cabero et al., 2012) indicated that the daughter (syenite porphyry) magma was formed by 76% crystallization of the parent (vaugnerite) magma coupled with ~30% crustal assimilation. The average composition of granulite from the Moldanubian Zone was used as a crustal contaminant in the mass balance calculations. The K_2O content is almost constant in both the vaugnerite and syenite porphyry and is suggestive of phlogopite buffering in the source magma (Williams et al., 2004). It is involved in biotite and K-feldspar, where modal content of K-feldspar increases proportionally with SiO_2 in the rock. As plagioclase is only a rare phase in the vaugnerite, the increase of Na_2O toward the syenite porphyry may also relate to contamination of crustal material.

Major and trace element variations in Figs. 6, 7 and 8a indicate close similarity between Mg-K syenite plutons and syenite porphyry dykes and hosting enclaves. The relatively high REE contents in the vaugnerite comparing to the syenite porphyry (Fig. 8b) probably reflect the original melt composition produced by partial melting of mantle.

2.7.3 Geodynamic implication

Textural and compositional relations of minerals from vaugnerite and syenite porphyry in combination with the ID-TIMS analyses on zircon and titanite allow clarification of the origin of ultrapotassic magmatism and to discuss the succession of Variscan magmatic and metamorphic events that belongs among the most debated topics in the Bohemian Massif (Faryad, 2011; Janoušek and Holub, 2007; Krmíček et al., 2016; Schulmann et al., 2005, 2014). Recent study from some eclogites (Faryad and Fišera, 2015; Scott et al., 2013), but mainly from felsic granulite in the Moldanubian Zone (Faryad et al., 2010, 2015; Jedlicka et al., 2015; Perraki and Faryad, 2014) showed that the felsic granulite and some other amphibolite facies rocks passed first an earlier eclogite and UHP event and were then overprinted by granulite-amphibolite facies metamorphism in the lower and middle crustal positions at 0.7–1.5 GPa. They also showed that the granulite and amphibolite facies overprint was not sufficiently long to homogenize the minerals formed during the eclogite facies and UHP conditions. Such partially equilibrated minerals are not suitable for PT estimate or geochronological dating as they may yield inaccurate or mixed results. The best example

is the wide range of ages (380 to 340 Ma) from granulite facies rocks that were obtained for Ordovician granitoids (Schulmann et al., 2005; Teipel et al., 2012). The age of 340 Ma is assumed as peak of the granulite facies metamorphism and this age overlaps with the available geochronological data (337–343 Ma) from ultrapotassic (durbachite) rocks (Holub et al., 1997; Kusiak et al., 2010; Verner et al., 2008). However, field relations suggest that the durbachite intruded granulites in their solid state (Verner et al., 2008). In addition to their sharp intrusive contacts, the orientation of magmatic fabrics in durbachite is discordant to the metamorphic fabrics in the granulites which were developed during granulite emplacement into the middle crustal level. The ultrapotassic rocks were thus emplaced into various levels of theMoldanubian Zone revealing variable structural relationships depending on the heterogeneous regional strain distribution and changes in rheological properties of the host rocks (Verner et al., 2006). As indicated by Faryad et al. (2015), the heat source for the short-lived granulite facies metamorphism was the ultramafic magma (norite, troctolite, gabbro), which intruded the Moldanubian crust between 360 and 340 Ma. This was documented by age dating and crystallization textures of mafic and ultramafic rocks (troctolite, gabbro), which show granulite facies conditions and occur adjacent or within felsic granulite. The new ages of ca. 338 Ma, obtained by ID-TIMS analyses, for vaugnerite and syenite porphyry dykes in combination with the field relations (chilled margins between dykes and host rocks) indicate that the ultrapotassic magmatism occurred after all basement rocks were already in their surface position.

Fig. 11 illustrates the succession of magmatic and metamorphic processes that related to subduction of the Moldanubian plate, slab break-off, generation of the asthenospheric magma, granulite facies metamorphism and finally the formation of ultrapotassic rocks. Subduction of the Moldanubian plate beneath the Teplá-Barrandian Block initiated formation of arc-related granitoid rocks of the CBPC (Fig. 11a). After exhumation of HP-UHP rocks by syn-convergent mechanism (Chemenda et al., 1995) and their emplacement into various crustal levels, slab break-off (Atherton and Ghani, 2002; Davies and von Blanckenburg, 1995; Mahéo et al., 2009) occurred. Consistent with the model by van Hunen and Allen (2011), the buoyant continental part was decoupled from its deeper counterpart (Fig. 11b) and resulted in uplift and further exhumation of the HP-UHP rocks within the accretionary complex. This process was associated with the mantle upwelling triggering melting and emplacement of magma in lower stress field beneath the accretionary complex and subsequent intrusions of gabbro-norite plutons into the overlying crustal basement rocks (Fig. 11b). Extreme heating produced by mafic-ultramafic intrusions resulted in granulite facies overprint of already exhumed HP-UHP bodies and migmatitization of their host lithologies. After this short-lived thermal process (Faryad and Fišera, 2015; Jedlicka et al., 2015), the high-grade rocks were transported to the upper crustal levels due to subduction of the Rheic oceanic plate (Finger et al., 2007) and subsequent underplating of the Brunovistulian Block beneath the Moldanubian Zone (Schulmann et al., 2005).

The ultrapotassic magmatism occurred subsequent to the granulite facies metamorphism and exhumation of the basement rocks to their present position. In the Bohemian Massif, dykes of lamprophyres and lamproite are present not only along the western and eastern border of the Moldanubian Zone (Holub, 1997; Krmíček et al., 2016), but they also occur along the Saxothuringian Zone (Erzgebirge, the West Sudetes) and in the Mid-German Crystalline Rise (Abdelfadil et al., 2014; Kovaříková et al., 2007; Siebel and Chen, 2009; Siebel et al., 2003; Štemprok et al., 2014; von Seckendorf et al., 2004). In the Saxothuringian Zone, they are represented by minetta, kersantite, spessartite and yield ages of 336–334 Ma (based on Ar-Ar dating), but younger dykes (297–293 Ma) are also reported (Abdelfadil et al., 2014; von Seckendorf et al., 2004). The lamprophyre dykes, occurring along the eastern border of the Moldanubian Zone are interpreted as result from closure of the Rheic oceanic basin (Krmíček et al., 2016). The distribution of potassic and ultrapotassic dykes within different crustal units in the Bohemian Massif probably reflects deep tectonic zones (plate boundaries). This is consistent with the generally accepted interpretations about the formation and emplacement of K-rich magma by melting of the metasomatized lithospheric mantle in the transcurrent shear zones (e.g. Vaughan and Scarrow, 2003) or by decompression melting of the lithospheric mantle by extensional post-orogenic tectonic movements (Bea et al., 1999; Scarrow et al., 2011; Villaseca et al., 2008). Within these zones opening of steep magma-controlled riedel fractures permits the transfer of metasomatized mantle lithosphere melts to shallow depths as the low degree, volatile-rich, melts use the tectonic weaknesses to ascend. The mantle lithosphere in the Bohemian Massif, is formed by several domains, including the Saxothuringian, Moldanubian, Teplá-Barrandian and Brunovistulian and each of these domains has its own mantle lithosphere with different mantle fabrics (Babuška and Plomerová, 2013). The boundaries among lithospheric domains functioned as strike-slip faults that could serve as feeding channels for potassic-ultrapotassic magma generated in the mantle (Fig. 11c). This process was probably partly operated by various degrees of clockwise and anticlockwise block rotations in the Bohemian Massif that was documented by paleomagnetic data since the Devonian (Edel et al., 2003; Krs et al., 1995; Tait et al., 1994).

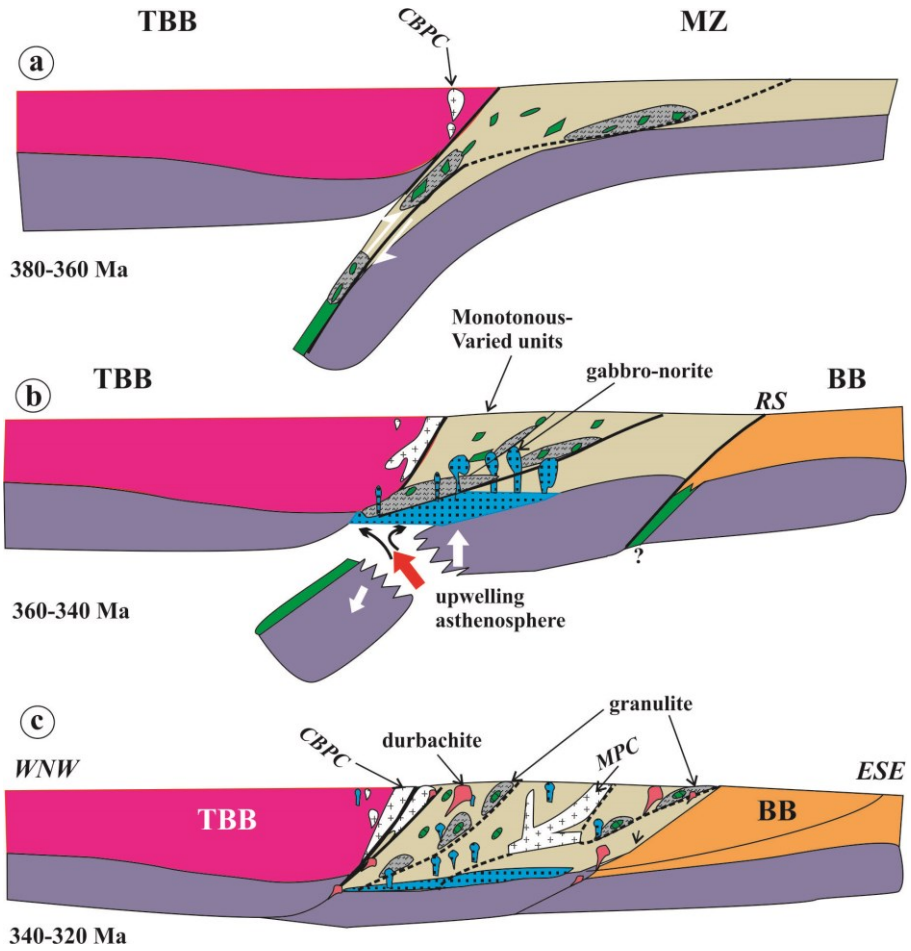

Fig. 11. Tentative WNW-ESE cross-sections illustrating the sequence of Variscan orogenic processes in the Moldanubian part of the Bohemian Massif (modified from Faryad et al., 2015). Exhumation of HP-UHP rocks (a) was followed by slab breakoff and upwelling of the asthenosphere belowthe accretionary complex (b). Note that bodies of HP-UHP mafic and ultramafic rocks are present within the amphibolite facies Monotonous/Varied units. (c) illustrates the final stage of the Variscan Orogeny with ultrapotassic magmatism followed by granitoid intrusions along the Moldanubian Plutonic Complex (MPC). TBB - Teplá-Barrandian Block, BB - Brunovistulian Block, MZ - Moldanubian Zone, RS - Rhenohercynian suture.

The generation of a large volume of durbachitic magma, forming relatively large plutons in the Moldanubian Zone, probably occurred by a combination of melting of the metasomatized mantle (Janoušek and Holub, 2007) and assimilation with crustal material. However, this process occurred subsequent to the intrusions of gabbro-norric magma and heating of the crust. As indicated by von Raumer et al. (2013), the presence of ultrapotassic rocks is not restricted only to the Bohemian Massif, but they are distributed along the whole European Variscan Belt (Fig. 1a). The swarm of lamprophyre dykes of Permian (265 Ma) age in Gredos (the Iberian Massif) occurred long after the Variscan collisional process was ended and the lamprophyre magma is interpreted as resulting from melting of metasomatized mantle lithosphere within the garnet stability field (Scarrow et al., 2011). Therefore, relation of the potassic and ultrapotassic magmatism with strike slip movement along

boundaries of lithospheric plates seems as a possible mechanism and it acts as markers of a change in mantle geodynamic regime. The whole process of the Variscan orogeny in the Moldanubian Zone was terminated by crustal thickening as a result of deep-level westward wedging (indentation) of the Brunovistulian Block (Finger et al., 2007; Schulmann et al., 2005) and formation of a dome-like structure with the Moldanubian Plutonic Complex (MPC, Žák et al., 2011) in the middle part of the Moldanubian Zone (Fig. 11c).

2.8 Conclusions

The mineral chemistry and bulk rock major and trace element concentrations in vaugnerite and syenite porphyry dykes demonstrate that their source magma was formed by very low-degrees of partial mantle melting. The primary minerals in the rocks are phlogopite, clinopyroxene, apatite, chromium-rich spinel and pseudomorphs of talc after olivine. The presence of F-rich apatite and phlogopite with carbonate suggest high concentration of F, H_2O and CO_2 in the source magma. The melting process likely occurred in the spinel stability field. Modal amounts of olivine pseudomorphs decrease but quartz increase from the vaugnerite to the syenite porphyry. Consistent with the bulk rock major and trace element chemistry, the change in modal amounts of minerals was the result of fractional crystallization and contamination with felsic crustal material during magma ascent. The new age data from both dykes are in the range of that known from Mg-K syenite plutons in the Moldanubian Zone. In addition, the syenite porphyry shows close mineralogical and geochemical similarity to Mg-K syenite plutonic rocks. The ultrapotassic magma was likely formed along transcurrent shear zones or boundaries of lithospheric blocks that occurred shortly after slab break-off and exhumation of the granulite facies rocks from the lower and middle crustal levels.

Acknowledgments

This work was supported by the Czech Science Foundation (research project number 13-06958S). The authors thank M. Racek and R. Jedlička for their help with microprobe analyses. We thank A. Fabbrizio for discussion during manuscript preparation. We are grateful to S. Couzinié and L. Krmíček for detailed reviews which helped us to considerably improve the manuscript. N. Eby is thanked for his editorial handling.

References

Abdelfadil, K.M., Romer, L.R., Glodny, J., 2014. Mantle wedge metasomatism revealed by Li isotopes in orogenic lamprophyres. Lithos 196–197, 14–26.

Ackerman, L., Pašava, J., Erban, V., 2013. Re-Os geochemistry and geochronology of the Ransko gabbro-peridotite massif, Bohemian Massif. Mineralium Deposita 48, 799–804.

Arai, S., 1984. Pressure-temperature dependent compositional variation of phlogopitic micas in upper mantle peridotites. Contributions to Mineralogy and Petrology 87, 260–264.

Atherton, M.P., Ghani, A.A., 2002. Slab breakoff: a model for Caledonian, Late Granite syncollisional magmatism in the orthotectonic (metamorphic) zone of Scotland and Donegal, Ireland. Lithos 62, 65–85.

Babuška, V., Plomerová, J., 2013. Boundaries of mantle-lithosphere domains in the Bohemian Massif as extinct exhumation channels for high-pressure rocks. Gondwana Research 23, 973–987.

Bea, F., Montero, P., Molina, J.F., 1999. Mafic precursors, peraluminous granitoids, and late lamprophyres in the Avila batholith: a model for the generation of Variscan batholiths in Iberia. Journal of Geology 107, 399–419.

Boynton, W.V., 1984. Chapter 3. Cosmochemistry of the rare earth elements: meteorite studies. In: Henderson, P. (Ed.), Rare Earth Element Geochemistry Developments in Geochemistry 2. Elsevier, Amsterdam, pp. 115–152.

Cabero, M.T., Mecoleta, S., López-Moro, F. J., 2012. OPTIMASBA: a Microsoft excel workbook to optimise the mass-balance modelling applied to magmatic differentiation processes and subsolidus overprints. Computers & Geosciences 42, 206–211.

Chemenda, A.I., Mattauer, M., Malavieille, J., Bokun, A. N., 1995. A mechanism for syncollisional rock exhumation and associated normal faulting: results from physical modelling. Earth and Planetary Science Letters 132, 225–232.

Clarke, D.B., 2007. Assimilation of xenocrysts in granitic magmas: principles, processes, proxies and problems. Canadian Mineralogist 45, 5–30.

Conceição, R.V., Green, D.H., 2004. Derivation of potassic (shoshonitic) magmas by decompression melting of phlogopite + pargasite lherzolite. Lithos 72, 209–229.

Condamine, P., Médard, E., 2014. Experimental melting of phlogopite bearing mantle at 1GPa: implications for potassic magmatism. Earth and Planetary Science Letters 397, 80–92.

Condon, D.J., Schoene, B., McLean, N.M., Bowring, S.A., Parrish, R.R., 2015. Metrology and traceability of U-Pb isotope dilution geochronology (EARTHTIME tracer calibration part I). Geochimica et Cosmochimica Acta 164, 464–480.

Conticelli, S., 1998. The effect of crustal contamination on ultrapotassic magmas with lamproitic affinity: mineralogical, geochemical and isotope data fromthe Torre Alfina lavas and xenoliths, Central Italy. Chemical Geology 149, 51–81.

Couzinié, S., Moyen, J.-F., Villaros, A., Paquette, J.-L., Scarrow, J.H., Marignac, C., 2014. Temporal relationships between Mg-K mafic magmatism and catastrophic melting of the Variscan crust in the southern part of Velay Complex (Massif Central, France). Journal of Geosciences 59 (1), 69–86.

Davies, J.H., von Blanckenburg, F., 1995. Slab breakoff: a model of lithospheric detachment and its test in the magmatism and deformation of collisional orogens. Earth and Planetary Science Letters 129, 85–102.

Davydov, V.I., Crowley, J.L., Schmitz,M.D., Poletaev, V.I., 2010. High-precision U-Pb zircon age calibration of the global Carboniferous time scale and Milankovitch-band cyclicity in the Donets Basin, eastern Ukraine. Geochemistry, Geophysics, Geosystems 11 (1), 1–22.

Edel, J.B., Schulmann, K., Holub, F.V., 2003. Anticlockwise and clockwise rotations of the Eastern Variscides accommodated by dextral lithospheric wrenching: palaeomagnetic and structural evidence. Journal of the Geological Society 160, 209–218.

Edgar, A.D., Arima, M., 1983. Conditions of phlogopite crystallization in ultrapotassic volcanic rocks. Mineralogical Magazine 47, 11–19.

Edgar, A.D., Mitchell, R.H., 1997. Ultra high pressure-temperature melting experiments on an SiO_2-rich lamproite from Smoky Butte, Montana: derivation of siliceous lamproite magmas from enriched sources deep in the continental mantle. Journal of Petrology 38, 457–477.

Edgar, A.D., Pizzolato, L.A., Sheen, J., 1996. Fluorine in igneous rocks and minerals with emphasis on ultrapotassic mafic and ultramafic magmas and their mantle source regions. Mineralogical Magazine 60, 243–257.

Faryad, S.W., 2011. Distribution and geological position of high-/ultrahigh-pressure units within the European Variscan Belt: a review. In: Dobrzhinetskaya, L., Faryad, S.W., Wallis, S., Cuthbert, S. (Eds.), Ultrahigh Pressure Metamorphism: 25 Years After the Discovery of Coesite and Diamond. Elsevier, pp. 361–397.

Faryad, S.W., Fišera, M., 2015. Olivine-bearing symplectites in fractured garnet from eclogite, Moldanubian Zone (Bohemian Massif) – a short-lived, granulite facies event. Journal of Metamorphic Geology 33, 597–612.

Faryad, S.W., Kachlík, V., 2013. New evidence of blueschist facies rocks and their geotectonic implication for Variscan suture(s) in the Bohemian Massif. Journal of Metamorphic Geology 31, 63–82.

Faryad, S.W., Žák, J., 2016. High-pressure granulites of the Podolsko complex, Bohemian Massif: an example of crustal rocks that were subducted to mantle depths and survived a pervasivemid-crustal high-temperature overprint. Lithos 246–247, 246–260.

Faryad, S.W., Jedlicka, R., Collett, S., 2013. Eclogite facies rocks of the Monotonous unit, clue to Variscan suture in the Moldanubian Zone (Bohemian Massif). Lithos 179, 353–363.

Faryad, S.W., Kachlík, V., Sláma, J., Hoinkes, G., 2015. Implication of corona formation in a metatroctolite to the granulite facies overprint of HP-UHP rocks in the Moldanubian Zone (Bohemian Massif). Journal of Metamorphic Geology 33, 295–310.

Faryad, S.W., Kachlík, V., Sláma, J., Jedlicka, R., 2016. Coincidence of gabbro and granulite formation and their implication for Variscan HT metamorphism in the Moldanubian Zone (Bohemian Massif), example from the Kutná Hora Complex. Lithos 264, 56–69.

Faryad, S.W., Nahodilová, R., Dolejš, D., 2010. Incipient eclogite facies metamorphism in the Moldanubian granulites revealed by mineral inclusions in garnet. Lithos 114, 54–69.

Finger, F., Gerdes, A., Janoušek, V., René, M., Riegler, G., 2007. Resolving the Variscan evolution of the Moldanubian sector of the Bohemian Massif: the significance of the Bavarian and the Moravo-Moldanubian tectonometamorphic phases. Journal of Geosciences 52 (1–2), 9–28.

Finger, F., Roberts, M.B., Haunschmid, B., Schermaier, A., Steyrer, H.B., 1997. Variscan granitoids of Central Europe: their typology, potential sources and tectonothermal relations. Mineralogy and Petrology 61, 67–96.

Foley, S.F., Venturelli, G., Green, D.H., Toscani, L., 1987. Ultrapotassic rocks: characteristics, classification and constraints for petrogenetic models. Earth-Science Reviews 24, 81–134.

Foster, M.D., 1960. Interpretation of the composition of trioctahedral micas. U. S. Geological Survey Professional Papers 354-B, pp. 11–46.

Franke,W., 2000. The mid-European segment of the variscides: tectonostratigraphic units, terrane boundaries and plate tectonic evolution. In: Franke,W., Haak, V., Oncken, O., Tanner, D. (Eds.), Orogenic Processes: Quantification and Modelling in the Variscan Belt. Geological Society, London, Special Publication 179, pp. 35–61.

Friedl, G., Finger, F., Paquette, J.L., von Quadt, A.,McNaughton, N.J., Fletcher, I.R., 2004. Pre-Variscan geological events in the Austrian part of the Bohemian Massif deduced from U-Pb zircon ages. International Journal of Earth Sciences 93, 802–823.

Gerdes, A., Friedl, G., Parrish, R.R., Finger, F., 2003. High-resolution geochronology of Variscan granite emplacement – the South Bohemian Batholith. Journal of the Czech Geological Society 48, 53–54.

Green, T.H., Pearson, N.J., 1986. Ti-rich accessory phase saturation in hydrous mafic-felsic compositions at high P, T. Chemical Geology 54, 185–201.

Guo, Z., Wilson, M., Liu, J., Mao, Q., 2006. Post-collisional, potassic and ultrapotassic magmatism of the northern Tibetan plateau: constraints on characteristics of the mantle source, geodynamic setting and uplift mechanisms. Journal of Petrology 47 (6), 1177–1220.

Gupta, A.K., 2015. Origin of Potassium-Rich Silica-Deficient Igneous Rocks. Springer, New York, 536 pp.

Holub, F.V., 1997. Ultrapotassic plutonic rocks of the durbachite series in the Bohemian Massif: petrology, geochemistry and petrogenetic interpretation. Journal of Geological Sciences - Economic Geology, Mineralogy 31, 5–26.

Holub, F.V., Cocherie, A., Rossi, P., 1997. Radiometric dating of granitic rocks from the Central Bohemian Plutonic Complex (Czech Republic): constraints on the chronology of thermal and tectonic events along the Moldanubian-Barrandian boundary. Comptes Rendus de l'Académie des Sciences Paris 325, 19–26.

Holub, F.V., Klečka, M., Matějka, D., 1995. Moldanubian zone: igneous activity. In: Dallmeyer, D., Franke, W., Weber, K. (Eds.), Pre-Permian Geology of Central and Eastern Europe. Springer, Berlin, pp. 444–452.

Hughes, C.J., 1982. Igneous Petrology. Elsevier (551 pp.).

Jaffey, A.H., Flynn, K.F., Glendenin, L.E., Bentley, W.C., Essling, A.M., 1971. Precision measurements of half-lives and specific activities of ^{235}U and ^{238}U. Physical Review C 4 (5), 1889–1906.

Janoušek, V., Gerdes, A., 2003. Timing the magmatic activity within the Central Bohemian Pluton, Czech Republic: conventional U-Pb ages for the Sázava and Tábor intrusions and their geotectonic significance. Journal of the Czech Geological Society 48, 70–71.

Janoušek, V., Holub, F.V., 2007. The causal link between HP-HT metamorphism and ultrapotassic magmatism in collisional orogens: case study from the Moldanubian Zone of the Bohemian Massif. Proceedings of the Geologists Association 118, 75–86.

Janoušek, V., Bowes, D.R., Rogers, G., Farrow, C.M., Jelínek, E., 2000. Modelling diverse processes in the petrogenesis of a composite batholith: the Central Bohemian Pluton, Central European Hercynides. Journal of Petrology 41, 511–543.

Janoušek, V., Gerdes, A., Vrána, S., Finger, F., Erban, V., Friedl, G., Braithwaite, C.J.R., 2006. Low-pressure granulites of the Lišov massif, southern Bohemia: Viséan metamorphism of Late Devonian plutonic arc rocks. Journal of Petrology 47, 705–744.

Janoušek, V., Wiegand, B., Žák, J., 2010. Dating the onset of Variscan crustal exhumation in the core of the Bohemian Massif: new U-Pb single zircon ages from the high-K calc-alkaline granodiorites of the Blatná suite, Central Bohemian Plutonic Complex. Journal of the Geological Society London 167, 347–360.

Jedlicka, R., Faryad, S.W., Hauzenberger, C., 2015. Prograde metamorphic history of UHP granulites from the Moldanubian Zone (Bohemian Massif) revealed by major element and Y + REE zoning in garnets. Journal of Petrology 56 (10), 2069–2088.

Kempton, P.D., 1987. Mineralogical and geochemical evidence for differing styles of metasomatism in spinel lherzolite xenoliths: enriched mantle source region of basalt? In: Menzies, M.A., Hawkesworth, C.J. (Eds.), Mantle Metasomatism. Academic, London, pp. 45–89.

Klemme, S., 2004. The influence of Cr on the garnet-spinel transition in the Earth's mantle: experiments in the system MgO-Cr_2O_3-SiO_2 and thermodynamic modelling. Lithos 77, 639–646.

Košler, J., Konopásek, J., Sláma, J., Vrána, S., 2014. U-Pb zircon provenance of Moldanubian metasediments in the Bohemian Massif. Journal of Geological Society 171, 83–95.

Kovaříková, P., Siebel, W., Jelínek, E., Štemprok, M., Kachlík, V., Holub, F.V., Blecha, V., 2007. Petrology, geochemistry and zircon ages for redwitzite at Abertamy, NW Bohemian Massif (Czech Republic): tracing the mantle component in Late Variscan intrusions. Chemie der Erde 67, 151–174.

Krmíček, L., Cempírek, J., Havlín, A., Přichystal, A., Houzar, S., Krmíčková, M., Gadas, P., 2011. Mineralogy and petrogenesis of a Ba-Ti-Zr-rich peralkaline dyke from Šebkovice (Czech Republic): recognition of the most lamproitic Variscan intrusion. Lithos 121, 74–86.

Krmíček, L., Romer, R.L., Ulrych, J., Glodny, J., Prelević, D., 2016. Petrogenesis of orogenic lamproites of the Bohemian Massif: Sr-Nd-Pb-Li isotope constraints for Variscan enrichment of ultra-depleted mantle domains. Gondwana Research 35, 198–2016.

Kroner, U., Romer, R.L., 2013. Two plates – many subduction zones: the Variscan orogeny reconsidered. Gondwana Research 24, 298–329.

Kröner, A., Wendt, I., Liew, T.C., Compston, W., Todt, W., Fiala, J., Vaňková, V., Vaněk, J., 1988. U-Pb zircon and Sm-Nd model ages of high-grade Moldanubian metasediments, Bohemian Massif, Czechoslovakia. Contributions to Mineralogy and Petrology 99, 257–266.

Krs, M., Krsová, M., Pruner, P., 1995. Palaeomagnetism and palaeogeography of Variscan formations of the Bohemian Massif, comparison with other regions in Europe. Studia Geophysica et Geodaetica 39, 309–319.

Kusiak, M.A., Dunkley, D.J., Suzuki, K., Kachlík, V., Kędzior, A., Lekki, J., Opluštil, S., 2010. Chemical (non-isotopic) and isotopic dating of Phanerozoic zircon. A case study of durbachite from the Třebíč Pluton, Bohemian Massif. Gondwana Research 17, 153–161.

Le Bas, M.J., Le Maitre, R.W., Streckeisen, A., Zanettin, B., 1986. A chemical classification of volcanic rocks based on the total alkali-silica diagram. Journal of Petrology 27, 745–750.

Ludwig, K.R., 1998. On the treatment of concordant uranium-lead ages. Geochimica et Cosmochimica Acta 62, 665–676.

Mahéo, G., Blichert-toft, J., Pin, C., Guillot, S., Pêcher, A., 2009. Partial melting of mantle and crustal sources beneath south Karakorum, Pakistan: implications for the Miocene geodynamic evolution of the India-Asia convergence zone. Journal of Petrology 50 (3), 427–449.

Mallik, A., Nelson, J., Dasgupta, R., 2015. Partial melting of fertile peridotite fluxed by hydrous rhyolitic melt at 2–3 GPa: implications for mantle wedge hybridization by sediment melt and generation of ultrapotassic magmas in convergent margins. Contributions to Mineralogy and Petrology 169 (48), 1–24.

Mattinson, J.M., 2005. Zircon U-Pb chemical abrasion ("CA-TIMS") method: combined annealing and multi-step partial dissolution analysis for improved precision and accuracy of zircon ages. Chemical Geology 220, 47–66.

McLean, N.M., Condon, D.J., Schoene, B., Bowring, S.A., 2015. Evaluating uncertainties in the calibration of isotopic reference materials and multi-element isotopic tracers (EARTHTIME tracer calibration part II). Geochimica et Cosmochimica Acta 164, 481–501.

Mitchell, R.H., Bergman, S.C., 1991. Petrology of Lamproites. Plenum Press, NewYork (447 pp.).

Moyen, J.-F., 2009. High Sr/Y and La/Yb ratios: the meaning of the "adakitic signature". Lithos 112, 556–574.

Parat, F., Holtz, F., René, M., Almeev, R., 2010. Experimental constraints on ultrapotassic magmatism from the Bohemian Massif (durbachite series, Czech Republic). Contribution to Mineralogy and Petrology 159, 331–347.

Perraki, M., Faryad, S.W., 2014. First finding of microdiamond, coesite and other UHP phases in felsic granulites in the Moldanubian Zone: implications for deep subduction and a revised geodynamic model for Variscan Orogeny in the Bohemian Massif. Lithos 202–203, 157–166.

Platt, R.G., Mitchell, R.H., 1982. The Marathon dikes: ultrabasic lamprophyres from the vicinity of McKellar Harbour. N. W. Ontario. American Mineralogist 67, 907–916.

Rickwood, P.C., 1989. Boundary lines within petrologic diagrams which use oxides of major and minor elements. Lithos 22, 247–263.

Roden, M.F., Frey, F.A., Francis, D.M., 1984. An example of consequent mantle metasomatism in peridotite inclusions from Nunivak Island, Alaska. Journal of Petrology 25, 546–577.

Sabatier, H., 1980. Vaugnérites and granites, a peculiar association of basic and acid rocks. Bulletin de Minéralogie 103, 507–522.

Scarrow, J.H., Bea, F., Montero, P., Molina, J.F., 2009. Shoshonites, vaugnerites and potassic lamprophyres: similarities and differences between 'ultra'-high-K rocks. Earth and Environmental Science Transactions of the Royal Society of Edinburgh 99, 159–175.

Scarrow, J.H., Molina, J.F., Bea, F., Montero, P., Vaughan, A.P.M., 2011. Lamprophyre dikes as tectonic markers of late orogenic transtension timing and kinematics: a case study from the Central Iberian Zone. Tectonics 30 (TC4007), 1–22.

Schalterger, U., 1997. Magma pulses in the Central Variscan Belt: episodic melt generation and emplacement during lithospheric thinning. Terra Nova 9 (5/6), 242–245.

Schmitz, M.D., Davydov, V.I., 2012. Quantitative radiometric and biostratigraphic calibration of the global Pennsylvanian - Early Permian time scale. Geological Society of America Bulletin 124, 549–577.

Schmitz, M.D., Schoene, B., 2007. Derivation of isotope ratios, errors and error correlations for U-Pb geochronology using ^{205}Pb-^{235}U-(^{233}U)-spiked isotope dilution thermal ionization mass spectrometric data. Geochemistry, Geophysics, Geosystems 8 (8), 1–20.

Schulmann, K., Konopásek, J., Janoušek, V., Lexa, O., Lardeaux, J.-M., Edel, J.-B., Štípská, P., Ulrich, S., 2009. An Andean type Palaeozoic convergence in the Bohemian Massif. Comptes Rendu Geoscience 341, 266–286.

Schulmann, K., Kröner, A., Hegner, E., Wendt, I., Konopásek, J., Lexa, O., Štípská, P., 2005. Chronological constraints on the pre-orogenic history, burial and exhumation of deep-seated rocks along the eastern margin of the Variscan orogen, Bohemian Massif, Czech Republic. American Journal of Science 305, 407–448.

Schulmann, K., Lexa, O., Janoušek, V., Lardeaux, J.M., Edel, J.B., 2014. Anatomy of a diffuse cryptic suture zone: an example from the Bohemian Massif, European Variscides. Geology 42 (4), 275–278.

Scott, J.M., Konrad-Schmolke, M., O'Brien, P.J., Günter, C., 2013. High-T, low-P formation of rare olivine-bearing symplectites in Variscan eclogite. Journal of Petrology 54, 1375–1398.

Shand, S.J., 1927. The problem of the alkaline rocks. Proceedings of the Geological Society of South Africa 25, 19–33.

Siebel, W., Chen, F., 2009. Zircon Hf isotope perspective on the origin of granitic rocks from eastern Bavaria, SW Bohemian Massif. International Journal of Earth Sciences 99, 993–1005.

Siebel, W., Chen, F., Satir, M., 2003. Late-Variscan magmatism revised: new implications from Pb-evaporation zircon ages on the emplacement of redwitzites and granites in NE Bavaria. International Journal of Earth Sciences 92, 36–53.

Slaughter, J., Kerrick, D.M., Wall, V.J., 1975. Experimental and thermodynamic study of equilibria in the system CaO-MgO-SiO_2-H_2O-CO_2. American Journal of Science 27S, 143–162.

Stacey, J.S., Kramers, J.D., 1975. Approximation of terrestrial lead isotope evolution by a two-stage model. Earth and Planetary Science Letters 26, 207–221.

Štemprok, M., Dolejš, D., Holub, F.V., 2014. Late Variscan calc-alkaline lamprophyres in the Krupka ore district, Eastern Krušné hory/Erzgebirge: their relationship to Sn-W mineralization. Journal of Geosciences 59, 41–68.

Sun, S.-S., McDonough, W.F., 1989. Chemical and isotopic systematics of oceanic basalts: implications for mantle composition and processes. Geological Society, London, Special Publications 42, 313–345.

Tait, J., Bachtadse, V., Soffel, H.C., 1994. Silurian paleogeography of Armorica: new paleomagnetic data from central Bohemia. Journal of Geophysical Research 99, 2897–2907.

Taylor, S.R., McLennan, S.M., 1985. The Continental Crust: Its Composition and Evolution. Blackwell, Oxford (312 pp.).

Teipel, U., Finger, F., Rohrmüller, J., 2012. Remnants of Moldanubian HP-HT granulites in the eastern part of the Bavarian Forest (southwestern Bohemian Massif); evidence from SHRIMP zircon dating and whole rock geochemistry. Zeitschrift der Deutschen Gesellschaft fuer Geowissenschaften 163, 137–152.

Thirlwall, M.F., Smith, T.E., Graham, A.M., Theodorou, N., Hollings, P., Davidson, J.P., Arculus, R.J., 1994. High field strength element anomalies in arc lavas: source or process? Journal of Petrology 35, 819–838.

Thorkelson, D.J., 1992. Volcanic and Tectonic Evolution of the Hazelton Group in Spatsizi River (104H) Map-area, north-Central British Columbia. (Ph.D. thesis). Carleton Univ., Ottawa, Ontario, pp. 1–121.

Turner, S.P., Platt, J.P., George, R.M.M., Kelley, S.P., Pearson, D.G., Noveww, G.M., 1999. Magmatism associated with orogenic collapse of the Betic-Alboran domain, SE Spain. Journal of Petrology 40, 1011–1036.

van Hunen, J., Allen, M.B., 2011. Continental collision and slab break-off: a comparison of 3-D numerical models with observations. Earth and Planetary Science Letters 302, 27–37.

Vaughan, A.P.M., Scarrow, J.H., 2003. K-rich mantle metasomatism control of localization and initiation of lithospheric strike-slip faulting. Terra Nova 15, 163–169.

Verner, K., Žák, J., Hrouda, F., Holub, F., 2006. Magma emplacement during exhumation of the lower- to mid-crustal orogenic root: the Jihlava syenitoid pluton, Moldanubian Unit, Bohemian Massif. Journal of Structural Geology 28, 1553–1567.

Verner, K., Žák, J., Nahodilová, R., Holub, F., 2008. Magmatic fabrics and emplacement of the cone-sheet-bearing Knížecí Stolec durbachitic pluton (Moldanubian Unit, Bohemian Massif): implications for mid-crustal reworking of granulitic lower crust in the Central European Variscides. International Journal of Earth Sciences 97, 19–33.

Villaseca, C., Pérez-Soba, C., Merino, E., Orejana, D., López-García, J.A., 2008. Contrasting crustal sources for peraluminous granites of the segmented Montes de Toledo Batholith. Journal of Geosciences 53, 263–280.

von Raumer, J., Bussy, F., Schaltegger, U., Schulz, B., Stampfli, G.M., 2013. Pre-Mesozoic Alpine basements - their place in the European Paleozoic framework. Geological Society of America Bulletin 125 (1/2), 89–108.

von Raumer, J.F., Finger, F., Veselá, P., Stampfli, G.M., 2014. Durbachites-vaugnerites - a geodynamic marker in the central European Variscan orogen. Terra Nova 26, 85–95.

von Seckendorf, V., Timmerman, M.J., Kramer, W., Wrobel, P., 2004. New $^{40}Ar/^{39}Ar$ ages and geochemistry of Late Carboniferous–Early Permian lamprophyres and related volcanic rocks in the Saxothuringian Zone of the Variscan Orogen (Germany). In: Wilson, M., Neumann, E.R., Timmermann, G.R., Heremans, M., Larsen, B.T. (Eds.), Permo-Carboniferous 106 Magmatism and Rifting in Europe. Geological Society, London, Special Publications 223, pp. 335–359.

Vrána, S., Blümel, P., Petrakakis, K., 1995. Metamorphic evolution of the Moldanubian Zone. In: Dallmeyer, R.D., Franke, W., Weber, K. (Eds.), Pre-Permian Geology of Central and Eastern Europe. Springer, Berlin, pp. 453–466.

Wendt, J.I., Kröner, A., Fiala, J., Todt,W., 1993. Evidence from zircon dating for existence of approximately 2.1 Ga old crystalline basement in southern Bohemia, Czech Republic. Geologische Rundschau 82, 42–50.

Williams, H.M., McCammon, C.A., Peslier, A.H., Halliday, A.N., Teutsch, N., Levasseur, S., Burg, J.P., 2004. Iron isotope fractionation and the oxygen fugacity of the mantle. Science 304, 1656–1659.

Žák, J., Verner, K., Finger, F., Faryad, S.W., Chlupáčová,M., Veselovský, F., 2011. The generation of voluminous S-type granites in the Moldanubian unit, Bohemian Massif, by rapid isothermal exhumation of the metapelitic middle crust. Lithos 121, 25–40.

Žák, J., Verner, K., Janoušek, V., Holub, F.V., Kachlík, V., Finger, F., Hajná, J., Tomek, F., Vondrovic, L., Trubač, J., 2014. A plate-kinematic model for the assembly of the Bohemian Massif constrained by structural relations around granitoid plutons. Geological Society, Special Publications 405, 169–196.

Zeitlhofer, H., Grasemann, B., Petrakakis, K., 2016. Variscan potassic dyke magmatism of durbachitic affinity at the southern end of the Bohemian Massif (Lower Austria). International Journal of Earth Sciences 105, 1175–1197.

CHAPTER 3

MINERAL TEXTURES OF OLIVINE MINETTE AND THEIR SIGNIFICANCE FOR CRYSTALLIZATION HISTORY OF PARENTAL MAGMA; AN EXAMPLE FROM THE MOLDANUBIAN ZONE (THE BOHEMIAN MASSIF)

Šárka Kubínová [a], Shah Wali Faryad [a]

[a] *Institute of Petrology and Structural Geology, Charles University, Albertov 6, Prague 12843, Czech Republic*

Status: Published in Mineralogy and Petrology (2019)

ABSTRACT

One of the best-preserved dykes of olivine minette among the lamprophyre dyke swarm in the Moldanubian Zone of the Bohemian Massif (Czech Republic) was investigated. The minette, exposed at Horní Kožlí Village (near Prachatice town), has porphyric texture with phenocrysts of olivine, clinopyroxene, orthopyroxene and biotite in a fine-grained matrix consisting of Kfeldspar, biotite, clinopyroxene and minor plagioclase and quartz. Accessory minerals are apatite, Cr-rich spinel and iron sulphides. Olivine is mostly replaced by talc and rimmed by two zones (coronas) - a talc-rich inner zone and a biotite-rich outer zone. Rarely, larger grains of quartz with a corona of clinopyroxene are present. The clinopyroxene grows mostly perpendicular to the quartz rim and radially penetrates the quartz crystal.

Three stages of mineral crystallization were distinguished. The first stage with apatite, olivine, biotite, spinel, orthopyroxene and part of the clinopyroxene occurred in the mantle position. During the second stage, felsic phases (K-feldspar, plagioclase, quartz) in the matrix were crystallized. The enrichment of the residual melt by silica and Na occurred as the result of both fractionation and contamination during magma ascent through the granulite facies crust during post-collision orogeny in the Bohemian Massif. Minerals related to the third stage were formed during filling of the vesicles (quartz with reaction rims of clinopyroxene) and subsequent alteration (talc after olivine). The origin of quartz with clinopyroxene reaction rims (‘quartz ocelli’) is explained by filling of cavities formed by the escape of volatiles.

Keywords*: minette, dyke swarm, ultrapotassic magmatism, Bohemian Massif*

3.1 Introduction

Lamprophyre dykes are considered as a tectonic marker of late orogenic processes and provide insights into large-scale mantle processes and mantle-crust interplay controlled by, or potentially controlling, the regional geodynamic evolution (Rock 1984, 1987, 1991; Scarrow et al. 2011). Compositional variation of lamprophyre depends on the source magma and degree of metasomatism of the upper mantle (Abdelfadil et al. 2014; Awdankiewicz 2010; Vaughan and Scarrow 2003). Therefore, its crystallization, fractionation and possibly contamination during magma ascent through the crust are essential to understand geodynamic processes operating during post-collision events in orogenic belts. As lamprophyre magma usually contains high volatile contents, which results in alteration of original minerals ascribed to subsolidus autometasomatic to deuteric processes (Bratzdrum et al. 2009; Rock 1991), most studies are focused on bulk rock and trace element chemistry and isotopic ratios of the rocks. Less information exists about mineral textures and compositional variations of primary phases, which give direct evidence about the succession of minerals and changes of magma composition during their crystallization.

Numerous lamprophyre dykes of (late)-Variscan age occur in the Bohemian Massif (Fig. 1). They are present both in the Saxothuringian (Kovaříková et al. 2007; Krmíček 2010; Siebel et al. 2003; Štemprok et al. 2014; von Seckendorf et al. 2004) and the Moldanubian Zone (Krmíček 2010; Krmíček et al. 2011, 2016). Available geochronological data from lamprophyre dykes in the Moldanubian Zone indicate crystallization ages around 335–342 Ma (e.g. Kubínová et al. 2017), which overlaps the ages of graniotoids from the Central Bohemian Plutonic Complex (Holub et al. 1997a) and some gabbro-troctolite intrusions associated with granulite facies metamorphism (for ref. see Faryad et al. 2016; Schulmann et al. 2005). Similar to other orogenic belts, the lamprophyres are strongly modified by alteration of primary minerals (Kubínová et al. 2017). Their classification and compositional variation, that ranges from high potassic to calc-alkaline members, are mostly based on their bulk rock and trace element chemistry (Holub 1997, 1999). Because of similarity in ages and spatial relation to other magmatic suites, mainly the presence of lamprophyre dykes in the vicinity of the arc related Central Bohemian Plutonic Complex (Janoušek et al. 2004), crystallization history of the source lamprophyre magma, its fractionation and/or possible interaction with magma generated in crustal levels are not always clear.

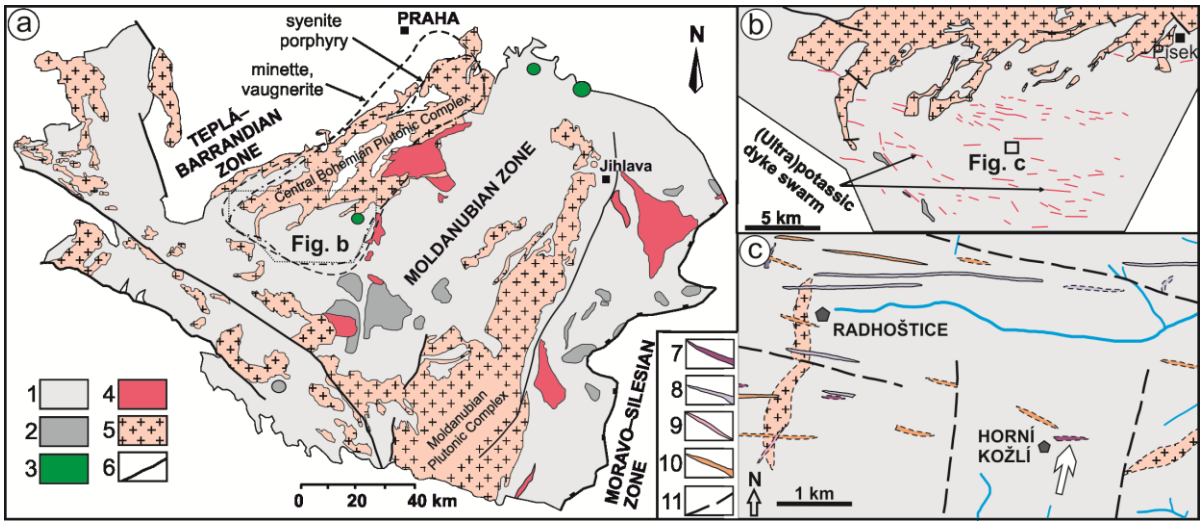

Fig. 1 a The Moldanubian Zone of the Bohemian Massif with Variscan granitoid plutons (Central Bohemian Plutonic Complex, Moldanubian Plutonic Colmplex) and ultrapotassic plutons. The dashed and dotdashed lines defines the occurrence of dykes of minette to vaugnerite and syenite porphyry, **b** Distribution of the (ultra)potassic dykes in the western part of the Moldanubian Zone, **c** a detailed map shows the localization of the dyke of olivine minette (labelled by white arrow) that is associated with syenite to granite porphyries. Explanations to (**a**) and (**c**): 1 - Moldanubian Zone (unspecified), 2 - high-pressure granulites, 3 - mafic-ultramafic complexes, 4 - ultrapotassic plutonic rocks (two-pyroxene mela-syenite, porphyric amph-bt melagranite to melasyenite (durbachite)), 5 - granitoids, 6 - main thrusts and faults, 7 - minette, 8 - syenite porphyry, 9 - granodiorite porphyry, 10 - leucocratic granite, 11 - presumed faults

In this paper we present mineral textures of an olivine minette dyke with relatively well preserved primary phases. It comes from the western part of the Moldanubian Zone, where predominantly west-east trending lamprophyre dykes of variable compositions penetrate the metamorphic basement and the Central Bohemian Plutonic Complex (Fig. 1). The aim of this study is to: 1) distinguish the original phases crystallized from the parental melt in the mantle depth, 2) verify compositional changes of minerals during crystallization and 3) constrain succession of mineral formation in various crustal positions, including replacement textures. The results are used to discuss the origin and possible implication of the lamprophyre dyke formation within post-Variscan collisional magmatic events in the Bohemian Massif.

3.2 Geological setting

The Bohemian Massif represents the eastern part of the Variscan orogenic belt and it is formed by two zones (Saxothuringian and Moldanubian) and two blocks (the Teplá-Barrandian and Brunovistulian, Fig. 1a). All they consist of metamorphic basement rocks with various amounts granitoid plutons. The zones differ from the blocks by the presence of high- to ultrahigh-pressure

(HP-UHP) rocks formed during Variscan orogeny. The HP-UHP rocks form boudins and lenses with gneisses, migmatite and granulite and they all experienced amphibolite-granulite facies metamorphism. (For more details about basement units, their metamorphism and age relations see Faryad et al. 2015; Košler et al. 2014; Kröner et al. 1988; Medaris et al. 2006; Schulmann et al. 2005; Wendt et al. 1993).

The contact of the Teplá-Barrandien Block and the Moldanubian Zone (Fig. 1) is a significant tectonic boundary that permits the formation of voluminous granitoid bodies and minor mafic intrusions of Variscan age and a large number of dykes of late-Variscan age. Based on their composition and ages, the magmatic rocks can be subdivided into four main groups (see e.g. Finger et al. 1997; Holub et al. 1995, 1997b; Janoušek et al. 1995; Schalterger 1997; Žák et al. 2014). The first two groups are represented by granitoid complexes that are exposed along two belts, the Central Bohemian plutonic complex (CBPC) and the Moldanubian Plutonic Complex (MPC) (Fig. 1a). These two complexes differ from each other by age and their relations to Variscan geotectonic processes (e.g. Finger et al. 1997; Holub et al. 1997b; Schalterger 1997; Žák et al. 2014). The older (c. 355–345 Ma) CBPC straddles the border of the Teplá-Barrandian Block and is formed by subduction related calc-alkaline plutons (Holub et al. 1997a, b; Janoušek et al. 2004; Žák et al. 2014). The younger MPC is composed of peraluminous (S-type) anatectic granitoids (c. 330–300 Ma) and it was formed by extensive migmatitization and isothermal decompression of the surrounding pelitic rocks (Žák et al. 2011). The third group is represented by potassic-ultrapotassic rocks (346–337 Ma) that form several isolated plutons and dyke swarms (Fig. 1a and b; Holub 1997; Janoušek and Gerdes 2003; Janoušek et al. 2010; Krmíček 2010; Kubínová et al. 2017). The last group of Variscan igneous rocks have mafic to ultramafic compositions (gabbro, norite, trocolite, pyroxenite, Fig. 1a) and around 340 Ma age (Ackerman et al. 2013; Faryad et al. 2015, 2016). Some of the mafic-ultramafic rocks are unmetamorphosed, but others record amphibolite-granulite facies conditions and therefore were assumed to be pre-Variscan in age.

The magmatic rocks of the CBPC and adjacent metamorphic rocks of the Moldanubian Zone and the Teplá-Barrandien Block are injected by numerous dykes and dyke swarms (~ 340 to 335 Ma; Holub et al. 1997b, 2009, 2012) with variable petrographic and geochemical composition. These dykes are mafic to felsic in composition and vary from calc-alkaline to (ultra)-potassic. The rock-types include lamprophyric rocks (spessartite, kersantite, minette, vaugnerite), gabbrodiorite to granodiorite porphyries and melasyenite to melagranite porphyries. Their diverse geochemical character indicates a variability of mantle and crustal sources of individual magma pulses (for a brief overview see Holub 1999, 2007). The ultrapotassic dykes (minettes, vaugnerites and melasyenite to melagranite porphyries) are distributed over about 30 × 100 km area that mostly covers the CBPC (Fig. 1a). They have a thickness of ~25 m for melagranite to melasyenite porphyries and about 3 m for minettes and vaugnerites. The remarkable feature of these dykes is their orientations, which are

parallel in a W-E to NW-SE direction (Fig. 1b, i.e. almost perpendicular to the CPBC and to the main foliation and nappe stocks basement rocks of the Moldanubian Zone). The formation of dykes reflects the regional stress field during the Variscan orogeny (Hrouda et al. 2016).

The minette studied here is located about 10 km northwest from the Prachatice town (Fig. 1c). A contact of the west-east trending dyke with the surrounding rocks is not well exposed, but based on the fragments at the surface it can be traced along a ca 300 m distance (Dudíková-Schulmannová et al. 2014). The country rock is migmatite that consists of quartz, feldspar and biotite, and rare sillimanite, garnet and cordierite for which peak metamorphic temperatures of 630–720 °C at 0.4 GPa are estimated (Vrána et al. 1995).

3.3 Analytical methods

3.3.1 Sample and thin section preparation

Samples selected for this study come from fragments (up to 20 × 30 cm in size) that are scattered at the top of a small hill formed by migmatite. Standard-sized thin sections ~ 26 × 48 mm of ~ 30 μm thickness were prepared following routine procedures and covered with a 0.17 mm glass slip for assessment in an optical petrographic microscope under transmitted polarized light. Thin sections for assessment by EPMA (see below) were not covered, but polished with diamond pastes 9, 6 and 3 μm on cloth, and finally covered with ~15 nm carbon to reduce charging in the electron beam.

3.3.2 Bulk whole-rock geochemistry

The bulk whole-rock composition of olivine minette (Table 1) was determined at Activation Laboratories Ltd. (Ontario, Canada; www.actlabs.com) according to Code 4Litho package following lithium metaborate/tetraborate fusion with inductively coupled plasma (ICP; for major elements) and inductively coupled plasma-mass spectrometry (ICP-MS; for trace elements); loss on ignition (LOI) was determined gravimetrically. The method uses a batch system that comprises reagent blank, one of the 7 standards (prepared USGS and CANMET certified reference materials) and 17 % replicates. At the first step, samples were mixed with a flux of lithium metaborate and lithium tetraborate and fused in an induction furnace. Then, the molten melt was poured into a solution of 5 % nitric acid containing an internal standard, and mixed continuously until completely dissolved (~ 30 min). Finally, the samples were run on a combination simultaneous/sequential Thermo Jarrell-Ash ENVIRO II ICP or a Varian Vista 735 ICP. Whole-rock geochemical compositions with lower limits of detection (LLD) are given in Table 1.

Table 1 The major elements concentrations (wt%) in olivine minette

Sample	LLD	LR 727	LR 728
SiO_2	0.01	58.07	57.53
TiO_2	0.001	1.01	1.05
Al_2O_3	0.01	12.69	13.12
Fe_2O_3*	0.01	6.18	6.27
MnO	0.001	0.09	0.09
MgO	0.01	8.14	7.48
CaO	0.01	3.65	3.53
Na_2O	0.01	1.81	1.65
K_2O	0.01	5.49	5.81
P_2O_5	0.01	0.66	0.73
LOI	0.01	1.50	1.39
Total		99.29	98.65
K_2O/Na_2O		3.03	3.52
Mg#		56.84	54.40

Fe_2O_3* = total Fe as Fe_2O_3, *LOI* = Loss On Ignition, Mg# = 100 MgO/(MgO + Fe_2O_3*), *LLD* - lower limit of detection.

3.3.3 Mineral chemistry by electron probe-microanalysis (EPMA)

Chemical analyses and compositional maps of minerals were obtained with a JEOL JXA-8530F microprobe instrument, equipped with wavelength and energy dispersive spectrometers (WDS and EDS) at the Institute of Petrology and Structural Geology, Charles University. The operating conditions were 15 kV and 30 nA beam current for spot analyses and 20 kVand 120 nA for element mappings. Lower limits of detection (LLD) are in the range of 50–150 ppm for elements, and are tabulated for the respective oxides together with composition data. The used standards were quartz (Si), corundum (Al), periclase (Mg), magnetite (Fe), rhodonite (Mn), calcite (Ca), rutile (Ti), chromium oxide (Cr), vanadinite (V), albite (Na), sanidine (K), apatite (P, F). Mineral abbreviations are according to Whitney and Evans (2010).

Selected mineral analyses and calculated mineral formulas are given in Tables 2, 3, 4 and 5. Proportions of Fe^{2+} and Fe^{3+} in orthopyroxene, clinopyroxene and spinel were calculated based on cation and charge balance (see eg. Droop 1987).

Olivine end-members are forsterite Fo = 100 Mg/(Mg + Fe^{2+} + Mn) and fayalite Fa = 100 Fe/(Mg + Fe^{2+} + Mn). Pyrexene end-members are wollastonite Wo = 100 Ca/(Ca + Mg + Mn + Fe^{2+} + Fe^{3+}), enstatite En = 100 Mg/(Ca + Mg + Mn + Fe^{2+} + Fe^{3+}) and ferrosilite Fs = 100 (Fe^{2+} + Mn+

Fe^{3+})/(Ca + Mg + Mn + Fe^{2+} + Fe^{3+}). Calculated parameters are magnesium number Mg# = 100 (MgO/(MgO + FeO_{total}) and chromium number Cr# = 100 (Cr_2O_3/(Cr_2O_3+Al_2O_3).

Table 2 Selected microprobe analysis of olivine and talc in olivine minette

mineral	LLD	Ol	Ol	Tlc
position		ph-c	ph-r	ps-c
wt. %				
SiO_2	0.01	40.69	39.14	56.85
TiO_2	0.02	0.00	0.02	0.04
Al_2O_3	0.01	0.00	0.01	0.43
Cr_2O_3	0.02	0.09	0.13	0.05
V_2O_5	0.05	-	-	-
NiO	0.02	0.21	0.07	0.12
ZnO	0.02	-	-	-
FeO	0.02	9.06	17.31	6.31
MnO	0.02	0.14	0.29	0.11
MgO	0.01	49.48	42.43	27.19
CaO	0.01	0.13	0.23	0.28
Na_2O	0.01	0.01	0.01	0.04
K_2O	0.01	-	-	-
BaO	0.04	-	-	-
F	0.06	-	-	-
Cl	0.01	-	-	-
Total		99.81	99.63	91.43
Per		4(O)		11(O)
Si		0.997	0.999	3.886
Ti		0.000	0.000	0.002
Al		0.000	0.000	0.035
Cr		0.002	0.003	0.003
Ni		0.004	0.001	0.007
Fe^{2+}		0.186	0.369	0.361
Mn		0.003	0.006	0.006
Mg		1.807	1.614	2.771
Ca		0.003	0.006	0.020
Na		0.001	0.001	0.005
Fo (%)		90.55	81.12	-
Fa (%)		9.45	18.88	-
Mg#		85.99	71.02	-

LLD Lower limit of detection, position of analyses: *ph* Phenocryst, *ps* Pseudomorph; *c* Core of grain, *r* Rim of grain.

Table 3 Selected microprobe analysis of biotite in olivine minette

mineral	Bt I	Bt II	Bt III	Bt IV
position	ph-c	a-c	in Cpx ph	around Ol ph
wt. %				
SiO_2	38.21	37.48	38.78	41.40
TiO_2	4.47	4.61	4.52	0.08
Al_2O_3	13.80	13.67	13.96	13.08
Cr_2O_3	0.41	-	1.00	0.02
FeO	8.20	16.36	9.18	3.54
MnO	0.05	0.19	-	0.03
MgO	18.18	13.00	18.14	24.92
CaO	0.00	-	-	0.08
Na_2O	0.15	-	0.13	0.09
K_2O	10.16	9.88	9.66	10.41
BaO	0.58	0.70	0.78	0.00
F	0.71	-	0.61	1.92
Cl	0.01	-	-	0.03
Total	94.62	95.89	96.14	94.77
Per			22(O)	
Si	5.646	5.653	5.630	5.952
Al	2.403	2.430	2.388	2.216
Ti	0.497	0.523	0.494	0.009
Cr	0.048	0.000	0.115	0.002
Fe^{2+}	1.013	2.064	1.114	0.425
Mn	0.006	0.024	0.000	0.003
Mg	4.005	2.924	3.926	5.341
Ca	0.000	0.000	0.000	0.012
Na	0.044	0.000	0.036	0.025
K	1.915	1.901	1.789	1.908
Ba	0.033	0.041	0.044	0.000
F	0.332	0.000	0.281	0.874
Cl	0.003	0.000	0.000	0.008
Mg#	68.92	44.28	66.40	87.56

Position of analyses: ph – phenocryst, a – automorphic grain in matrix; c – core of grain.

Table 4 Selected microprobe analysis of Cr-spinel in olivine minette

mineral	Spl	Spl
position	in Ol ph	bt-zone of Ol
wt. %		
TiO_2	1.79	1.69
Al_2O_3	8.44	8.18
Cr_2O_3	52.66	54.60
V_2O_5	-	1.01
FeO	32.61	31.39
MnO	0.41	-
MgO	3.30	2.23
CaO	0.12	-
ZnO	-	1.50
Total	99.34	100.60
Per	32(O)	
Ti	0.378	0.357
Al	2.789	2.707
Cr	11.672	12.128
V	0.000	0.188
Fe^{3+}	0.783	0.000
Fe^{2+}	6.864	7.375
Mn	0.097	0.000
Mg	1.381	0.934
Ca	0.036	0.000
Zn	0.000	0.311
Mg#	86.19	86.97
Cr#	9.19	6.63

Position of analyses: *ph* Phenocryst.

Table 5 Selected microprobe analysis of pyroxenes in olivine minette

mineral	Cpx I	Cpx I	Cpx II	Cpx III	Cpx IV	Opx
type	augite	augite	augite	diopside	augite	enstatite
position	ph-c	ph-r	ph-r	a-c		ph-c
wt. %						
SiO_2	52.59	52.11	52.00	53.78	54.81	55.03
TiO_2	0.39	0.38	0.38	-	-	0.16
Al_2O_3	1.89	1.73	1.94	0.29	0.30	1.26
Cr_2O_3	0.39	0.02	0.22	-	-	0.72
FeO	6.67	8.99	7.02	10.91	8.09	10.01
MnO	0.23	0.28	0.22	0.61	0.31	0.24
MgO	16.27	14.87	16.00	11.88	15.11	30.04
CaO	21.35	21.24	21.35	23.02	21.87	1.94
Na_2O	0.17	0.14	0.17	-	-	0.02
Total	99.94	99.75	99.30	100.49	100.45	99.43
Per			6(O)			6(O)
Si	1.940	1.946	1.936	2.016	2.016	1.955
Ti	0.011	0.011	0.011	0.000	0.000	0.004
Al	0.082	0.076	0.085	0.013	0.013	0.053
Cr	0.011	0.001	0.006	0.000	0.000	0.020
Fe^{3+}	0.025	0.030	0.043	0.000	0.000	0.014
Fe^{2+}	0.181	0.250	0.175	0.344	0.250	0.284
Mn	0.007	0.009	0.007	0.019	0.010	0.007
Mg	0.895	0.828	0.888	0.664	0.829	1.592
Ca	0.844	0.850	0.851	0.924	0.862	0.074
Na	0.012	0.010	0.012	0.000	0.000	0.001
Wo (%)	43.24	43.21	43.34	47.37	44.20	3.75
En (%)	45.85	42.09	45.21	34.01	42.49	80.79
Fs (%)	10.91	14.69	11.44	18.62	13.31	15.46
Mg#	70.92	62.32	69.50	52.13	65.64	75.01

Position of analyses: *ph* Phenocryst, *a* Automorphic grain in matrix; *c* Core of grain, *r* Rim of grain.

3.4 Mineral textural relations

The studied dyke has a porphyric texture with phenocrysts of olivine, clinopyroxene, biotite (Fig. 2a-d) and orthopyroxene (Fig. 3). Rare large (up to 0.5 mm) oval grains of quartz with reaction rims of clinopyroxene are present (Fig. 2e-g). Olivine is usually replaced by talc with a biotite corona. The matrix is fine-grained and it is composed of K-feldspar, biotite, clinopyroxene and small amounts of plagioclase and quartz. The rock shows a weak magmatic foliation that is defined by

tabular grains of biotite and occasionally clinopyroxene. Accessory minerals are apatite (1.5 % molar volume), Cr-spinel (0.5 %) and Fe-sulphides (1 %). The minette shows various degrees of alteration. A relatively less altered hand sample (LR 727) was selected for detailed study. Based on the criteria of modal amounts of mafic and felsic minerals (Le Maitre et al. 2002), mainly the relatively high amount of biotite (17 %), elevated amount of olivine (15 %), lesser amount of clinopyroxene (14 %), small amount of orthopyroxene (6 %), predominance of alkali feldspar (20 %) over plagioclase (13 %), and presence of quartz (12 %), the rock can be classified as an olivine minette. The olivine minette is intermediate in composition (~ 58 wt% SiO_2; Table 1) and has high $K_2O + Na_2O$ ~ 7.4 wt%. Furthermore, based on its high contents of MgO (> 7.5 wt%) and K_2O (> 5.5wt%), and K_2O/Na_2O ratios > 3, it can be classified as ultrapotassic (Foley et al. 1987). The analyzed samples have high magnesium number (Mg# = 100 MgO/(MgO + $Fe_2O_{3\ total}$), on average Mg# = 55.6), low concentrations of CaO (~ 3.6 wt%) and Na_2O (~ 1.7 wt%) and moderate amounts of TiO_2 (~ 1 wt%) and P_2O_5 (~ 0.7 wt%).

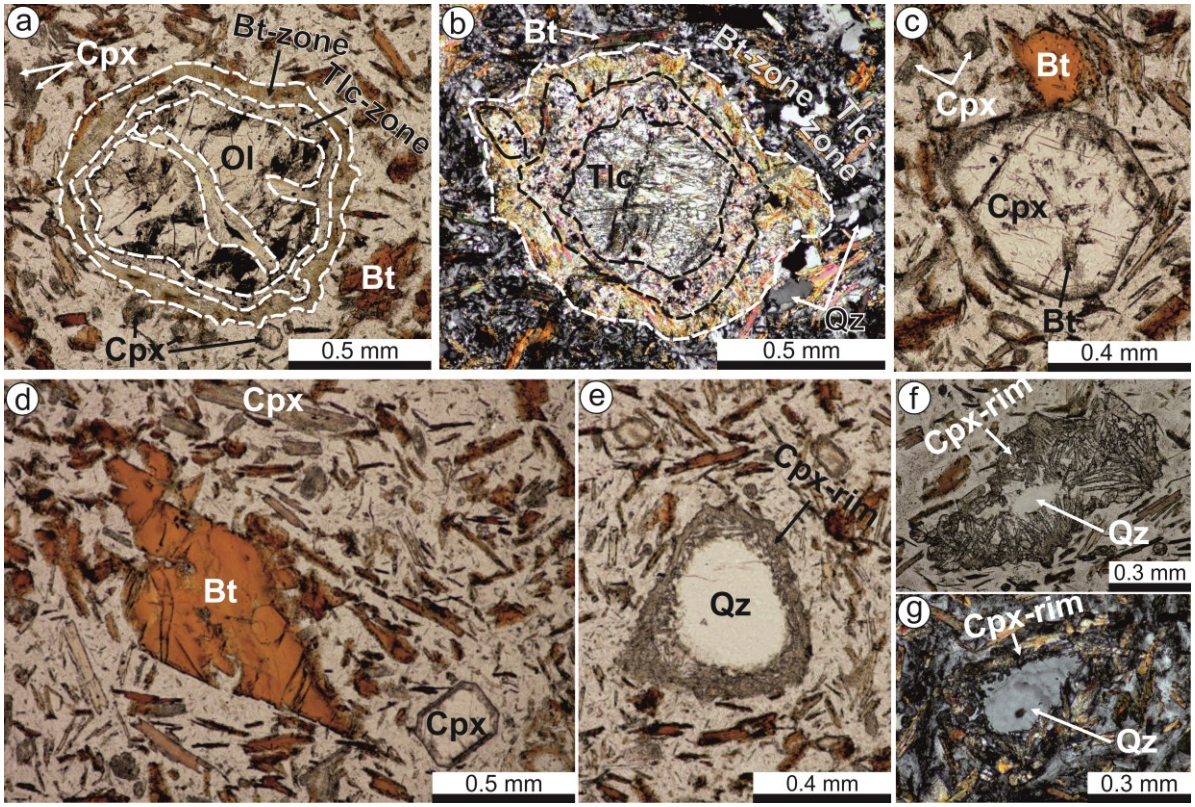

Fig. 2 Microphotographs (a, c, d-f plane polarized, b and g cross polarized) of minette from Horní Kožlí (sample LR 727). Olivine phenocryst (**a**) and its talc pseudomorph (**b**) with two reaction zones - the inner with talc and outer with biotite. Note that talc in the central part of the pseudomorph has uniform optical orientation. **c**) Clinopyroxene phenocryst with inclusion of biotite. The darker zone around the phenocryst consists of undefined alteration products. **d**) Two varieties of biotite, phenocryst and small tabular grains in the matrix. Note that the tubular grains of biotite and clinopyroxene in the matrix show a weak preferred orientation. **e**)

Oval quartz (amygdaloidal) grain with clinopyroxene-rich corona. **f**) Columnar clinopyroxene overgrowing inwards the quartz vesicle. **g**) Centric microstructure of quartz in the vesicle

3.4.1 Olivine and its pseudomorphs

Olivine forms pale pink phenocrysts 0.6–1.6 mm (occasionally up to 2.5 mm) in size and may contain inclusions of Cr-spinel and Fe-sulphide (Fig. 4a). It has corona with inner and outer zones dominated by talc and biotite, respectively (Fig. 2a). The thickness of each zone is about 0.1–0.3 mm. The outer zone additionally contains K-feldspar. Olivine is usually fractured and along the fractures replaced by talc. The pale yellow-brown to green coloured pseudomorphs after olivine are formed by talc with accessory amounts of iron sulphides and Cr-spinel. Similar to olivine phenocrysts, they have coronas with two talc- and biotite-rich zones. Talc in the central part of the pseudomorphs has optical orientation in one direction suggesting topotactic replacement along the crystal shape (Fig. 2b).

3.4.2 Biotite

Biotite has brown to brown-orange colour and texturally four different varieties (types) can be recognized. *Type I* forms tabular phenocrysts (0.3–1.0 mm in size, Fig. 2c, d) that contain inclusions of apatite and opaque phases. In some cases, it may also contain rutile exsolutions that mostly occur along the cleavage planes. *Type II* are small tabular grains (below 0.2 mm in length) and occurs in the matrix (Fig. 2d). *Type III* forms inclusions in clinopyroxene (Fig. 2c). *Type IV* occurs in the corona around olivine phenocrysts and talc pseudomorphs. It is fine-grained (< 0.2 mm) with random orientation of tabular crystals.

3.4.3 Pyroxenes

Clinopyroxene is colourless in thin section and forms four textural types (varieties). *Type I* forms phenocrysts (0.3–0.5 mm in size; Fig. 2c, d) and show oscillatory zoning (the thickness of individual compositional zones is variable and ranges from 10 to 40 μm). They may contain inclusions of apatite and rare of biotite. *Type II* represents clinopyroxene (0.5–0.8 mm in size), which overgrows orthopyroxene phenocrysts (Fig. 3c). *Type III* is fine-grained (< 0.15 mm in size) and occurs in the matrix. A specific type (*type IV*) of clinopyroxene occurs in the coronas of oval quartz (Fig. 2e-g). It forms fine columnar grains that grow mostly perpendicular to the quartz rim and radially penetrate the quartz crystal.

Orthopyroxene is rarely present and occurring only as relict grains rimed by clinopyroxene (Fig. 3c). It is overgrown by clinopyroxene along its crystallographic planes or penetrated by clinopyroxene along the cleavage (see white domains inside the grain, Fig. 3c).

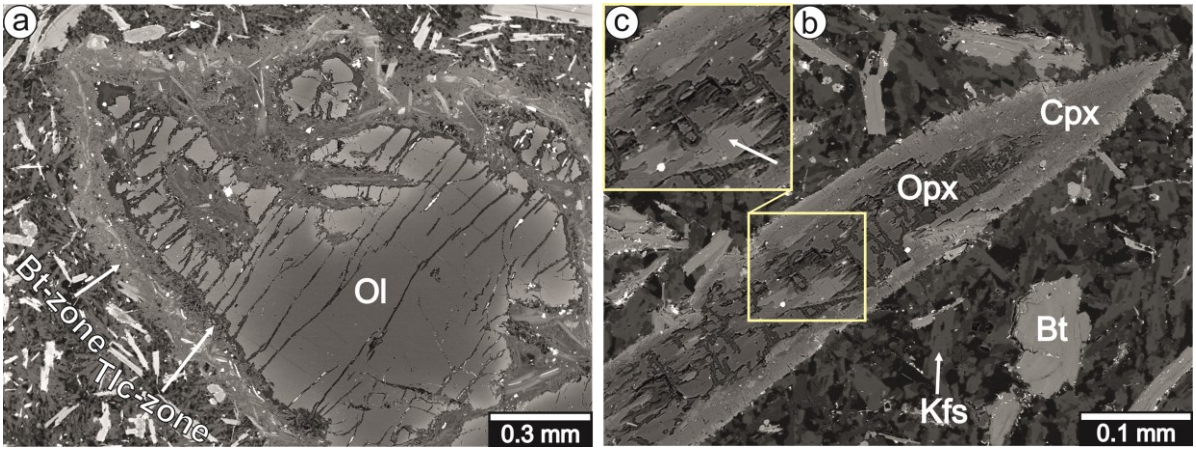

Fig. 3 Backscatter electron images of olivine and pyroxenes. **a** Partially replaced olivine phenocryst with reaction rims of inner talc and outer biotite zones, **b** Orthopyroxene phenocryst is along its rims overgrown by clinopyroxene (the lightest rim of clinopyroxene shows a transition in composition from clinopyroxene to amphibole). Note that the clinopyroxene has different domains of light and grey colour. The close up in **c** shows thin light zones of clinopyroxene at contact with orthopyroxene and with the matrix. The light grey domain labelled by arrow indicates clinopyroxene replacing orthopyroxene

3.4.4 Feldspars

Both K-feldspar and plagioclase are present in the rock. They are very fine-grained (< 0.1 mm in size) and irregularly distributed in the matrix.

3.4.5 Quartz

In addition to small amounts of interstitial quartz in the matrix, rare large (up to 0.4 mm) oval quartz grains are also present (Fig. 2e). They are characterized by reaction rims formed by fine grains (about 0.1 mm long and smaller, rarely up to 0.25 mm in length) of clinopyroxene and minor K-feldspar (< 0.05 mm in size). The thickness of the corona around individual quartz grains is variable and ranges between 0.03 and 0.1 mm. In the case of small quartz grains, it is preserved only in the central part (Fig. 2f) or totally overgrown by clinopyroxene that forms clusters instead of quartz. Crossed polarized microphotographs of some oval quartz grains (Fig. 2g) show patchy zoning that is typical for quartz in vesicles in volcanic rocks and cavities filled by minerals.

3.4.6 Apatite

Apatite is present both as inclusions in mafic minerals as well as in the matrix. In the first case, it has small (< 0.04 mm) grains, but may reach up to 0.1 mm long columnar crystals in the matrix.

3.4.7 Cr-spinel

Two varieties of Cr-spinel are present in the rock. *Type I* is primary and forms inclusions in olivine phenocrysts (Fig. 4a). *Type II* is present in the pseudomorphs after olivine or in cracks with talc. Both types of spinel are < 0.02 mm in size.

3.5 Mineral chemistry

3.5.1 Olivine

Olivine is rich in forsterite (77.8–90.6 % Fo) with magnesium number Mg# (= 100 MgO/ ($MgO + FeO_{total}$) = 66.7–86.0 and shows core to rim normal zoning in Mg, Fe and Mn contents (Fig. 4b). The decrease of MgO from 49.5 to 40.3 wt% towards the rims is compensated by increase of FeO and MnO. Cr_2O_3 and NiO contents are < 0.2 and < 0.2 wt%, respectively and both shows no systematic zoning. The CaO concentration varies from 0.1 to 0.2 wt%.

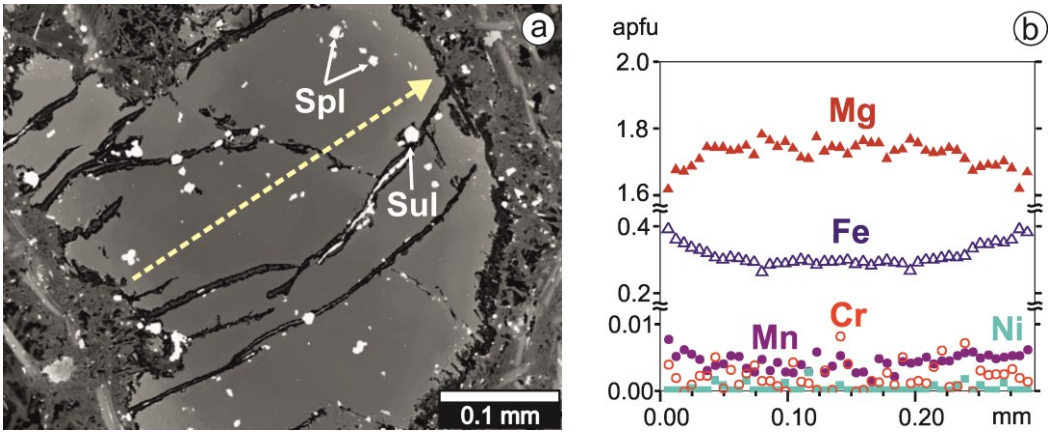

Fig. 4 BSE image and compositional profile across the olivine phenocryst. The olivine contains inclusions of spinel and sulphides

3.5.2 Biotite

Based on the classification by Foster (1960), both biotite (X_{Mg} = Mg/ (Mg + Fe) < 0.64) and phlogopite (XMg > 0.64) are present in the rock. As there is transition from biotite to phlogopite in each textural type, for simplification we used a term biotite for all observed textural varieties. The phenocrysts (*type I*) have composition from biotite to phlogopite (X_{Mg} = 0.57–0.80) with Mg# = 42.3–69.9, and grains in the matrix (*type II*) are biotite (X_{Mg} = 0.53–0.59) with Mg# = 38.8–44.3 (Fig. 5). They both have similar TiO_2 (4.3–5.7 wt%), F (< 0.7 wt%) and Al_2O_3 (13.1–14.4 wt%) contents. Phlogopite (*type III*, X_{Mg} = 0.78) with Mg# = 66.4, TiO_2 = 4.5 wt%, F = 0.6 wt% and Al_2O_3 = 14.0 wt% occurs as inclusions in clinopyroxene phenocrysts. *Type IV* in the corona of quartz shows wide compositional variation from biotite to phlogopite (X_{Mg} = 0.59–0.93) with Mg# = 44.4–87.6, TiO_2 0.1–6.0 wt%, F = 0.3–2.1 wt% and Al_2O_3 = 11.5–14.7 wt% (Fig. 5).

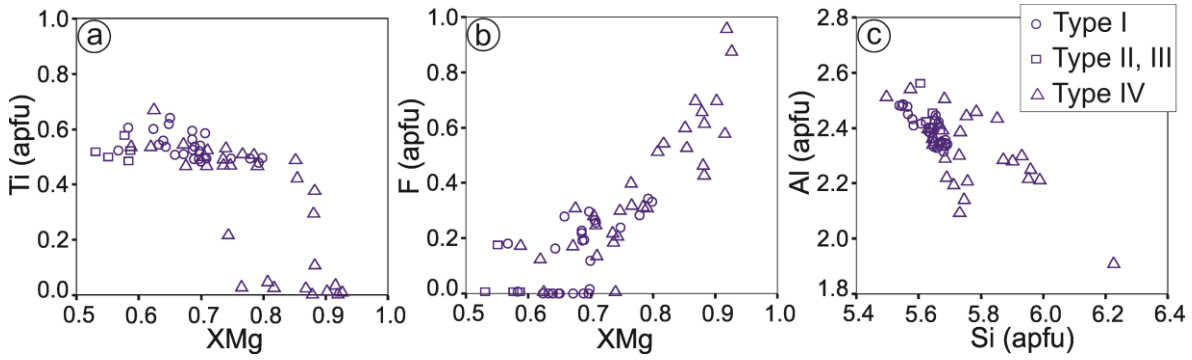

Fig. 5 Composition of various textural varieties (I–IV) of biotite in olivine minette

3.5.3 Clinopyroxene

Based on the classification of Morimoto et al. (1989), clinopyroxene is augite to diopside in composition. Phenocrysts of clinopyroxene (*type I*) have enstatite (En) content of 28.3–55.2 %, ferrosilite (Fs) content of 9.1–23.5 % and wollastonite (Wo) content of 33.2–48.2 %, and are compositionally zoned with Mg# = 41.6–76.5. Compositional maps and profiles (Figs. 6 and 7) show multiple growth zones, where the increase of Fe and Mn towards the rim is compensated for by Mg, Cr and Ti. Compositional maps (Fig. 6a, b) and detailed profiles (Fig. 7) show a jump of Mg and Fe values from one zone to another, but within each zone they show little variation. The Cr_2O_3, TiO_2 and MnO contents are low (< 0.8 wt%) but also exhibit the multiple zoning observed for Mg and Fe (Fig. 7). Furthermore, Ca content also shows variation in the individual zones of grains (Fig. 6c). The core zone has relatively low Ca but high Fe and Mg, which changes towards the interface with the surrounding zone by the decrease of Mg and increase of both Fe and Ca. It is not clear, if this variation is due to diffusion or it reflects continuous growth zoning. Although Na_2O content is low

(< 0.2 wt%), it shows a weak zoning (Fig. 6d), which does not correlate well with the Ca distribution.

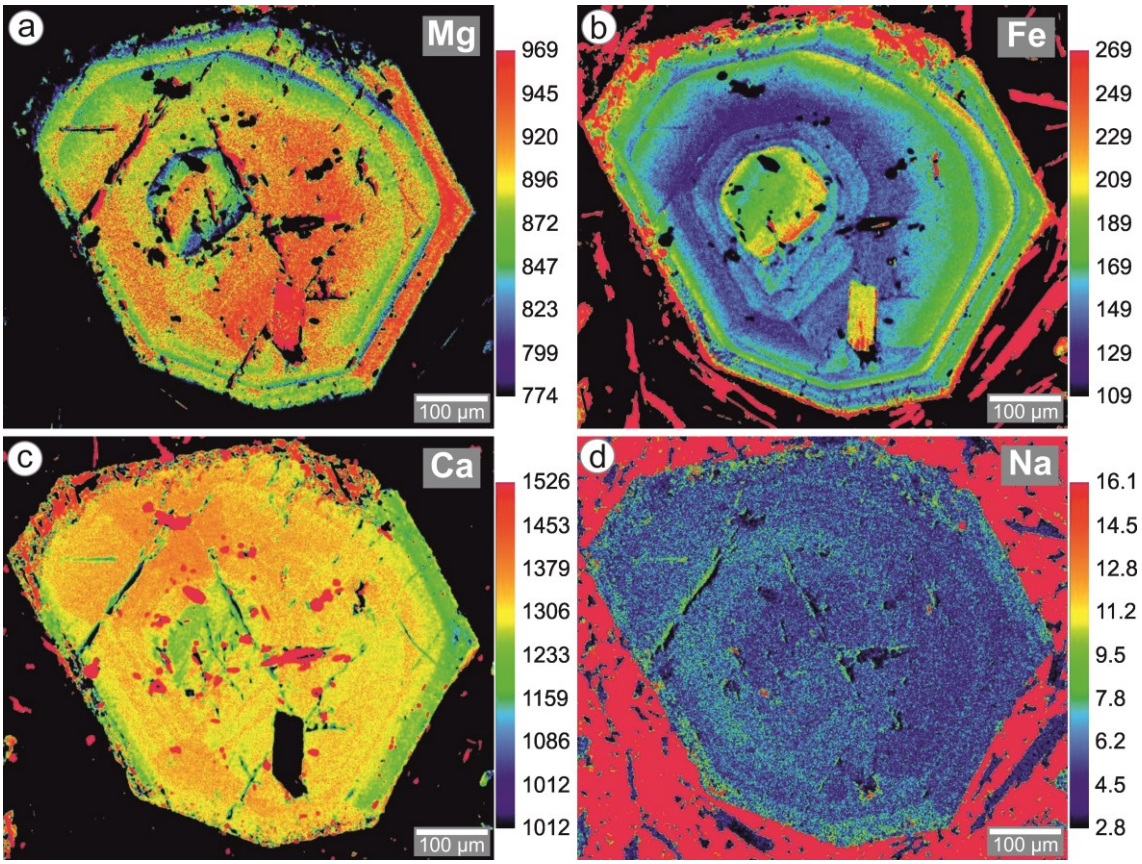

Fig. 6 Compositional maps of Mg, Fe, Ca and Na from zoned clinopyroxene phenocryst as shown in Fig. 2c. The tabular inclusions of biotite and several grains of apatite are characterized by high Fe (b) and Ca (c) contents, respectively

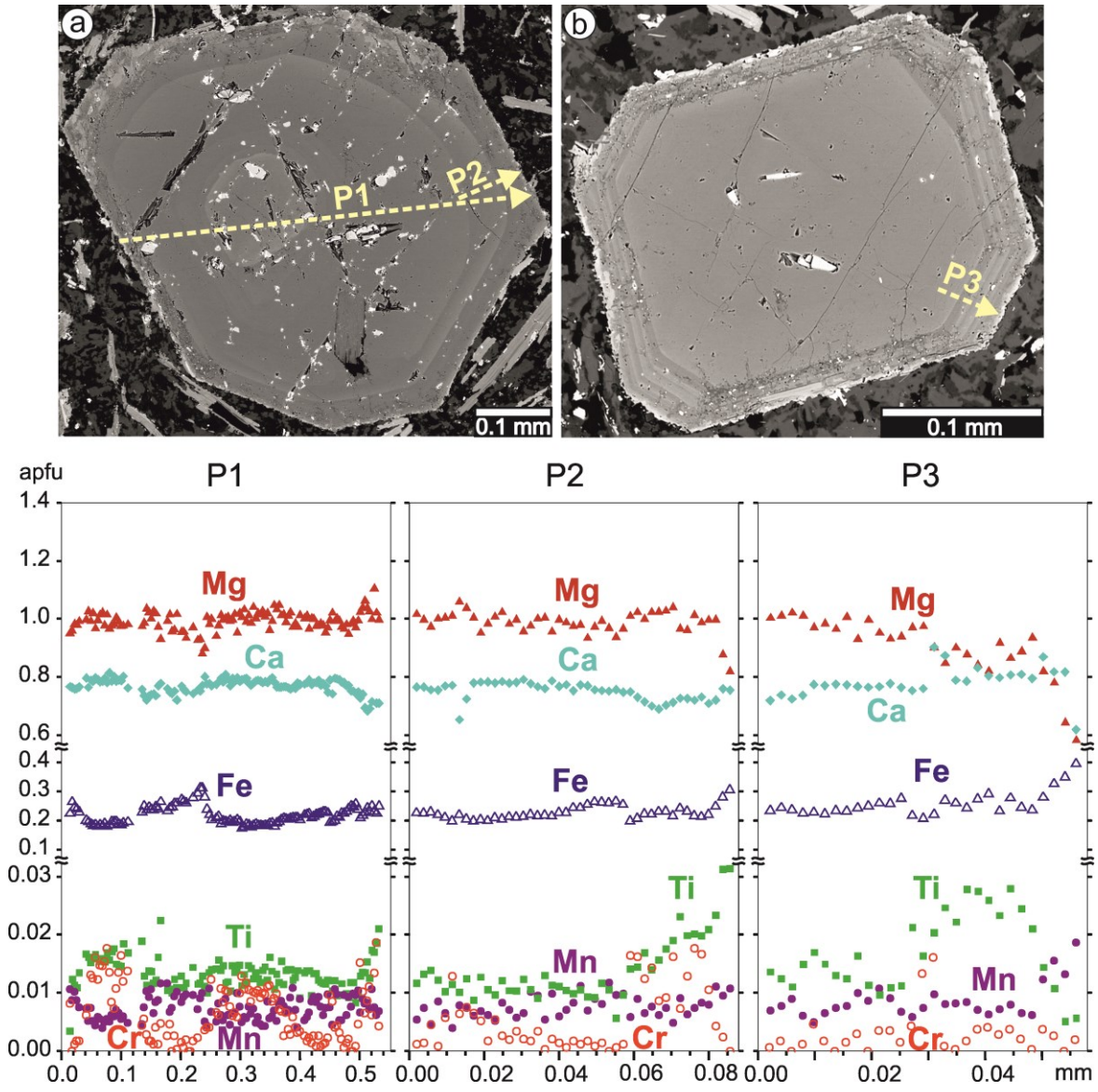

Fig. 7 Compositional profiles of zoned clinopyroxene phenocrysts. Positions of profiles P1, P2 and P3 are also indicated

The *type II* clinopyroxene, which encloses orthopyroxene, has 26.7–46.8 % En, 9.6–25.0 % Fs and 38.1–48.3 % Wo, and Mg# = 38.6–73.9. The compositional variation is due to different domains (light and grey colour, Fig. 3b) or thin zones that are developed both at the contact with orthopyroxene and matrix (Fig. 3c).

Similar wide compositional variation of En = 25.3–50.0 %, Fs = 11.0–25.9 % and Wo 34.2–49.2 %, and Mg# = 37.1–71.2 occurs in fine-grained clinopyroxene in the matrix (*type III*). No clear difference in composition among clinopyroxene I, II and III was found. Generally, FeO and Al_2O_3 in all types indicate a weak negative correlation with MgO, which decrease towards the rim. In contrast to large variation of Mg# values in types I–III, the *type IV* clinopyroxene (in the corona of quartz)

show very small variation in composition with Mg# = 65.1–70.5 and with content of 42.5–47.5 % En, 11.7–13.5 % Fs, 40.9–44.2 % Wo.

3.5.4 Orthopyroxene

In contrast to the zoned clinopyroxene, orthopyroxene is homogeneous with 80.5–81.2 % En, 15.5–16.1 % Fs and 3.6–3.8 % Wo contents, and Mg# = 74.3–75.1. It has low Al_2O_3 < 1.3 wt% and MnO < 0.3 wt%. Avarege TiO_2 and Cr_2O_3 contents are 0.2 and 0.7 wt%, respectively.

3.5.5 Feldspars

Alkali feldspar in the matrix shows compositions with 75.7–96.0 % orthoclase and contains small amount of barium (0.0–0.7 % celsian). Relatively high orthoclase content of 96.7–97.2 % is present in alkali feldspar in the reaction rims of quartz. Plagioclase in the matrix is oligoclase in composition (~ 30% An).

3.5.6 Cr-spinel

Both textural varieties of spinel, forming inclusions in olivine and occurring in the pseudomorphs after olivine, are Cr-spinel with very similar chromium number (Cr# = 100 $Cr_2O_3/(Cr_2O_3 + Al_2O_3)$) Cr# = 86.2–87.8 and 87.0–87.6. The spinel enclosed in olivine has slightly higher Mg# (9.2–14.3) and lower ZnO (< 0.7 wt%) comparing to that in the pseudomorphs (Mg# = 6.0–7.3 and ZnO = 0.7–1.5 wt%).

3.5.7 Apatite

All analysed apatite, forming inclusions in olivine, biotite, clinopyroxene and occurring in the matrix, are rich in F = 3.5–4.1 wt% with Cl < 0.2 wt%. No Sr was detected in apatite.

3.6 Equilibrium mineral assemblages in the parental magma

To estimate equilibrium conditions of minerals crystallized from the source magma, a short summary of textural and compositional relations is given below. In addition to apatite and olivine, the early crystallized phases are biotite, Cr-spinel, orthopyroxene and possibly clinopyroxene. As no systematic compositional variation among the different textural types of biotite was observed, the wide compositional range of biotite could be due to various degrees of partial reequilibration and alteration during the later stage of magma crystallization. This is supported by the presence of rutile

exsolutions along the cleavage plane of biotite. Cr-spinel, occurring in the pseudomorphs after olivine could be formed due to olivine replacement, but its presence as inclusions in fresh olivine crystals represents a primary phase enclosed by olivine rather than formation by exsolution. No systematic distribution of spinel grains or its relations to crystallographic plane of the host olivine were observed. Orthopyroxene stabilized after fractionation proceeded and the host magma became richer in silica. The crystallization process was followed by clinopyroxene, which crystallized by multiple growing events with changing composition of the host melt. Although, there is no significant compositional difference among the various zones, except the compositional jump at the interface of two zones, the core of the phenocrysts have compositions indicative of equilibrium with olivine and orthopyroxene.

The olivine-spinel thermometer of O'Neill and Wall (1987) and two-pyroxene thermometer of Lindsley (1983) were used to estimate temperatures during their crystallization or their equilibrium conditions. The olivine-spinel thermometer is based on the Fe-Mg exchange reaction between olivine and spinel, but also considers Al, Cr, Ti and Fe^{3+} in spinel. Temperature calculated for different compositions of olivine and spinel range between 850 and 1200 °C and the high values were obtained for spinel with the highest Mg content. It decreases with increase of Fe in the olivine. It should be noted that the observed Cr-spinel inclusions occur near the rim of olivine phenocryst with slightly lower Mg/Fe ratios. The lower temperature can be due to reequilibration of Cr-spinel and/or during cooling (e.g. Arai, 1978). The results of two-pyroxene thermometry (Lindsley, 1983) with using core composition of clinopyroxene yielded temperature in the range of 1000–1150 °C at 1.0 GPa and 1050–1150 °C at 1.5 GPa. The ortho- and clinopyroxene compositions were used also for pressures estimate using the method by Putirka (2008). The results are in the range of 0.8 (± 0.37) GPa at 1100 °C and 1.0 (± 0.37) GPa at 1150 °C. These pressures correspond to the boundary of plagioclase and spinel stability fields in mantle peridotite, but the presence of Cr-spinel is clear evidence for the spinel stability field. It should be noted that the high Cr/(Cr + Al) ratios in spinel peridotite progressively shifts the spinel-garnet transition to higher pressures (Grütter et al. 2006; Klemme 2004; MacGregor 1970; O'Neill 1981). Considering phase relations of minerals in the system SiO_2-Al_2O_3-MgO-CaO (Gasparik 2003), the low Al content in combination with Ca in orthopyroxene indicate garnet stability field above 2.5 GPa at the temperature range of 800–1000 °C.

We also used the olivine-orthopyroxene-spinel oxygen geobarometer of Ballhaus et al. (1991) to estimate oxidation state of the source melt generation in the mantle. The result showed $\Delta\log(fO_2)^{FMQ}$ value ranging from -3.9 to -5.9, which is consistent with the lamprophyre magma that is believed to form by partial melting, under reduced (carbon-water buffer) H_2O-rich volatile conditions, of an ancient enriched harzburgite source (Foley 1990; Mitchell and Bergman 1991).

3.7 Discussion

3.7.1 Crystallization history and formation of mineral textures

Combining the observed textural relations in the studied minette, at least two, even three stages of mineral crystallization can be distinguished. Minerals formed during the first stage are apatite, Cr-spinel, olivine, orthopyroxene, clinopyroxene (type I and probably type II, and also type III) and biotite (type I–III). During the second stage, felsic phases (K-feldspar, plagioclase, quartz) in the matrix, biotite type IV and rim parts of zoning clinopyroxene were crystallized. Minerals related to the third stage were formed during filling of the vesicles (quartz with reaction rims of clinopyroxene) and subsequent alteration (talc after olivine). In the following we discuss phase relations and the mineral crystallization succession as a result of changes in the compositions of melt and fluid and temperature/pressure conditions.

Generation of lamprophyre melt from mica peridotite and the importance of volatiles, particularly H_2O and CO_2 for the genesis of alkaline or calc-alkaline rocks are commonly accepted (e.g. Falloon and Green 1988). The presence of F-rich apatite and biotite as well as of carbonates in some similar rock samples (Hrouda et al. 2016; Kubínová et al. 2017), suggests that F-H_2O-CO_2 played an important role in the stabilization of minerals. These phase relations can be explained in the section of the kalsilite-forsterite-quartz system (Fig. 8), which fits well with the observed textural relations in the investigated minette. By crystallization of apatite, olivine and phlogopite, the composition of the system shifts towards quartz and increases the activity of CO_2. Consistent with the textural relations, stabilization of orthopyroxene was governed by the enrichment of silica in the system and the increase of CO_2/H_2O that occurred due to crystallization of biotite and olivine (Ryabchikov and Green 1978). According to Foley (1990), an increase of CO_2 activity stabilizes also clinopyroxene in the system. While a major role for CO_2 is precluded for most lamproites by their very low CO_2 contents, it might be important for some clinopyroxene-rich lamproites (Edgar et al. 1980; Foley 1990; Ryabchikov and Green 1978). The multiple oscillatory zoning in clinopyroxene with compositional gaps suggests that crystallization of the residual melt did not occur in a closed system, but it benefited from magma mixing, which resulted in compositional changes on various scales. This can be deduced from compositional profiles in Fig. 7, where a drop of Fe content at the beginning of each growth zone is followed by its increase towards the rim.

To quantify modal amounts of minerals crystallized from parental melt and to analyse possible changes in the composition of magma during crystallization, the calculated normative mineral contents and estimated modal amount of minerals present in the thin section were compared. Simple calculation of normative minerals based on CIPW norm (Verma et al. 2003) for the bulk rock composition yielded no olivine, but high amounts of orthopyroxene (~ 1.7 % Ap, 24 % Opx, 2 %

Cpx, 28 % Pl, 36 % Kfs and 5 % Qz), which is not consistent with the observed mineral contents in the thin-section. However, calculation of mineral contents by combination of the bulk rock composition and observed modal amounts of minerals in the thin section and their microprobe analyses gave molar volume of ~ 1 % Ap, 15 % Ol, 17 % Bt, 1 % Opx, 10 % Cpx, 20 % Pl, 20 % Kfs, 16 % Qz. The difference of calculated modal contents of minerals by CIPW and from thin section suggests that the parental melt was SiO_2-undersaturated and the increased silica was controlled not only by fractionation but by mixing of Si-rich melt/fluid in the system. Most K_2O from the parental melt was involved in phlogopite associated with olivine.

Enrichment of the residual melt by silica is supported by the presence of quartz in the matrix. In the first stage, it was stabilized during fractional crystallization as can be seen in Fig. 8. But its further enrichment could occur due to magma mixing as mentioned above. Na is involved in plagioclase crystallized during the second stage. If Na was present during crystallization of minerals during the first stage, it could be incorporated into clinopyroxene. The low Na content in the clinopyroxene core domain and its variable zoning in the mantle- rim part suggest that, together with Si, Al and Ti, it was added into system after the first stage minerals crystalized. As external source for these elements could be felsic magma, generated during coeval granulite facies metamorphism and migmatisation (see next chapter). Biotite in the coronas around olivine was formed as a result of reaction between olivine with residual melt or K-feldspar in the matrix during second stage. Its high Mg content is due to local compositional gradient with olivine.

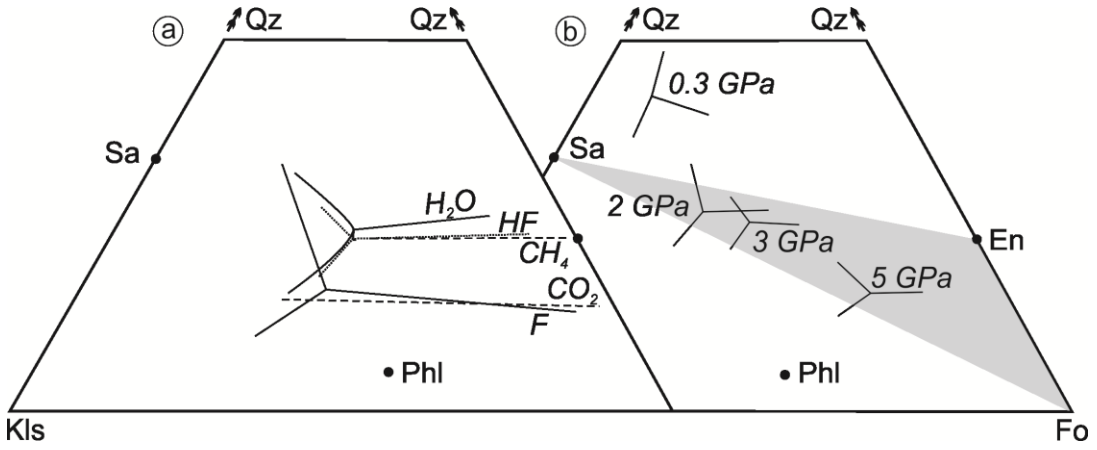

Fig. 8 Positions of peritectic melting points of phlologopite + olivine + orthopyroxene + L in the system kalsilite-forsterite-quartz (Foley 1990) in various volatile (**a**) and pressure conditions (**b**). Curves in (a) are experimentally determined positions for either the peritectic point or the enstatite-forsterite cotectic except for HF and CH_4 which are estimated positions. Positions in (b) are determined in H_2O saturation conditions for 0.3 and 2.8 GPa are from Luth (1967) and Gupta and Green (1989), respectively. The shaded zone between the critical planes of oversaturation and undersaturation indicates that the peritectic melts from mica harzburgite are hyperstene-normative even at 5.0 GPa

The clinopyroxene forming coronas around vesicles of quartz or its intergrowing suggest that the vesicles were filled at high temperature in the stability field of clinopyroxene. The whole process was closed by subsolidus alteration of primary phases, mainly of olivine, which due to excess silica was replaced by talc with Fe oxides instead of serpentine.

The oval quartz forming „quartz ocelli“ textures are common in lamprophyres and some basaltic rocks (Bussy and Ayrton 1990; Har and Rusu 2000; Rock 1991). They consist of single quartz grains that can be rimmed by coronas of ferromagnesian minerals (amphibole and/or clinopyroxene and/or biotite depending on the rock-type), and by alkali feldspar (K-feldspar, sanidine), even carbonate or glass (silica- or alkali-rich). The origin of quartz ocelli is usually explained by filling of cavities formed by the escape of volatiles or that they represent quartz xenocrysts (Bussy and Ayrton 1990). In our case, the first alternative is supported by patchy zoning structure of quartz and by radial arrangement of clinopyroxene crystals around quartz as a result of reaction between Si-rich fluid with the matrix.

3.7.2 Implication to post-Variscan collisional events in the Bohemian Massif

The wide compositional range of lamprophyre or lamprophyre-related rocks (minette, vaugnerite, kersantite, spessartite, melasyenite) of similar ages to that of gabbro-troctolite, even norite intrusions in the Bohemian Massif suggest selective melting of variably metasomatized mantle. Faryad et al. (2015, 2016) indicated that gabbro-norite intrusions were coeval with the granulite facies metamorphism that occurred in the middle to lower crustal depths. Based on the corona textures in gabbro-trocrolite and peak mineral assemblages in the surrounding felsic granulites with lenses of HP-UHP rocks in the Moldanubian Zone, they concluded that the mafic-ultramafic magmas, generated by slab breakoff and mantle upwelling, were the main heat sources for granulite facies metamorphism. Although the available age data from lamprophyres (for ref. see Kubínová et al. 2017) overlap with gabbro-troctolite magmatism and granulite facies metamorphism, field relations show that the lamprophyre dykes penetrated the already consolidated Moldanubian crust with amphibolite-granulite facies rocks near the surface. Formation of lamprophyre magma after the last stages of the collisional process in the Bohemian Massif is supported also by the younger, even Permian (297–293 Ma) lamprophyre dykes reported from the Saxothuringian Zone (Abdelfadil et al. 2014; von Seckendorf et al. 2004).

The very narrow age interval of gabbro-norite intrusions, granulite facies metamorphism and lamprophyre dyke formation in the Moldanubian Zone have important implication to understand the rate of crustal dynamics after slab breakoff and exhumation of HP-UHP rocks into the middle and lower crust (Faryad et al. 2018). In contrast to the gabbro-norite magmatism, which occurred by extension due to slab rifting, when the lower part of slab was sinking away (Davies and von

Blanckenburg 1995), the lamprophyre melt was produced after the upper part of the slab moved upward and resulted in uplift of the hot orogen. Compared to gabbro-troctolite, where almost pure anorthite plagioclase with olivine, orthopyroxene and clinopyroxene is present (Faryad et al. 2015, 2016), the early stage phases in the minette crystallized in the Cr-spinel stability field at temperature about 1200 °C. Based on the composition of the early crystallized minerals (low-Al orthopyroxene) and phase-fluid relations in Fig. 8, formation of the original melt and its partial crystallization in the garnet stability field is not excluded. Generation of the lamprophyre source melt in the garnet stability field is not exceptional as this is known from other regions, e.g. the presence of garnet-lherzolite xenolith in minette from the Colorado Plateau (Ehrenberg 1982). Although, the lamprophyre dykes penetrated consolidated amphibolite to granulite facies rocks on the surface, the Moldanubian crust at its deeper levels was still hot or partially molten (Faryad et al. 2010; Nahodilová et al. 2011) and could result in compositional changes of the ascending mantle-related magma.

3.8 Conclusions

Mineral textures and their compositional relations in the studied minette indicated at least two, even three stages of mineral crystallization. Minerals formed during the first stage are apatite, Cr-spinel, olivine, orthopyroxene, clinopyroxene (type I and III, and probably also type II) and biotite (type I–III). Crystallization succession of the early formed minerals was controlled by changes of main components in the melt, fluid composition and temperature/pressure conditions. After crystallization of olivine and biotite, stabilization of orthopyroxene was controlled by the enrichment of silica in the system and increase of CO_2/H_2O. Incorporation of F and H_2O into apatite and biotite could result in an increase of CO_2 activity and stabilize clinopyroxene. Based on the presence of Cr-rich spinel and low Al content in orthopyroxene, formation of the original melt and its partial crystallization could occur in the garnet stability field.

During the second stage, felsic phases in the matrix were crystallized. Enrichment of the residual melt by silica and Na is supported by the presence of quartz and plagioclase in the matrix. Introduction of Na into the system is supported by its low content in clinopyroxene, which is the only possible Na-bearing phase crystallized during this stage. Biotite in the coronas around olivine was formed as a result of reaction between olivine with residual melt or matrix dominated by K-feldspar. Its high Mg content is due to a local compositional gradient with olivine.

Minerals related to the third stage were formed during filling of the vesicles (quartz with reaction rims of clinopyroxene called „quartz ocelli“) and subsequent alteration (talc after olivine). The origin of quartz ocelli is explained by the filling of cavities formed by the escape of volatiles. The clinopyroxene forming corona around quartz or its intergrowing with quartz suggest that

vesicles were filled at high temperature in the stability field of clinopyroxene. The whole process was closed by subsolidus alteration of primary phases, mainly of olivine, which due to excess silica was replaced by talc with Fe oxides instead of serpentine.

Acknowledgements

This work was supported by the Czech Science Foundation (research project number 18-03160S) and by Charles University through project Progress Q45. We thank R. Jedlicka and M. Racek for help with microprobe analyses. We thank C.-J. De Hoog for very helpful reviews and M.A.T.M. Broekmans for editorial handling.

References

Abdelfadil KM, Romer LR, Glodny J (2014) Mantle wedge metasomatism revealed by Li isotopes in orogenic lamprophyres. Lithos 196–197:14–26

Ackerman L, Pašava J, Erban V (2013) Re-Os geochemistry and geochronology of the Ransko gabbro-peridotite massif, Bohemian Massif. Miner Deposita 48:799–804

Arai S (1978) Chromian spinel lamellae in olivine from the Isanai-Dake peridotite mass, Hokkaido, Japan. Earth and Planet Sci Lett 39:267–273

Awdankiewicz M (2010) Petrogenesis of the Late Paleozoic lamprophyres and related mafic rocks of the Sudetes, SW Poland. Mineralogia, Special Papers 37:20–25

Ballhaus C, Berry RF, Green DH (1991) High pressure experimental calibration of the olivine-orthopyroxene-spinel oxygen geobarometer: implications for the oxidation state of the upper mantle. Contrib Mineral Petrol 107:27–40

Bratzdrum C, Grapes R, Gieré R (2009) Late-stage hydrothermal alteration and heteromorphism of calc-alkaline lamprophyre dykes in Late Jurassic Granite, Southeast China. Lithos 113:820–830

Bussy F, Ayrton S (1990) Quartz textures in dioritic rocks of hybrid origin. Schweiz Mineral Petrogr Mitt 70:223–235

Davies JH, von Blanckenburg F (1995) Slab breakoff: amodel of lithospheric detachment and its test in the magmatismand deformation of collisional orogens. Earth Planet Sci Lett 129:85–102

Droop GTR (1987) A general equation for estimating Fe^{3+} concentrations in ferromagnesian silicates and oxides from microprobe analyses, using stoichiometric criteria. Mineral Mag 51:431–435

Dudíková-Schulmannová B, Barnet I, Čížek D, Hejmánková P, Hroch T, Holub F, Janderková J, Košuličová M, Kotková J, Kryštofová E, Krupička J, Martínek K, Nahodilová R, Pacherová P, Poňavič M, Skácelová Z, Trubačová A, Verner K, Žáčková E (2014) Explanatory notes to the basic geological map of the Czech Republic 1: 25 000, 22-344 Vlachovo Březí (in Czech). Česká geologická služba, Praha, 178 pp

Edgar AD, Condliffe E, Barnett RL, Shirran RJ (1980) An experimental study of an olivine ugandite magma and mechanisms for the formation of its K-enriched derivatives. J Petrol 21:475–497

Ehrenberg SN (1982) Rare earth element geochemistry of garnet lherzolite and megacrystalline nodules from minette of the Colorado Plateau province. Earth Planet Sci Lett 57:191–210

Falloon TJ, Green DH (1988) Anhydrous partial melting of peridotite from 8 to 35 kb and the petrogenesis of MORB. Journal of Petrology, Special Lithosphere Issue, 379–414

Faryad SW, Jedlicka R, Hauzenberger C, Racek M (2018) High-pressure crystallization vs. recrystallization origin of garnet pyroxenite-eclogite within subduction related lithologies. Miner Petrol 112(5):603–616

Faryad SW, Kachlík V, Sláma J, Hoinkes G (2015) Implication of corona formation in a metatroctolite to the granulite facies overprint of HP-UHP rocks in the Moldanubian Zone (Bohemian Massif). J Metamorph Geol 33:295–310

Faryad SW, Kachlík V, Sláma J, Jedlicka R (2016) Coincidence of gabbro and granulite formation and their implication for Variscan HT metamorphismin in the Moldanubian Zone (Bohemian Massif), example from the Kutná Hora Complex. Lithos 264:56–69

Faryad SW, Nahodilová R, Dolejš D (2010) Incipient eclogite facies metamorphism in the Moldanubian granulites revealed by mineral inclusions in garnet. Lithos 114:54–69

Finger F, Roberts MB, Haunschmid B, Schermaier A, Steyrer HB (1997) Variscan granitoids of Central Europe: their typology, potential sources and tectonothermal relations. Miner Petrol 61:67–96

Foley SF (1990) A review and assessment of experiments on Kimberlites, Lamproites and Lamprophyres as a guid to their Origin. Proceedings of the Indian Academy of Sciences - Earth and Planetary Sciences 99:57–80

Foley SF, Venturelli G, Green DH, Toscani L (1987) Ultrapotassic rocks: characteristics, classification and constraints for petrogenetic models. Earth Sci Rev 24:81–134

Foster MD (1960) Interpretation of the composition of trioctahedral micas. U. S. Geol Surv Prof Pap 354-B:11–46

Gasparik T (2003) Phase diagrams for geoscientists. An atlas of the Earth's interior. Springer, New York, 462 pp

Grütter H, Latti D, Menzies A (2006) Cr-saturation arrays in concentrate garnet compositions from kimberlite and their use in mantle barometry. J Petrol 47:801–820

Gupta AK, Green DH (1989) The liquidus surface of the system forsterite-kalsilite-quartz at 28 kbar under dry conditions, in the presence of H_2O, and of CO_2. Miner Petrol 39:163–174

Har N, Rusu A-M (2000) Diffusion coronas around quartz xenocrysts in basaltic andesite from Capus (Cionca Hill, Gilau Mountains - Romania). Studia Universitatis Babes-Bolyai, Geologia XLV:35–45

Holub FV (1997) Ultrapotassic plutonic rocks of the durbachite series in the Bohemian Massif: petrology, geochemistry and petrogenetic interpretation. Journal of Geological Sciences - Economic Geology, Mineralogy 31:5–26

Holub FV (1999) Geochemistry and significance of dyke swarms in the Central Bohemian Plutonic Complex. Geolines 8:28

Holub FV (2007) Dyke swarms in the area of the Central Bohemian Plutonic Complex: their matter variations and relationships to the plutonic rocks (in Czech). vol 3. sjezd České geologické společnosti,Volary

Holub FV, Cocherie A, Rossi P (1997a) Radiometric dating of granitic rocks from the Central Bohemian Plutonic Complex (Czech Republic): constraints on the chronology of thermal and tectonic events along the Moldanubian-Barrandian boundary. C R Acad Sci Ser IIA Earth Planet Sci 325:19–26

Holub FV, Klečka M, Matějka D (1995) Moldanubian zone: igneous activity. In: Dallmeyer D, Franke W, Weber K (eds) Pre-Permian Geology of Central and Eastern Europe. Springer, Berlin, pp. 444–452

Holub FV, Machart J, Manová M (1997b) The Central Bohemian Plutonic Complex: Geology, chemical composition and genetic interpretation. Sborník geologických věd, Ložisková geologie, mineralogie LG 31:27–50

Holub FV, Verner K, Schmitz MD (2012) Temporal relations of melagranite porphyry dykes and durbachitic plutons in South Bohemia (in Czech). Zprávy o geologických výzkumech v roce 2011, Česká geologická služba 23–25

Holub FV, Verner K, Studená M, Orságová L (2009) Dyke swarms of ultrapotassic melasyenite to melagranite porphyries from the Central Bohemian Plutonic Complex and the Šumava part of the Moldanubicum (in Czech). Zprávy o geologických výzkumech v roce 2008, Česká geologická služba 17–20

Hrouda F, Verner K, Kubínová Š, Buriánek D, Faryad SW, Chlupáčová M, Holub F (2016) Magnetic fabric and emplacement of dykes of lamprophyres and related rocks of the Central Bohemian Dyke Swarm (Central European Variscides). J Geosci 61:335–354

Janoušek V, Brainthwaite CJR, Bowes DR, Gerdes A (2004) Magma mixing in the genesis of Hercynian calc-alkaline granitoids: an integrated petrographic and geochemical study of the Sázava intrusion, Central Bohemian Pluton, Czech Republic. Lithos 78:67–99

Janoušek V, Gerdes A (2003) Timing the magmatic activity within the Central Bohemian Pluton, Czech Republic: conventional U-Pb ages for the Sázava and Tábor intrusions and their geotectonic significance. J Czech Geol Soc 48:70–71

Janoušek V, Rogers G, Bowes DR (1995) Sr-Nd isotopic constraints on the petrogenesis of the Central Bohemian Pluton, Czech Republic. Geol Rundsch 84:520–534

Janoušek V, Wiegand B, Žák J (2010) Dating the onset of Variscan crustal exhumation in the core of the Bohemian Massif: new U-Pb single zircon ages from the high-K calc-alkaline granodiorites of the Blatná suite, Central Bohemian Plutonic Complex. J Geol Soc, London 167:347–360

Klemme S (2004) The influence of Cr on the garnet-spinel transition in the Earth's mantle: experiments in the system MgO-Cr_2O_3-SiO_2 and thermodynamic modelling. Lithos 77:639–646

Košler J, Konopásek J, Sláma J, Vrána S (2014) U-Pb zircon provenance of Moldanubian metasediments in the Bohemian Massif. J Geol Soc 171:83–95

Kovaříková P, Siebel W, Jelínek E, Štemprok M, Kachlík V, Holub FV, Blecha V (2007) Petrology, geochemistry and zircon ages for redwitzite at Abertamy, NW Bohemian Massif (Czech Republic): tracing the mantle component in Late Variscan intrusions. Chem Erde 67:151–174

Krmíček L (2010) Pre-Mesozoic lamprophyres and lamproites of the Bohemian Massif (Czech Republic, Poland, Germany, Austria). Mineralogia, Special Papers 37:37–46

Krmíček L, Cempírek J, Havlín A, Přichystal A, Houzar S, Krmíčková M, Gadas P (2011) Mineralogy and petrogenesis of a Ba-Ti-Zr-rich peralkaline dyke from Šebkovice (Czech Republic): recognition of the most lamproitic Variscan intrusion. Lithos 121:74–86

Krmíček L, Romer RL, Ulrych J, Glodny J, Prelević D (2016) Petrogenesis of orogenic lamproites of the Bohemian Massif: Sr-Nd-Pb-Li isotope constraints for Variscan enrichment of ultra-depleted mantle domains. Gondwana Res 35:198–2016

Kröner A, Wendt I, Liew TC, Compston W, Todt W, Fiala J, Vaňková V, Vaněk J (1988) U-Pb zircon and Sm-Nd model ages of high-grade Moldanubian metasediments, Bohemian Massif, Czechoslovakia. Contrib Mineral Petrol 99:257–266

Kubínová Š, Faryad SW, Verner K, Schmitz M, Holub F (2017) Ultrapotassic dykes in the Moldanubian Zone and their significance for understanding of the post-collisional mantle dynamics during Variscan orogeny in the Bohemian Massif. Lithos 272–273:205–221

LeMaitre RW, Streckeisen A, Zanettin B, Le Bas MJ, Bonin B, Bateman P, Bellieni G, Dudek A, Efremova S, Keller J, Lameyre J, Sabine PA, Schmid R, Sørensen H, Woolley AR (2002) Igneous Rocks. A Classification and Glossary of Terms. Recommendations of the International Union of Geological Sciences Subcommission on the Systematics of Igneous Rocks, 2nd edn. Cambridge University Press, Cambridge, 236 pp

Lindsley DH (1983) Pyroxene thermometry. Am Mineral 68:477–493

Luth WC (1967) Studies in the system $KAlSiO_4$-Mg_2SiO_4-SiO_2-H_2O: I, Inferred phase relations and petrologic applications. J Petrol 8:372–416

MacGregor ID (1970) The effect of CaO, Cr_2O_3, Fe_2O_3 and Al_2O_3 on the stability of spinel and garnet peridotites. Phys Earth Planet Inter 3:372–377

Medaris LG, Beard BL, Jelínek E (2006) Mantle-derived, UHP garnet pyroxenite and eclogite in the Moldanubian Gföhl Nappe, Bohemian Massif: a geochemical review, new P-T determinations, and tectonic interpretation. Int Geol Rev 48:765–777

Mitchell RH, Bergman SC (1991) Petrology of Lamproites. Plenum Press, NewYork, 447 pp

Morimoto N, Fabries J, Ferguson AK, Ginzburg IV, Ross M, Seifert FA, Zussman J, Aoki K, Gottardi G (1989) Nomenclature of pyroxenes. Can Mineral 27:143–156

Nahodilová R, Faryad SW, Dolejš D, Tropper P, Konzett J (2011) High-pressure partial melting and melt loss in felsic granulites in the Kutná Hora complex, Bohemian Massif (Czech Republic). Lithos 125:641–658

O'Neill HSC (1981) The transition between spinel lherzolite and garnet lherzolite, and its use as a geobarometer. Contrib Mineral Petrol 77:185–194

O'Neill HSC, Wall VJ (1987) The olivine-orthopyroxene-spinel oxygen geobarometer, the nickel precipitation curve, and the oxygen fugacity of the earth's upper mantle. J Petrol 28:1169–1191

Putirka KD (2008) Thermometers and barometers for volcanic systems. Rev Mineral Geochem 69(1):61–120

Rock NMS (1984) Nature and origin of calc-alkaline lamprophyres: minettes, vogesites, kersantites and spessartites. Earth Sci 74:193–227

Rock NMS (1987) The nature and origin of lamprophyres: an overview. Geol Soc Lond, Spec Publ 30:191–226

Rock NMS (1991) Lamprophyres. Blackie and Son Ltd, London, 275 pp

Ryabchikov ID, Green DH (1978) The role of carbon dioxide in the petrogenesis of highly potassic magmas. Akademiya Nauk SSSR, Institute of Geology and Geophysics 403:49–64

Scarrow JH, Molina JF, Bea F, Montero P, Vaughan APM (2011) Lamprophyre dikes as tectonic markers of late orogenic transtension timing and kinematics: a case study from the Central Iberian Zone. Tectonics 30(TC4007):1–22

Schalterger U (1997) Magma pulses in the Central Variscan Belt: episodic melt generation and emplacement during lithospheric thinning. Terra Nova 9:242–245

Schulmann K, Kröner A, Hegner E, Wendt I, Konopásek J, Lexa O, Štípská P (2005) Chronological constraints on the pre-orogenic history, burial and exhumation of deep-seated rocks along the

eastern margin of the Variscan orogen, Bohemian Massif, Czech Republic. Am J Sci 305:407–448

Siebel W, Chen F, Satir M (2003) Late-Variscan magmatism revised: new implications from Pb-evaporation zircon ages on the emplacement of redwitzites and granites in NE Bavaria. Int J Earth Sci 92:36–53

Štemprok M, Dolejš D, Holub FV (2014) Late Variscan calc-alkaline lamprophyres in the Krupka ore district, Eastern Krušné hory/Erzgebirge: their relationship to Sn-W mineralization. J Geosci 59:41–68

Vaughan APM, Scarrow JH (2003) K-rich mantle metasomatism control of localization and initiation of lithospheric strike-slip faulting. Terra Nova 15:163–169

Verma SP, Torres-Alvarado IS, Velasco-Tapia FT (2003) A revised CIPW norm. Schweiz Mineral Petrogr Mitt 83:197–216

von Seckendorf V, Timmerman MJ, Kramer W, Wrobel P (2004) New $^{40}Ar/^{39}Ar$ ages and geochemistry of Late Carboniferous–Early Permian lamprophyres and related volcanic rocks in the Saxothuringian Zone of the Variscan Orogen (Germany). In: Wilson M, Neumann ER, Timmermann GR, Heremans M, Larsen BT (eds) Permo-Carboniferous 106 Magmatism and Rifting in Europe, vol 223. Geological Society, London, Special Publications, pp. 335–359

Vrána S, Blümel P, Petrakakis K (1995) Metamorphic evolution of the Moldanubian Zone. In: Dallmeyer RD, Franke W, Weber K (eds) Pre-Permian Geology of Central and Eastern Europe. Springer, Berlin, pp. 453–466

Wendt JI, Kröner A, Fiala J, Todt W (1993) Evidence from zircon dating for existence of approximately 2.1 Ga old crystalline basement in southern Bohemia, Czech Republic. Geol Rundsch 82:42–50

Whitney DL, Evans BW (2010) Abbreviations for names of rock-forming minerals. Am Mineral 95:185–187

Žák J, Verner K, Finger F, Faryad SW, Chlupáčová M, Veselovský F (2011) The generation of voluminous S-type granites in the Moldanubian unit, Bohemian Massif, by rapid isothermal exhumation of the metapelitic middle crust. Lithos 121:25–40

Žák J, Verner K, Janoušek V, Holub FV, Kachlík V, Finger F, Hajná J, Tomek F, Vondrovic L, Trubač J (2014) A plate-kinematic model for the assembly of the Bohemian Massif constrained by structural relations around granitoid plutons. Geol Soc Spec Publ 405:169–196

CHAPTER 4

MAGNETIC FABRIC AND EMPLACEMENT OF DYKES OF LAMPROPHYRES AND RELATED ROCKS OF THE CENTRAL BOHEMIAN DYKE SWARM (CENTRAL EUROPEAN VARISCIDES)

František Hrouda [1,2], Kryštof Verner [1,3], Šárka Kubínová [1], David Buriánek [4], Shah Wali Faryad [1], Marta Chlupáčová [5], František V. Holub [1]

[1] Institute of Petrology and Structural Geology, Charles University, Albertov 6, 128 43 Prague 2

[2] Agico Inc., Ječná 29a, 621 00 Brno, Czech Republic

[3] Czech Geological Survey, Klárov 3, 118 21 Prague 1, Czech Republic

[4] Czech Geological Survey, Leitnerova 22, 621 00 Brno, Czech Republic

[5] Boháčova 866/4, 149 00 Prague 4, Czech Republic

Status: Published in Journal of Geosciences (2016)

ABSTRACT

Numerous dykes of lamprophyres and various types of granitoid, syenitoid, dioritoid, and gabbroid porphyries of Variscan age crop out in the area of the Central Bohemian Plutonic Complex and adjacent high- to low-grade metamorphic units of the Moldanubian Zone and Teplá-Barrandian Unit. Magnetic fabric in fourteen dykes of lamprophyres and related rocks was investigated. Mostly, the magnetic foliation is roughly parallel to the dyke plane and the magnetic lineation is horizontal with the relics of originally steep fabrics. This type of magnetic fabric originated through magma flow in which the larger surfaces of the magnetic minerals were oriented parallel to the dyke plane and their longer dimensions were parallel to the magma flow. In two localities, the so-called inverse fabrics were found in which the maximum and minimum susceptibility directions were swapped.

The dykes of lamprophyres and related rocks were emplaced into already juxtaposed and cooled Teplá-Barrandian Zone, Central Bohemian Plutonic Complex and western Moldanubian Zone not later than 339 Ma. Parallel orientation of dykes giving a steep intrusive contacts mainly in W(NW)-E(SE) trend was caused by the regional stress field of ~WNW-ESE convergence (arc-parallel stretching) during the Variscan Orogeny.

***Keywords**: anisotropy of magnetic susceptibility (AMS), dyke-swarm, emplacement, Bohemian Massif, Variscides*

4.1 Introduction

Magma ascent and emplacement in dykes is one of important mechanisms of the mass transport within the Earth's crust and the upper mantle. Structural aspects of this mass transfer can be advantageously studied using the anisotropy of magnetic susceptibility (AMS), which is a rapid and efficient geophysical (petrophysical) method for investigation of the preferred orientation of magnetic minerals (magnetic fabric) in rocks (for more details see Tarling and Hrouda 1993). This method is very sensitive and extremely fast (an order of magnitude faster than the classical methods of structural analysis). In addition, there are extensive data-bases of the AMS data in various volcanic bodies and dykes (for summary see Cañón-Tapia 2004; Raposo 2011) and their deformed equivalents (e.g., Henry 1977; Hrouda and Přichystal 1995).

In dykes, the most common magnetic fabric type is characterized by the magnetic foliation approximately parallel to the dyke plane and the magnetic lineation, also parallel to the dyke plane, can be vertical, horizontal, or even oblique according to the magma flow in a dyke (e.g. Knight and Walker 1988; Rochette et al. 1991; Ernst and Baragar 1992; Raposo 2011). This fabric type was called *normal* by Rochette et al. (1991) or *Type I* by Raposo and Ernesto (1995) (see Fig. 1). During magma flow, the larger surfaces of magnetic minerals align approximately parallel to the dyke, while the longer dimensions orient parallel to the magma flow direction. The second and much less frequent type is characterized by the approximately perpendicular orientation of magnetic foliation to the dyke plane and magnetic lineation parallel to the dyke (*intermediate* fabric of Rochette et al. 1991, *Type II* fabric of Raposo and Ernesto 1995; Fig. 1). This orientation may originate through a compaction of a static magma column along the dyke and the magnetic minerals reorient with their larger surfaces perpendicular to the flow direction (Park et al. 1988; Bates and Mushayandebvu 1995; Raposo and Ernesto 1995). The third, scarce type is characterized by the magnetic foliation and magnetic lineation perpendicular to the dyke. This type was termed *reverse* by Rochette et al. (1991) or *inverse* by Raposo (2011) or *Type III* by Raposo and Ernesto (1995) (Fig. 1). This magnetic fabric is attributed to secondary processes such as hydrothermal alteration (Rochette et al. 1991) or to single domain effect if very small magnetic grains carry the AMS (Stephenson et al. 1986). There is also a fourth type showing almost random orientations of magnetic foliations and lineations, which may result from very complex flow patterns or from severe post-magmatic changes of magnetic minerals (Hrouda 1985; Raposo 2011).

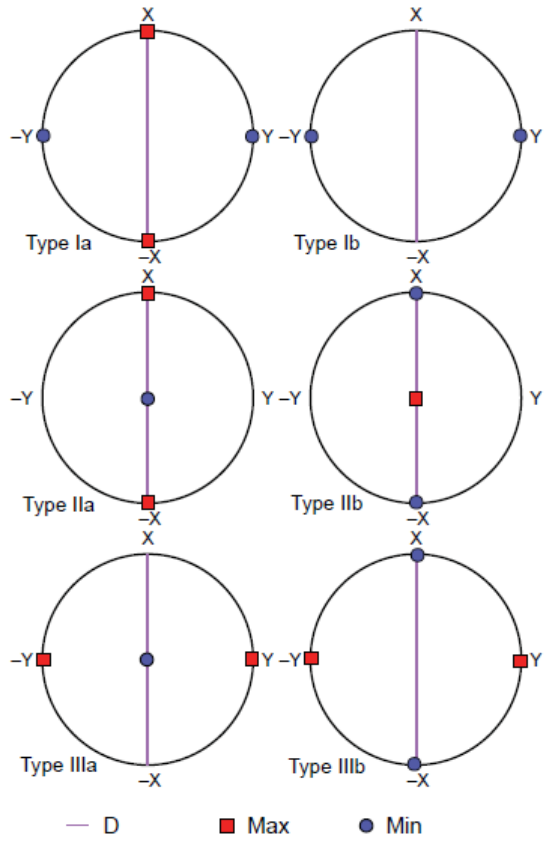

Fig. 1 Schematic sketch of variable types of magnetic fabrics in dykes. Dyke plane is denoted by vertical great circle in grey. Equal-area projection on lower hemisphere. Adapted from Raposo and Ernesto (1995).

The relationship between magnetic fabric and dyke orientation described in preceding paragraph was revealed through investigation of crustally derived intermediate to mafic dykes. Much less information is available about magnetic fabric in mafic and ultramafic ultrapotassic dykes (e.g. Holub et al. 2012; Machek et al. 2014) generated from the mantle (e.g. Edgar and Mitchell 1997; Guo et al. 2006; Chalapathi Rao and Srivastava 2012; Gupta 2015).

The (ultra-) potassic dykes are abundant late members of the Central Bohemian Dyke Swarm spatially associated to the Variscan Central Bohemian Plutonic Complex (CBPC) but also cut the adjacent parts of the upper-crustal Teplá-Barrandian Unit and mid- to lower crustal western Moldanubian Zone (Fig. 2). The Central Bohemian Dyke Swarm has an asymmetric area of extent, elongated predominantly in the NNE-SSW direction along the border between western Moldanubian and Teplá-Barrandian zones. The individual dykes are approximately perpendicular to the asymmetric Central Bohemian Dyke Swarm and are mostly perpendicular to the regional fabrics in host units. The studied dykes penetrate the older medium- and high-K calc-alkaline granitoid rocks of the CBPC dated at 354.1 ± 3.5 Ma (Janoušek et al. 2004) and 346.4 ± 1.1 Ma (Janoušek et al. 2010), respectively. Concurrently they must be older than the emplacement of the Tábor Pluton (dated at 336.9 ± 0.6 Ma; Janoušek et al. 2013). This means that despite the extensive area of

occurrence and compositional variations these dykes show only a limited variation in age (~ 346 to 337 Ma; Holub 1997; Holub et al. 1997a).

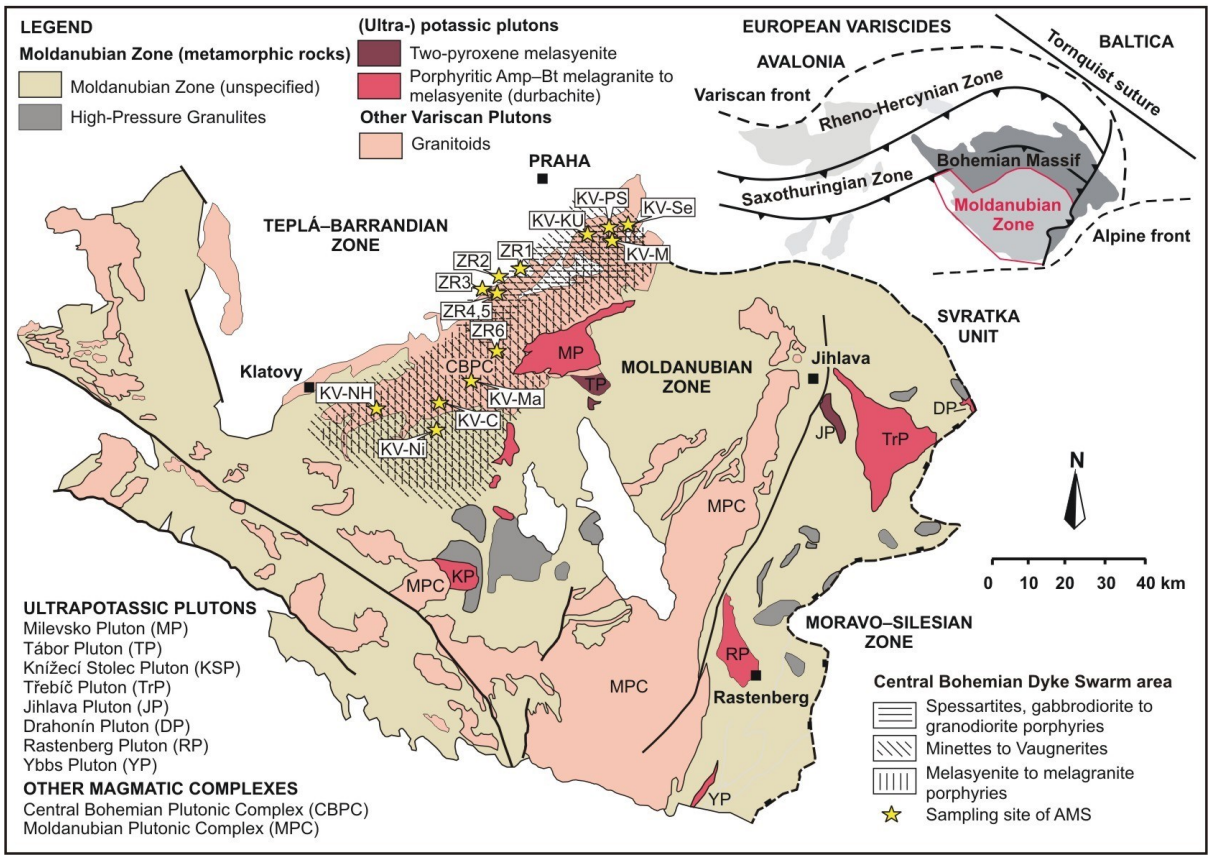

Fig. 2 Geological sketch map of the Bohemian Massif and its position in the European Variscides (inset). Geological map of the southern and central parts of the Bohemian Massif showing the extent of occurrence of the Central Bohemian Dyke Swarm (hatch pattern) and locations of the dykes investigated. Adapted from Chlupáč et al. (2002).

In this paper we discuss the petrology and AMS of the dykes of calc-alkaline and potassic lamprophyres and related rocks of the Central Bohemian Dyke Swarm. This study aims to analyse the magma ascent and emplacement during the dyke formation that occurred along the western border of the Moldanubian Zone at the contact with the Teplá-Barrandian Unit. This event dated the final stage of regional ~ WNW-ESE convergence and crustal exhumation that occurred at around 340 Ma (e.g. Schulmann et al. 2009).

4.2 Geological setting

4.2.1 Metamorphic and magmatic units hosting the dyke swarm

4.2.1.1. Teplá-Barrandian Unit

The Teplá-Barrandian Unit consists of low- to medium-grade Neoproterozoic metasediments, originally forming a part of the Cadomian accretionary wedge, later intruded by Cambro-Ordovician granitoids and containing unmetamorphosed mid-Cambrian to mid-Devonian volcanosedimentary sequences (for review see Chlupáč et al. 1998; Schulmann et al. 2009; Žák et al. 2014; Hajná et al. 2017).

4.2.1.2. Moldanubian Zone

The Moldanubian Zone represents exhumed lower- to mid-crustal orogenic root that builds up the internal part of the Variscan orogenic belt in central Europe (Fig. 2). The Moldanubian Zone experienced polyphase metamorphism and complex deformational history (e.g. Franke 2006; Schulmann et al. 2009; Faryad et al. 2010; Lardeaux et al. 2014). In general, the overall structure of the orogenic root resulted from stacking of several lithotectonic units at ~ 360 to 345 Ma followed by HT/LP metamorphism, anatexis and late-Variscan wrench tectonics (for review see Schulmann et al. 2009; Žák et al. 2014). The Moldanubian Zone consists of metasedimentary sequences of Neoproterozoic to Lower Palaeozoic protolith age (Košler et al. 2014) dominated by sillimanite-biotite (± cordierite) paragneisses to migmatites with variable presence of small bodies of metaquartzites, marbles, calc-silicate rocks, graphite-bearing schists and amphibolites (e.g. Urban and Synek 1995).

The Variscan geodynamic evolution in the Moldanubian Zone was characterized by 380 to 335 Ma subduction-collision tectonics and metamorphism, magmatic activity, and fast exhumation and cooling from ~ 346 to 335 Ma onward (e.g. Schulmann et al. 2009; Dörr and Zulauf 2010; Žák et al. 2012, 2014; Faryad et al. 2013).

4.2.1.3. Central Bohemian Plutonic Complex (CBPC)

Syn-collisional Late Devonian-Early Carboniferous (~ 370 to 340 Ma) crustal thickening broadly overlapped with the emplacement of medium- and high-K calc-alkaline, I-type plutons of the prevailing part of the CBPC (Holub et al. 1997a, b; Žák et al. 2011). The CBPC crops out along significant tectonic boundary between the upper-crustal Barrandian Unit (eastern Teplá-Barrandian Zone) and high-grade western part of the Moldanubian Zone (WMZ). It covers an area of about

3,000 km^2 and comprises a number of various granitoid and subordinate mafic rocks that can be divided into several suites (e.g. Janoušek et al. 1995, 2000; Holub et al. 1997b; Žák et al. 2005b).

Widely distributed are mainly medium-K calc-alkaline rocks (quartz diorites to granodiorites of the Sázava Pluton) dated by conventional zircon U-Pb method to 354.1 ± 3.5 Ma (Janoušek et al. 2004). The high-K to shoshonitic rocks (monzogabbros, quartz monzonites to granodiorites of the Blatná Composite Pluton) gave the SHRIMP U-Pb zircon age of 346.4 ± 1.1 Ma (Janoušek et al. 2010). The ultrapotassic rocks (melasyenites to melagranites of the durbachitic Milevsko and Tábor plutons) were dated at 343 ± 6 Ma by Pb-Pb zircon evaporation (Holub et al. 1997a) and at 336.9 ± 0.6 Ma by conventional U-Pb dating of zircon (Janoušek et al. 2013), respectively. Rapid exhumation and cooling of the lower- to mid-crustal level at ~ 343 to 337 Ma was associated with formation of one of the largest calc-alkaline and (ultra-) potassic lamprophyre dyke-swarms in the Central European Variscides (e.g. Žežulková 1982; Holub et al. 1995, 1997b, 2012; Janoušek and Holub 2007).

4.2.2 Central Bohemian Dyke Swarm

The Central Bohemian Dyke Swarm (Fig. 2) has been emplaced predominantly into older magmatic units of the CBPC, but also into adjacent parts of the Teplá-Barrandian and Moldanubian zones (Žežulková 1982; Holub et al. 1997b, 2012). The composition of these dykes varies from mafic to felsic and from calc-alkaline (spessartites, kersantites, gabbrodiorite to granodiorite porphyries) to (ultra)-potassic (minettes, vaugnerites and melasyenite to melagranite porphyries). The latter dykes reveal geochemical similarities to the (ultra-) potassic (durbachitic) plutonic rocks (Holub 1997; Holub et al. 1997b).

The overall occurrence of the Central Bohemian Dyke Swarm defines a rectangle c. 115 km long stretched approximately in the NNE-SSW direction from northeastern flank of the CBPC to its southwestern tip (Fig. 2).

The calc-alkaline spessartite to gabbrodiorite dykes were emplaced mainly into the oldest granitoids of the CBPC (medium-K calc-alkaline Sázava Pluton) and also into the adjacent upper-crustal Teplá-Barrandian Zone (Fig. 2). The average thickness of these dykes is ~ 1 to 6 meters. Prevailing intrusive contacts are steep and mostly discordant with respect to the regional fabrics in host rocks (Fig. 3a). The orientation of the dykes is mainly E-W to NW-SE; rarely, also NE-SW or N-S trending intrusive contacts have been observed.

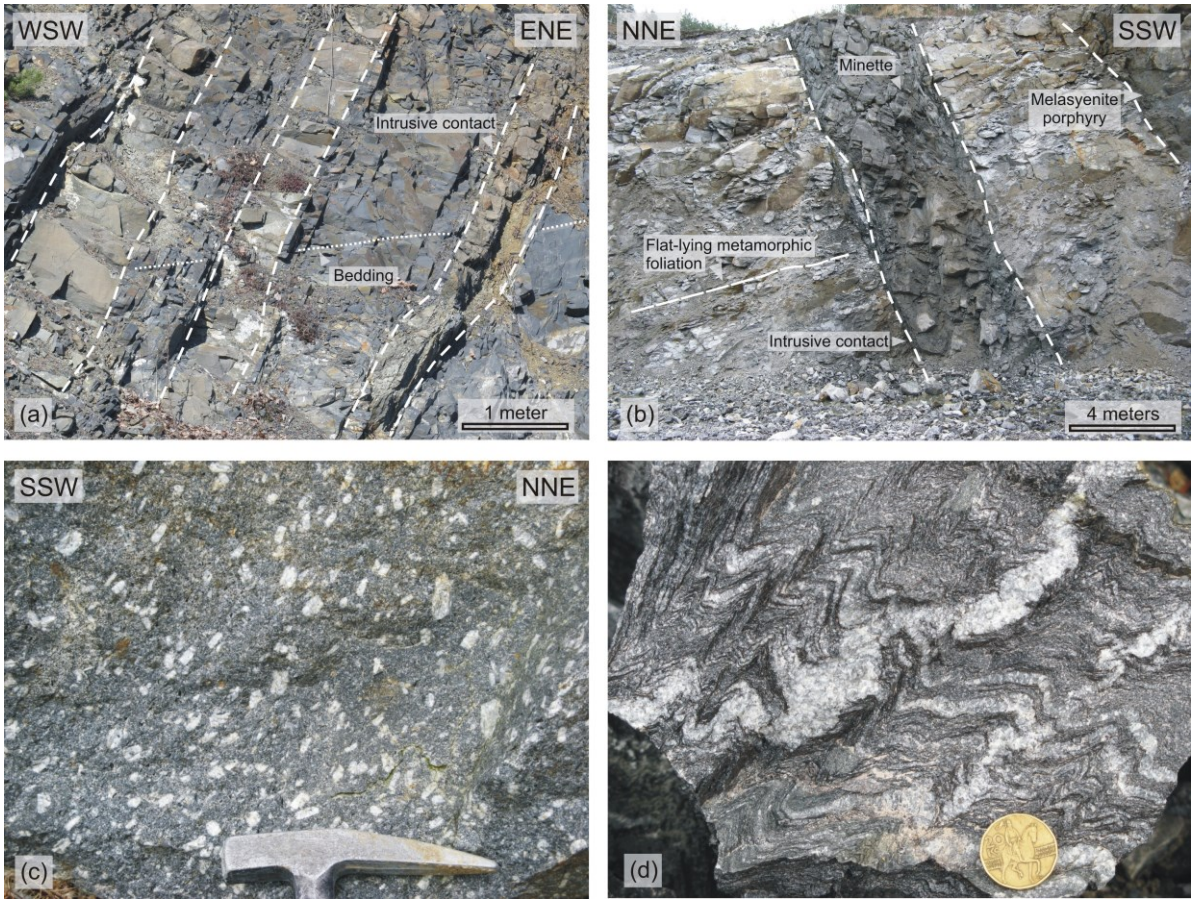

Fig. 3 Field photographs to show intrusive relationships of the dykes to host metamorphic rocks and fabric patterns. **a** – Originally steep discordant intrusive contacts between several kersantite dykes and host Neoproterozoic sequences of the Teplá-Barrandian Zone (Dobříš). **b** – Subparallel ~E-W trending steeply dipping ultrapotassic dykes (minette and syenite porphyry) which are discordant to regional metamorphic foliation in the host migmatite of the western Moldanubian Zone (Nihošovice). **c** – Magmatic (flow) foliation in syenite porphyry dyke defined by planar preferred orientation of K-feldspars (Nihošovice). Hammer for scale. **d** – Folded metamorphic foliation (compositional banding) in migmatites of western Moldanubian Zone which is discordantly intruded by the dyke-swarm (Nihošovice). Coin for scale.

All the (ultra-) potassic dykes (minettes, vaugnerites and melasyenite to melagranite porphyries) were emplaced into partly exhumed mid-crustal paragneisses to migmatites of the WMZ and into older intrusive bodies of the CBPC (medium-K calc-alkaline Sázava and high-K calc-alkaline Blatná suites dated at 354 and 346 Ma, respectively), but not into ultrapotassic plutons and younger intrusions of the CBPC c. 340–335 Ma old (Holub et al. 1997).

The individual melasyenite to melagranite porphyries (U-Pb zircon age 337.87 ± 0.21 Ma; Kubínová et al. 2017) are oriented W-E to WNW-ESE and are nearly vertical or steeply dipping southwards (Fig. 3b). Dyke thickness varies from 5 to 20 m, the lengths are often limited to less than 1–2 km, perhaps due to segmentation of dykes by younger faults. Horizontal distances between parallel porphyry dykes vary considerably being about 0.5–1.0 km in districts with the highest

density of dyking. These dykes show well-developed magmatic (flow) foliation, which is defined by planar preferred orientation of K-feldspar phenocrysts (Fig. 3c). External contacts of porphyry dykes are sharp and generally discordant to folded metamorphic foliations of host gneisses and migmatites (Fig. 3d). At southern margin of the CBPC, dykes of the same rock type are discordant to the fabric of the host granodiorites.

Minettes are commonly parallel to porphyry dykes (Fig. 3b) and their field relations are comparable. However, owing to their apparently lower magma viscosity, minette dykes are generally much narrower, frequently with offshoots and strings. The most frequent thickness ranges 0.5–1.5 m, only rarely exceeding 2 meters. Their intrusive contacts are mostly sharp and discordant with respect to regional fabrics and older plutons. All ultrapotassic dykes have similar trend, ~ W(WNW) to E(ESE), with steeply dipping intrusive contacts. Repeated intrusions of magma portions from dykes of almost uniform strikes exemplify the long-lasting uniformity of the regional stress field with the least compressional stress oriented roughly N(NNE)-S(SSW) thus allowing a limited extension in this direction.

4.3 Analytical techniques

The oriented specimens were drilled in 14 selected dykes of the Central Bohemian Dyke Swarm using portable drilling machine and oriented using geological compass mounted on special orientating fixture (see Tab. 1).

The AMS was measured with the KLY-3S (Jelínek and Pokorný 1997) and MFK1-FA kappabridges (Pokorný et al. 2011) in the driving field 425 A/m peak at the operating frequencies 920 Hz and 976 Hz, respectively, using the 3D rotator in the latter instrument (Studýnka et al. 2014), and the results were calculated by the SAFYR program (version 5).

The mean bulk susceptibility (K_m), degree of AMS (P) and shape of the AMS ellipsoid (T) are defined as follows (Nagata 1961; Jelínek 1981)

$$K_m = (k_1 + k_2 + k_3) / 3$$

$$P = k_1 / k_3$$

$$T = (2\,\eta_2 - \eta_1 - \eta_3) / (\eta_1 - \eta_3) = 2 \ln F / \ln P - 1$$

where $k_1 \geq k_2 \geq k_3$ are the principal susceptibilities, $\eta_1 = \ln k_1$, $\eta_2 = \ln k_2$, $\eta_3 = \ln k_3$.

Tab. 1 Dykes of lamprophyres and related rocks investigated (location and geological characteristics)

Latitude	Longitude	Locality No.	Locality Name	Rock Type	Host Unit	Thickness	Orientation	Mesoscopic fabric
49.80185	14.20024	ZR-1	Dobříš	Kersantite	TBZ Proterozoic Unit	8.5 m	NW-SE 41/86, 60/85	no apparent
49.72086	14.01888	ZR-2	Příbram - Trhové Dušníkv	Spessartite	TBZ Proterozoic Unit	~ 3 m	NE-SW 145/48	no apparent
49.62877	14.05309	ZR-3	Milín - Kojetín	Spessartite	CBPC Marginal granite	1.5 m	NW-SE 47/88	no apparent
49.62538	14.05157	ZR-4	Milín W	Minette	CBPC Marginal granite	1.7 m	NW-SE 60/85, 63/79	contact parallel
49.62688	14.05196	ZR-5	Milín E	Minette	CBPC Marginal granite	0.45 m	N-S 90/89	no apparent
49.54967	14.10815	ZR-6	Zalužany - Kozárovice	Minette	CBPC Blatná pluton	1.60 m	W-E 170/85	no apparent
49.86089	14.51760	KV-KU	Kamenný Újezdec	Syenite porphyry	CBPC Sázava pluton	~ 8 m	WNW-ESE 27/62	contact parallel
49.84214	14.69152	KV-PS	Poříčí nad Sázavou	Minette	CBPC Sázava pluton	4 m	NW-SE 51/88, 206/86	contact parallel
49.85915	14.66266	KV-Ne	Městečko - Nespeky	Minette	CBPC Sázava pluton	1.5 m	NW-SE 62/86	contact parallel
49.40026	13.70356	KV-C	Újezd u Chanovic	Minette	CBPC Blatná pluton	8 m	W-E 186/81	no apparent
49.32149	13.53378	KV-NH	Nalžovské Hory - Letovy	Syenite porphyry	CBPC Blatná pluton	7 m	WNW-ESE 194/87	contact parallel
49.18331	13.85323	KV-Ni	Nihošovice	Syenite porphyry	Moldanubian Zone	21 m	W-E 189/82	magmatic foliation
49.38048	14.05131	KV-Ma	Malčice	Syenite porphyry	CBPC Blatná pluton	6 m	W-E 7/72, 358/84	magmatic foliation
49.88826	14.75448	KV-Se	Senohraby	Spessartite	TBZ Proterozoic Unit	2.5 m	NW-SE not known	no apparent

TBZ - Teplá Barrandien Zone; CBPC - Central Bohemian Plutonic Complex

The statistical evaluation of the AMS at individual localities was made using the ANISOFT program package (Jelínek 1978; Hrouda et al. 1990; Chadima and Jelínek 2008). The orientation of magnetic foliations and magnetic lineations, the respective mean directions and corresponding confidence areas are presented in equal-area projections on the lower hemisphere in the dyke coordinate system (dyke was rotated about its strike to vertical position and about the vertical axis to N-S position).

The magnetic minerals carrying the AMS were investigated through the Maximum Theoretical Paramagnetic Susceptibility (MTPS) method (Aydin et al. 2007) and through the susceptibility variation with magnetizing field, with operating frequency, and with temperature. The susceptibility was measured in the magnetizing fields ranging from 2 A/m to 700 A/m at the operating frequency 976 Hz using the automated mode of the MFK1-FA Kappabridge. It can be concisely characterized by the V_m parameter defined as follows (Hrouda et al. 2006):

$$V_m = 100\ (k_{max} - k_{min}) / k_{min}\ [\%]$$

where k_{max} and k_{min} are the maximum and minimum susceptibilities, respectively, obtained during one measuring run. The susceptibility variation with operating frequency was investigated at the frequencies 976 Hz and 15,616 Hz in the driving field 200 A/m. It can be represented quantitatively by the commonly accepted percentage loss of susceptibility (Dearing et al. 1996):

$$X_{FD} = 100\ (k_{LF} - k_{HF}) / k_{LF}\ [\%]$$

where k_{LF} and k_{HF} are susceptibilities measured at low and high frequencies, respectively. The susceptibility variation with temperature was measured on coarsely powdered pilot specimens at -194 to 0 °C, 25 to 700 °C (heating curve) and back to 40 °C (cooling curve), and then again between -194 and 0 °C, using the CS-L Cryostat, CS-4 Furnace (Parma et al. 1993) and the MFK1-FA Kappabridge. The Curie temperatures were determined using the Petrovský and Kapička (2006) method looking for the beginning of the paramagnetic hyperbola exactly at the Curie temperature.

4.4 Petrology

The selected 14 dykes of lamprophyres and related rocks show a compositional range from calc-alkaline to (ultra)potassic. Most dykes are represented by one rock type, but texturally they may change from relatively coarse-grained in the core to fine-grained or even to aphanitic variety at the contact with the host lithology. In one case (locality of Dobříš), a composite dyke, formed by symmetric zones of three rock types, is present (Holub 2003). Based on modal composition and textures, the rocks from selected dykes can be classified into four groups as outlined below.

4.4.1 The composite dyke from Dobříš

The overall thickness of the dyke is about 8.5 m and it consists of three symmetric zones. The dyke is dominated by the outermost kersantite (Fig. 4a) that is separated from c. 1 m thick axial hornblendite zone by a thin transitional zone of spessartite composition. In general, there are gradual transitions between individual zones and the grain size of mafic minerals increases inwards. The whole dyke is characterized by ocellar texture, with the spherical ocelli filled by carbonate and partly by quartz. In addition to clinopyroxene phenocrysts with spinel inclusions, the kersantite contains pseudomorphs of talc after olivine. Spinel is also present in the talc pseudomorphs. The matrix is fine-grained and consists of plagioclase, clinopyroxene, biotite and small amounts of quartz, carbonate and accessory apatite and opaque phases. In addition to high amphibole content, the hornblendite contains pseudomorphs after olivine, clinopyroxene, plagioclase, biotite and spinel. The amphibole is magnesio-hornblende and shows optical zoning with green-brown cores and green rims.

4.4.2 Spessartite

It is a dark-grey, medium- to fine-grained rock dominated by amphibole, biotite and plagioclase with minor alkali feldspar, secondary chlorite, actinolite, carbonate and quartz (Fig. 4b). Spessartite from Dobříš contains also diopsidic augite and pseudomorphs of talc after olivine. Amphibole forms euhedral prismatic phenocrysts up to 4 mm long. It is magnesio-hornblende-tschermakite that is partly replaced by actinolite, chlorite or overgrown by biotite. The matrix is formed by biotite, plagioclase and amphibole. Biotite is very fine-grained and occurs in the matrix. Apatite, Fe-Ti oxides and chromium spinel are common accessory phases. Spessartite from Milín (Fig. 4b) contains xenocrysts of quartz within plagioclase, amphibole and biotite matrix. The quartz appears as monocrystals but it forms round grains similar to vesicles.

4.4.3 Minette

Minette is a dark-grey, fine-grained and porphyritic rock with hypidiomorphic texture. The grain size usually decreases towards the outer contact with the host rocks, where it becomes glassy or more aphanitic in appearance. Olivine and/or clinopyroxene phenocrysts are typically subhedral to euhedral and c. 1 mm in size. Olivine phenocrysts are replaced by talc. The matrix consists of biotite (phlogopite), alkali feldspar, amphibole, and small amounts of albite and calcite. In cases, the minettes have amygdaloidal texture; the vesicles are filled by calcite (Fig. 4c). Biotite and amphibole may define magmatic foliation in the rock (Fig. 4d). Apatite, titanite and Fe-Ti oxides can occur as accessory phases. Amphibole is actinolite and it is mostly formed by replacement of clinopyroxene.

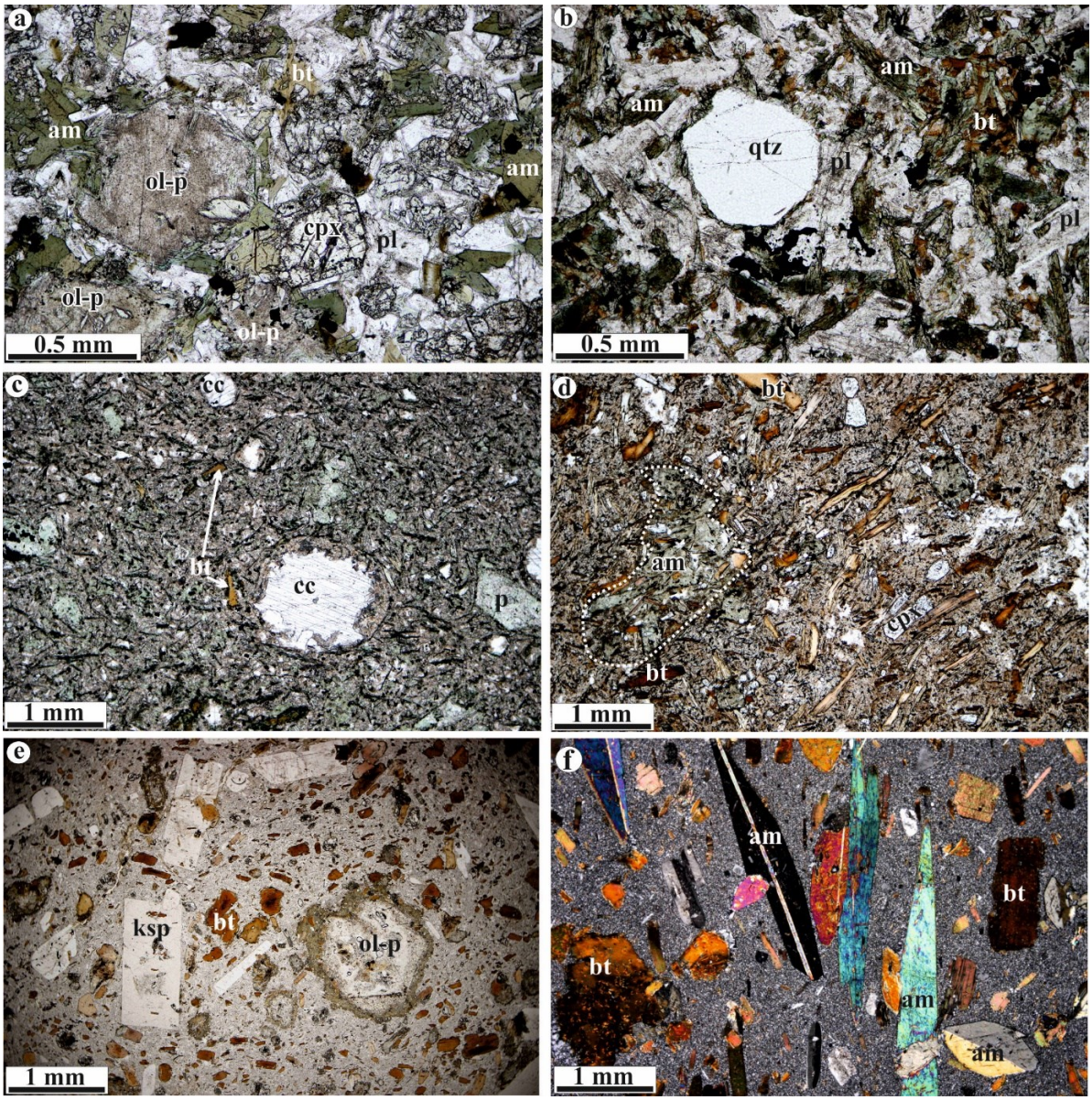

Fig. 4 Selected photomicrographs from rocks of the Central Bohemian dyke swarm (a–e: PPL, f: XPL). **a** – Kersantite/spessartite dykes, Dobříš (ZR-1) with pseudomorphs of talc after olivine (ol-p), clinopyroxene (cpx), amphibole (am), plagioclase (pl) and biotite (bt). The black grains are opaque phases. Note the hexagonal talc pseudomorphs that are partly overgrown by amphibole. **b** – Spessartite from Milín (dyke ZR-3) with porphyric grains of quartz (qtz) in plagioclase, amphibole and biotite matrix. Amphibole is mostly overgrown by biotite. Note the opaque minerals (black) following a zone from upper-right to lower-left corner of the image. **c** – Minette from Milín (dyke ZR-5) with vesicles filled by calcite (cc). The angular grains are pseudomorphs (p) of chlorite with calcite after clinopyroxene. The thin dark grains are biotite replaced by chlorite with opaque phases. The matrix consists of chlorite, calcite, and opaque phases with relicts of feldspars. **d** – Minette from Zalužany (dyke ZR-6) with biotite, amphibole (dashed field labelled am) and clinopyroxene in the fine-grained, almost glassy matrix. The white irregular grains are K-feldspar and quartz. Note that biotite, amphibole and some clinopyroxene grains show orientation in one direction. **e** – Syenite porphyry from Nihošovice (dyke KV-Ni) with phenocrysts of K-feldspar (ksp) and biotite as well as

pseudomorphs of talc after olivine. The matrix consists of K-feldspars, biotite and quartz. **f** – Syenite porphyry from Nihošovice with almost parallel phenocrysts of amphibole and biotite, in fine-grained matrix.

4.4.4 Quartz syenite to melagranite porphyry

This is a grey, fine-grained porphyritic rock dominated by plagioclase or K-feldspar with biotite and amphibole. In cases, it may contain pseudomorphs of talc after olivine, rimmed by biotite (Fig. 4e). Euhedral to subhedral K-feldspar phenocrysts are up to 6 mm in size. Amphibole occurs as euhedral, prismatic phenocrysts up to 5 mm long (Fig. 4f). It is usually actinolite, which formed by replacement of clinopyroxene or possibly also of primary hornblende. The feldspar laths and prismatic amphibole phenocrysts show locally a magmatic flow alignment. The matrix is formed by plagioclase and/or alkali feldspar, biotite, occasionally amphibole and rare quartz. Accessory phases are Fe-Ti oxides and apatite.

4.5 Whole rock geochemistry

Based on the TAS diagram (Le Bas et al. 1986), the above-mentioned four groups range from basalt, through basaltic trachyandesite to trachyte/trachydacite (Fig. 5a). The mafic varieties (hornblendite, spessartite and kersantite) show calc-alkaline affinity, while the minette and quartz syenite porphyry belong to high-K calc-alkaline series or, more commonly, shoshonite series (Fig. 5b). A continuous compositional change exists in the MgO, FeO and CaO variations, where all three oxides decrease from hornblendite and spessartite/kersantite to minette and quartz syenite porphyry (Fig. 5c–d). Both FeO and CaO show positive correlation with MgO.

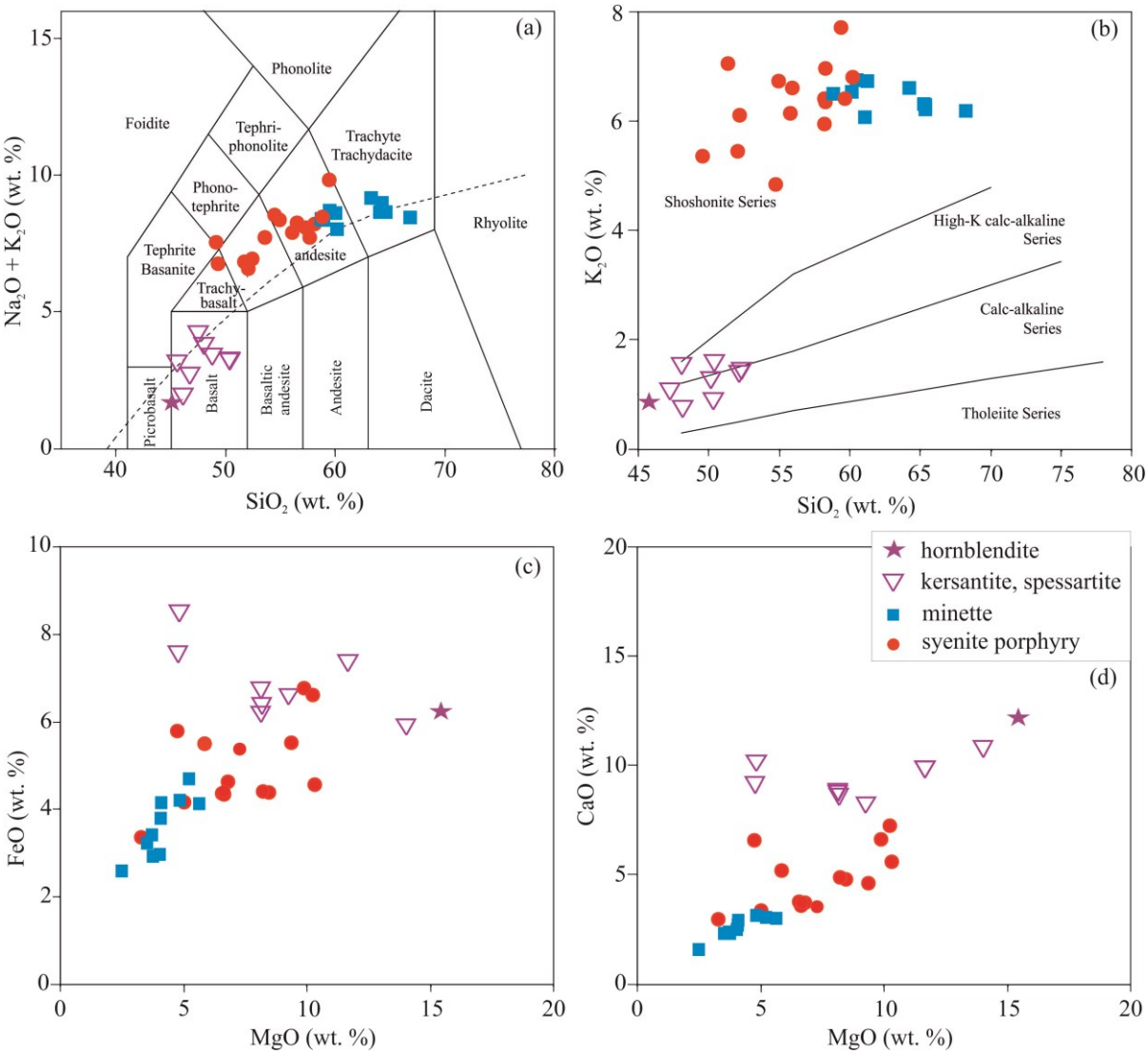

Fig. 5 Geochemical classification of lamprophyres and related rocks: **a** – Total alkali-silica (TAS) classification diagram (Le Bas et al. 1986); **b** – K_2O vs. SiO_2 (wt. %) diagram (according to Peccerillo and Taylor 1976); **c** – FeO vs. MgO (wt. %); **d** – CaO vs. MgO (wt. %). The major element data have been recalculated to 100 wt. % on a volatile-free basis. Based on data from Holub et al. (2007, 2009, 2010), Kubínová et al. (2017) and unpublished data of F.V. Holub.

4.6 Magnetic mineralogy

The mean volume susceptibility of the dykes investigated is variable, ranging from the order of 10^{-4} to the order of 10^{-2} (Fig. 6, Tab. 2). The MTPS method, which calculates the rock paramagnetic susceptibility from the Fe and Mn contents obtained from the whole-rock chemical analyses, shows that the contribution of paramagnetic minerals to the whole-rock susceptibility is relatively low, ranging from 0.2×10^{-3} to 0.7×10^{-3}. Consequently, in weakly magnetic dykes ($K_m < 0.7 \times 10^{-3}$), the susceptibility can be significantly affected by paramagnetic minerals, while in the

dykes with higher susceptibility the ferromagnetic minerals play a more important, sometimes even dominant, role.

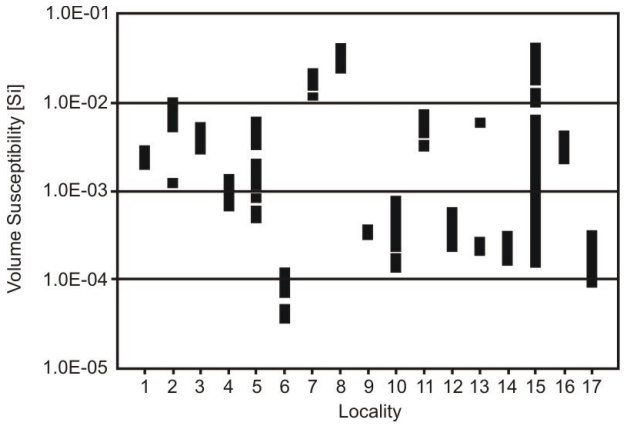

Fig. 6 Point diagram of bulk magnetic susceptibility in individual dykes. (1) ZR-1 hornblendite, (2) ZR-1 kersantite, (3) ZR-1 spessartite, (4) ZR-2 spessartite, (5) ZR-3 spessartite, (6) ZR-3 host granite, (7) ZR-4 minette, (8) ZR-5 minette, (9) ZR-6 minette, (10) KV-C minette, (11) KV-KU syenite porphyry, (12) KV-Ma syenite porphyry, (13) KV-Ne minette, (14) KV-NH syenite porphyry, (15) KV-Se spessartite, (16) KV-PS minette, (17) KV-Ni syenite porphyry.

The susceptibility variation with field is either nondetectable practically (Fig. 7a), very weak (Fig. 7b), or even very strong (Fig. 7c). The mean values of the V_m parameter for individual dykes are presented in Tab. 2. Among ferromagnetic minerals *sensu lato*, pure magnetite shows virtually field-independent susceptibility, while in titanomagnetite, pyrrhotite and hematite the susceptibility may be clearly field-dependent even in low fields used in common AMS meters (e.g., Worm et al. 1993; Jackson et al. 1998; Hrouda 2002, 2006; de Wall and Nano 2004). From this point of view, none or very weak susceptibility variation of most specimens investigated may indicate presence of more or less pure magnetite. The susceptibility vs. field curves of the specimens from the locality ZR-3 showing strong susceptibility increase with field resembling curves of some types of pyrrhotite (cf. Hrouda et al. 2006, 2009). This conclusion is supported by very strong variation of out-of-phase susceptibility with field (Fig. 7d). The out-of-phase susceptibility originates in materials in which, if measured in alternating magnetic field, the magnetic response delays behind the magnetizing field. The susceptibility may then be formally resolved into the component that is in-phase (almost exclusively used in rock magnetism) and that which is out-of-phase with respect to magnetizing field. The strong field variation of the out-of-phase component is characteristic of minerals with wide hysteresis loop such as pyrrhotite.

Tab. 2 Magnetic characteristics of individual dykes

Locality No.	Locality Name	Rock Type	Fabric Type	K_m [10^{-3}]	MTPS [SI u.]	V_m [%]	X_{FD} [%]	T_v, T_C [°C]	A_{40} [%]	Main AMS Carrier
ZR-1	Dobříš	Spessartite	IIIa	3.899	560	1.2	2.74	-169, 585		magnetite
		Kersantite	IIIb	6.091	587	2.3	2.87	510, 585 -155, 335	-11.2	magnetite
		Hornblendite	Ia	2.361	655	0.7	2.86	497, 585	-10.2	magnetite
ZR-2	Příbram - Trhové Dušníky	Spessartite	IIIb	1.121		0.2	3.16	550	16.6	Fe-Ti oxide
ZR-3	Milín - Kojetín	Spessartite		3.578	484	85	2.91	327, 505	-68.8	pyrrhotite
ZR-4	Milín W	Minette	Ib, IIb	18.47	443	0.5	2.55			magnetite
ZR-5	Milín E	Minette	Ia	34.12		1.4	2.46	-155, 600	-22.2	magnetite
ZR-6	Zalužany - Kozárovice	Minette	Ia	0.346	371	1.6	5.68	-156, 582	684.2	magnetite
KV-KU	Kamenný Újezdec	Syenite porphyry	Ia-b	4.807	299	2.4	1.61	562	165.7	magnetite
KV-PS	Poříčí nad Sázavou	Minette	Ib	3.546		0.5	4.68	585	150.0	magnetite
KV-Ne	Městečko - Nespeky	Minette	Ia	1.762	375	0.4	2.37	549	116.2	paramag.
KV-C	Újezd u Chanovic	Minette	Ia-b	0.385	356	10.1	1.27	322, 575	37.9	paramag.
KV-NH	Nalžovské Hory - Letovy	Syenite porphyry	Ia	0.226		7.6	-0.9	563	521.1	paramag.
KV-Ni	Nihošovice	Syenite porphyry		0.180	229	3.9	-0.2	555	94.0	paramag.
KV-Ma	Malčice	Syenite porphyry	Ia-b	0.355	346	1.1	1.77	528, 580	150.0	paramag.
KV-Se	Senohraby	Spessartite	IIIb	21.4 0.909	518	0.5	-1.3	578	46.8	magnetite paramag.

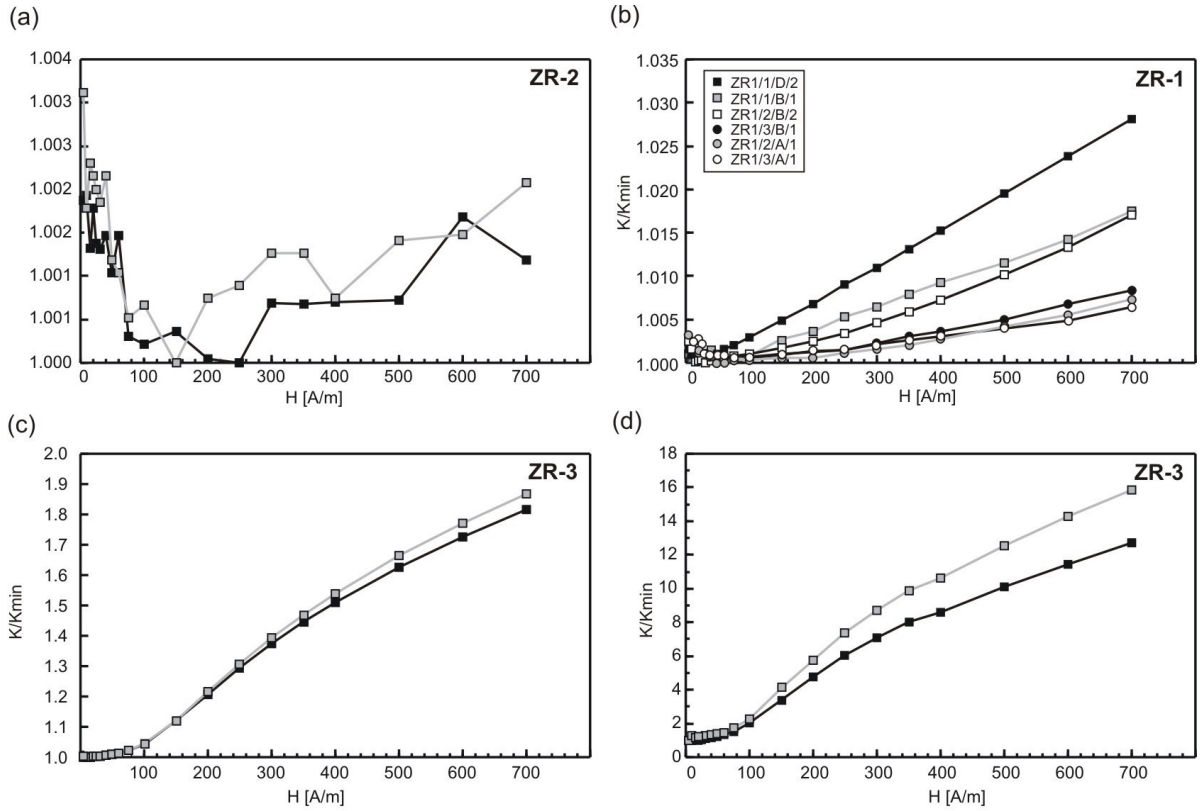

Fig. 7 Examples of variation of bulk susceptibility K/K_{min} with measuring field H.

The grain size of ferromagnetic *sensu lato* minerals can be assessed, at least partially, through frequency-dependent susceptibility. Namely, the frequency-dependent susceptibility is effectively zero in multi-domain (MD) and single-domain (SD) grains of magnetite (titanomagnetite) as well as in its ultra-fine superparamagnetic (SP) grains (e.g. Dearing et al. 1996; Hrouda 2011). On the other hand, it can be clearly non-zero in magnetically viscous grains that are on the transition from SP state to SD state. The X_{FD} parameter in the dykes investigated ranges from 2.5 % to 6.5 %. If we realize that the detection limit of the X_{FD} parameter is less than 1 % (Hrouda and Pokorný 2011) and the X_{FD} parameter is mostly less than 15 % (Dearing et al. 1996; Eyre 1997; Worm 1998), it is obvious that the dykes investigated contain magnetic grains that are on the transition from SP to SD states in non-negligible amounts. Assuming that the magnetic particles show continuous size distribution, it is likely that the rocks investigated contain also SD particles.

The heating curves mostly show one acute susceptibility decrease due to Curie temperature at 500–600 °C (Figs 8a–d). The Curie temperatures that are near 585 °C correspond to those of magnetite, whose presence is confirmed by the susceptibility decrease at c. -155 °C at Verwey transition, which is typical of relatively pure magnetite (Dunlop and Özdemir 1997). The Curie temperatures less than 550 °C probably indicate Ti-richer Fe-Ti oxides. In the dyke ZR-1, there are three susceptibility decreases on the heating curves, at 335 °C, c. 500 °C, and 585 °C (Fig. 8b). The last temperature probably points to magnetite, the second may reflect the presence of

titanomagnetite. The susceptibility decrease at 335 °C may indicate Fe-Ti oxide with relatively high content of Ti or pyrrhotite. As the Curie temperature of pyrrhotite is usually very near 325 °C, the first interpretation seems more likely. It is interesting that the curves of kersantite/spessartite and hornblendite are very similar thus supporting the observation of Holub (2003) of gradual transitions between individual rock types within this dyke. In the dykes ZR-3 and KV-C, the heating susceptibility vs. temperature curves show the most conspicuous and acute susceptibility decrease due to Curie temperature at 327 and 322 °C, respectively, and very minor decreases at 505 and 575 °C, respectively (Fig. 8c). The former undoubtedly indicates pyrrhotite and the latter probably Fe-Ti oxides to magnetite.

The cooling curves may run higher than the heating ones (see Fig. 8d, Tab. 2). This difference indicates that the assemblage of magnetic minerals is rather unstable and prone to activating various magnetic phases due to specimen heating. This may for instance result from post-magmatic alterations during magma cooling or from the effect of epigenetic fluids. On the other hand, the cooling curves may also run lower than the heating ones (see Fig. 8d, Tab. 2). This may indicate dissolution of the earlier separated phases resulting in the creation of a less magnetic phase.

In weakly magnetic specimens, the most conspicuous feature of the heating curves is paramagnetic hyperbola (for example see the low temperature segment of the curve KV-C in Fig. 8c). The paramagnetic susceptibilities determined through resolution of the susceptibility vs. temperature curve into paramagnetic hyperbola and ferromagnetic straight line using the method by Hrouda (1994) are mostly in the order of 10^{-4}, thus being of the same order as those obtained by the MTPS method.

Magnetite is dominant contributor to the rock susceptibility and AMS in strongly magnetic dykes ZR-1, ZR-4, ZR-5, KV-KU, KV-PS, and partially also KV-Ne. As the magnetite AMS is controlled by its grain shape, the rock AMS is determined by the magnetite grain-shape preferred orientation. Even though there may be some other magnetic phases in the above dykes, their contributions to the rock susceptibility are relatively low. In the dyke ZR-3, the AMS is dominantly carried by pyrrhotite preferentially oriented by mineral lattice. In weakly magnetic dykes, the AMS signal is often dominated by paramagnetic mafic silicates; sometimes the magnetic fabric is composite, due to both paramagnetic minerals and Fe-Ti oxides.

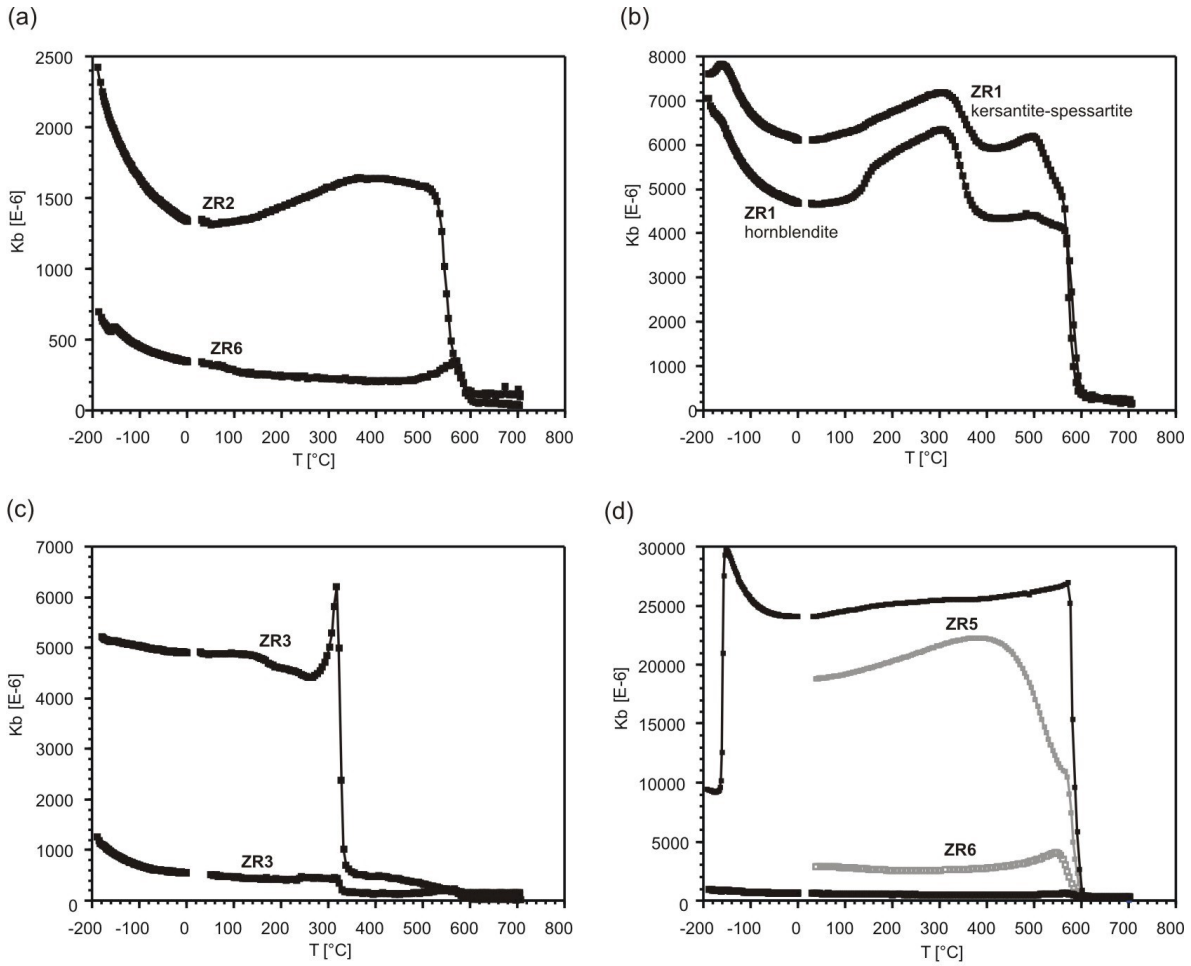

Fig. 8 Temperature variation of susceptibility for pilot specimens. In black are heating curves, in grey cooling curves.

4.7 Magnetic fabrics

4.7.1 Dobříš composite dyke

The degree of AMS is very low in all rock types (Fig. 9a). The shape of the AMS ellipsoid ranges from prolate to oblate in kersantite, from neutral (on the transition between prolate and oblate) to moderately oblate in spessartite and from moderately prolate to moderately oblate in hornblendite (Fig. 9).

Both the magnetic foliations and lineations are always relatively well defined. In the central hornblendite, the magnetic foliation is approximately parallel to the dyke plane, while the magnetic lineation is horizontal and also parallel to the dyke plane (Fig. 9b). This fabric corresponds to the *Type Ia*. In kersantite, the magnetic foliation is sometimes oblique to the dyke plane but in the most specimens vertical and perpendicular to the dyke plane; the magnetic lineation is mostly

perpendicular to the dyke (Fig. 9c). The magnetic fabric of the most specimens corresponds to the *Type IIIb*. In spessartite, both the magnetic foliations and magnetic lineations are virtually horizontal, approximately perpendicular to the dyke plane (*Type IIIa*; see Fig. 9d).

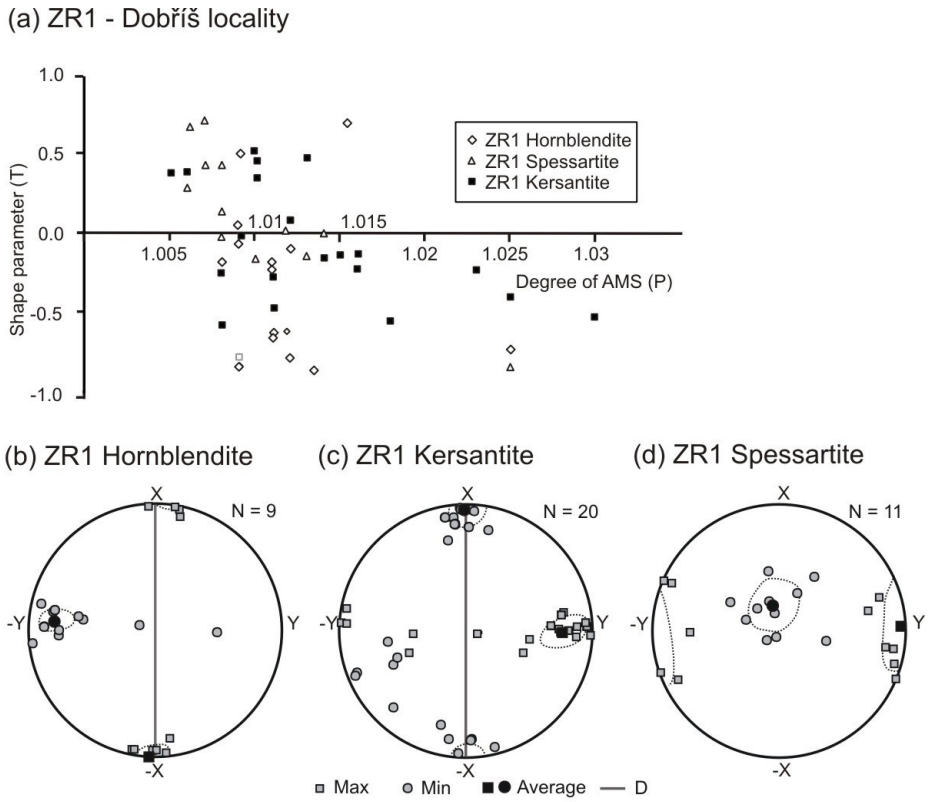

Fig. 9 Pattern of the AMS in the composite dyke ZR-1 (Dobříš). **a** – Magnetic anisotropy P-T plot. Orientations of magnetic lineations (squares) and magnetic foliation poles (circles): in hornblendite (**b**), kersantite (**c**) and spessartite (**d**). Equal-area projection on lower hemisphere. Ellipses represent confidence areas.

The fact that the magnetic fabrics are conspicuously different in the individual rock types excludes a possibility of post-magmatic origin and can be interpreted in terms of magma flow. The *Type Ia* magnetic fabric in central hornblendite that is the most frequent in the intermediate and mafic dykes the world over, evidently indicates relatively free flow during which the magnetic minerals orientate parallel with their larger surfaces to the dyke and with their longer dimensions parallel to the magma flow. The horizontal flow direction indicates that the hornblendite part of the dyke was not fed by vertical flow along the entire dyke length, but only locally and then the magma propagated through horizontal flow.

In kersantite and spessartite dykes, the magnetic foliations are perpendicular to the dyke, being vertical in kersantite and horizontal in spessartite, and the magnetic lineations are also perpendicular to the dyke and approximately horizontal. These fabric types belong to the most

controversial *Types IIIa* and *b*, the origins of which are disputable. The magnetic foliation perpendicular to the dyke could indicate the magma movement mechanism hypothesized by Raposo and Ernesto (1995) for the *Type II*, i.e. compaction of a static magma column along the dyke in which the magnetic minerals reoriented with their larger surfaces perpendicular to the magma movement. If true, the magma movement would be horizontal in kersantite and vertical in spessartite. The origin of magnetic lineations perpendicular to the dyke is extremely difficult to explain. One explanation would be that of Rochette et al. (1991) ascribing this magnetic lineation to secondary processes such as hydrothermal alteration. The other assumes squeezing of some portions of magma due to the pressure of the other portions of magma resulting in thickening of the dyke and faint magma movement in the direction perpendicular to the dyke.

4.7.2 Minette dykes

The magnetic fabric of minette dykes was investigated at six localities. The degree of AMS is mostly very low, only in the KV-C dyke it ranges from very low to moderately high (Fig. 10a). The shape of the AMS ellipsoid is mostly oblate, prolate one was found only in a few specimens in ZR-4 and KV-C dykes (Fig. 10a). In each of the minette dykes investigated, the magnetic foliation of either almost all (dykes ZR-5, ZR-6, KV-Ne) or at least majority of specimens (dykes ZR-4, KV-PS, KV-C) is near the dyke plane (Fig. 10b–g). Some dykes (ZR-4, KV-PS, KV-C) yielded also a few specimens with magnetic foliation at a large angle to the dyke plane, being sometimes even perpendicular. The magnetic lineation is roughly parallel to the dyke plane in all dykes, being virtually vertical in two (ZR-4, KV-PS), horizontal in three (ZR-5, ZR-6, KV-Ne), and ranging from vertical to horizontal in one (KV-C) of them (Fig. 10b–g).

The magnetic fabric in the majority of specimens corresponds to the *Type Ia*. This type evidently originates from relatively free flow during which the magnetic minerals orientate parallel with their larger surfaces to the dyke margins and with their longer dimensions parallel to the magma flow. The vertical orientation of magnetic lineation in the dykes ZR-4 and KV-PS indicate vertical magma flow. The horizontal magnetic lineations in the dykes ZR-5, ZR-6, KV-Ne probably document that these dykes were fed by vertical flow only locally and then the magma propagated through horizontal flow. In some dykes, there are rare specimens with magnetic foliation roughly perpendicular to the dyke plane. They suggest that the magma movement need not be represented by free flow in the entire volume of the dyke, but could have been rather represented by compressive deformation in which the magnetic minerals reorient with their larger surfaces perpendicular to the magma movement. In the KV-C dyke one can observe gradual transitions from one mechanism to the other.

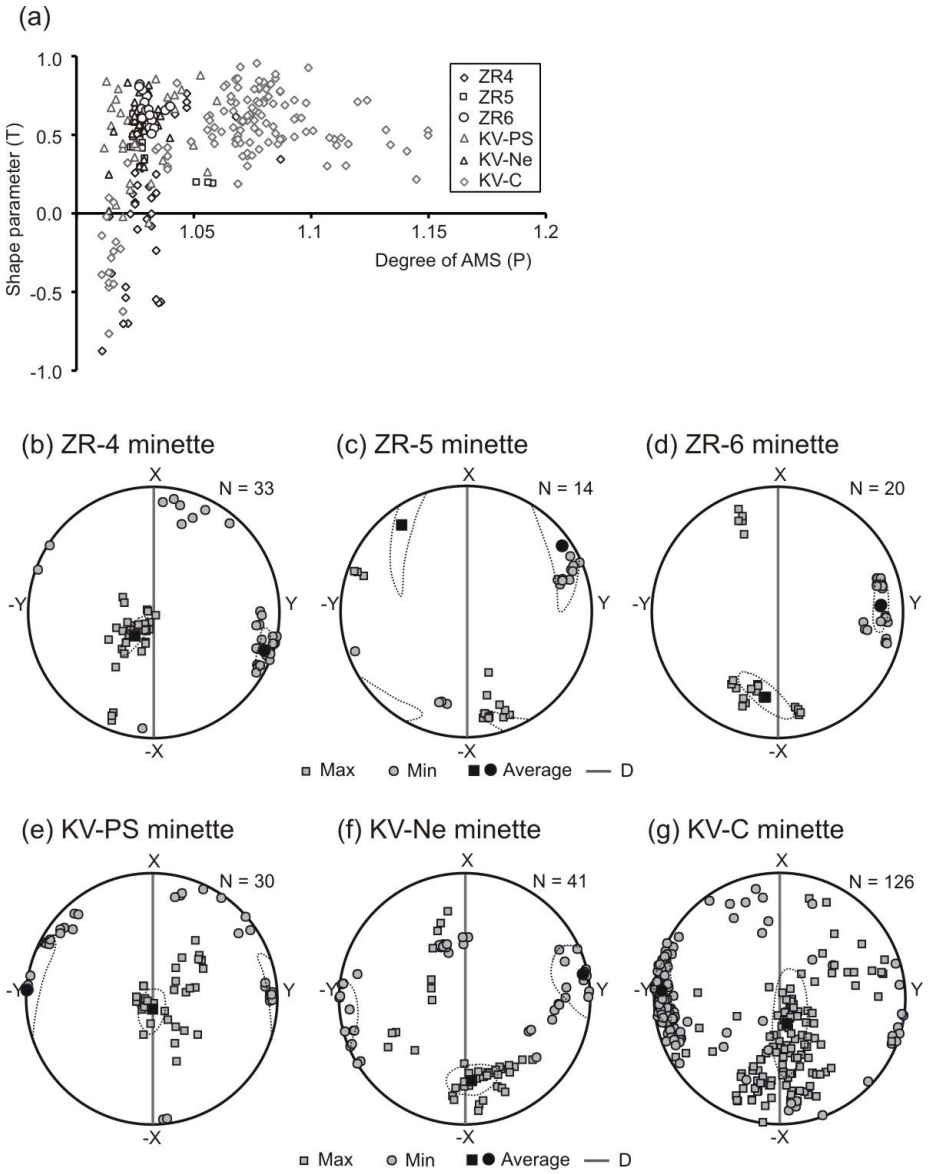

Fig. 10 Pattern of the AMS in minette dykes. **a** – Magnetic anisotropy P-T plot. **b–g** – Orientations of magnetic lineations (squares) and magnetic foliation poles (circles). Equal-area projection on lower hemisphere. Ellipses represent confidence areas.

4.7.3 Quartz syenite to melagranite porphyry dykes

The magnetic fabric of syenite porphyry dykes was investigated at four localities. The degree of AMS is very low in most specimens, only rarely slightly higher (mainly in KV-Ma dyke) (Fig. 11a). The shape of the AMS ellipsoid ranges from very prolate to almost perfectly oblate (Fig. 11a). In three dykes (KV-KU, KV-NH, KV-Ma), the magnetic foliation is relatively near the dyke plane (Figs 11b–d; 12a–b). At two localities (KV-Ni and KV-Ma), the magnetic foliation scatters widely, creating a wide girdle in its poles, at a large angle with the dyke margins (Figs 11d–e; 12a–b). The magnetic lineation is very roughly parallel to the dyke plane in all four dykes, being virtually

horizontal in KV-NH and creating girdles very near to dyke plane in KV-KU and KV-Ma (Fig. 11b–d). In the dyke KV-Ni, the magnetic lineations of the most specimens are sub-horizontal or show only mild plunges, even though there are also a few specimens that plunge moderately to steeply (Figs 11e, 12a). In the dyke KV-NH, the magnetic fabric corresponds well to the *Type Ib* fabric which evidently originated from relatively free flow. The horizontal magnetic lineations indicate that the flow was horizontal. The magnetic fabric in the dykes KV-KU and KV-Ma in principle also corresponds to the *Type I* (in fact transition between *Type Ia* and *Type Ib*). However, the mean magnetic foliation differs from the dyke azimuthally by c. 20°. We ascribe this difference rather to measurement error in the dyke orientation due to local unevenness of the dyke plane rather than to the flow oblique with respect to the dyke plane. The girdle in magnetic lineations suggests that the magma flow may have been complex, spatially varying from vertical to horizontal.

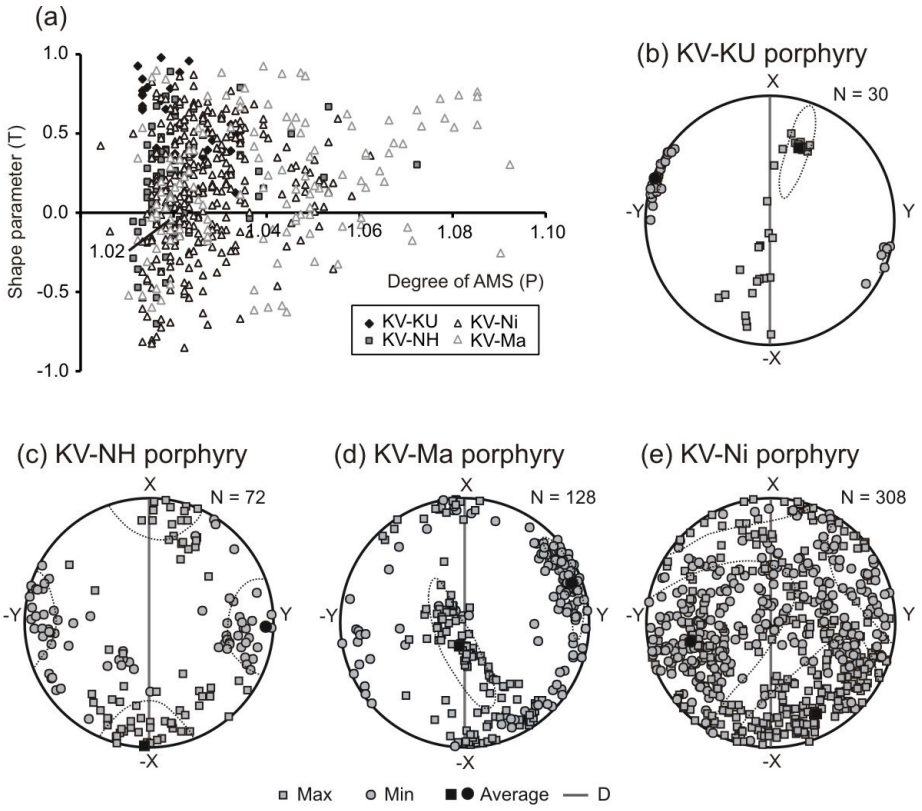

Fig. 11 Pattern of the AMS in porphyry dykes. **a** – Magnetic anisotropy P-T plot. **b–e** – Orientations of magnetic lineations (squares) and magnetic foliation poles (circles). Equal-area projection on lower hemisphere. Ellipses represent confidence areas.

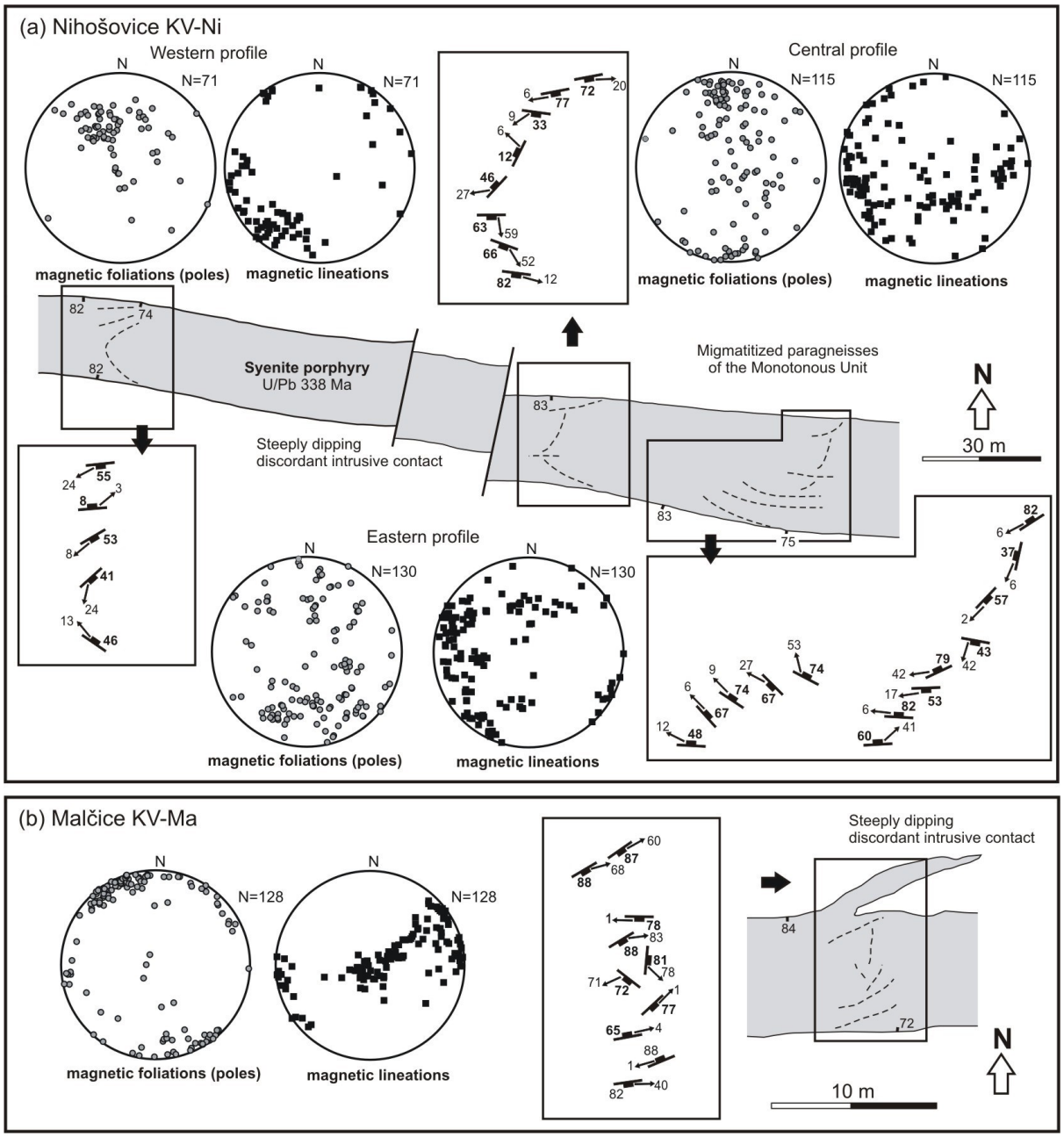

Fig. 12 Structural scheme of porphyry dykes showing magnetic fabric pattern and trajectories of the magnetic foliation at: **a** – Nihošovice (KV-Ni) and **b** – Malčice (KV-Ma).

4.7.4 Spessartite dykes

In addition to the locality ZR-1 where spessartite occurs in a composite dyke consisting of three rock types (see Section 6.1) and whose degree of AMS is very low (see Fig. 9a), this rock was investigated in the dykes ZR-3 and KV-Se. In the dyke ZR-3, the degree of AMS is an order of magnitude higher but in the host granite it is very low. The dyke KV-Se (Fig. 13a) shows highly variable, low to high, degree of AMS.

The shape of the AMS ellipsoid ranges from moderately prolate to strongly oblate at all three localities (Fig. 13a). In the most strongly anisotropic specimens, it is neutral to weakly prolate. Both the magnetic foliation and lineation in the dyke ZR-3 are oblique with respect to the dyke (Fig. 13b). The magnetic foliation and lineation in the host granite are almost precisely perpendicular to the dyke (Fig. 13c). In KV-Se dyke, both magnetic foliation and magnetic lineation are perpendicular to the dyke margins (*Type IIIb*; Fig. 13d). In neither of the spessartite dykes investigated, the magnetic fabric corresponds to the generally most common *Type I*. It means that the movement of the spessartite magma did not resemble the free flow known mainly from minette magmas but was much more complex.

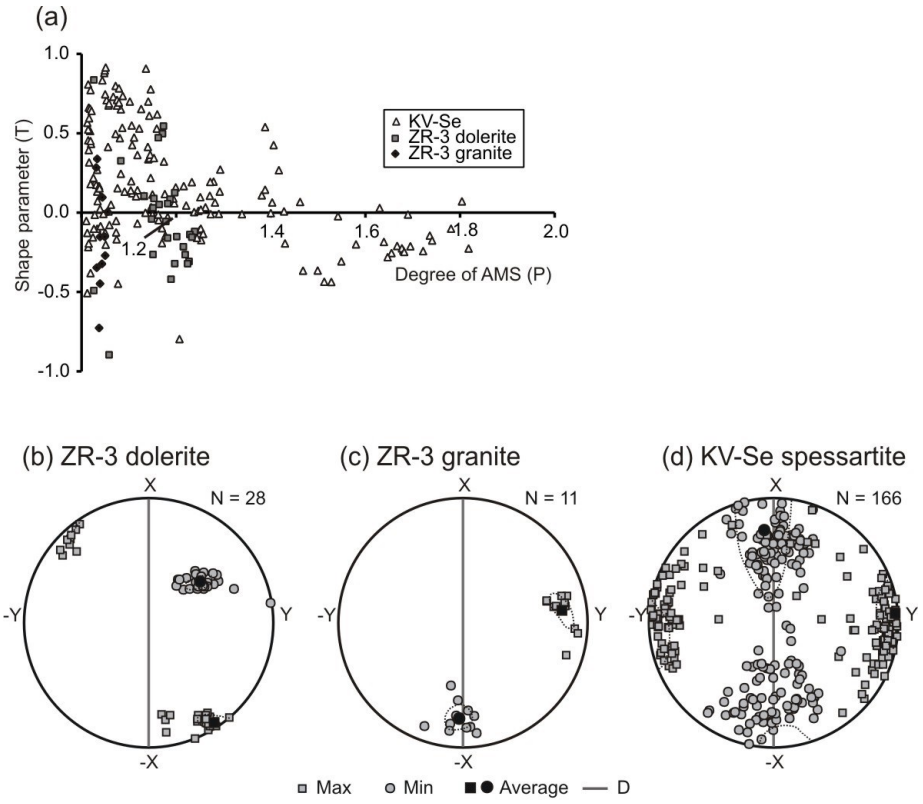

Fig. 13 Pattern of the AMS in spessartite/dolerite dykes (ZR-3 and KV-Se) and host granite. **a** – Magnetic anisotropy P-T plot. Orientations of magnetic lineations (squares) and magnetic foliation poles (circles): **b** – in spessartite/dolerite dyke (locality ZR-3); **c** – in host-rock granite (locality ZR-3) and **d** – in spessartite dyke (locality KV-Se). Equal-area projection on lower hemisphere. Ellipses represent confidence areas.

4.8 Discussion

Almost two thirds of the dykes investigated show *Type I* magnetic fabric characterized by approximate parallelism of the magnetic foliation and magnetic lineation to the dyke plane. The magnetic lineation is mostly nearly horizontal and only exceptionally vertical. This magnetic fabric type is commonly assumed to originate through magma flow within the dyke (e.g. Raposo 2011). It

is interesting that the flow directions inferred from magnetic lineations are horizontal and only exceptionally vertical. Consequently, the dyke magma propagated through horizontal flow, which may indicate that the dykes investigated are not located above the magma source.

In the Dobříš composite dyke, the innermost hornblendite shows *Type Ia* magnetic fabric, the outermost spessartite *Type IIIa*, and the kersantite in between *Type IIIb*. Only hornblendite therefore experienced relatively free flow of magma, while the mechanisms of kersantite and spessartite magma movement were more complex.

The magnetic fabric in kersantite is precisely inverse to that in hornblendite. The first, geological explanation of this phenomenon assumes dramatically different magma movement in both rock types and the second, physical explanation assumes that the grains of the magnetic minerals carrying the AMS were very small, virtually single domain (SD) particles in one of the rock types. As shown by Potter and Stephenson (1988) for example, the maximum susceptibility is along the minimum axis, while the minimum susceptibility is along the maximum dimension of a SD particle.

Were the second, physical explanation true, the magnetic particles would define the most frequent fabric type whereby the larger planes of magnetic minerals are aligned parallel to the dyke plane and their longer dimensions are parallel to the flow direction within the dyke. However, the susceptibility variation with temperature is very similar in hornblendite and kersantite. In addition, the frequency-dependent susceptibility is in these rock types relatively low (mostly X_{FD} = 2–3 %) indicating that the ultrafine magnetically viscous particles on transition from superparamagnetic (SP) to SD state are indeed present, albeit in relatively small amounts. Assuming grain-size distribution continuous from SP, through SD to MD, and realizing that the susceptibility of SD particles is lower than that of MD or SP particles, the relatively low values of frequency-dependent susceptibility may indicate that the SD particles are not abundant enough to dominate the rock magnetism. All this makes the physical explanation very unlikely and the above phenomenon should be ascribed to different mechanisms in detail magma movement.

In spessartite, the magnetic fabric is of the *Type IIIa*. We assume that the magma flow was not free because the injected joint was not fully open or was filled in with initial portions of magma. Consequently, the magma movement resembled that of forceful injection. The magnetic minerals were then orientated with their larger surfaces perpendicular to the magma movement and the magnetic foliation was horizontal. The existence of magnetic lineations perpendicular to the dyke can be explained by a mechanism when joint, gradually filled with the magma, was simultaneously widened and the magma also flew horizontally on a small scale.

The studied dykes are mostly perpendicular to the elongation of the CBPC as well as to magmatic to subsolidus fabrics in individual plutons and regional metamorphic fabrics in the WMZ. In addition, the dykes are parallel with the direction of regional ~ WNW-ESE crustal convergence

during the main phase of the Variscan Orogeny at ~ 355 to 340 Ma (e.g. Žák et al. 2005a, b, 2009; Schulmann et al. 2009; Faryad and Žák 2016). Therefore, we can assume that NW(W)-SE(E) trending extensional joints and accompanying dykes originated synchronously during dilatation (orogen arc-parallel stretching) which was perpendicular to their intrusive contacts.

Analyses of fabric pattern and AMS have been applied for identification of the direction of initial magma flow through dykes (e.g. Varga et al. 1998; Geoffroy et al. 2002). In general, magnetic lineations are usually subparallel to the direction of magma flow (Callot et al. 2001; Callot and Geoffroy 2004). Relics of steeply dipping magnetic lineations which have been identified mainly in the central parts of the dykes indicate an originally vertical flow direction during magma ascent after dyke propagation, mainly in marginal parts of the dykes. However, predominant subhorizontal magmatic lineation (0 to 40° to ~ W to WNW) suggests changes in rate and direction of magma flow. The reason can be increasing viscosity of the magma (e.g. Petford 1996; Mathieu et al. 2008) and/or effect of regional stress field (Féménias et al. 2004). Indeed, the regional stress conditions in the WMZ changed from the NW–SE compression to subvertical shortening of the crust due to exhumation of orogenic root domain (e.g. Verner et al. 2008; Žák et al. 2012). In addition, rare imbrication of magnetic foliation (e.g. Geoffroy et al. 2002) with respect to the intrusive contacts of the dyke (e.g. at Nihošovice; Figs 11e, 12a) indicates the redirection of magma flow from east to west.

4.9 Conclusions

The investigations of magnetic fabrics in the calc-alkaline to (ultra)potassic lamprophyre dykes of the Central Bohemian Dyke Swarm (Bohemian Massif, Czech Republic) have drawn the following conclusions:

(a) Even though various magnetic phases, represented by various Fe-Ti oxides, were identified in the dykes investigated, it is magnetite or low-Ti titanomagnetite that is evidently the principal carrier of rock susceptibility as well as of the AMS. As the AMS of this mineral is controlled by the grain shape, the rock's AMS reflects its grain-preferred orientation. The contributions of the other Fe-Ti oxides to the rock susceptibility are low. In one dyke, the predominating carrier of susceptibility is pyrrhotite, the AMS of which is controlled by the lattice-preferred orientation of grains. The intensity of this effect depends on the pyrrhotite and magnetite/titanomagnetite proportions.

(b) The magnetic fabric in the most dykes is conformable to the dyke shapes. This corresponds to the most common type of magnetic fabric in dykes the world over (*Type I*; Raposo and Ernesto 1995), which no doubt originates through a magma flow, during which the larger surfaces of magnetic minerals orient approximately parallel to the dyke, while the longer dimensions

orient parallel to the magma flow direction. It is considered to be relatively free flow that requires relatively open, likely extensional structures. The flow directions inferred from magnetic lineations are horizontal and only exceptionally vertical suggesting that the magma propagated through horizontal flow within the dyke. This may indicate that the dykes investigated were not located immediately above the magma source.

(c) In most spessartite dykes, both the magnetic foliation and magnetic lineation are perpendicular to the dyke, thus corresponding to the magnetic fabric *Type III* of Raposo and Ernesto (1995). We assume that the magma movement had character of forceful injection. The larger surfaces of the magnetic minerals were oriented perpendicular to the magma movement and the long dimensions of the same minerals oriented perpendicular to the progressively widened dyke.

(d) In the Dobříš composite dyke, the innermost hornblendite shows *Type Ia* magnetic fabric, the outermost spessartite *Type IIIa*, and the kersantite located in between *Type IIIb*. Only hornblendite, therefore, indicates relatively free flow of magma, while the mechanisms of magma movement in kersantite and spessartite were more complex, possibly changing during the generation of that single composite dyke.

(e) Studied dykes were emplaced into already juxtaposed the Teplá-Barrandian Zone, Central Bohemian Plutonic Complex and exhumed western Moldanubian Zone at ~ 346 to 337 Ma. Identical orientation of dykes (steep intrusive contacts in W(NW)-E(SE) trend was caused by the regional stress field of ~ WNW-ESE convergence (arc-parallel stretching) and subvertical shortening of due to crustal exhumation of the Variscan orogen root.

Acknowledgements

We would like to gratefully acknowledge the contribution of Michael Petronis and Arnošt Dudek through their very constructive reviews, which greatly assisted in improving the original manuscript. Vladislav Rapprich is acknowledged for his helpful comments and careful editorial handling of the manuscript. Lucie Orságová and Martina Studená are greatly thanked for assistance with sampling and measuring AMS. The research was financially supported by the Czech Science Foundation (GACR-FWF No. 15-34621L to K. Verner).

Electronic supplementary material

The values of the mean susceptibility (K_m), degree of AMS (P), shape parameter (T) as well as the orientations of the maximum (K_1), intermediate (K_2), and minimum (K_3) susceptibilities in terms of azimuth (prefix d) and plunge (prefix i) in geographic coordinates for individual specimens are available online at the Journal web site (*http://dx.doi.org/10.3190/jgeosci.222*).

References

Aydin A, Ferré EC, Aslan Z (2007) The magnetic susceptibility of granitic rocks as a proxy for geochemical differentiation: example from the Saruhan granitoids, NE Turkey. Tectonophysics 441: 85–95

Bates MP, Mushayandebvu MF (1995) Magnetic fabric in the Umvimeela Dyke, satellite of the Great Dyke, Zimbabwe. Tectonophysics 242: 141–254

Callot JP, Geoffroy L (2004) Magma flow in the East Greenland dyke swarm inferred from study of anisotropy of magnetic susceptibility: magmatic growth of a volcanic margin. Geophys J Inter 159: 816–830

Callot JP, Geoffroy L, Aubourg C, Pozzi JP, Mege D (2001) Magma flow directions of shallow dykes from the East Greenland volcanic margin inferred from magnetic fabric studies. Tectonophysics 335: 3–4

Cañón-Tapia E (2004) Anisotropy of magnetic susceptibility of lava flows and dykes: a historical account. In: Martin-Hernandez F, Luneburg CM, Aubourg C, Jackson M (eds) Magnetic Fabric: Methods and Applications. Geological Society of London Special Publications 238: pp 205–225

Chadima M, Jelínek V (2008) Anisoft 4.2 – anisotropy data browser. Contrib Geophys Geodesy 38: 41 (Special Issue)

Chalapathi Rao NV, Srivastava RK (2012) Kimberlites, lamproites, lamprophyres, their entrained xenoliths, mafic dykes and dyke swarms: highlights of recent Indian Research. Proc Indian Nat Sci Acad 78: 431–444

Chlupáč I, Havlíček V, Kříž J, Kukal Z, Štorch P (1998) Paleozoic of the Barrandian (Cambrian to Devonian). Czech Geological Survey, Prague, pp 1–183

Chlupáč I, Brzobohatý R, Kovanda J, Stráník Z (2002) Geological History of the Czech Republic. Academia, Prague, pp 1–436 (in Czech)

Dearing JA, Dann RJL, Hay K, Lees JA, Loveland PJ, Maher BA, O'Grady K (1996) Frequency-dependent susceptibility measurements of environmental materials. Geophys J Int 124: 228–240

Dunlop DJ, Özdemir Ö (1997) Rock Magnetism. Fundamentals and Frontiers. Cambridge University Press, Cambridge, pp 1–573

De Wall H (2000) The field dependence of AC susceptibility in titanomagnetites: implications for the anisotropy of magnetic susceptibility. Geophys Res Lett 27: 2409–2411

De Wall H, Nano L (2004) The use of field dependence of magnetic susceptibility for monitoring variations in titanomagnetite composition: a case study on basanites from the Vogelsberg 1996 Drillhole, Germany. Stud Geophys Geod 48: 767–776

Dörr W, Zulauf G (2010) Elevator tectonics and orogenic collapse of a Tibetan-style plateau in the European Variscides: the role of the Bohemian shear zone. Int J Earth Sci (Geol Rundsch) 99: 299–325

Edgar AD, Mitchell RH (1997) Ultra high pressure-temperature melting experiments on an SiO_2-rich lamproite from Smoky Butte, Montana: derivation of siliceous lamproite magmas from enriched sources deep in the continental mantle. J Petrol 38: 457–477

Ernst RE, Baragar WRA (1992) Evidence from magnetic fabric for the flow pattern of magma in the Mackenzie giant radiating dyke swarm. Nature 356: 511–513

Eyre JK (1997) Frequency dependence of magnetic susceptibility for populations of single-domain grains. Geophys J Int 129: 209–211

Faryad SW, Žák J (2016) High-pressure granulites of the Podolsko complex, Bohemian Massif: an example of crustal rocks that were subducted to mantle depths and survived a pervasive mid-crustal high-temperature overprint. Lithos 246–247: 246–260

Faryad SW, Nahodilová R, Dolejš D (2010) Incipient eclogite facies metamorphism in the Moldanubian granulites revealed by mineral inclusions in garnet. Lithos 114: 54–69

Faryad SW, Jedlicka R, Collett S (2013) Eclogite facies rocks of the Monotonous unit, clue to Variscan suture in the Moldanubian Zone (Bohemian Massif). Lithos 179: 353–363

Féménias O, Diot H, Berza T, Gauffriau A, Demaiffe D (2004) Asymmetrical to symmetrical magnetic fabric of dikes: paleo-flow orientations and paleo-stresses recorded on feeder-bodies from the Motru Dike Swarm (Romania). J Struct Geol 26: 1401–1418

Franke W (2006) The Variscan orogen in Central Europe: construction and collapse. In: Gee DG, Stephenson RA (eds), European Lithosphere Dynamics. Geological Society of London Memoirs 32: pp 333–343

Geoffroy L, Callot JP, Aubourg C, Moreira M (2002) Magnetic and plagioclase linear fabric discrepancy in dykes: a new way to define the flow vector using magnetic foliation. Terra Nova 14: 183–190

Guo Z, Wilson M, Liu J, Mao Q (2006) Post-collisional, potassic and ultrapotassic magmatism of the northern Tibetan plateau: constraints on characteristics of the mantle source, geodynamic setting and uplift mechanisms. J Petrol 47: 1177–1220

Gupta AK (2015) Origin of Potassium-Rich Silica-Deficient Igneous Rocks. Springer, Berlin, New York, pp 1–536

Hajná J, Žák J, Dörr W (2017) Time scales and mechanisms of growth of active margins of Gondwana: a model based on detrital zircon ages from the Neoproterozoic to Cambrian Blovice accretionary complex, Bohemian Massif. Gondwana Res 42: 63–83

Henry B (1977) Relations entre deformations et proprietes magnétiques dans des roches volcaniques des Alpes francaises. Mem BRGM 91: 79–86

Holub FV (1997) Ultrapotassic plutonic rocks of the durbachite series in the Bohemian Massif: petrology, geochemistry and petrogenetic interpretation. Sbor geol Věd, ložisk Geol Mineral 31: 5–26.

Holub FV (2003) Zonal dyke of ocelli lamprophyre to hornblendite from Dobříš. Zpr Geol Výzk v r 2003: 106–108 (in Czech)

Holub FV, Klečka M, Matějka D (1995) Moldanubian zone: igneous activity. In: Dallmeyer RD, Franke W, Weber K (eds) Pre-Permian Geology of Central and Eastern Europe. Springer Verlag, Berlin, pp. 444–452

Holub FV, Cocherie A, Rossi P (1997a) Radiometric dating of granitic rocks from the Central Bohemian Plutonic Complex (Czech Republic): constraints on the chronology of thermal and tectonic events along the Moldanubian-Barrandian boundary. C R Acad Sci Paris, Sciencies de la Terre et des planétes 325: 19–26

Holub FV, Machart J, Manová M (1997b) The Central Bohemian Plutonic Complex: geology, chemical composition and genetic interpretation. Sbor geol Věd, ložisk Geol Mineral 31: 27–50

Holub FV, Studená M, Vosk M (2007) Dolerites and gabbro to diorite porphyries in the Central Bohemian Plutonic Complex. Zpr geol Výzk v r 2006: 127–129 (in Czech)

Holub FV, Verner K, Studená M, Orságová L (2009) Dyke swarms of ultrapotassic melasyenite to melagranite porphyries from the Central Bohemian Plutonic Complex and the Šumava part of the Moldanubicum. Zpr geol Výzk v r 2008: 17–20 (in Czech)

Holub FV, Schmitz MD, Verner K, Janoušek V, Veselovský F (2010) Geochemical and temporal relations of ultrapotassic plutons and dyke swarms in South Bohemia. In: Kohút M (eds) Datovanie 2010. Zborník abstraktov. Štátny geologický ústav Dionýza Štúra, Bratislava, pp 13–14

Holub FV, Verner K, Schmitz MD (2012) Temporal relations of melagranite porphyry dykes and durbachitic plutons in South Bohemia. Zpr geol Výzk v r 2011: 23–25 (in Czech)

Hrouda F (1985) The magnetic fabric in the Brno Massif. Sbor Geol Věd, Už Geol 19: 89–112

Hrouda F (2002) Low-field variation of magnetic susceptibility and its effect on the anisotropy of magnetic susceptibility of rocks. Geophys J Int 150: 715–723

Hrouda F (2011) Models of frequency-dependent susceptibility of rocks and soils revisited and broadened. Geophys J Int 187: 1259–1269

Hrouda F, Pokorný J (2011) Extremely high demands for measurement accuracy in precise determination of frequency-dependent magnetic susceptibility of rocks and soils. Stud Geophys Geod 55: 667–681

Hrouda F, Přichystal A (1995) Magnetic fabric relationship between Palaeozoic volcanic and sedimentary rocks in the Nízký Jeseník Mts. (NE Moravia). J Czech Geol Soc 40: 91–102

Hrouda F, Jelínek V, Hrušková L (1990) A package of programs for statistical evaluation of magnetic anisotropy data using IBM-PC computers. Eos Trans Am Geophys Union (Fall meeting 1990), Conference Abstract, pp 1289

Hrouda F, Chlupáčová M, Mrázová Š (2006) Low-field variation of magnetic susceptibility as a tool for magnetic mineralogy of rocks. Phys Earth Sci Inter 154: 323–336

Hrouda F, Faryad SW, Chlupáčová M, Jeřábek P, Vitouš P (2009) Determination of field-independent and field-dependent components of anisotropy of susceptibility through standard AMS measurements in variable low fields II: An example from the ultramafic body and host granulitic rocks at Bory in the Moldanubian Zone of Western Moravia, Czech Republic. Tectonophysics 466: 123–134

Jackson M, Moskowitz B, Rosenbaum J, Kissel C (1998) Field-dependence of AC susceptibility in titanomagnetites. Earth Planet Sci Let 157: 129–139

Janoušek V, Holub FV (2007) The causal link between HP-HT metamorphism and ultrapotassic magmatism in collisional orogens: case study from the Moldanubian Zone of the Bohemian Massif. Proc Geol Assoc 118: 75–86

Janoušek V, Rogers G, Bowes DR (1995) Sr-Nd isotopic constraints on the petrogenesis of the Central Bohemian Pluton, Czech Republic. Geol Rundsch 84: 520–534

Janoušek V, Bowes DR, Rogers G, Farrow CM, Jelínek E (2000) Modelling diverse processes in the petrogenesis of a composite batholith: the Central Bohemian Pluton, Central European Hercynides. J Petrol 41: 511–543

Janoušek V, Brainthwaite CJR, Bowes DR, Gerdes A (2004) Magma mixing in the genesis of Hercynian calc-alkaline granitoids: an integrated petrographic and geochemical study of the Sázava intrusion, Central Bohemian Pluton, Czech Republic. Lithos 78: 67–99

Janoušek V, Wiegand B, Žák J (2010) Dating the onset of Variscan crustal exhumation in the core of the Bohemian Massif: new U-Pb single zircon ages from the high-K calc-alkaline granodiorites of the Blatná suite, Central Bohemian Plutonic Complex. J Geol Soc, London 167: 347–360

Janoušek V, Holub FV, Gerdes A, Verner K (2013) Two-pyroxene syenitoids from the Moldanubian Zone of the Bohemian Massif: peculiar magmas derived from a strongly enriched lithospheric mantle source. Geophys Res Abstr 15: EGU2013-11746

Jelínek V (1978) Statistical processing of magnetic susceptibility measured on groups of specimens. Stud Geophys Geod 22: 50–62

Jelínek V (1981) Characterization of the magnetic fabric of rocks. Tectonophysics 79: 63–67

Jelínek V, Pokorný J (1997) Some new concepts in technology of transformer bridges for measuring susceptibility anisotropy of rocks. Phys Chem Earth 22: 179–181

Knight MD, Walker GPL (1988) Magma flow directions in dykes of the Koolan Complex, Oahu, determined from magnetic fabric studies. J Geophys Res 93: 4308–4319

Košler J, Konopásek J, Sláma J, Vrána S (2014) U-Pb zircon provenance of Moldanubian metasediments in the Bohemian Massif. J Geol Soc 171: 83–95

Kubínová Š, Faryad SW, Verner K, Schmitz M, Holub FV (2017) Ultrapotassic dykes in the Moldanubian Zone and their significance for understanding of the post-collisional mantle dynamics during Variscan orogeny in the Bohemian Massif. Lithos 272–273: 205–221

Lardeaux JM, Schulmann K, Faure M, Janoušek V, Lexa O, Skrzypek E, Edel JB, Štípská P (2014) The Moldanubian Zone in French Massif Central, Vosges/Schwarzwald and Bohemian Massif revisited: differences and similarities. In: Schulmann K, Martínez Catalán JR, Lardeaux JM, Janoušek V, Oggiano G (eds) The Variscan Orogeny: Extent, Timescale and the Formation of the European Crust. Geological Society, London, Special Publications 405, pp 7 –44

Le Bas MJ, Le Maitre RW, Streckeisen A, Zanettin B (1986) A chemical classification of volcanic rocks based on the total alkali-silica diagram. J Petrol 27: 745–750

Machek M, Roxerová Z, Závada P, Silva PF, Henry B, Dědeček P, Petrovský E, Marques FO (2014) Intrusion of lamprophyre dyke and related deformation effects in the host rock salt: a case study from the Loule diapir, Portugal. Tectonophysics 629: 165–178

Mathieu L, De Vries BVW, Holohan EP, Troll VR (2008) Dykes, cups, saucers and sills: analogue experiments on magma intrusion into brittle rocks. Earth Planet Sci Lett 271: 1–13

Nagata T (1961) Rock Magnetism. Maruzen, Tokyo, pp 1–366

Park JK, Tanczyk EI, Desbarats A (1988) Magnetic fabric and its significance in the 1400 Ma Mealy diabase dykes of Labrador, Canada. J Geophys Res 93: 689–704

Parma J, Hrouda F, Pokorný J, Wohlgemuth J, Suza P, Šilinger P, Zapletal K (1993) A technique for measuring temperature dependent susceptibility of weakly magnetic rocks. EOS Trans AGU 1993: 113

Peccerillo A, Taylor SR (1976) Geochemistry of Eocene calc-alkaline volcanic rocks from the Kastamonu area, Northern Turkey. Contrib Mineral Petrol 58: 63–81

Petford N (1996) Dykes or diapirs? In: Brown M, Candela PA, Peck DL, Stephens WE, Walker RJ, Zen EA (eds) The Third Hutton Symposium on the Origin of Granites and Related Rocks. Geological Society of America Special Papers 315: pp 105–114

Petrovský E, Kapička A (2006) On determination of the Curie point from thermomagnetic curves. J Geophys Res 111: B12S27

Pokorný J, Pokorný P, Suza P, Hrouda F (2011) A multifunction Kappabridge for high precision measurement of the AMS and the variations of magnetic susceptibility with field, temperature and frequency. In: Petrovský E, Herrero-Bervera T, Harinarayana DI (eds) The Earth's Magnetic Interior. IAGA Special Sopron Book Series 1: Springer, Berlin, pp 292–301

Potter DK, Stephenson A (1988) Single-domain particles in rocks and magnetic fabric analysis. Geophys Res Lett 15: 1097–1100

Raposo MIB (2011) Magnetic fabric of the Brazilian dike swarms. A review. In: Petrovský E, Herrero-Bervera E, Harinarayana T, Ivers D (eds) The Earth's Magnetic Interior. IAGA Special Sopron Book Series 1: Springer, Berlin, pp 247–262

Raposo MIB, Ernesto M (1995) Anisotropy of magnetic susceptibility in the Ponta Grossa dyke swarm (Brazil) and its relationship with magma flow direction. Phys Earth Planet Inter 87: 183–196

Rochette P, Jenatton L, Dupuy C, Boudier F, Reuber I (1991) Diabase dykes emplacement in the Oman ophiolite: a magnetic fabric study with reference to geochemistry. In: Peters TJ, Nicolas A, Coleman R (eds) Ophiolite Genesis and Evolution of the Oceanic Lithosphere. Kluwer, Dordrecht, pp 55–82

Schulmann K, Konopásek J, Janoušek V, Lexa O, Lardeaux J-M, Edel J-B, Štípská P, Ulrich S (2009) An Andean type Palaeozoic convergence in the Bohemian Massif. C R Geosci 341: 266–286

Stephenson A, Sadikum S, Potter DK (1986) A theoretical and experimental comparison of the anisotropies of magnetic susceptibility and remanence in rocks and minerals. Geophys J Astron Soc 84: 185–200

Studýnka J, Chadima M, Suza P (2014) Fully automated measurement of anisotropy of magnetic susceptibility using 3D rotator. Tectonophysics 629: 6–13

Tarling DH, Hrouda F (1993) The Magnetic Anisotropy of Rocks. Chapman & Hall, London, pp 1–217

Urban M, Synek J (1995) Moldanubian Zone: Structure. In: Dallmeyer RD, Franke W, Weber K (eds) Pre-Permian Geology of Central and Eastern Europe. Springer Verlag, Berlin, pp 429–424

Varga RJ, Gee JS, Staudigel H, Tauxe L (1998) Dike surface lineations as magma flow indicators within the sheeted dike complex of the Troodos ophiolite, Cyprus. J Geophys Res 103: 5241–5256

Verner K, Žák J, Nahodilová R, Holub F (2008) Magmatic fabrics and emplacement of the cone-sheet-bearing Knížecí Stolec durbachitic pluton (Moldanubian Unit, Bohemian Massif): implications for mid-crustal reworking of granulitic lower crust in the Central European Variscides. Int J Earth Sci 97: 19–33.

Worm HU (1998) On the superparamagnetic-stable single domain transition for magnetite, and frequency dependence of susceptibility. Geophys J Int 133: 201–206

Worm HU, Clark D, Dekkers MJ (1993) Magnetic susceptibility of pyrrhotite: grain size, field and frequency dependence. Geophys J Int 114: 127–137

Žák J, Schulmann K, Hrouda F (2005a) Multiple magmatic fabrics in the Sázava pluton (Bohemian Massif, Czech Republic): a result of superposition of wrench-dominated regional transpression on final emplacement. J Struct Geol 27: 805–822

Žák J, Holub FV, Verner K (2005b) Tectonic evolution of a continental magmatic arc from transpression in the upper crust to exhumation of mid-crustal orogenic root recorded by episodically emplaced plutons: the Central Bohemian Plutonic Complex (Bohemian Massif). Int J Earth Sci 94: 385–400

Žák J, Dragoun F, Verner K, Chlupáčová M, Holub FV, Kachlík V (2009) Forearc deformation and strain partitioning during growth of a continental magmatic arc: the northwestern margin of the Central Bohemian Plutonic Complex, Bohemian Massif. Tectonophysics 469: 93–111

Žák J, Kratinová Z, Trubač J, Janoušek V, Sláma J, Mrlina J (2011) Structure, emplacement, and tectonic setting of Late Devonian granitoid plutons in the Teplá-Barrandian Unit, Bohemian Massif. Int J Earth Sci (Geol Rundsch) 100: 1477–1495

Žák J, Verner K, Holub FV, Kabele P, Chlupáčová M, Halodová P (2012) Magmatic to solid state fabrics in syntectonic granitoids recording early Carboniferous orogenic collapse in the Bohemian Massif. J Struct Geol 36: 27–42

Žák J, Verner K, Janoušek V, Holub FV, Kachlík V, Finger F, Hajná J, Tomek F, Vondrovic L, Trubač J (2014) A plate-kinematic model for the assembly of the Bohemian Massif constrained by structural relations around granitoid plutons. In: Schulmann K, Martínez Catalán JR, Lardeaux JM, Janoušek V, Oggiano G (eds) The Variscan Orogeny: Extent, Timescale and the Formation of the European Crust. Geological Society, London, Special Publications 405, pp 169–196

Žežulková V (1982) Žilné horniny jižní části středočeského plutonu. Sbor geol Věd, Geol 37: 71–102

CHAPTER 5

SIMULTANEOUS FREE FLOW AND FORCEFULLY DRIVEN MOVEMENT OF MAGMA IN LAMPROPHYRE DYKES AS INDICATED BY MAGNETIC ANISOTROPY: CASE STUDY FROM THE CENTRAL BOHEMIAN DYKE SWARM, CZECH REPUBLIC

František Hrouda *, Shah Wali Faryad, Šárka Kubínová, Kryštof Verner, Marta Chlupáčová

Institute of Petrology and Structural Geology, Charles University, Albertov 6, 128 43 Praha, Czech Republic

Status: Published in Geosciences (2019)

ABSTRACT

A composite lamprophyre dyke from the Central Bohemian Dyke Swarm (Czech Republic) shows both indications of magma free flow (normal magnetic fabric with magnetic foliation and lineation parallel to the dyke plane) as well as those of forcefully driven magma movement (intermediate and inverse magnetic fabrics with magnetic foliation perpendicular to the dyke plane). The overall characteristics of the magnetic parameters across the dyke indicate the existence of at least two slightly differing parts that probably represent two magma pulses. The marginal part of the dyke is formed by kersantite, while toward the axial part, the composition gradually changes to spessartite, and obtains an increasing degree of amphibolization. The rocks of the dyke are inhomogeneous, both compositionally and structurally. It is likely that some portions of ascending magma were more viscous than the others, and the magnetic minerals in the more viscous magma portions may have oriented according to their longer dimensions perpendicular to the dyke, creating an inverse fabric. The lengthening perpendicular to the dyke was compensated by the vertical escape of neighboring more fluid magma, creating a normal magnetic fabric. The frequent oblique magnetic fabrics may represent transitions between the above two mechanisms.

***Keywords**: composite lamprophyre dyke; normal and inverse magnetic fabrics; emplacement mechanism*

5.1 Introduction

The magnetic fabric of igneous dykes has been intensely investigated because their creation and propagation signify important mechanisms of mass transport within the Earth's crust and the upper mantle. For example, there are dykes that originated through the almost free flow of magma infilling more or less open fractures in host rocks (close to the surface) as well as dykes that originated through a forceful magma intrusion of the host rocks with no open fractures (in deeper portions of the crust) (see [1]). The structural aspects of these processes have been investigated both from the theoretical and practical points of views (see, for example, [2,3] and references therein). These investigations used various indicators of magma flow, which are unfortunately scarce, and the anisotropy of magnetic susceptibility (AMS), which can be easily measured on almost all types of dyke rocks (e.g., [4–14]).

The different mechanisms of dyke formation are reflected in the type of the preferred orientation of magnetic minerals by grain shape within a dyke, viz. the magnetic fabric. In the free flow of magma within the dyke, the large surfaces of magnetic minerals orient approximately parallel to the dyke, while the longer dimensions orient parallel to the magma flow direction. This type of preferred orientation gives rise to the most common *normal* (*Type I*) magnetic fabric [11,12], with magnetic foliation approximately parallel to the dyke plane and magnetic lineation approximately parallel to the dyke plane and to the direction of the flow. In a forceful intrusion, the large surfaces of magnetic minerals orient approximately perpendicular to the dyke, and the longer dimensions orient parallel to the dyke plane [11,15,16], giving rise to the *intermediate* or *Type II* magnetic fabric with an approximately perpendicular orientation of magnetic foliation to the dyke plane and magnetic lineation parallel to the dyke [11,12]. In addition, there are two other types of magnetic fabric whose origin is unfortunately less known. One of them is the *reverse* or *inverse* (*Type III*) magnetic fabric with magnetic foliation and magnetic lineation perpendicular to the dyke [10–12], the origin of which is attributed to secondary processes such as hydrothermal alteration [12] or to a single-domain effect if the AMS is carried by very small (single domain, SD) magnetic grains [17]. The last type shows almost random orientations of magnetic foliation and lineation, which may result from very complex flow patterns or from severe post-magmatic changes of magnetic minerals [10,18].

The above types of magnetic fabric are assumed to originate in such a way that the dyke walls simply open gradually, and the space between them is infilled by magma. In addition to simple opening, the dyke walls can also be subject to shear movements during dyke formation, with the movements being vertical (dip-slip), horizontal (strike-slip) or even oblique; this process gives rise to more frequent oblique magnetic fabrics (e.g., [7]).

The above magnetic fabric types were most frequently revealed in intermediate and mafic dykes. Much less information is available about magnetic fabric in potassic-lamprophyre dykes (e.g., [19,20]) with source magma generated in the mantle depths (e.g., [21–24]). Among the potassic-ultrapotassic dykes of the Central Bohemian Dyke Swarm, Hrouda et al. [8] revealed the first three of the above four magnetic fabric types. Interestingly, there is one dyke, the composite lamprophyre dyke near the town of Dobříš, where all three magnetic fabrics can be found: *normal* in the central part, and *intermediate* and even *inverse* magnetic fabrics in the other parts of the dyke. A question arises: how it is possible that the magma movement in one dyke shows indications of both free flow (*normal* magnetic fabric in central parts) and forceful intrusion (*intermediate* magnetic fabric in marginal and rim parts)? One explanation of this phenomenon assumes that the central (amphibolized spessartite), marginal (spessartite), and rim (kersantite) parts represent different injections undergoing different mechanisms of magma movement. The other explanation assumes that the dyke originated by one injection within which the petrographical rock types changed gradually to one from another (see [25]), and the rheological state of the moving magma varied accordingly.

In order to evaluate these explanations, new samples were collected along a profile (with dense spacing of 0.5 m in average) across the dyke. They were investigated by standard AMS, which is the anisotropy of the in-phase component of susceptibility (ipAMS), by the anisotropy of the out-of-phase component of susceptibility (opAMS), and by the anisotropy of anhysteretic magnetic remanence (AAMR). The results were combined with detail petrological and geochemical analyses.

5.2 Concise Geological Setting

The Bohemian Massif, representing the easternmost segment of the European Variscides, is formed by two crustal blocks (the Brunovistulian and the Teplá-Barrandian, Figure 1) and two zones (the Moldanubian and the Saxothuringian), with rocks affected by various degrees of metamorphism and deformation. The Saxothuringian Zone occupies the northern part of the Bohemian Massif, while the Moldanubian Zone is located in the southeastern part between the Teplá-Barrandian Block in the northwest and the Brunovistulian Block in the east (Figure 1). The Moldanubian Zone is formed by medium-grade (the monotonous and varied units) and high-grade (the Gföhl Unit) metamorphic rocks. The Variscan geodynamic evolution in the Moldanubian Zone was characterized by 380 to 335 Ma long subduction-collision tectonics that resulted in various degrees of metamorphism, magmatic activity, and fast exhumation and cooling (e.g., [26–30]). In general, the overall structure of the Moldanubian Zone is the result of the stacking of several lithotectonic units at ~ 360 to 345 Ma followed by HT-LP (high temperature, low pressure) metamorphism, anatexis, and late-Variscan wrench tectonics (for a review, see [28,30,31]).

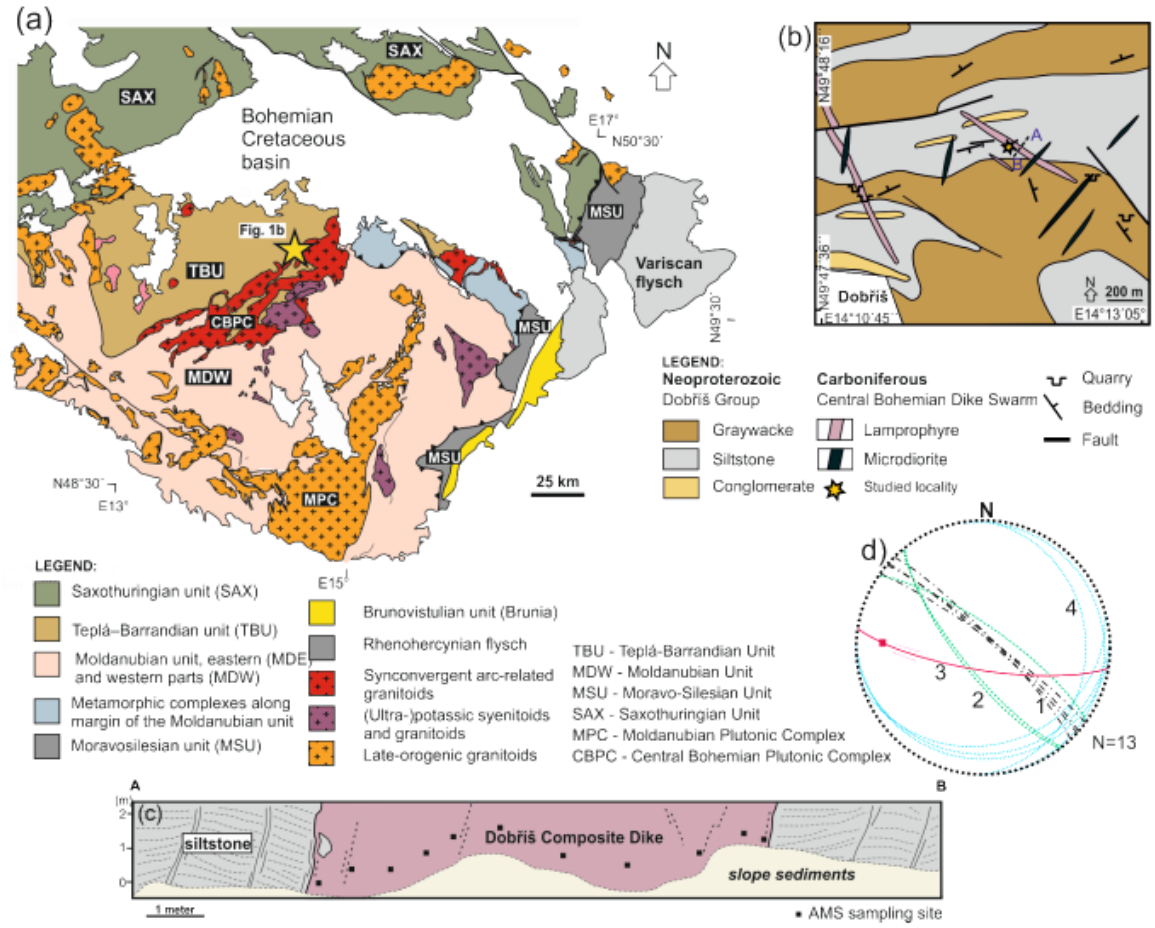

Figure 1. (**a**) Simplified geological map of the Bohemian Massif. (**b**) detailed situation of the dyke near Dobříš. (**c**) Field scheme of NE-SW cross-section with schematic locations of samples for anisotropy of magnetic susceptibility (AMS) and petrological analysis. (**d**) Orientations of mesoscopic structural elements (equal area projection to lower hemiscphere): intrusive contacts (1), cleavage (2), fault plane (slickensides) (3), bedding (4), The map (a) is compiled using [30].

In the Moldanubian Zone, magmatic rocks of Variscan age can be classified into four groups. The first two groups are represented by granitoid complexes that are exposed along two belts, the Central Bohemian Plutonic Complex (CBPC) and the Moldanubian Plutonic Complex (MPC) (Figure 1a). These two complexes differ from each other by age and their relations to Variscan geotectonic processes (e.g., [29,30,32–35]). The older (c. 355–345 Ma) CBPC straddles the border of the Teplá-Barrandian Block, and is formed by subduction-related calc-alkaline plutons. The younger MPC is composed of peraluminous (S-type) anatectic granitoids (c. 330–300 Ma), and it was formed by extensive migmatitization and isothermal decompression of the surrounding pelitic rocks. The third group is represented by potassic-ultrapotassic rocks (346–337 Ma) that form several isolated plutons (Figure 1a) and dyke swarms [8,36–38]. The last group of Variscan igneous rocks have mafic and ultramafic composition (gabbro, norite, troctolite, pyroxenite) and an age of around 340

Ma [39–41]. Some of the mafic-ultramafic rocks are unmetamorphosed, but others record amphibolite-granulite facies conditions, and therefore were assumed to be pre-Variscan in age.

The potassic to ultrapotassic rocks form large plutons and dykes having a composition of spessartite, gabbrodiorite, minette, vaugnerite, kersantite, melasyenite, and melagranite. In the western part of the Moldanubian Zone, they are distributed over about a 30 × 100 km area that mostly covers the CBPC (Figure 1a). The dykes have an orientation that is almost E-W and intrudes on not only the basement rocks, but also the granitic rocks of the CBPC. Their thickness varies from five to 20 m, the lengths are often limited to less than one to two km, which is perhaps due to the segmentation of dykes by younger faults. External contacts of porphyry dykes are sharp and generally discordant to folded metamorphic foliations of host gneisses and migmatites.

The studied dyke near Dobříš penetrates the low-grade Neoproterozoic metasediments (slates, metagraywackes, and metasiltstones with thin layers of metaconglomerates). The host rocks belong to the eastern part of the Teplá-Barrandian unit, which was heterogeneously deformed by the ~ NW-SE-oriented regional compression during the early stages of Variscan orogeny (for review, see [28,30]). The dyke is about 10 m thick, and has sharply discordant contact, dipping steeply to NNE to NE, in respect to both the regional gently SE dipping bedding and moderately SW dipping cleavage in the host metasiltstones and metagraywackes. A narrow chilled margin (up to 10 cm in thickness) and minor xenoliths of the host rock are present along the contacts. Contact-parallel magmatic foliation (planar preferred orientation of rock-forming minerals) has been identified in some places across the dyke.

5.3 Sampling, Technique of Measurement, Data Presentation

Twenty-two oriented samples were drilled across the dyke (Figure 1c) using a portable petrol-powered drilling machine and oriented using a geological compass mounted on a special orientating fixture. From each sample, thin sections for petrological analysis and powder specimen for magnetic mineralogy were made, as well as two to three cylindrical (25 mm in diameter and 21–22 mm in height) specimens for magnetic anisotropy measurement. The standard AMS (ipAMS) and the opAMS were measured with the KLY-5 Kappabridge [42] using the three-dimensional (3D) rotator [43], and computed by the SAFYR (ver. 6) program. The AAMR was measured using the LDA-5 anhysteretic magnetizer / AF Demagnetizer and JR-6A Spinner Magnetometer (both produced by Agico Inc. Brno). The bias field was 500 μT, and the AF field was 40 mT; before anhysteretic magnetizing in each direction, the specimen was tumble AF demagnetized in the field of 50 A/m. The measurement was processed using the program REMA (ver. 6.20, M. Chadima) based on the theory by Jelínek [44].

Until now, the dominant method for measuring the AMS of rocks is that of an induction bridge, which measures the susceptibility and its anisotropy in an alternating magnetic field. The susceptibility that is measured in this way can in general be resolved into a component that is in-phase with the magnetizing field, and a component that is out-of-phase. The standard AMS is in fact the anisotropy of the in-phase component (ipAMS). The technique for measuring the anisotropy of the out-of-phase component (opAMS) was developed only recently [42].

The mean bulk susceptibility, eccentricity, and shape of the anisotropy ellipsoid can be characterized by the following parameters [45,46]:

$$K_m = (k_1 + k_2 + k_3) / 3$$

$$P = k_1 / k_3$$

$$T = (2\,\eta_2 - \eta_1 - \eta_3) / (\eta_1 - \eta_3) = 2 \ln F / \ln P - 1$$

where $k_1 \geq k_2 \geq k_3$ are the principal vaalues, and $\eta_1 = \ln k_1$, $\eta_2 = \ln k_2$, $\eta_3 = \ln k_3$.

The parameter P, which is called the degree of anisotropy, indicates the intensity of the preferred orientation of the magnetic minerals in a rock. The parameter T characterizes the shape of the anisotropy ellipsoid. If $0 < T < +1$, the ellipsoid is oblate (the magnetic fabric is planar); $T = +1$ means that the ellipsoid is rotationally symmetric (uniaxial oblate). If $-1 < T < 0$, the ellipsoid is prolate (the magnetic fabric is linear); $T = -1$ means that the ellipsoid is uniaxial prolate.

In order to obtain a statistical evaluation of the AMS/AAMR at individual localities, the ANISOFT package of programs [47–49] was used, which enable a complete statistical evaluation of a group of specimens. The orientations of magnetic foliations and magnetic lineations, the respective mean directions, and the corresponding confidence areas are presented in equal-area projections on the lower hemisphere in the dyke coordinate system (the dyke was rotated about its strike to a vertical position, and about the vertical axis to the N-S position).

The magnetic minerals carrying the rock magnetism were investigated through the method of the maximum theoretical paramagnetic susceptibility (MTPS, see [50]), using the susceptibility variation with the magnetizing field, the operating frequency, and the temperature. The susceptibility variation with magnetizing field was measured in the fields ranging from five A/m to 700 A/m at the operating frequency 1220 Hz using the automated mode of the KLY-5 Kappabridge. The variation can be concisely characterized by the V_m parameter defined as follows [51]:

$$V_m = 100\,(k_{max} - k_{min}) / k_{min}\ [\%]$$

where k_{max} and k_{min} are the maximum and minimum susceptibilities, respectively, that were obtained during one measuring run. The susceptibility variation with operating frequency was investigated at the frequencies 976 Hz and 15,616 Hz in the driving field of 200 A/m using the MFK1-FA

Kappabridge. It can be represented quantitatively by the commonly accepted percentage loss of susceptibility [52]:

$$X_{FD} = 100\ (k_{LF} - k_{HF}) / k_{LF}\ [\%]$$

where k_{LF} and k_{HF} are susceptibilities measured at low and high frequencies, respectively. The low and high frequencies were 976 Hz and 15,616 Hz. The susceptibility variation with temperature was measured on coarsely powdered pilot specimens in temperature intervals between -194 °C and 0 °C and between 25–700 °C using the CS-L Cryostat, CS-4 Furnace [53], and the MFK1-FA Kappabridge. The susceptibility versus temperature curve that is measured between -194 °C and 700 °C is called the heating curve, while the curve measured between 40–700 °C is called the cooling curve. The high-temperature curves were measured in the atmosphere of flowing argon (10 l/min). The Curie temperatures were determined using the Petrovský and Kapička [54] method based on searching for the beginning of the paramagnetic hyperbola just at the Curie temperature.

The bulk rock density was determined through simply measuring the dimensions of cylindrical specimens for measuring the AMS using vernier and weighing the specimens using analytical scales.

5.4 Petrology and Bulk Rock Chemistry

Modal contents of minerals and their textures show a gradual change from the rim to the central part of the dyke. After Holub [25], the dyke is formed by kersantite (plagioclase > K-feldspar with high biotite content) upon contact with the host siltstone, and by hornblendite in the axial part of the dyke. The bulk rock composition of three main varieties is given in Table 1. It should be noted that the different composition and mineral mode is partially due to the degree of amphibolization (see later). Both axial and rim parts are separated by a thin zone of spessartite (plagioclase > K-feldspar with high amphibole content). The dyke margin, up to several cm from contact with the host rocks, consists of a very fine-grained (< 0.15 mm) matrix with phenocrysts (up to 1.5 mm) of clinopyroxene and pseudomorphs of talc after olivine (Figure 2a). The minerals that are present in the matrix are plagioclase > biotite > clinopyroxene, and small amounts of amphibole, K-feldspar, quartz, carbonate, magnetite, and sulphides. The amphibole content increases toward the central part of the dyke, and the biotite content is about 8 vol%. The pseudomorphs of talc after olivine instead of orthopyroxene are assumed by their shapes and comparison with other lamprophyre dykes with similar phenomena of olivine replacement to talc [38]. In addition to talc, the pseudomorphs contain accessory amounts of quartz and Cr-spinel. The phenocrysts of clinopyroxene may contain inclusions of apatite and opaque minerals. A striking feature of this part of the rock is the presence of multiphase ocelli (1.55–4.5 mm), which are formed by tabular grains (< 0.5 mm in size) of plagioclase and brown biotite with small amounts of green amphibole and a smaller amount of K-

feldspar (Figure 2b). The minerals in the ocelli show random orientation (Figure 2b,c). Some ocelli contain also carbonate and minor quartz.

Table 1. Bulk rock composition of different rock varieties in the dyke.

Sample	LR 1123	LR 1145	LR 1113
Rock	kersantite	spessartite	hornblendite
SiO_2	48.05	50.31	45.78
TiO_2	0.55	0.71	0.51
Al_2O_3	12.46	15.43	9.72
Fe_2O_3*	9.76	8.62	9.45
MnO	0.17	0.15	0.16
MgO	11.65	9.25	15.46
CaO	9.94	8.31	12.21
Na_2O	1.27	2.66	0.87
K_2O	1.57	0.92	0.89
P_2O_5	0.28	0.18	0.16
LOI	2.35	2.70	3.2
Total	98.05	99.24	99.41

Fe_2O_3* = total Fe as Fe_2O_3

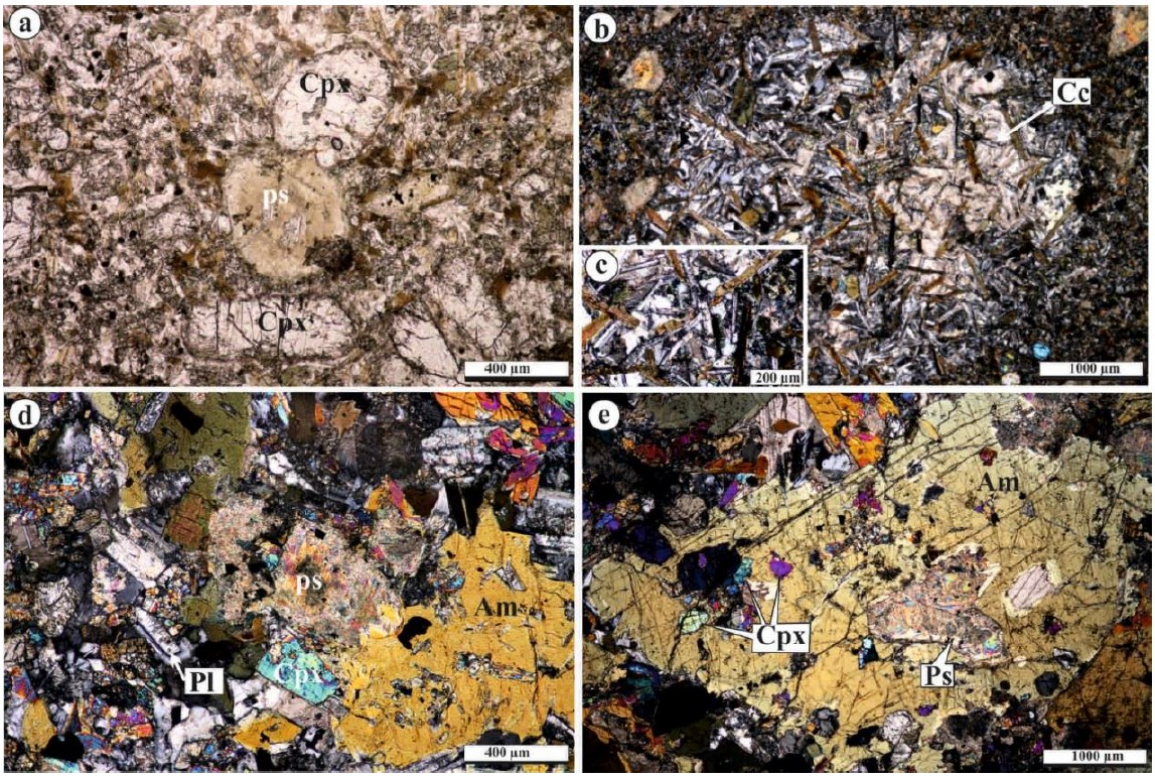

Figure 2. Photomicrographs of zoned lamprophyre dyke from Dobříš. (**a–c**) show minerals and textures of kersantite at the contact zone with the host siltstone. Note that the fine-grained matrix (**a**) contains phenocrysts of clinopyroxene (Cpx) and pseudomorphs of talc (ps) after olivine. (**b**) indicates ocellus filled by plagioclase, biotite, amphibole, and calcite (Cc). (**c**) is a detail of randomly oriented tabular grains of plagioclase, biotite, and amphibole. (**d**) Relatively coarse-grained matrix (about 80 cm from the contact zone) with large amphiboles containing or overgrowing clinopyroxene and pseudomorphs of talc. Note the zoning of

plagioclase (Pl) in the matrix. (**e**) is from the central part of the dyke with large poikiloblasts of amphibole with inclusions of clinopyroxene, plagioclase, and talc pseudomorphs.

Farther from the dyke rim, the rock gradually becomes coarse-grained. Although the matrix phases can have a size of up 0.4 mm, the coarsening is mainly due to amphibole grains (up to 1.5 mm in size) that overgrow or enclose clinopyroxene and pseudomorphs after olivine (Figure 2d). It has a brown color that transitions to green rims. In contrast to the contact zone, biotite content decreases (< 1 vol%), and that of amphibole increases (up 60 vol%). The amounts of clinopyroxene phenocrysts and talc pseudomorphs also decrease due to their replacement by amphibole. Matrix minerals are similar to those from the contact zone and consist of plagioclase, amphibole, K-feldspar, clinopyroxene, biotite, and minor quartz and carbonate.

The axial part of the dyke is coarse-grained and consists mostly of amphiboles that reach a grain size of up to five mm (Figure 2e). Biotite is not present, or can occur as an accessory phase. Amphibole contains relics of clinopyroxene, talc pseudomorphs, and encloses plagioclase. The original matrix is locally preserved and consists of amphibole, clinopyroxene, plagioclase, minor carbonate, and quartz.

No significant variation in the composition of minerals was observed between the rim and central parts of the dyke. Clinopyroxene is augite to diopside (X_{Mg} = 81.58–87.50 mol %). Amphibole corresponds to tschermakite, magnesio-hornblende, magnesio-hastingstite, and edenite in composition. Its Mg (X_{Mg} = Mg/(Mg + Fe^{2+})) ratios slightly increase from the marginal part of the dyke (0.63–0.72) to the central part (0.67–0.86). Some amphibole grains in the central part are replaced along the rims by actinolite. Biotite has X_{Mg} = 0.55–0.65, but rarely, phlogopite (0.70–0.72 X_{Mg}) is also present. Plagioclase is zoned, and shows a wide compositional range, from andesine-labradorite (37.80–69.83% An) in the marginal part of the dyke to andesine-bytownite (31.16–85.34% An) in the central part of the dyke. K-feldspar is orthoclase with 72.30–76.74% Or and a mixture of celsian (1.89–3.82% Cn).

In addition to a fast-cooled matrix and the presence of ocelli textures at the contact zone, the main difference between the rim and central part of the dyke is related to the presence and amounts of biotite and amphibole. Biotite with high X_{Mg} content could represent the original phase, but it is not clear whether some amphibole was also formed among the early crystallized phases. As shown above, amphibole is a late crystallized phase, and it clearly replaces or overgrows the early crystallized minerals (plagioclase, clinopyroxene, and olivine). Based on the original minerals, the rim part corresponds to kersantite, which is consistent with the findings of Holub [25], but the central part is represented by spessartite, with an inward increase of amphibolization degrees. Bulk rock chemistry indicates that the central part has less silica, aluminum, and potassiumm but higher amounts of MgO and CaO. Calculated normative contents of minerals reveal that the rim part has

higher content of plagioclase, orthoclase, and hypersthene, but lower amounts of diopside and olivine compared to the central part. As shown above, the pseudomorphs are after olivine, but the presence of small amounts of orthopyroxene among the primary phases is not excluded. In addition, some Ca could be incorporated into the original carbonate.

5.5 Magnetic Mineralogy

The mean volume susceptibility of the Dobříš dyke is moderate, covering the entire order of 10^{-3} (Figure 3). The MTPS method, which calculates the rock paramagnetic susceptibility from the Fe and Mn contents obtained from the whole-rock chemical analyses (see [50]), shows that the contribution of paramagnetic minerals to the whole-rock susceptibility is an order of magnitude lower: about 0.6×10^{-3}. Consequently, the rock's susceptibility is dominantly carried by ferromagnetic minerals (encompassing ferrimagnetic, antiferromagnetic, and ferromagnetic *sensu stricto* ones).

The variation of susceptibility with temperature was investigated on 11 pilot specimens that cover all rock types in the dyke. The susceptibility versus temperature curves of the high-temperature segment (between room temperature and 700 °C) mostly show three susceptibility decreases in the heating curves: one between 300–360 °C, the second between 495–515 °C, and the third between 570–590 °C (Figure 4a,c). The last temperature probably indicates magnetite, the other two may indicate Fe-Ti oxides with different contents of Ti. The hump of susceptibility between ca. 150–350 °C can be ascribed to a new phase that may have been created during specimen heating. It should be emphasized that the curves of all the specimens are similar, even though they come from different positions within the dyke and represent different rock types, thus supporting gradual inward changes in mineral and bulk rock chemistry within the dyke. The cooling curves run lower than the heating ones and show only one susceptibility decrease, i.e., that at 570–590 °C (Figure 4b,d). This probably indicates the dissolution of the earlier separated phases, resulting in the creation of one phase.

The low-temperature curves (between -190 °C and 0 °C) show susceptibility decreases at -160 °C and -170 °C at the Verwey transition, which is typical of relatively pure magnetite [55], in six specimens, and paramagnetic hyperbola in five specimens (Figure 4a,c).

In specimens that showed no Verwey transition, but indicated the existence of paramagnetic hyperbola, the low-temperature segments of the curves were resolved into paramagnetic hyperbola and a ferromagnetic straight line using the method by Hrouda [56]. This technique revealed that the paramagnetic susceptibilities are mostly in the order of 10^{-4}, thus indicating that the rock's susceptibility is even in such cases dominantly carried by ferromagnetic minerals (magnetite).

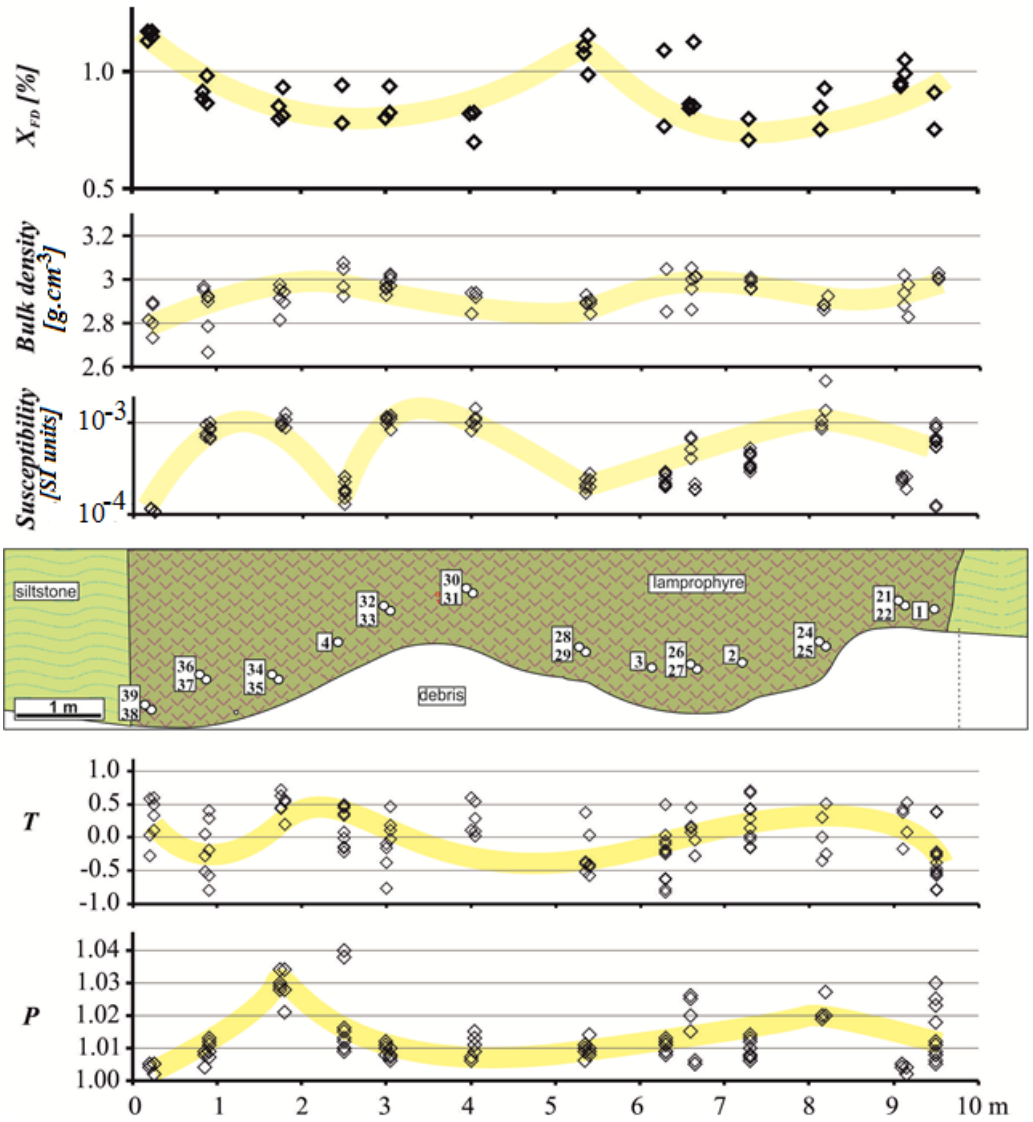

Figure 3. Sample locations (open circles with numbers 1–39), bulk susceptibility, bulk density, percentage loss of susceptibility (X_{FD}), degree of anisotropy of magnetic susceptibility (AMS) (P), and shape parameters (T) within the dyke.

The variation of in-phase susceptibility with field is very weak, with the K/K_{min} ratio being less than 1.02 (Figure 5a). Among ferromagnetic minerals, pure magnetite shows virtually field-independent susceptibility, while in titanomagnetite, pyrrhotite, and hematite, the susceptibility may be clearly field-dependent, even in low fields that are commonly used in AMS meters [51,57–62]. From this point of view, the weak in-phase susceptibility variation of most of the investigated specimens probably indicates the presence of only slightly impure magnetite or very low amounts of titanomagnetites.

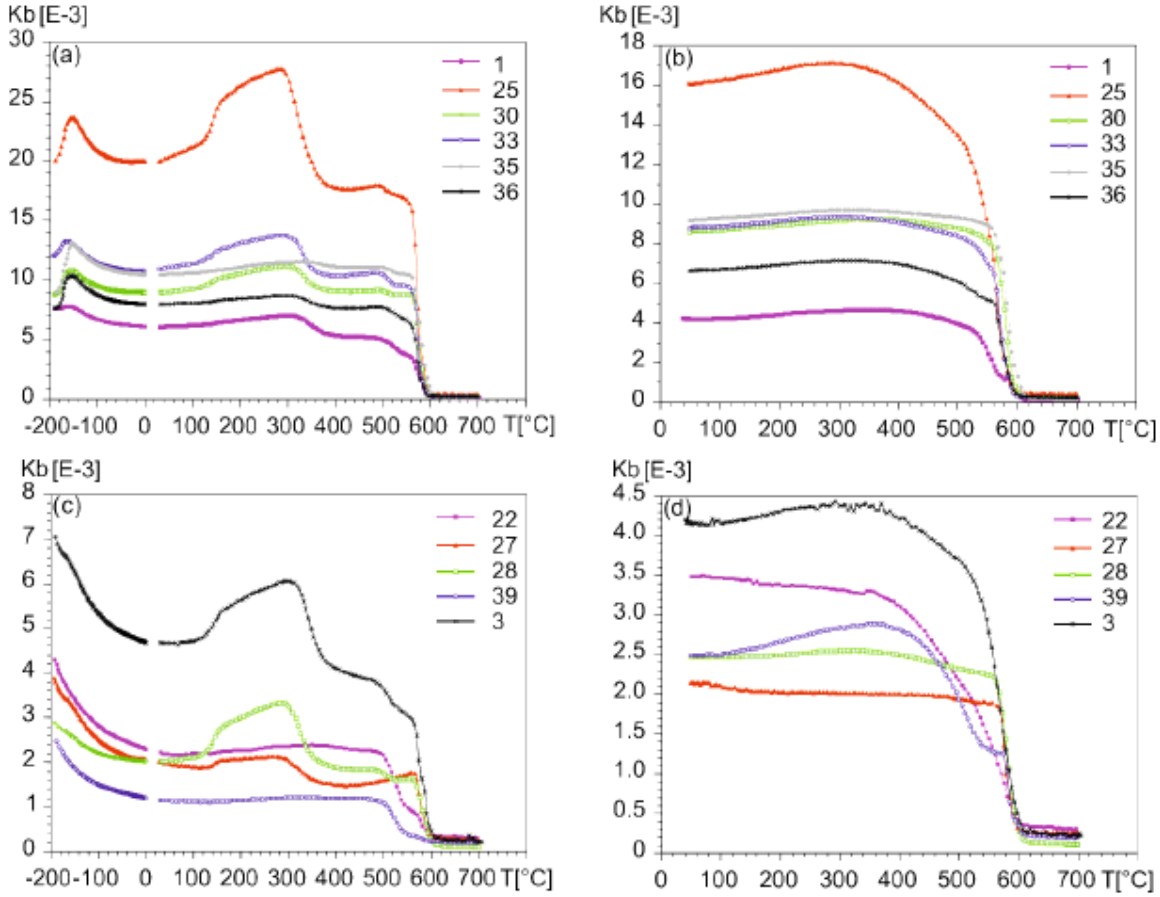

Figure 4. Susceptibility vs. temperature curves for pilot specimens. (**a**) Heating curves for specimens showing Verwey transitions in low-temperature segments, (**b**) cooling curves for the same specimens, (**c**) heating curves for specimens showing paramagnetic hyperbola in the low-temperature segment, (**d**) cooling curves for the same specimens.

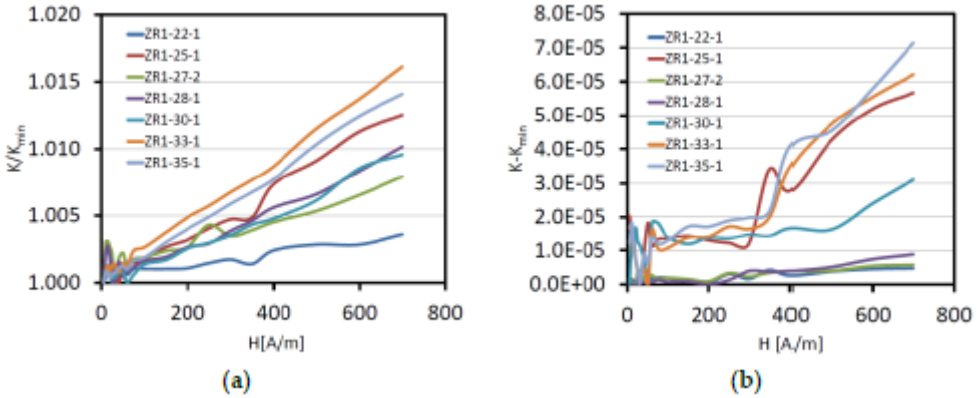

Figure 5. Field variation of in-phase (**a**) and out-of-phase (**b**) susceptibility in pilot specimens.

The out-of-phase susceptibility is about two orders lower than the in-phase susceptibility. To visualize its variation with field, the K - K_{min} difference is used instead of the K/K_{min} ratio to avoid problems with normalizing by very low numbers. Nevertheless, it clearly shows an observable

increase with field (Figure 5b). As the out-of-phase susceptibility of pure magnetite is effectively zero, while it is clearly non-zero in titanomagnetite, pyrrhotite, and hematite (see [63], the low, but non-zero, out-of-phase susceptibility probably indicates the presence of either impure magnetite or very low amounts of titanomagnetite.

The grain size of ferromagnetic minerals can be assessed, et least partially, through frequency-dependent susceptibility. Namely, the frequency-dependent susceptibility is effectively zero in multi-domain (MD) and single-domain (SD) grains of magnetite (titanomagnetite) as well as in its ultrafine superparamagnetic (SP) grains (e.g., [51,64]). On the other hand, it can be clearly non-zero in magnetically viscous grains that are transitioning from the SP state to the SD state. The values of the X_{FD} parameter characterizing the frequency-dependent susceptibility quantitatively are low, mostly lower than 1 % (see Figure 3), approaching the detection limit of the method [65]. Consequently, the investigated dyke contains very low amounts of magnetically viscous grains, if any.

It can be concluded that the dominant carrier of the ipAMS is magnetite, even though some other magnetic phases are also present. As the AMS of magnetite is controlled by its grain shape, the rock ipAMS is controlled by the preferred orientation of magnetite by grain shape. The opAMS is controlled either by impure magnetite of very low amounts of titanomagnetite. The AAMR in the measuring configuration used (without using magnetization/demagnetization windows) is controlled by the mineral(s) that can be easily magnetized anhysteretically and subsequently demagnetized before changing the magnetizing direction, which is probably represented by low-Ti titanomagnetite.

5.6 Magnetic Fabric

5.6.1 Standard Anisotropy of Magnetic Susceptibility (AMS)

The degree of AMS is very low, mostly about $P \sim 1.01$, and reaching $P = 1.04$ (Figure 3). The shape of the AMS ellipsoid ranges from very prolate to moderately oblate (Figure 3). Both the magnetic foliations and lineations are relatively well defined. From the point of view of the orientations of magnetic foliations and magnetic lineations with respect to the dyke plane, the dyke can be divided into seven domains showing different, but relatively homogeneous, orientations. In two domains, D1 (samples 34 and 35) and D2 (samples 3, 28, and 29), the magnetic foliation is approximately parallel to the dyke plane, while the magnetic lineation is horizontal and also parallel to the dyke plane (Figure 6); this fabric can be denoted as *normal* or *Type Ia*. In domain D3 (samples 4 and 30), the magnetic foliation is almost perfectly vertical and perpendicular to the dyke, and the magnetic lineation is also mostly perpendicular to the dyke (Figure 6). This fabric type is no doubt *inverse* or *Type IIIb*. In domain D4 (samples 2, 24–27), the magnetic foliation is mostly

perpendicular to the dyke, varying in the dip from horizontal to vertical, and magnetic lineation is mostly horizontal, perpendicular to the dyke (Figure 6). This magnetic fabric can be also denoted as *inverse*, transitioning from *Type IIIa* to *IIIb*. In the domains D5 (samples 36–39), D6 (samples 31–33), and D7 (samples 1, 21, 22), both the magnetic foliations and magnetic lineations are oblique with respect to the dyke plane (Figure 6), and the magnetic fabrics cannot be described in simple terms such as *normal* or *inverse*. It is likely that the rocks in these domains suffered local strike-slip movements that rotated the magnetic fabrics.

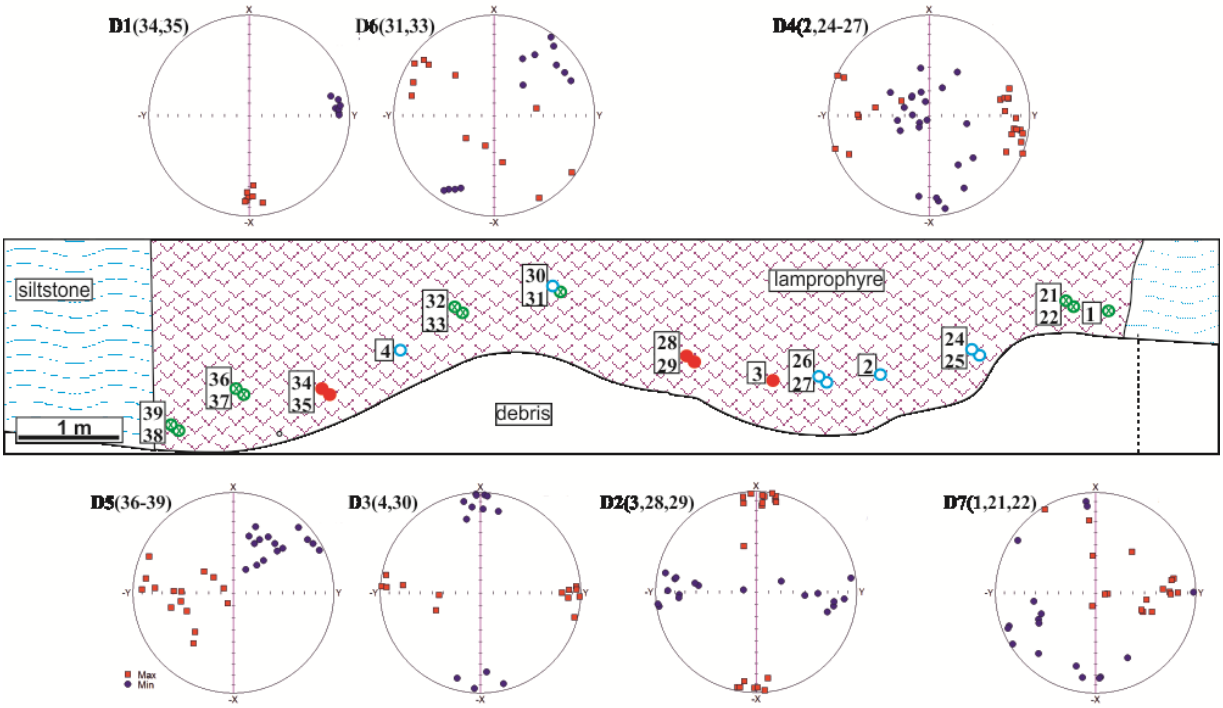

Figure 6. Positions of samples and orientations of magnetic foliation poles and magnetic lineations in homogenous domains within the dyke. Symbols of sampling points indicate the type of magnetic fabric within the sample (solid, red - normal; open, magenta - inverse; x, green - oblique fabrics). The upper left corners of the diagrams show the domain numbers (with numbers of samples creating the individual domains in brackets). Dyke coordinate system, equal-area projection on lower hemisphere.

5.6.2 Anisotropy of Anhysteretic Magnetic Remanence (AAMR) and Anisotropy of Out-of-Phase Magnetic Susceptibility (opAMS)

The reason for investigating the AAMR was to find out whether the inverse AMS fabric results from the perpendicular orientation of larger dimensions of magnetic minerals with respect to the dyke plane or from the grains of magnetic minerals being very small and SD in state. Namely, as shown by Potter and Stephenson [66] for example, the maximum susceptibility is along the maximum dimension in the MD particle, while it is along the minimum dimension in the SD particle. The minimum susceptibility is along the minimum dimension in the MD particle and along the

maximum dimension in the SD particle. As the measurement of AAMR is an order-of-magnitude more laborious and time-consuming than that of AMS, the AAMR was not measured in all the available specimens, but preferably in a selection of those coming from domains with normal (domains D1, D2) and inverse (domains D3, D4) AMS fabrics.

In both the domains showing *normal* ipAMS fabric (D1, D2), the ipAMS foliation and ipAMS lineation are parallel to the dyke plane; the latter is horizontal (Figure 7a,d). The AAMR and opAMS foliations are parallel to the dyke in the D2 domain, while they deflect azimuthally from the dyke in the D1 domain; the AAMR and opAMS lineations are very steep in the D1 domain and gentle to very steep in the D2 domain (Figure 7b,c,e,f).

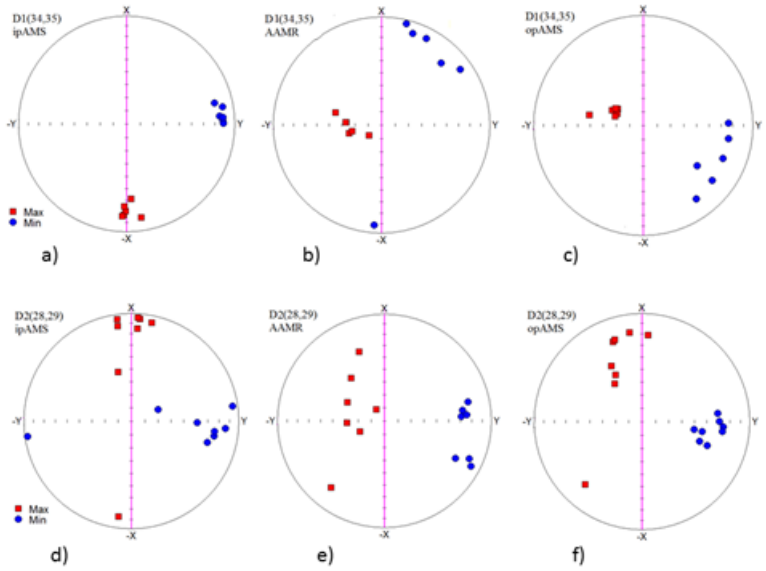

Figure 7. Domains D1 and D2 with normal magnetic fabric (**a**, **d** - anisotropy of the in-phase component of susceptibility, ipAMS; **b**, **e** - anisotropy of anhysteretic magnetic remanence, AAMR; **c**, **f** - out-of-phase component of susceptibility, opASM). Dyke coordinate system, equal-area projection on lower hemisphere.

In both the domains with *inverse* AMS fabric (D3, D4), the ipAMS foliation is perpendicular to the dyke plane, being horizontal in the D4 domain and vertical in the D3 domain; meanwhile, the ipAMS lineation is perpendicular to the dyke (Figure 8a,d). The AAMR foliations are very steep, and mostly perpendicular to the dyke; the AAMR lineations are perpendicular to the dyke and horizontal in the D4 domain, and mostly parallel to the dyke and vertical in the D3 domain (Figure 8b,e). The opAMS foliations are vertical and perpendicular to the dyke in both domains, and the opAMS lineations are horizontal and perpendicular to the dyke in the D4 domain, and show a variable plunge within the vertical plane perpendicular to the dyke in the domain D3 (Figure 8c,f).

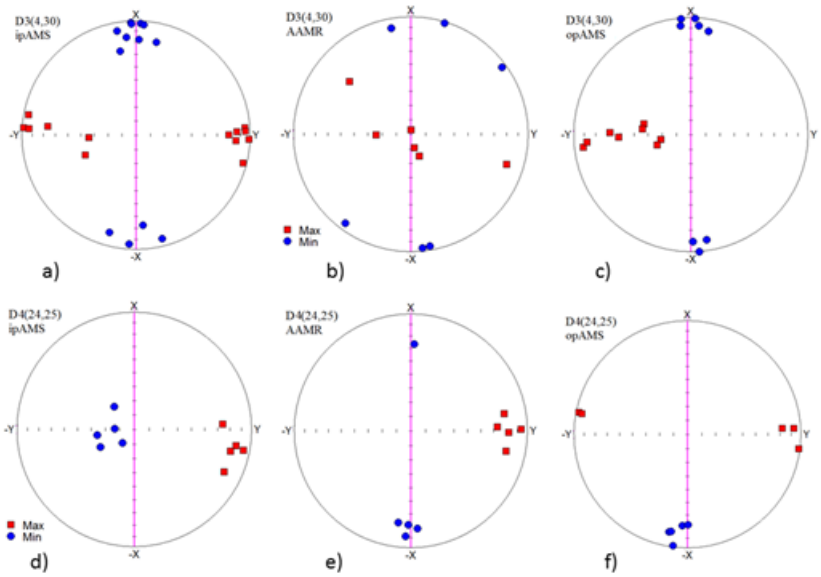

Figure 8. Domains D3 and D4 with inverse magnetic fabric (**a**, **d** - ipAMS; **b**, **e** - AAMR; **c**, **f** - opAMS). Dyke coordinate system, equal-area projection on lower hemisphere.

In summary, the ipAMS foliation poles are not parallel to the AAMR lineations as well as the ipAMS lineations are not parallel to the AAMR foliation poles in any domain. In addition, the frequency-dependent susceptibility is very low (mostly X_{FD} < 1%), indicating that the ultrafine magnetically viscous particles in transition from the SP state to the SD state are present in very low amounts. Assuming continuous grain-size distribution from SP to MD, and realizing that the susceptibility of SD particles is lower than that of MD or SP particles, the very low values of the X_{FD} parameter may indicate that the SD particles are not abundant enough to dominate the rock magnetism. One can conclude that the inverse AMS fabrics are very unlikely due to the dominance of SD particles, and their existence should be ascribed to specific mechanisms in detailed magma movement.

The magnetism of the dyke is dominantly carried by MD ferromagnetic minerals. If different subpopulations of those minerals had similar geological histories, one would expect coaxial orientations of ipAMS, AAMR, and opAMS. However, this is true only partially. The ipAMS, AAMR, and opAMS foliations and lineations all show moderate to large differences. These may be ascribed to slightly different subpopulations of magnatic grains controlling the individual anisotropies. They may reflect a transition from vertical feeding flow to horizontal flow, representing advanced magma propagation.

In the D1 and D2 domains, in which the ipAMS, AAMR, and ipAMS fabrics can be classified as *normal*, all the three magnetic fabrics evidently indicate relatively free flow, during

which the magnetic minerals orient parallel, with their larger surfaces to the dyke, and with their longer dimensions probably parallel to the magma flow. The titanomagnetite longer axes, being oblique to vertical as indicated by AARM and opAMS lineations, probably represent the direction of the feeding flow of the dyke. The horizontal longer axes of magnetite indicated by ipAMS probably represent the advanced magma propagation along the dyke. We hypothesize that the magnetic minerals crystallized only during magma feeding a joint and creating the dyke. Then, the titanomagnetites crystallized earlier at higher temperatures than magnetite.

In the D3 and D4 domains, whose ipAMS, AAMR, and ipAMS fabrics can be classified as *inverse*, the magnetic minerals are oriented with their larger surfaces perpendicular to the dyke and with their longer dimensions also perpendicular to the dyke. Such a magnetic fabric may have originated as follows. The magma movement is no longer represented by free flow. Rather, it is akin to forceful injection when the later magma batches push on the earlier ones. In this process, the larger surfaces as well as the longer axes of magnetic minerals orient perpendicular to the compression direction. It is interesting that in the D4 domain, the ipAMS foliations, although perpendicular to the dyke, are horizontal, while the AAMR and opAMS foliations are also perpendicular to the dyke, but vertical. This would mean that titanomagnetites indicate horizontal compression along the dyke, while the magnetite indicates vertical compression.

5.7 Discussion

5.7.1 Variation of Mineral Textures and AMS Fabrics across the Composite Dyke

As shown above, the dyke at Dobříš is represented by various domains differing in composition and fabrics. Its compositional change from kersantite occurring mostly at the margin parts to spessartite in the central part is accompanied by an increase in the degrees of amphibolization. This inward transition is gradual, and can be seen in the grain sizes of minerals, mainly of amphibole, with its high volume content in the central part. It seems that the original magma of kersantite composition intruded into a relatively cold environment, making chilled contacts with the host siltstone. Although phenocrysts of clinopyroxene and talc pseudomorphs reach sizes of up to 1.5 mm, the rock still has a fine-grained matrix. The continuous change in grain size, modal amounts of original mineral (biotite), mineral composition (plagioclase, X_{Mg} values of clinopyroxene), and bulk rock composition suggest a gradual change of the source magma to spessartite, which intruded through the central part of the dyke. Based on the early crystallized minerals, both magmas were generated by partial mantle melting, but kersantite melt came from the mica-bearing peridotite part [38]. The presence of spectacular ocelli textures at areas in contact with the rim suggests that the bubbles were filled at high temperature by infiltration of the residual melt

from the matrix, which crystallized into plagioclase, biotite, amphibole, and quartz, with or without calcite. As there is no sharp boundary between kersantite and spessartite, the more mafic magma penetrated the axial part of the dyke in the still relatively warm environment formed by kersantite. Consistent with textural relations, amphibole was formed during the last stage of crystallization. The presence of amphibole enclosing both phenocrysts and matrix minerals suggests that it formed in subsolidus conditions after the emplacement of the dyke. The assumption about high temperature being sufficient for amphibole formation of magnesio-hornblende and tschermakite composition is supported by the ocelli textures filled by plagioclase, amphibole, and biotite.

As illustrated in Figure 3, except for the percentage loss of susceptibility (X_{FD}), the values of bulk density, mean susceptibility, shape parameter (T), and degree of AMS (P) show generally bimodal distribution and divide the dyke into two NE and SW segments. Each segment is characterized by an elevated central part and depressions at the marginal parts. The values of the X_{FD} parameter are roughly inverted to those of the above parameters. This bimodal distribution of magnetic parameters implies that the dyke was formed by two magma pulses: one creating the NE segment, and the other creating the SW one. Based on the results of petrology, the two pulses do not represent timely and mechanically separated magma batches, but rather represent the gradual development of one slowly moving magma, changing its composition from kersantite to spessartite.

5.7.2 Implications of AMS Fabrics to Multistage Evolution of Magmatic Dykes

Several theoretical models of the dyke formation can be basically considered. They either assume that the dyke walls simply open gradually and the space between them is infilled by magma, or they also consider that during dyke formation, the dyke walls are subject to shear movements, which can be vertical (dip-slip), horizontal (strike-slip), or even oblique. The moving magma is supposed to resemble the flow of the Newtonian or Binghamian liquid or a transition between these two (e.g., [7]). The magma movement is advantagenously described in terms of intrusive strain; four different cases (model 1–4 in Figures 9 and 10) can occur. The predicted orientations of the magnetic foliations and lineations are obtained from our own program based on the line/plane and viscous models (for details, see [67, 68]).

Model 1 (Figure 9) considers that a vertical dyke opens without the transcurrent component being fed with vertically flowing magma, resembling the Newtonian liquid (Figure 9a,b). The AMS ellipsoid is nearly neutral, and the magnetic foliation is very steep, striking parallel to the dyke wall and dipping toward the wall; the magnetic lineation is also very steep, being roughly parallel to the dip of the magnetic foliation (Figure 9f). This magnetic fabric can be classified as *normal*. In the tip parts of the dyke (Figure 9b), the magma movement resembles pure shear, the AMS ellipsoid is predominantly oblate, and the magnetic foliation and magnetic lineation are roughly horizontal, making them perpendicular to the dyke, and creating the *intermediate* magnetic fabric (Figure 9g)

[7]. If the uppermost part of the dyke does not open sufficiently rapidly, the flow direction may change to horizontal (Figure 9c); as a result, the magnetic foliation orients near the dyke walls, and the magnetic lineation becomes horizontal (Figure 9h). If the horizontal flow is no longer possible for mechanical reasons, the magnetic foliation and magnetic lineation also may become vertical (Figure 9i). If the magma flow resembles the Binghamian liquid (Figure 9e), the magnetic foliation is parallel to the dyke walls, and the magnetic lineation is vertical (Figure 9j).

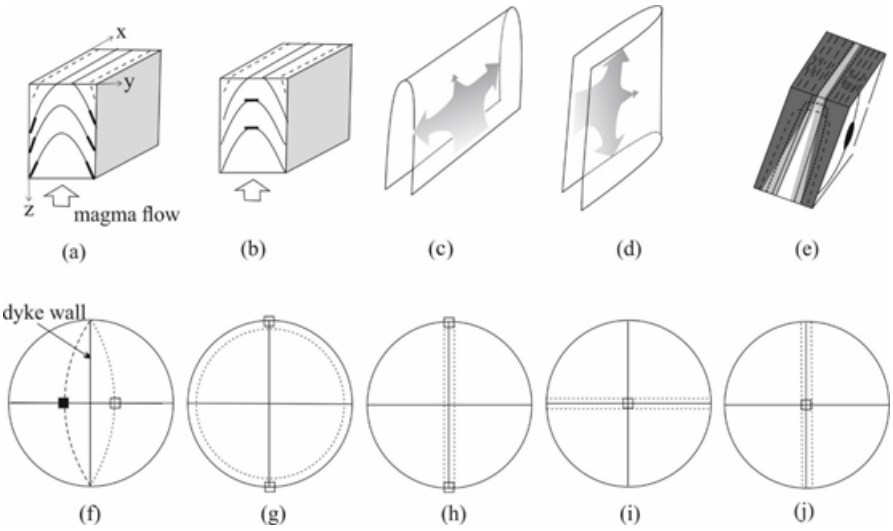

Figure 9. Schematic sketch of the magma flow and the AMS in the dyke without transcurrent movement of dyke walls. In **a**–**d**, the magma flow resembles the flow of the Newtonian liquid; in **e**, the magma movement resembles flow of the Binghamian liquid. **a**, **b** - vertical magma flow, **c** - change of vertical magma flow to horizontal flow, **d** - change from horizontal flow to vertical flow, **f** - orientations of magnetic foliation (great circles) and magnetic lineation (squares) in the marginal parts of the model a (dashed circles and close squares - left margin, dotted circles and open squares - right margin), **g** - magnetic foliation and lineation in the model b, **h** - magnetic foliation and lineation in the model c, **i** - magnetic foliation and lineation in the model d, **j** - magnetic foliation and lineation in the model e. Dyke coordinate system (*x, y, z*), equal-area projection on the lower hemisphere. Adapted from [5,7] using our own program for modeling magnetic particle orientations during flow and simple shear movements.

Model 2 (Figure 10a–e) assumes that a vertical dyke is vertically fed with magma, and the dyke walls move in a dip-slip way (Figure 10a). In the marginal areas, the basic orientations of magnetic foliation and magnetic lineation remain steep (Figure 10b). In the tip areas, the magnetic foliation deflects from the horizontal position, and the magnetic lineation remains more or less horizontal (Figure 10c). If the magma movement changes to horizontal, while the wall movements remain dip-slip oriented, the magnetic foliation may slightly deflect from the vertical, and the magnetic lineation may remain more or less horizontal if the shear movement is weak, or more or less vertical if the shear movement is relatively strong (Figure 10d). If the magma feeding magnetic

foliation is vertical and oriented in a perpendicular way to the dyke, the magnetic lineation deflects from the vertical due to dip-slip movements, and the magnetic foliation does not substantially change its orientation (Figure 10e).

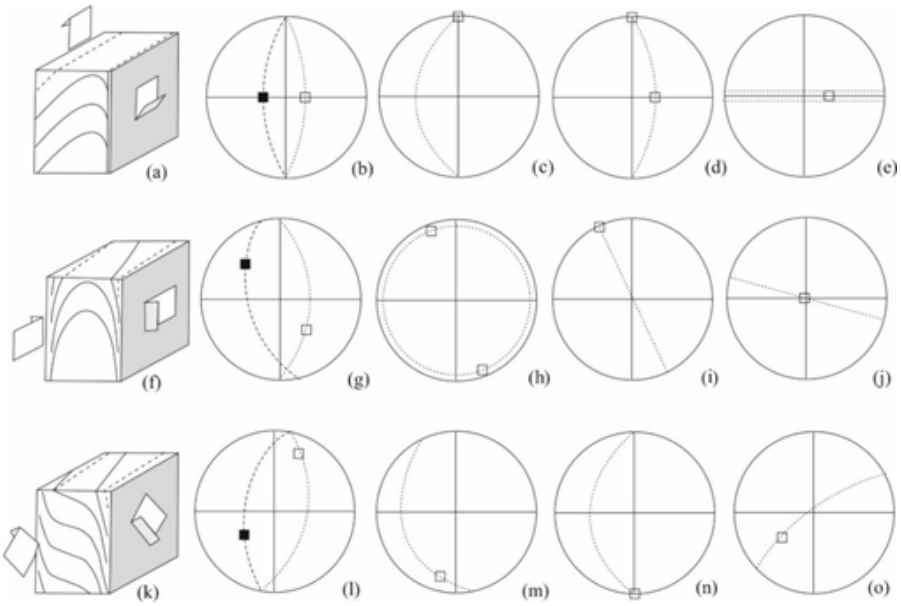

Figure 10. Schematic sketch of the magma flow and the AMS in the dyke showing various transcurrent movements of the dyke walls. (**a**–**e**) - vertical dextral shear, (**f**–**j**) - horizontal dextral shear, (**k**–**o**) - oblique shear. Equal-area projection on the lower hemisphere. Adapted from [5,7] using our own program for modeling magnetic particle orientations during flow and simple shear movements.

Model 3 (Figure 10f–j) assumes the same dyke, but with its walls making a strike-slip movement (Figure 10f). In the marginal parts, the magnetic foliation gradually deflects from the approximate parallelism to the dyke toward the perpendicularity to the dyke, and the magnetic lineation moves along the great circle from the vertical toward the horizontal (Figure 10g). In the tip parts, the magnetic foliation remains nearly horizontal, and the magnetic lineation gradually deflects from the dyke strike direction (Figure 10h). If the magma feeding direction is horizontal, the magnetic foliation remains more or less vertical, but deflects azimuthally from the dyke plane; the magnetic lineation remains nearly horizontal and rotates azimuthally from the dyke strike (Figure 10i). If the magma feeding magnetic foliation is vertical and oriented in a perpendicular way to the dyke, the magnetic lineation remains more or less vertical, and the magnetic foliation rotates azimuthally due to strike-slip movements (Figure 10j).

Model 4 (Figure 10k–o) considers the same dyke, but with its walls performing oblique shear movements (Figure 10k). In this case, the magnetic foliation and lineation show movements, combining the previous three models.

Based on the above outlined analysis on magma flow within dykes (with or without shear movements of the walls), the magnetic fabrics in different parts of the Dobříš dyke indicate analogies with some model types in Figures 9 and 10. For example, the ipAMS fabrics in the D1 (Figure 7a) and D2 (Figure 7d) domains correspond to model 1 (Figure 9c,h), and those in the D5 and D6 domains (Figure 6) correspond to model 3 in Figure 10g,i,j, respectively. The AAMR fabric in the D1 domain (Figure 10b) is similar to that in model 3 (Figure 10j), and the fabric in the D2 domain (Figure 7e) corresponds to that of model 1 (Figure 9a). There is also an additional type showing both magnetic foliation and magnetic lineation perpendicular to the dyke, which is represented by the D3 domain (Figure 8a) and the D4 domain (Figure 8d). All this indicates that the magma movement must have been very complex.

Even though the magnetic fabric in the Dobříš dyke shows features in some domains that can be due to shear movements (corresponding to models 2 and 3), we cannot find the effects of these movements on the whole dyke. In our opinion, the above features are due to small-scale shear movements within the dyke, rather than overall dyke wall movements.

As indicated in Figure 6, the orientations of magnetic foliation poles and magnetic lineations across the dyke can be classified into seven domains (Figure 11). The two domains (D1, D2) with normal fabrics (magnetic foliation parallel to the dyke plane) are in contact with the D3 and D4 domains, which have inverse fabrics (magnetic foliation and lineation perpendicular to the dyke plane). The domains D5 and D7 with mixed fabrics between normal and inverse are located in areas in contact with surrounding siltstone, while the D6 domain, which has similar fabrics, is located in the central part of the dyke. The detailed textural relations and bulk rock chemistry of the rocks in domain D5 indicate that its composition is kersantite, and that it intruded first into the cold surrounding environment. We also showed that the formation of the dyke was evolved toward the central part, where new magma of more mafic composition intruded. Therefore, the fabrics of the marginal domains (D5 and D7) were controlled both by friction with the wall of the host siltstone, and by the movement of ascending magma.

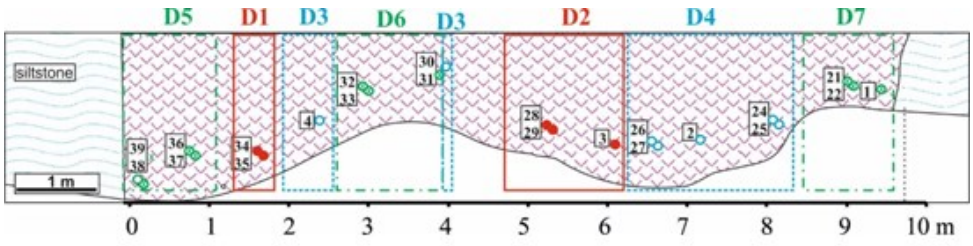

Figure 11. Locations of different domains with normal (open circles), inverse (solid circles), and oblique (crossed circles) magnetic fabrics across the lamprophyre dyke in Dobříš.

Although the degrees of amphibolization and coarsening of the rocks increase inward, the original texture and bulk rock chemistry is not uniform in the central part of the dyke. This suggest that the whole dyke was fed by different portions of melt that intruded in different time intervals that were close to each other. The presence of the D6 domain with mixed magnetic fabrics in the central part of the dyke can be explained by reopening of the dyke on both sides of the D6 domain, where two normal and inverse domains occur. We assume that the D1 and D2 domains with vertical magnetic fabrics represent the younger portions of melt that penetrated the dyke after the D3 and D4 domains were partly solidified. Consequently, the magnetic minerals in the more viscous magma portions may have oriented by their longer dimensions perpendicular to the dyke, because the lengthening perpendicular to the dyke was compensated by the vertical escape of neighboring, less viscous magma.

The investigated dyke at Dobříš shows a rare phenomena, viz. the occurence of both *normal* and *inverse* magnetic fabrics within one dyke. The question arises of how it is possible that the magma movement in one dyke shows indications of both free flow (*normal* magnetic fabric) and forceful injection (*intermediate* or *inverse* magnetic fabric). Following the results of petrological and rock magnetism studies, the answer can be found in the strong inhomogenity of the rocks, both compositionally and structurally. It may have happened that some portions of the ascending magma were more viscous than others. Consequently, the magnetic minerals in the more viscous magma portions may have oriented by their longer dimensions parpendicular to the dyke, because the lengthening perpendicular to the dyke was compensated for by the vertical escape of neighboring less viscous magma. The frequent oblique magnetic fabrics may represent transitions between the above two mechanisms.

5.8 Conclusions

The results of petrological and magnetic fabric investigations of a composite lamprophyre dyke from the Central Bohemian Dyke Swarm, showing domains with gradual change in composition and having *normal* and *inverse* magnetic fabrics, can be summarized as follows:

1. The composite dyke near Dobříš was formed by the intrusion of two subsequent magmas of kersantite and spessartite compositions, respectively. Both magmas were generated by partial mantle melting, but the former seemed to evolve from metasomatized mica-bearing peridotite. Kersantite occupies mostly the NE margin of the dyke, while the spessartite forms the central and SW parts of the dyke.

2. In addition to the changes in mineral composition and bulk rock chemistry, there is a gradual change in the grain size and degree of amphibolization that occurred in subsolidus conditions.

3. The dominant carrier of rock susceptibility and AMS is slightly oxidized magnetite, even though some other magnetic phases (represented by Fe-Ti oxides with different contents of Ti) are also present. As the AMS of magnetite is controlled by its grain shape, the rock AMS is controlled by the preferred orientation of magnetite by grain shape.

4. The magnetite is dominantly represented by relatively large MD grains, while the SD particles and the ultrafine magnetically viscous grains are present in very low amounts; the AMS is dominantly controlled by the preferred orientation of MD grains.

5. The overall courses of the magnetic parameters investigated across the dyke indicate the existence of two slightly differing sections, one between 0–500 cm, and the other between 500–1000 cm. These two sections may represent two magma pulses.

6. The magnetic fabric is *normal*, i.e., with magnetic foliation and magnetic lineation parallel to the dyke plane, in some domains of the dyke, *inverse*, i.e., with magnetic foliation and magnetic lineation perpendicular to the dyke plane, in some other domains, and oblique, with both magnetic foliation and lineation with respect to the dyke, in most domains.

7. The existence of the domains with both *normal* and *inverse* magnetic fabric within the dyke is ascribed to dramatically different mechanisms of magma movement in the respective domains. It is hypothesized that some portions of the ascending magma were more viscous than others. The magnetic minerals in the more viscous magma portions may have oriented by their longer dimensions perpendicular to the dyke, because the lengthening perpendicular to the dyke was compensated by the vertical escape of neighboring, less viscous magma.

Acknowledgments

We thank anonymous reviewers for very helpful reviews. Macie Ma and R. Li are thanked for editorial handling.

Funding

The research was financially supported by the Czech Science Foundation (Project 18-03160S) and by Charles University through project Progress Q45.

References

1. Silva, P.F.; Marques, F.O.; Henry, B.; Madureira, P.; Hirt, A.M.; Font, E.; Lourenco, N. Thick dyke emplacement and internal flow: A structural and magnetic fabric study of the deep-seated dolerite dyke on Foum Zguid (Southern Morocco). *J. Geophys. Res.* **2010**, *115*, B12109.
2. Correa-Gomes, L.C.; Souza Filho, C.R.; Martins, C.J.F.N.; Oliveira, E.P. Development of symmetrical and asymmetrical fabrics in sheet-like igenous bodies: The role of magma flow and wall-rock displacements in theoretical and natural cases. *J. Struct. Geol.* **2001**, *23*, 1415–1428.
3. Skarmeta, J. Interaction between magmatic and tectonic stresses during dyke intrusion. *And. Geo.* **2011**, *38*, 393–413.
4. Callot, J.-P.; Geoffroy, L.; Aubourg, C.; Pozzi, J.P.; Mege, D. Magma flow directions of shallow dykes from the East Greenland volcanic margin inferred from magnetic fabric studies. *Tectonophysics* **2001**, *335*, 3–4.
5. Clemente, C.S.; Amoros, E.B.; Crespo, M.G. Dike intrusion under shear stress: Effects on magnetic and vesicle fabrics in dikes from rift zones of Tenerife Canary Islands). *J. Struct. Geol.* **2007**, *29*, 1931–1942.
6. Ernst, R.E.; Baragar, W.R.A. Evidence from magnetic fabric for the flow pattern of magma in the Mackenzie giant radiating dyke swarm. *Nature* **1992**, *356*, 511–513.
7. Féménias, O.; Diot, H.; Brza, T.; Gauffriau, A.; Demaiffe, D. Assymetrical to symmetrical magnetic fabric of dikes: Paleo-flow orientations and Paleo-stresses recorded on feeder-bodies from the Motru Dike Swarm (Romania). *J. Struct. Geol.* **2004**, *26*, 1401–1418.
8. Hrouda, F.; Verner, K.; Kubínová, Š.; Buriánek, D.; Faryad, S.W.; Chlupáčová, M.; Holub, F.V. Magnetic fabric and emplacement of dykes of lamprophyres and related rocks of the Central Bohemian Dyke Swarm (Central European Variscides). *J. Geosci.* **2016**, *61*, 335–354.
9. Knight, M.D.; Walker, G.P.L. Magma flow directions in dykes of the Koolan Complex, Oahu, determined from magnetic fabric studies. *J. Geophys. Res.* **1988**, *93*, 4308–4319.
10. Raposo, M.I.B. Magnetic Fabric of the Brazilian Dike Swarms: A Review. In The Earth's Magnetic Interior; IAGA Special Sopron Book Series 1; Petrovský, E., Herroro-Bervera, E., Harinarayana, T., Ivers, D., Eds.; IAGA: Hong Kong, China, 2011; pp. 247–262.
11. Raposo, M.I.B.; Ernesto, M. Anisotropy of magnetic susceptibility in the Ponta Grossa dyke swarm (Brazil) and its relationship with magma flow direction. *Phys. Earth Planet. Int.* **1995**, *87*, 183–196.
12. Rochette, P.; Jenatton, L.; Dupuy, C.; Boudier, F.; Reuber, I. Diabase dykes emplacement in the Oman ophiolite: A magnetic fabric study with reference to geochemistry. In *Ophiolite Genesis*

and Evolution of the Oceanic Lithosphere; Peters, T., Nicolas, A., Coleman, R., Eds.; Springer: Dordrecht, The Netherlands, 1991; pp. 55–82.

13. Staudigel, H.; Gee, J.; Tauxe, L.; Varga, R.J. Shallow intrusive directions of sheeted dykes in the Troodos ophiolite: Anisotropy of magnetic susceptibility and structural data. *Geology* **1992**, *20*, 841–844.
14. Varga, R.J.; Gee, J.S.; Staudigel, H.; Tauxe, L. Dike surface lineations as magmaflow indicators within the sheeted dike complex of the Troodos ophiolite, Cyprus. *J. Geophys. Res.* **1998**, *103*, 5241–5256.
15. Bates, M.P.; Mushayandebvu, M.F. Magnetic fabric in the Umvimeela Dyke, satelite of the Great Dyke, Zimbabwe. *Tectonophysics* **1995**, *242*, 141–254.
16. Park, J.K.; Tanczyk, E.I.; Desbarats, A. Magnetic fabric and its significance in the 1400 Ma Mealy diabase dykes of Labrador, Canada. *J. Geophs. Res.* **1988**, *93*, 13689–13704.
17. Stephenson, A.; Sadikum, S.; Potter, D.K. A theoretical and experimental comparison of the anisotropies of magnetic susceptibility and remanence in rocks and minerals. *Geophys. J. Astron. Soc.* **1986**, *84*, 185–200.
18. Hrouda, F. The magnetic fabric in the Brno massif. *Sbor. Geol. Věd*. **1985**, *19*, 89–112.
19. Holub, F.V.; Verner, K.; Schmitz, M.D. Temporal relations of melagranite porphyry dikes and durbachitic plutons in South Bohemia. *Geos. Res. Rep.* **2011**, *2012*, 23–25.
20. Machek, M.; Roxerová, Z.; Závada, P.; Silva, P.F.; Henry, B.; Dědeček, P.; Petrovský, E.; Marques, F.O. Intrusion of lamprophyre dyke and related deformation effects in the host rock salt: A case study from the Loule diapir, Portugal. *Tectonophys* **2014**, *629*, 165–178.
21. Chalapathi Rao, N.V.; Srivastava, R.K. Kimberlites, lamproites, lamprophyres, their entrained xenoliths, mafic dykes and dyke swarms: Highlights of Recent Indian Research. Proc. Indian natn. *Sci. Acad.* **2012**, *78*, 431–444.
22. Edgar, A.D.; Mitchell, R.H. Ultra high pressure–temperature melting experiments on an SiO_2-rich lamproite from Smoky Butte, Montana: Derivation of siliceous lamproite magmas from enriched sources deep in the continental mantle. *J. Petrol.* **1997**, *38*, 457–477.
23. Guo, Z.; Wilson, M.; Liu, J.; Mao, Q. Post-collisional, potassic and ultrapotassic magmatism of the northern Tibetan Plateau: Constraints on characteristics of the mantle source, geodynamic setting and uplift mechanisms. *J. Petrol.* **2006**, *47*, 1177–1220.
24. Gupta, A.K. *Origin of Potassium-Rich Silica-Deficient Igneous Rocks*; Springer: Berlin, Germany; New York, NY, USA, 2015.

25. Holub, F. Zonal dyke of ocelli lamprophyre to hornblendite from Dobříš. *Zprávy Geol. Výzk.* **2003**, *2003*, 106–108. (In Czech)

26. Dörr, W.; Zulauf, G. Elevator tectonics and orogenic collapse of a Tibetan-style plateau in the European Variscides: The role of the Bohemian shear zone. *Int. J. Earth Sci.* **2010**, *99*, 299–325.

27. Faryad, S.W.; Jedlička, R.; Collett, S. Eclogite facies rocks of the Monotonous unit, clue to Variscan suture in the Moldanubian Zone (Bohemian Massif). *Lithos* **2013**, *179*, 353–363.

28. Schulmann, K.; Konopásek, J.; Janoušek, V.; Lexa, O.; Lardeaux, J.M.; Edel, J.B.; Štípská, P.; Ulrich, S. An Andean type Palaeozoic convergence in the Bohemian Massif. *Comptes Rendus Geosci.* **2009**, *341*, 266–286.

29. Žák, J.; Verner, K.; Finger, F.; Faryad, S.W.; Chlupáčová, M.; Veselovský, F. The generation of voluminous S-type granites in the Moldanubian unit, Bohemian Massif, by rapid isothermal exhumation of the metapelitic middle crust. *Lithos* **2011**, *121*, 25–40.

30. Žák, J.; Verner, K.; Janoušek, V.; Holub, F.V.; Kachlík, V.; Finger, F.; Hajná, J.; Tomek, F.; Vondrovic, L.; Trubač, J. A plate–kinematic model for the assembly of the Bohemian Massif constrained by structural relationships around granitoid plutons. In *The Variscan Orogeny: Extent, Timescale and the Formation of the European Crust*; Special Publications 405; Schulmann, K., Martínez Catalán, J.R., Lardeaux, J.M., Janoušek, V., Oggiano, G., Eds.; Geological Society: London, UK, 2014; pp. 169–196.

31. Jedlička, R.; Faryad, S.W.; Hauzenberger, C. Prograde metamorphic history of UHP granulites from the Moldanubian Zone (Bohemian Massif) revealed by major element and Y + REE zoning in garnets. *J. Petrol.* **2015**, *56*, 2069–2088.

32. Finger, F.; Roberts, M.P.; Haunschmid, B.; Schermaier, A.; Steyrer, H.P. Variscan granitoids of central Europe: Their typology, potential sources and tectonothermal relations. *Miner. Petrol.* **1997**, *61*, 67–96.

33. Holub, F.V.; Klečka, M.; Matějka, D. Igneous activity. In *Pre-Permian Geology of Central and Eastern Europe*; Dallmeyer, R.D., Franke,W.,Weber, K., Eds.; Springer: Berlin, Germany, 1995; pp. 444–452.

34. Janoušek, V.; Braithwaite, C.J.R.; Bowes, D.R.; Gerdes, A. Magma-mixing in the genesis of Hercynian calc-alkaline granitoids: An integrated petrographic and geochemical study of the Sázava intrusion, Central Bohemian Pluton, Czech Republic. *Lithos* **2004**, *78*, 67–99.

35. Schaltegger, U. Magma pulses in the Central Variscan Belt: Episodic melt generation and emplacement during lithospheric thinning. *Terra Nova* **1997**, *9*, 242–245.

36. Janoušek, V.; Gerdes, A. Timing the magmatic activity within the Central Bohemian Pluton, Czech Republic: Conventional U-Pb ages for the Sázava and Tábor intrusions and their geotectonic significance. *J. Geosci.* **2003**, *48*, 70–71.

37. Janoušek, V.; Wiegand, B.; Žák, J. Dating the onset of Variscan crustal exhumation in the core of the Bohemian Massif: New U–Pb single zircon ages from the high-K calcalkaline granodiorites of the Blatná suite, Central Bohemian Plutonic Complex. *J. Geol. Soc.* **2010**, *167*, 347–360.

38. Kubínová, Š.; Faryad, S.W.; Verner, K.; Schmitz, M.; Holub, F.V. Ultrapotassic dykes in the Moldanubian Zone and their significance for understanding post-collisional mantle dynamics during the Variscan orogeny in the Bohemian Massif. *Lithos* **2017**, *272*, 205–221.

39. Ackerman, L.; Pašava, J.; Erban, V. Re-Os geochemistry and geochronology of the Ransko gabbro-peridotite massif, Bohemian Massif. *Miner. Depos.* **2013**, *48*, 799–804.

40. Faryad, S.W.; Kachlík, V.; Sláma, J.; Hoinkes, G. Implication of corona formation in a metatroctolite to the granulite facies overprint of HP-UHP rocks in the Moldanubian Zone (Bohemian Massif). *J. Metamorph. Geol.* **2015**, *33*, 295–310.

41. Faryad, S.W.; Kachlík, V.; Sláma, J.; Jedlička, R. Coincidence of gabbro and granulite formation and their implication for Variscan HT metamorphism in the Moldanubian Zone (Bohemian Massif), example from the Kutná Hora Complex. *Lithos* **2016**, *264*, 56–69.

42. Pokorný, P.; Pokorný, J.; Chadima, M.; Hrouda, F.; Studýnka, J.; Vejlupek, J. KLY5 Kappabridge: High sensitivity and anisotropy meter precisely decomposing in-phase and out-of-phase components. In Proceedings of the EGU General Assembly 2016, Vienna, Austria, 17–22 April 2016; p. 18.

43. Studýnka, J.; Chadima, M.; Suza, P. Fully automated measurement of anisotropy of magnetic susceptibility using 3D rotator. *Tectonophysics* **2014**, *629*, 6–13.

44. Jelínek, V. Theory and measurement of the anisotropy of isothermal remanent magnetization of rocks. *Trav. Geophys.* **1993**, *37*, 124–134.

45. Jelínek, V. Characterization of the magnetic fabric of rocks. *Tectonophysics* **1981**, *79*, 63–67.

46. Nagata, T. *Rock Magnetism*; Maruzen: Tokyo, Japan, 1961.

47. Chadima, M.; Jelínek, V. Anisoft 4.2—Anisotropy Data Browser. *Contrib. Geophys. Geodesy* **2008**, *38*, 41.

48. Hrouda, F.; Jelínek, V.; Hrušková, L. A package of programs for statistical evaluation of magnetic anisotropy data using IBM-PC computers (abstract). *Eos Trans. AGU* **1990**, *71*, 1289.

49. Jelínek, V. Statistical processing of magnetic susceptibility measured on groups of specimens. *Studia Geophys. Geod.* **1978**, *22*, 50–62.

50. Aydin, A.; Ferré, E.C.; Aslan, Z. The magnetic susceptibility of granitic rocks as a proxy for geochemical differentiation: Example from the Saruhan granitoids, NE Turkey. *Tectonophysics* **2007**, *441*, 85–95.

51. Dearing, J.A.; Dann, R.J.L.; Hay, K.; Lees, J.A.; Loveland, P.J.; Maher, B.A.; O'Grady, K. Frequency-dependent susceptibility measurements of environmental materials. *Geophys. J. Int.* **1996**, *124*, 228–240.

52. Hrouda, F.; Chlupáčová, M.; Mrázová, Š. Low-field variation of magnetic susceptibility as a tool for magnetic mineralogy of rocks. *Phys. Earth Sci. Int.* **2006**, *154*, 323–336.

53. Parma, J.; Hrouda, F.; Pokorný, J.;Wohlgemuth, J.; Suza, P.; Šilinger, P.; Zapletal, K. A technique for measuring temperature dependent susceptibility of weakly magnetic rocks. In Proceedings of the Eos, Transactions American Geophysical AGU, Spring Meeting, Portland, OR, USA, 18–21 October 1993; Volume 1993, p. 113.

54. Petrovský, E.; Kapička, A. On determination of the Curie point from thermomagnetic curves. *J. Geophys. Res.* **2006**, *111*, B12S27.

55. Dunlop, D.J.; Özdemir, Ö. Rock Magnetism. In *Fundamentals and Frontiers*; Cambridge University Press: Cambridge, UK, 1997.

56. Hrouda, F. A technique for the measurement of thermal changes of magnetic susceptibility of weakly magnetic rocks by the CS-2 apparatus and KLY-2 Kappabridge. *Geophys. J. Int.* **1994**, *118*, 604–612.

57. De Wall, H. The field dependence of AC susceptibility in titanomagnetites: Implications for the anisotropy of magnetic susceptibility. *Geophys. Res. Lett.* **2000**, *27*, 2409–2411.

58. De Wall, H.; Nano, L. The use of field dependence of magnetic susceptibility for monitoring variations in titanomagnetite composition—A case study on basanites from the Vogelsberg 1996 Drillhole, Germany. *Stud. Geophys. Geod.* **2004**, *48*, 767–776.

59. Hrouda, F. Low-field variation of magnetic susceptibility and its effect on the anisotropy of magnetic susceptibility of rocks. *Geophys. J. Int.* **2002**, *150*, 715–723.

60. Jackson, M.; Moskowitz, B.; Rosenbaum, J.; Kissel, C. Field-dependence of AC susceptibility in titanomagnetites. *Earth Planet. Sci. Lett.* **1998**, *157*, 129–139.

61. Markert, H.; Lehmann, A. Three-dimensional Rayleigh hysteresis of oriented core samples from the German Continental Deep Drilling program: Susceptibility tensor, Rayleigh tensor, three-dimensional Rayleigh law. *Geophys. J. Int.* **1996**, *127*, 201–214.

62. Worm, H.-U.; Clark, D.; Dekkers, M.J. Magnetic susceptibility of pyrrhotite: Grain size, field and frequency dependence. *Geophys. J. Int.* **1993**, *114*, 127–137.

63. Hrouda, F.; Chadima, M.; Ježek, J.; Pokorný, J. Anisotropy of out-of-phase magnetic susceptibility of rocks as a tool for direct determination of magnetic subfabrics of some minerals: An introductory study. *Geophys. J. Int.* **2017**, *208*, 385–402.

64. Hrouda, F. Models of frequency-dependent susceptibility of rocks and soils revisited and broadened. *Geophys. J. Int.* **2011**, *187*, 1259–1269.

65. Hrouda, F.; Pokorný, J. Extremely high demands for measurement accuracy in precise determination of frequency-dependent magnetic susceptibility of rocks and soils. *Stud. Geophys. Geod.* **2011**, *55*, 667–681.

66. Potter, D.K.; Stephenson, A. Single-domain particles in rocks and magnetic fabric analysis. *Geophys. Res. Lett.* **1988**, *15*, 1097–1100.

67. Owens,W.H. Mathematical model studies on factors affecting the magnetic anisotropy of deformed rocks. *Tectonophysics* **1974**, *24*, 115–131.

68. Hrouda, F. Theoretical models of magnetic anisotropy to strain relationship revisited. *Phys. Earth Planet. Int.* **1993**, *77*, 237–249.

CHAPTER 6

GENERAL CONCLUSIONS

The studied potassic to ultrapotassic dyke rocks from the contact area between the Moldanubian Zone and the Teplá-Barrandian Block of the Bohemian Massif are classified as *minettes, vaugnerite, spessartites*, *kersantites* and *syenite porphyries*. Special attention was paid to *vaugnerite*, *syenite porphyry* (both from Nihošovice) and *olivine minette* (from Horní Kožlí), mainly to their mineral textures, mineral chemistry, temperature-pressure conditions and crystallization history of the rocks. Also, the estimation of oxidation state of source melt was established. In addition, the study was completed by the bulk rock geochemistry that can provide information about the melt generation and subsequent differentiation processes. According to these approaches, we tried to compile the crystallization succession of rock-forming minerals and to identify possible mantle source of melts and its successive modifications. The U-Pb dating of *vaugnerite* and *syenite porphyry* dykes was used to determine the ages of this type of magmatic activity in the Bohemian Massif. The magnetic anisotropy study was applied on 14 dyke rocks (*minettes*, *spessartites*, *kersantites* and *syenite porphyries*) and it was aimed to constrain magnetic fabrics and mode of magma flow within the dykes. The relationship between the magnetic fabrics and dyke orientations allow us to analyse the mechanism of magma emplacement during the dyke propagation.

In summary, the dykes reflect the composition of lithospheric mantle under the Bohemian Massif and they preserve the record of thermal conditions and tectonic evolution of the study area. The results of their petrological, mineralogical, geochemical, magnetic and structural investigations can be summarized by the following findings:

1. The results of petrographic study show that the dyke rocks have similar original mineral textures and contain very close mineral assemblages.

   (i) As primary mineral phases they contain olivine, orthopyroxene, clinopyroxene, biotite, apatite, Cr-spinel. Accessory amounts of titanite, zircon and opaque phases (Fe-Ti oxides and sulphides of Fe, Cu, Ni) can be also observed. Additional (medium stage-formed) minerals are amphibole, K-feldspar, plagioclase, calcite and quartz. Late stage secondary minerals are talc, serpentine, calcite, amphibole, chlorite and quartz.

   (ii) The common feature of all rocks is the presence of pseudomorphs of talc and amphibole (mainly after olivine, minor after clinopyroxene) and various types of ocelli (quartz ocelli, carbonate ocelli and multiphase ocelli).

(iii) The weak magmatic foliations are defined by the flow alignment of tabular biotite grains, feldspar laths, grains of clinopyroxene and/or columnar amphibole grains were locally observed in rock samples.

2. Detailed study of mineral textures and mineral chemistry in *vaugnerite*, *syenite porphyry* and *olivine minette* indicate changes in melt and fluid compositions accompanied by decrease in temperature-pressure conditions during mineral crystallization. The rock samples preserve the evidence of multistage crystallization.

   (i) Two up to three mineral crystallization stages were recognized. The first stage led to crystallization of primary minerals in the mantle position. The second stage included creation of minerals from enriched residual melt by light elements in the crustal level and partly due to fractional crystallization. The third stage of mineral formation occurred in subsolidus conditions and includes minerals filling the vesicles after escape of volatiles and low-temperature alteration.

   (ii) The equilibrium phases of early stage of mineral crystallization were olivine, Cr-spinel, apatite, biotite, orthopyroxene and partly clinopyroxene. The second and third stage minerals are feldspars, titanite, clinopyroxene, biotite, amphibole, quartz, talc, serpentine, carbonate and chlorite.

   (iii) The main elements and components that affected crystallization succession and that were responsible for mineral formations, their stability and reactions in the different crystallization stages were CO_2, H_2O, F, Si and Na. The melts in the early crystallization stage were relatively rich in CO_2, H_2O and F, whereas the late-stage melts were enriched in Si and Na.

   (iv) The presence of olivine together with quartz and the replacement of olivine by talc instead of serpentine indicate melt enrichment by silica (assimilation of crustal material or mixing with crustal melts) in crustal level.

   (v) The presence of biotite coronae around olivine phenocrysts and talc pseudomorphs suggests that reaction of olivine with the matrix occurred prior to its replacement by talc. The occurrence of these pseudomorphs in vaugnerite and syenite porphyry supports origin of their parental magma similar to that of the olivine mineta.

3. Element concentrations in some primary minerals in *vaugnerite*, *syenite porphyry* and *olivine minette* shows both normal and oscillatory zoning. The normal zoning showed olivine, biotite and part of clinopyroxene. These minerals crystalized at the early stage and their zoning was the result of crystallization of original melt. The oscillatory zoning was observed in clinopyroxene and it occurred due to multiple changes in melt composition as the result from assimilation and/or magma mixing.

4. The mineral chemistry together with the bulk rock major and trace element concentrations in *vaugnerite* and *syenite porphyry* and *olivine minette* indicate that the source melt was formed by a low-degree partial melting of metasomatized upper mantle peridotite. The melting probably took place in the depth of spinel stability field or even at the boundary between spinel and garnet stability fields. This is supported by:

   (i) The lack of plagioclase phenocrysts that suggests mineral crystallization below the depths of its stability field.

   (ii) The presence of Cr-spinel inclusions in olivine (and its pseudomorphs).

   (iii) The pressure estimated from pyroxene compositions that corresponds to the depth of plagioclase-spinel stability field boundary probably reflects reequilibration during magma ascent to crustal levels.

   (iv) The REE concentrations in the bulk rocks show smooth curves in the chondrite-normalized diagram with enrichment of LREE in relation to HREE (e.g. low La/Yb ratio) that indicate the presence of spinel in the mantle source.

5. The bulk rock chemistry of all analyzed samples show close geochemical features. They have high contents of Mg, Cr and Ni and characterized by enrichment in LILE (mainly the most mantle-incompatible elements such as Cs, Rb and Ba, and also K), Th, U and Pb which is in contrast with the lower concentrations of HFSE (i.e. lesser mantle-incompatible elements such as Ta, Nb or Ti). They have high REE contents with enrichment of LREE relative to HREE. Also, they contain high amounts of volatiles (mainly CO_2, H_2O). These fundamental geochemical signatures are a clear evidence of magma formation in a subduction environment. The high rations of LILE/HFSE indicate the einrichment by fluids generated from the subducted slab.

6. The rocks also show variations in some element concentrations that are not consistent or systematic (mainly the oscillations in the ratios of some incompatible elements such as Ce, Sr, Nb, Zr). These signatures could be ascribed to an inhomogenous mantle source from which melts were originated. Generally, the low degree of partial mantle melting produce small volumes of melts and thus their mixing is limited and the formation of various dyke rocks in relatively small area and in narrow time intervals could be caused.

7. The newly determined ages of *vaugnerite* and *syenite porphyry* yield 338.59 ± 0.68 Ma and 337.87 ± 0.21 Ma. These ages are very close to the ages of Mg-K syenite plutons from the Moldanubian Zone. This suggests the existence of several magmatic pulses in relatively narrow time-intervals that are very close, but post-date the granulite facies metamorphism in the Moldanubian Zone.

8. The mode of magma ascent and its final emplacement in the dyke constrained by the magnetic fabrics in *minettes*, *spessartites*, *kersantites* and *syenite porphyries* dykes indicated that:

   (i) All studied dykes originated through flow magma within dykes.

   (ii) The *kersantite-spessartite composite dyke* shows domains with two types of magnetic fabrics (normal and inverse) which provide evidence of both magma free flow and forcefully driven magma movement. In addition, the variations of determined magnetic parameters across the dyke, and also the gradual changes in modal composition and in grain size across dyke together with variations in bulk rock chemistry from rims to core of the dyke were observed. Based on these observations, these phenomena were interpreted as the result of intrusion of two subsequent magma pulses with the slightly different composition (kersantite and spessartite) and viscosity that affect the orientation of magnetic minerals.

9. The structural field relations of all dykes indicate their creation in response to the regional stress field of WNW-ESE convergence during the formation of Variscan Orogeny.

   (i) The individual dykes have parallel orientation in W-E to NW-SE direction.

   (ii) They are almost perpendicular to the CBPC trend as well as to the magmatic fabrics in the individual plutons of CBPC and to the regional metamorphic fabrics observed in the metamorphic rocks of the Moldanubian Zone.

Although, the new results obtained by this thesis answer some principal questions, more detailed study is needed to confirm the achieved results and their interpretations. The future research should be aimed to:

- Study the trace element concentrations in bulk rock and primary minerals in olivine minette which is in elaboration.
- Study mineral textures and mineral chemistry in other selected potassic dyke rocks from contact area between the Moldanubian Zone and the Teplá-Barrandian Block of the Bohemian Massif.
- Analyse and investigate major and trace element concentrations and isotopic composition in bulk rock from selected dyke rocks.
- Determine the ages of selected dykes.

- Comparison of mineral textures and mineral chemistry in the studied dykes with those occurring in the eastern border of the Moldanubian Zone will help to clear geodynamics and mantle melting processes during Variscan Orogeny in the Bohemian Massif.
- As the dykes were generated by low-degree partial melting that formed small volumes of melt, they have much more predictive value about the composition of primary melts, mantle inhomogenitites and/or about mantle metasomatism in comparison to some larger plutonic bodies. The obtaining and processing of more data will help to better understand the origin of primary melts and their subsequent modifications, and also provide information about the heterogenity of lithospheric mantle beneath the Bohemian Massif.